INFORMATION TO USERS

This manuscript has been reproduced from the microfilm master. UMI films the text directly from the original or copy submitted. Thus, some thesis and dissertation copies are in typewriter face, while others may be from any type of computer printer.

The quality of this reproduction is dependent upon the quality of the copy submitted. Broken or indistinct print, colored or poor quality illustrations and photographs, print bleedthrough, substandard margins, and improper alignment can adversely affect reproduction.

In the unlikely event that the author did not send UMI a complete manuscript and there are missing pages, these will be noted. Also, if unauthorized copyright material had to be removed, a note will indicate the deletion.

Oversize materials (e.g., maps, drawings, charts) are reproduced by sectioning the original, beginning at the upper left-hand corner and continuing from left to right in equal sections with small overlaps. Each original is also photographed in one exposure and is included in reduced form at the back of the book.

Photographs included in the original manuscript have been reproduced xerographically in this copy. Higher quality 6" x 9" black and white photographic prints are available for any photographs or illustrations appearing in this copy for an additional charge. Contact UMI directly to order.

U·M·I

University Microfilms International
A Bell & Howell Information Company
300 North Zeeb Road, Ann Arbor, MI 48106-1346 USA
313 761-4700 800 521-0600

Order Number 9218250

Redox reagents based on 2,2′,4,4″,4′,4‴—quaterpyridyl and 4,7′—phenanthrolino—5′,6′:5,6 —pyrazine

Morgan, Robert John, Ph.D.

City University of New York, 1992

U·M·I
300 N. Zeeb Rd.
Ann Arbor, MI 48106

REDOX REAGENTS BASED ON 2,2',4,4'',4',4'''– QUATERPYRIDYL AND 4,7'–PHENANTHROLINO–5',6':5,6–PYRAZINE

by

ROBERT J. MORGAN

A dissertation submitted to the Graduate Faculty in Chemistry in Partial fulfillment of the requirements for the degree of Doctor of Philosophy, The City University of New York.

1992

This manuscript has been read and accepted for the Graduate Faculty in Chemistry in satisfaction of the dissertation requirement for the degree of Doctor of Philosophy.

1/27/92 — Arthur D. Bakelas

date — Chairman of Examining Committee

1/27/92 — Michael Hopkins

date — Executive Officer

Thomas C. Stekas

Harry D. Gafney

Klaus Schulten

Supervisory Committee

The City University of New York

Abstract

REDOX REAGENTS BASED ON 2,2',4,4'',4',4''– QUATERPYRIDYL (qpy)

AND 4,7'–PHENANTHROLINO–5',6':5,6–PYRAZINE (ppz)

by

Robert J. Morgan

Adviser: Professor A. D. Baker

The title ligands, and a series of Ru(II) polypyridine complexes containing the title ligands, have been prepared and characterized. The ground and excited state redox and acid–base properties of the quaterpyridyl complexes $[Ru(bpy)_2qpy]^{2+}$ (bpy = 2,2'–bipyridine), and its N–methylated derivatives ([qpyme]$^+$ and $[qpyme_2]^{2+}$), have been measured. $[Ru(bpy)_2qpy]^{2+}$ is highly luminescent (660 nm) and has a large quantum yield (0.053 in water), a long excited state lifetime (569 ns in water), and a first pK_a of 4.2. Quaternization on the remote pyridine rings of the quaterpyridyl generally decreases the quantum yield, and red shifts the emission and absorption maxima. $[Ru(qpy)_3]^{2+}$ is also a powerful emitter, with a quantum yield of emission of 0.14 in methanol, and an excited state lifetime of 991 ns in water.

The photoredox properties of monomeric, dimeric, and Pt(II) heterobinuclear Ru(II) complexes containing the bis–bidentate bridging ligand ppz reveal that the metal centers of luminescent, homobinuclear $[(bpy)_2RuppzRu(bpy)_2]^{4+}$ are not coupled. $[(bpy)_2RuppzPtCl_2]^{2+}$, the first Ru(II)/Pt(II) compound in which the two metal centers share the same π– system, is non–luminescent and its metal centers are strongly coupled.

The interaction of mixed ligand complexes of the type $[Ru(bpy)_2L]^{2+}$ L= ppz, $ppzPtCl_2$, qpy, [qpyme]$^+$ or $[qpyme_2]^{2+}$ with calf thymus DNA has been investigated by absorption, emission and circular dichroism (CD) spectroscopy, and equilibrium dialysis binding studies. Resolved spectral features of the ligand L simplify interpretation of the spectra regarding

intercalation.

A novel method for the enantiomeric resolution of certain tris–chelates of ruthenium(II) has been developed. Passing an aqueous solution of $[Ru(phen)]_3^{2+}$ or $Ru(bpy)_2ppz^{2+}$ through a column containing DNA adsorbed onto hydroxylapatite, gives fractions which are > 95% enantiomerically pure, and an additional pass results in pure isomers. We report the $\Delta\varepsilon$ values for the Δ and Λ isomers of the ppz complex. Qualitative results for the complex $[Ru(bpy)_2phen]^{2+}$ indicate that a minimal complement of ligands, in which only one is competent to intercalate within the major groove of B-form DNA can form the basis for highly enantioselective interaction.

ACKNOWLEDGEMENTS

There are so many people whose efforts made this work possible. First and foremost I wish to thank the staff of the chemistry department. Thanks to all the technicians, especially to Leon, Dianne, Maria, Bob, Randy, Tom and Joe. I could not have done any of this without the gracious help of the department secretaries. Thanks to Alice Brickman, Jeanne Deutsch and Claire Rosenblatt who could get *even me* through the paper work. A special thanks to Dr. Ronn who alone had to bear the burden of keeping me enrolled.

This work was only possible through the dedication of my committee members who always had time to assist and advise me. Thanks to Dr. Leddy for her electrochemical expertise, but more so for just listening. Dr. Gafney, who is responsible for everything I know about ruthenium. Dr. Strekas, who introduced me to DNA and Raman spectroscopy.

I am indeed grateful to Dr. Axelrad for his continued support for me and his faith in me,

Thanks to Dr. Baker for his support, encouragement, guidance and most of all friendship.

Finally, this work is dedicated to my mother for her love and support.

Preface

Bipyridines, phenanthrolines, and related heterocycles have attracted great attention in recent years as building blocks for the construction of several classes of highly useful compounds. These include the viologens, and α–diimine complexes of metal ions.

Viologens are quaternized bipyridines. Methyl viologen (N, N'–dimethyl–4,4'–bipyridinium dichloride) is the most common viologen; it is the common herbicide paraquat. Methyl viologen and other viologens are also extensively used as electron acceptors in redox schemes. On accepting an electron, the viologens form radicals that are generally stable in the absence of air, and highly colored.

Polypyridines and phenanthrolines possessing an α–diimine linkage form stable chelates with Ru(II) and other metal ions. These too figure prominently in redox schemes, particularly those involving photocatalysis. The cation $[Ru(bpy)_3]^{2+}$ (bpy = 2,2'–bipyridine)can be regarded as the parent member of this family. Because of its properties $[Ru(bpy)_3]^{2+}$ is often used in photoredox schemes. In addition to a long lived excited state, $[Ru(bpy)_3]^{2+}$ absorbs light of < 480 nm and throughout the ultraviolet region, and undergoes both oxidative and reductive quenching. Other α–diimine complexes share these properties to a greater or lesser degree depending on the structure of the α–diimine ligand.

Both viologens and Ru(II) α–diimine complexes have been used in photoredox schemes that generate hydrogen from water on irradiation with visible light. In this process, $[Ru(bpy)_3]^{2+}$ is used as the sensitizer, and methyl viologen mediates the transfer of an electron to a catalytic metal, which can act as a site for water reduction. The process is complicated by the need to use a sacrificial electron donor, and much work has been devoted to rendering the process catalytic. These ideas are elaborated in Chapter I, where a discussion of the photophysical properties of $[Ru(bpy)_3]^{2+}$, and the use of the cation as a light absorption sensitizer is presented.

The use of α–diimine ligands other than bpy, and viologens other than methyl viologen allows the redox properties of the sensitizer, and the electron acceptor to be fine–tuned. However,

the modified ligands on the sensitizer must closely resemble 2,2'–bipyridine or many of the desirable photophysical properties, in particular luminescence, are lost.

A new use for Ru(II) α–diimine complexes has recently been found. Some complexes are effective structural probes of B–DNA. The most effective ligands are thought to intercalate into the grooves of B–DNA, and are either planar, or contain planar groups, such as phenyl, on their periphery. There is also growing interest in the usage of these complexes in the photocleavage of DNA.

The work of this dissertation is concerned with preparation of two distinct families of redox reagents, and an investigation of their photophysical properties and their interaction with DNA. The first family is based on 2,2':4,4":4',4"'-quaterpyridine (qpy), which contains a diimine site and two "*remote*" *pyridine nitrogen atoms*. The *diimine site* can be used to bind to a metal and structural elaboration, the simplest of which is quaternization, may be performed on the remote pyridine nitrogen atoms. Chapter IV presents the preparation of qpy, Chapter V its quaternization, and Chapters VI through VIII, a study of the photophysical properties of Ru(II) complexes containing qpy, and two of its quaternized derivatives. Chapters I–III put this work in perspective by surveying relevant background material. After an introductory opening Chapter, Chapter II offers a discussion of structurally modified ruthenium α–diimine complexes, and Chapter III reviews the methodology by which novel α–diimine ligands can be prepared.

Many photochemical processes that could result in the production of useful fuels, such as the reduction of carbon dioxide to methane, or water to hydrogen, are multi–electron reactions. Yet ruthenium(II) complexes, as is true of most sensitizers, are capable of transferring only a single electron. The usage of single electron steps in multi–electron processes presents mechanistic and kinetic difficulties. A goal of this research was to prepare bimetallic Ru(II) complexes and evaluate the possibility of observing two–photon, two–electron events. Luminescence, a powerful probe of excited state properties, allows a simple calculation of excited state energies, which are pivotal in the design of photoredox systems. However, luminescence is rare in multimetallic compounds. We

sought luminescent binuclear complexes in order to investigate their photophysics and defining their potential for use in photocatalytic processes. The second portion of this dissertation focuses on ruthenium(II) complexes containing 4,7'–phenanthrolino–5',6':5,6– pyrazine (ppz). This planar phenanthroline– type ligand contains two diimine linkages, capable of bridging two metal centers. Chapter IX contains the preparation of luminescent monomeric and homobinuclear Ru(II) complexes, based on ppz, and an evaluation of their properties.

A major disadvantage in developing catalytic cycles with several components in solution, is the lack of control over their transport. A key to developing and maximizing the efficiency of catalytic processes may be to enforce structural organization the system. One approach is to prepare a "supermolecule" containing all the components of the redox system: sensitizer, catalyst and relay, bind it onto a suitable heterogeneous surface, and cleave it, regenerating the individual components in a localized zone. Chapter IX presents the first steps in this approach, and the evaluation of its feasibility. Novel heterobimetallic Ru(II)/Pt(II) complexes containing either ppz or dpp (2,3–di–(2–pyridyl)pyrazine), in which the metal centers share the same ligand π system, are prepared, diffused onto porous Vycor glass (PVG) and reductively cleaved.

Chapter XI is concerned with investigating the behavior of both the qpy, and ppz families of Ru(II) complexes on B–DNA. Chapter XII discusses the use of a DNA–hydroxylapatite in the resolution of the racemic Ru(II) α–diimine complexes; the enantomers of $[Ru(bpy)_2ppz]^{2+}$ and $[Ru(phen)_3]^{2+}$ are resolved. Finally, Chapter XIII is the experimental section. It contains all the experimental procedures used in this work, and the preparation of all the compounds.

TABLE OF CONTENTS

Part I: Survey

Part II: The Present Work

LIST OF TABLES

LIST OF FIGURES

Chapter II

Chapter III

Chapter IV

Chapter V

Chapter VI

Chapter VII

Chapter VIII

Chapter IX

Chapter X

Chapter XI

Chapter XII

LIST OF SCHEMES

Part I: Survey

Chapter I. Photophysical Properties of $[Ru(bpy)_3]^{2+}$

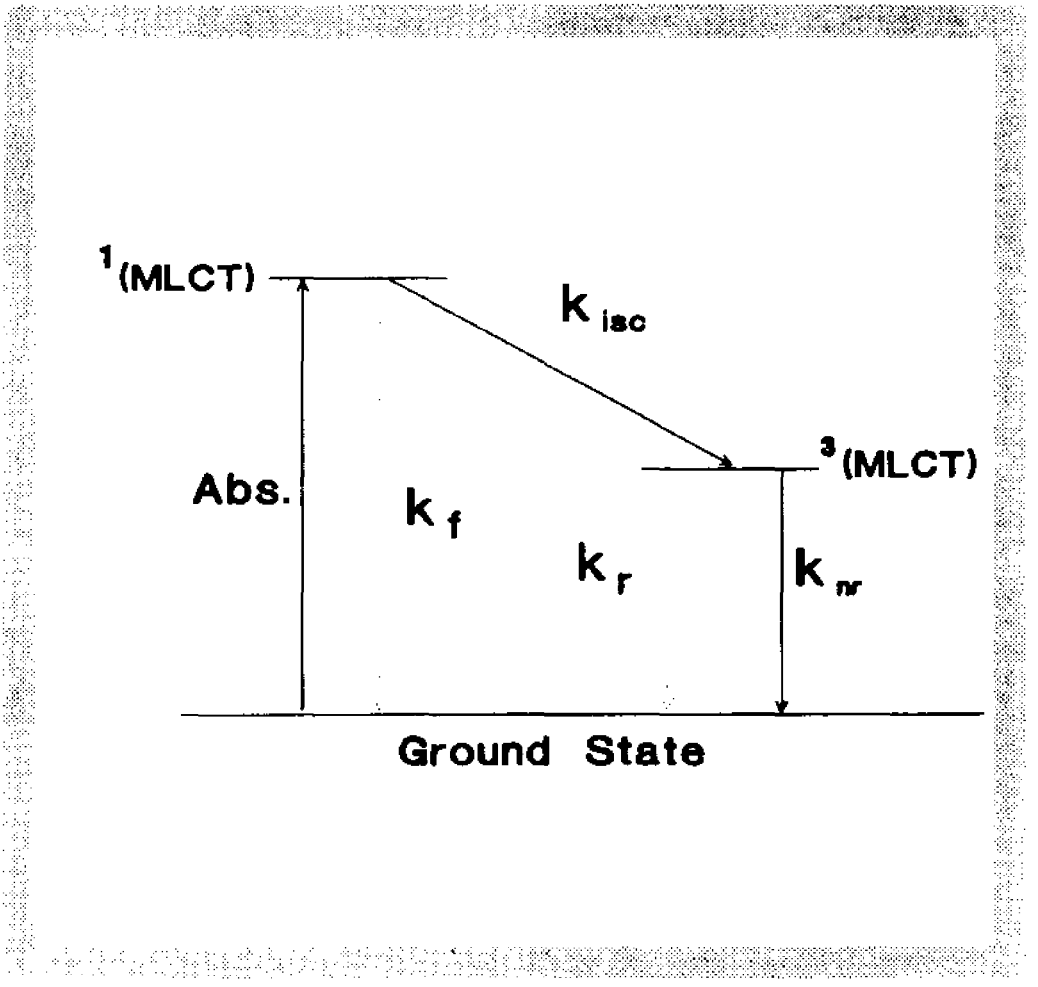

Discussion

Since the discovery of the potentially useful photophysical properties of the tris-(2,2'-bipyridine)ruthenium(II) cation[1], a tremendous amount of work been devoted to the modification of the metal environment. This has been achieved by substituting different α-diimine ligands for 2,2'-bipyridine. The parent complex has become the standard, and the properties of any novel tris-α-diimine complex are invariably compared to those of $[Ru(bpy)_3]^{2+}$. Thus any study of ruthenium(II) diimine complexes is incomplete without an overview of the photophysical properties of this

important complex ion.

Luminescence from the tris-(2,2'-bipyridine)ruthenium(II) cation was first observed by Paris and Brandt[1] in 1959. Yet, it was the discovery of excited state quenching by Co(III)[2] which precipitated an avalanche of studies attempting to exploit the excited state properties of the ion in various applications.

Photophysical Properties of $[Ru(bpy)_3]^{2+}$.

$[Ru(bpy)_3]^{2+}$ absorbs throughout the visible and ultraviolet regions of the spectrum. Excitation of $[Ru(bpy)_3]^{2+}$ throughout the visible and UV spectral regions results in a singlet metal to ligand charge transfer state (^{1}(MLCT)). The initially formed ^{1}(MLCT) state rapidly (< 10 ps) undergoes intersystem crossing (isc), resulting in a triplet metal to ligand charge transfer state (^{3}(MLCT))[2]. This triplet state is luminescent (λ_{max} = 608 nm in aqueous solution[3b], ϕ^{em} = 0.4 in alcoholic glass at 77K[3b]) and has a long lifetime (~800 ns in water at room temperature[3b]). The long lifetime allows the possibility of encountering a solute molecule while in the excited state, and $^*[Ru(bpy)_3]^{2+}$ (the ^{3}(MLCT) excited state of $[Ru(bpy)_3]^{2+}$) is a potent excited state oxidant, and reductant (Scheme 1).

$$[Ru(bpy)_3]^{2+} + h\upsilon \longrightarrow {}^*[Ru(bpy)_3]^{2+} \quad 2.1\ eV \quad (1)$$

$$^*[Ru(bpy)_3]^{2+} + e^- \longrightarrow [Ru(bpy)_3]^{+} \quad 0.84\ V \quad (2)$$

$$^*[Ru(bpy)_3]^{2+} - e^- \longrightarrow [Ru(bpy)_3]^{3+} \quad -0.86\ V \quad (3)$$

The quenching of the excited state, $^*[Ru(bpy)_3]^{2+}$, has been studied for a large variety of molecules[2,4,5]. Both reductive[2,4] and oxidative[5] quenching (Scheme 2) have been observed.

$$^*[Ru(bpy)_3]^{2+} + Q \longrightarrow [Ru(bpy)_3]^{+} + Q^+ \quad \text{Reductive}$$

$$^{*}[Ru(bpy)_3]^{2+} + Q \longrightarrow [Ru(bpy)_3]^{3+} + Q^{-} \quad \text{Oxidative}$$

It is this ability to undergo chemical reactions induced by absorption of visible light that has made $[Ru(bpy)_3]^{2+}$ a popular component in energy conversion applications.

Applications

Light Absorption Sensitizer (LAS)

An active area of research over the last decade has been the photochemical decomposition of water[3].

$$1/2\ H_2O + h\upsilon \longrightarrow 1/2\ H_2 + 1/4\ O_2 \qquad \Delta G = +1.23\ eV \quad (4)$$

The energetics of $[Ru(bpy)_3]^{2+}$ as a LAS in the process is summarized below.

$$^{*}[Ru(bpy)_3]^{2+} + H^{+} \longrightarrow [Ru(bpy)_3]^{3+} + 1/2\ H_2 \qquad \Delta G = -0.44\ eV \quad (5)$$

$$[Ru(bpy)_3]^{3+} + 1/2\ H_2O \longrightarrow [Ru(bpy)_3]^{2+} + 1/4\ O_2 + H^{+} \qquad \Delta G = -0.45\ eV \quad (6)$$

Although, reaction 5 is thermodynamically favorable, it is too slow to compete with the deactivation of the excited state of the sensitizer[3b] (the reverse of reaction 1). In spite of this, several systems for water photo–reduction have been developed. These use an electron acceptor (A), a metal catalyst (M), a sacrificial electron donor (S), and $[Ru(bpy)_3]^{2+}$ as the sensitizer.

$$[Ru(bpy)_3]^{2+} + h\upsilon \longrightarrow {}^{*}[Ru(bpy)_3]^{2+} \quad (1)$$

$$^{*}[Ru(bpy)_3]^{2+} + A \longrightarrow [Ru(bpy)_3]^{3+} + A^{-} \quad (7)$$

$$A^{-} + M \longrightarrow M^{-} + A \quad (8)$$

$$M^{\cdot} + H_2O \longrightarrow H_2 \quad (9)$$

$$[Ru(bpy)_3]^{3+} + S \longrightarrow [Ru(bpy)_3]^{2+} + S^{+} \quad (10)$$

The sacrificial electron donor is commonly EDTA or TEOA, the catalyst colloidal platinum or semiconductors[3a] such as TiO_2. Different acceptors have been used including, methyl[6] and other viologen[6a,6f], cobalt complexes[7] and others[8]. The major disadvantage of the method is that it is not catalytic, but stoichiometric as the electron donor is consumed. The sacrificial electron donor is required because rapid energy–robbing, back electron transfer

$$A^{\cdot} + [Ru(bpy)_3]^{3+} \longrightarrow A + [Ru(bpy)_3]^{2+} \quad (11)$$

not only returns the electron to the sensitizer, but also returns the sensitizer to the ground state.

Photoxidation of water using $[Ru(bpy)_3]^{2+}$ as the LAS has been given less attention in the recent literature than photoreduction. Cruetz and Sutin[9] first observed oxygen evolution from water according to the stoichiometry below.

$$[Ru(bpy)_3]^{3+} + OH^{-} \longrightarrow [Ru(bpy)_3]^{2+} + 1/2\ H_2O + 1/4\ O_2 \quad (12)$$

Later, it was discovered that trace levels of metals such as Fe^{3+} and Co^{2+} greatly enhanced the yield of oxygen[10] which is only about 10% in highly purified samples. From these results, it was proposed that hydroxo complexes of metal ions are intermediates[10]. The catalysis of oxygen in aqueous solution by $[Ru(IV)(py)L_2]^{2+}$ and $[(bpy)_2(H_2O)_2Ru]O^{4+}$ with Ce^{4+} supports this proposition[11,12]. These observations are focusing considerable attention[13] on oxo-bridged dimers of ruthenium with bipyridine ligands.

$[Ru(bpy)_3]^{2+}$ has also been used as a LAS in photoelectrochemical cells[14]. A photocurrent is achieved with a net oxidation of water by $Co(C_2O_4)_3^{2-}$. There are many other examples of $[Ru(bpy)_3]^{2+}$ as a LAS cited in the reviews in reference 3, but none has received as much attention as the photodecomposition of water. The quest to photochemically reduce water to hydrogen has generated in a tremendous amount of information about ruthenium(II) complexes and their excited states. The plethora of modified ruthenium complexes[3b] has generated a large database by which clear relationships between ligand structure and excited state properties of their complexes can be derived. We will draw upon these relationships to interpret the properties of the new complexes described in this dissertation.

Chapter II. Ruthenium(II) Diimine Complexes

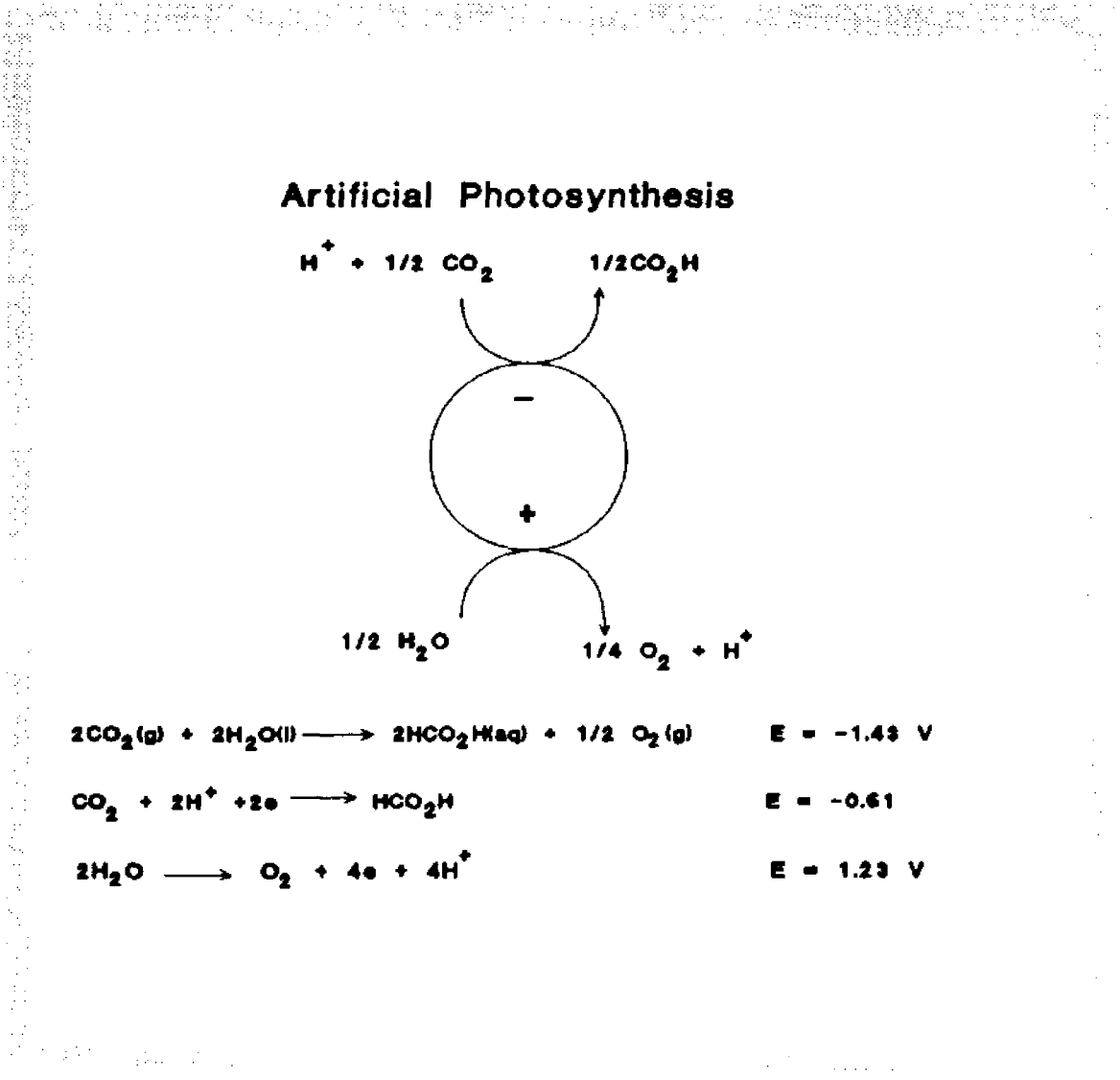

Introduction

The purpose of this chapter is to explore, in a general way, the uses of ruthenium(II) diimine complexes. A survey of important work on a variety of applications is given, and subjects with direct bearing on the present work are treated in more detail.

Ruthenium (II) polypyridine complexes have a unique combination of spectroscopic[3b] and electrochemical[15] properties. The ion $[Ru(bpy)_3]^{2+}$ has proven to be ideal for many fundamental

studies of photophysical and photochemical electron–transfer[16] and energy transfer[17] properties. The photophysical properties of this and related cations in diverse media such as micelles[18], vesicles[18], colloids[18], clays[19], cellulose[20], and silica[21] have also been determined. Significant applications of ruthenium (II) bipyridine complexes as photocatalysts have been demonstrated. Among these are the photoinduced cleavage of water[22,23] and the photoreduction of carbon dioxide[24], both major goals of research in the area of artificial photosynthesis[25]. In addition, some ruthenium polypyridine complexes have potential as components of electrochromic devices[26]. Increasingly, emphasis is attached to the rational design and synthesis of complexes with desired properties. "Fine–tuning" of advantageous properties has been achieved through the synthesis of many polypyridines and related compounds, and a recent review lists many examples[3b].

Among the most interesting modified Ru(II) polypyridine complexes are those containing ligands that have additional metal binding sites, thus allowing the preparation of bimetallic and multimetallic species. There has been much recent effort to prepare multielectron transfer agents containing Ru(II) chromophores. The preparation of Ru(II) polypyridine homonuclear dimers has been an important step in the understanding of electron transfer in multimetallic species. Initial efforts were directed toward the preparation of dimeric species in which two Ru(II) centers share the π system of a bridging ligand. In early studies, the metal centers of the 2,2'–bipyrimidine[27] (bpym) dimers (Figure 1a) were found to be strongly coupled, and the complexes were found to be non–luminescent. The same result was obtained for its methylated analog[28] (Figure 1b). Other diimine compounds with extended π systems were also used to form dimeric Ru(II) species. For example, dimers based on the quinoxaline ligands (Figure 2) were characterized, but were found to be non–luminescent[28a,29]. These were disappointing results because luminescence is an invaluable probe of excited state properties.

The first luminescent homonuclear dimers of this type were in fact synthesized in our laboratory. These complexes contained dpp (2,3–di–(2–pyridyl)pyrazine (Figure 3a) and ppz, 4,7'–phenanthrolino–5',6':5,6–pyrazine (Figure 3b) as the bridging ligands[30,31]. The excited state

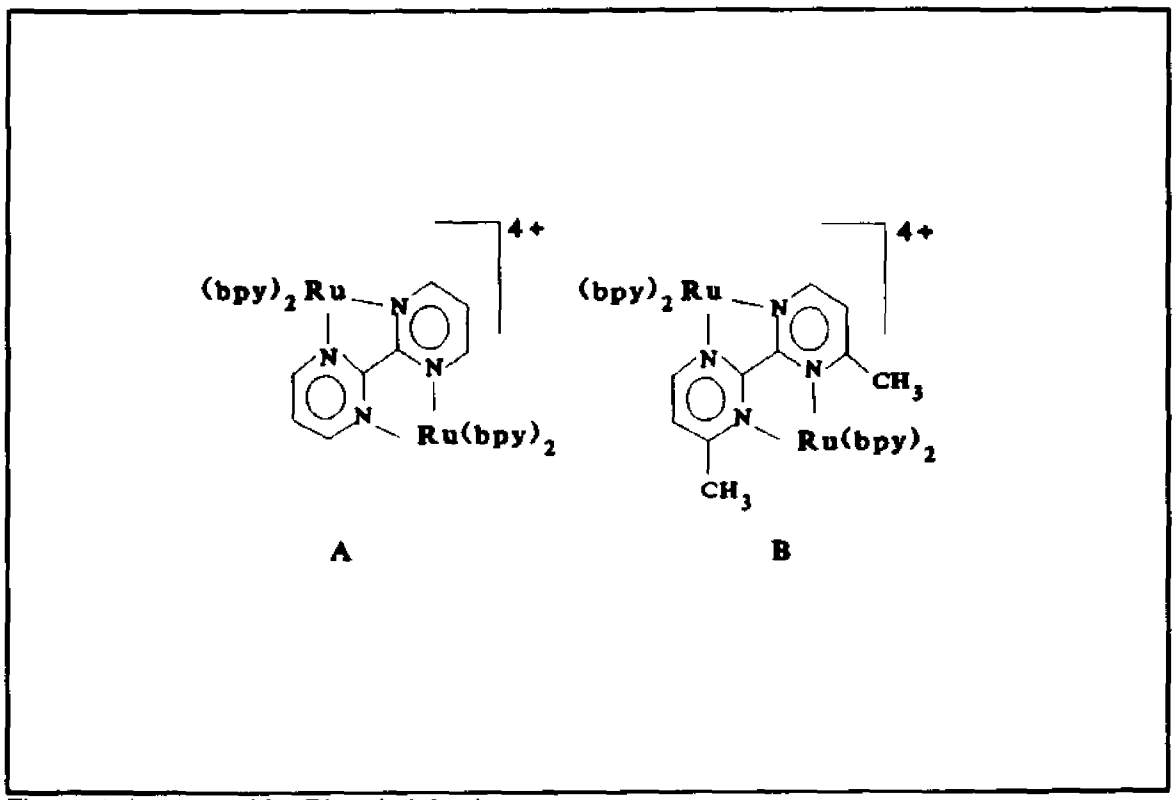

Figure 1. bpym and its Dimethyl Analog.

redox potentials of both the dpp and ppz dimers were measured. These studies revealed that the dimers are very weak excited state reductants, but potent excited state oxidants[31]. Subsequently mono–, bi– and trimetallic species of the tridentate hat (1,4,5,8,9,12–hexaazatriphenylene) ligand have been prepared (*Figure 4*)[32]. In general though, the usefulness of this type of multimetallic species as excited state reductants in redox systems is hampered by the low energy of the excited state.

Another class of multimetallic species currently being investigated have the metal centers insulated from one another by a covalent linkage. Examples of this type of complex include mononuclear, homobinuclear, and Ru(II)/Pt(II) heterobinuclear complexes incorporating the Mebpy–Mebpy bridging ligand (Figure 5)[33]. Spectroscopic properties of the series are dominated by the presence of the $[(bpy)_2RuMebpy–Mebpy–]^{2+}$ component, and there is no indication of intramolecular quenching. The $[(bpy)_2RuMebpy–MebpyRu(bpy)_2]^{4+}$ dimer displays emission and

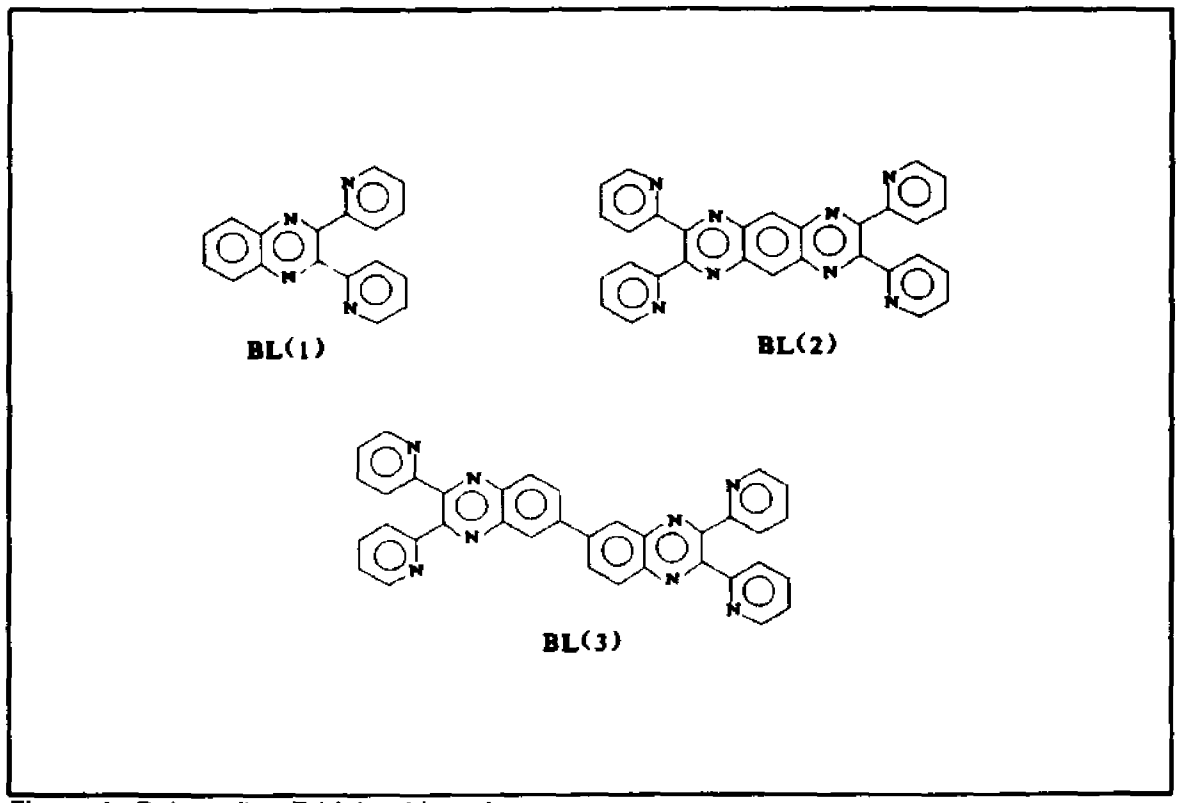

Figure 2. Quinoxaline Bridging Ligands

absorption spectra which indicate the two chromophores are not interacting with one another. The bridging ligand bb (Figure 5) has also been prepared[34], and the emission from the ruthenium bipyridine centers in the mixed iron–ruthenium cluster $\{[(bpy)_2Rubb]_3]Fe\}^{8+}$ has been found to be efficiently quenched. Using the bb (Figure 5a) ligand, Schmehl and co–workers prepared multimetallic species containing as many as four Ru(II) centers[35]. A novel intramolecular quenching mechanism has been proposed to be operative in the unsymmetrical dimer $[(dmb)_2RubbRu(decb)_2]^{4+}$ (where dmb = 4,4'–dimethyl–2,2'–bipyridine and decb = 4,4'–bis–(carboxyethyl)–2,2'–bipyridine). An excited state localized on the $[(dmb)_2Rubb–]$ chromophore is thermodynamically favored to quench the $Ru(decb)_2$– chromophore[35]. Multimetallic species in which the chromophores are separated by an aliphatic linkage have some favorable properties. They retain the high excited state potential, exhibited by the monomers, and similar to those of $[Ru(bpy)_3]^{2+}$. The length and the character of the linkage between metal centers affect the

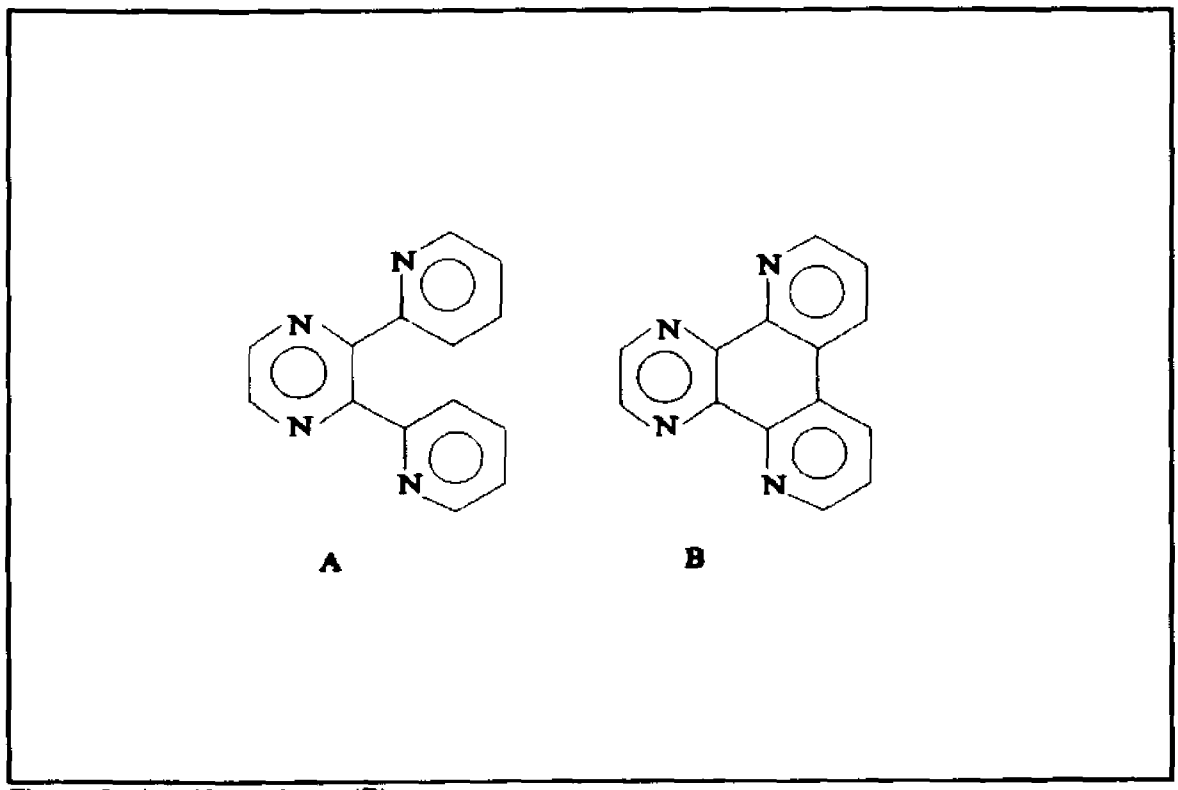

Figure 3. dpp (A) and ppz (B)

mechanism by which quenching occurs. Intramolecular quenching has the advantage of being spatially oriented, and could potentially, be modified to create a difference between the rates of forward and back electron transfer[3a,24].

A rapidly growing application of modified Ru(II) α–diimine complexes is in their use as site specific probes of DNA. It has been demonstrated[37–49] that various six-coordinate metal complexes in which the ligands are bidentate diimines with several fused aromatic rings are capable of enantiomerically selective interaction with double stranded DNA's. The basis of this enantioselectivity is usually assumed to be more favorable intercalative interaction of the one isomer within the major groove of DNA via one of the metal bonded aromatic ligands. One of the most intriguing cases is provided by tris-chelates of ruthenium(II) with heterocyclic aromatic fused-ring systems, such as 1,10-phenanthroline (phen), which have been shown[37,40,41,44,48] to bind enantioselectively to DNA. Here enantioselective binding is accomplished via an intercalative

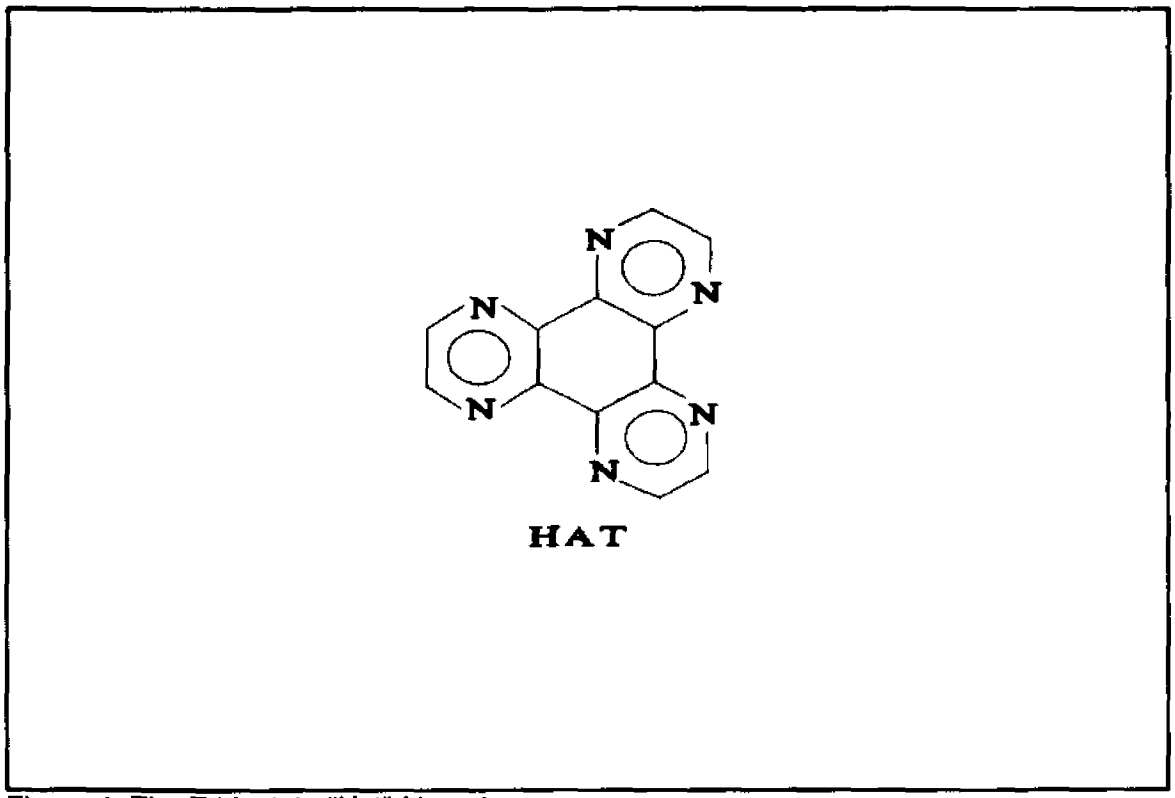

Figure 4. The Tridentate "Hat" Ligand

interaction of one ligand with base pairs within the major groove of B-form DNA. This mode of binding favors the fit of the Δ isomer by more favorable steric interactions with atoms forming the surface of the major groove. Hypochromicity of the visible region metal to ligand charge transfer (MLCT) absorption bands associated with the phen (or other ligands), circular dichroism spectra of DNA dialysates, increases in emission intensities (and quantum yields for emission) of LMCT transitions and fluorescence polarization anisotropies have all been presented as evidence of this unique mode of binding to DNA. The Λ isomer also shows enantioselectivity, but binds mainly in the minor groove. Exclusive binding of the Δ isomer of $[Ru(DIP)_3]^{2+}$ (DIP=4,7-diphenylphenanthroline) to B-form DNA by an intercalative mode[44,49] provides evidence that the optimum choice of ligand can maximize an enantioselective effect. However, a recent report, based on linear dichroism and circular dichroism studies, has challenged[48] the conclusions of Barton et al. regarding the favored intercalative binding of the Δ isomer within the major groove

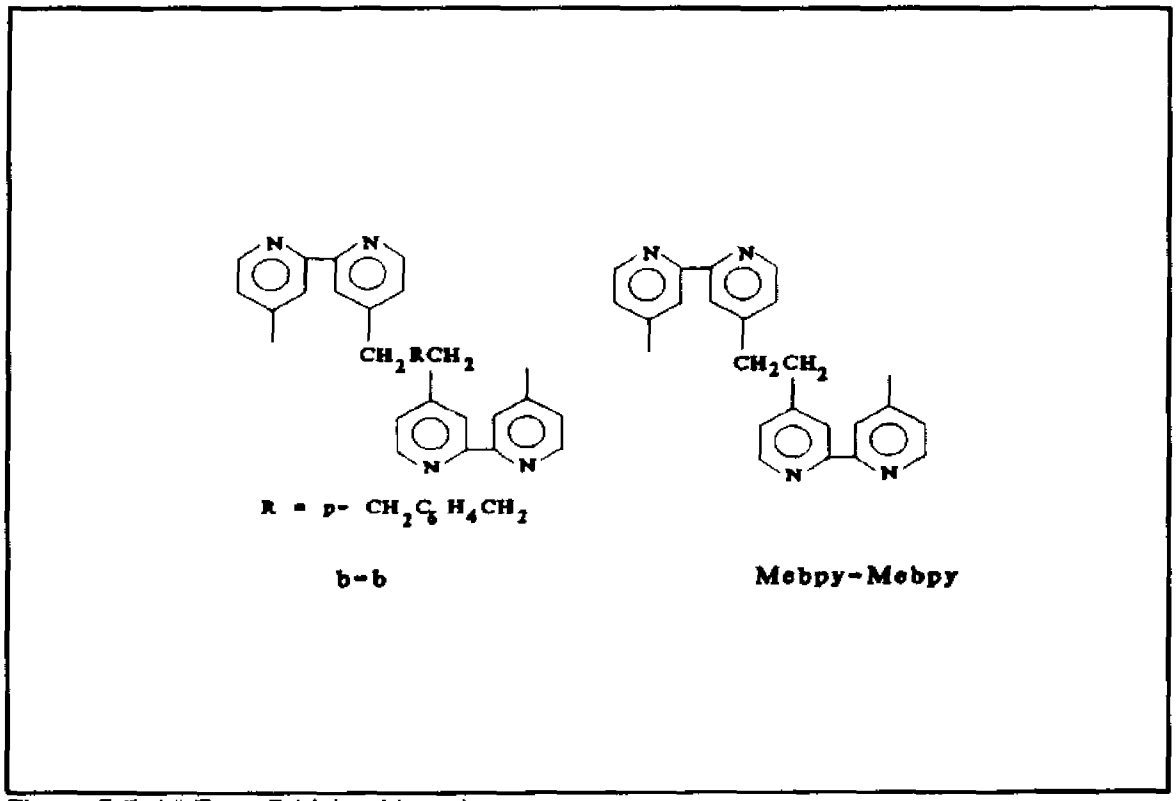

Figure 5 "b-b" Type Bridging Ligands.

of DNA. In contrast, a model is proposed in which both isomers bind via intercalation within the major groove.

Chapter III. Synthesis of Diimine Compounds Based on 2,2'–Bipyridine

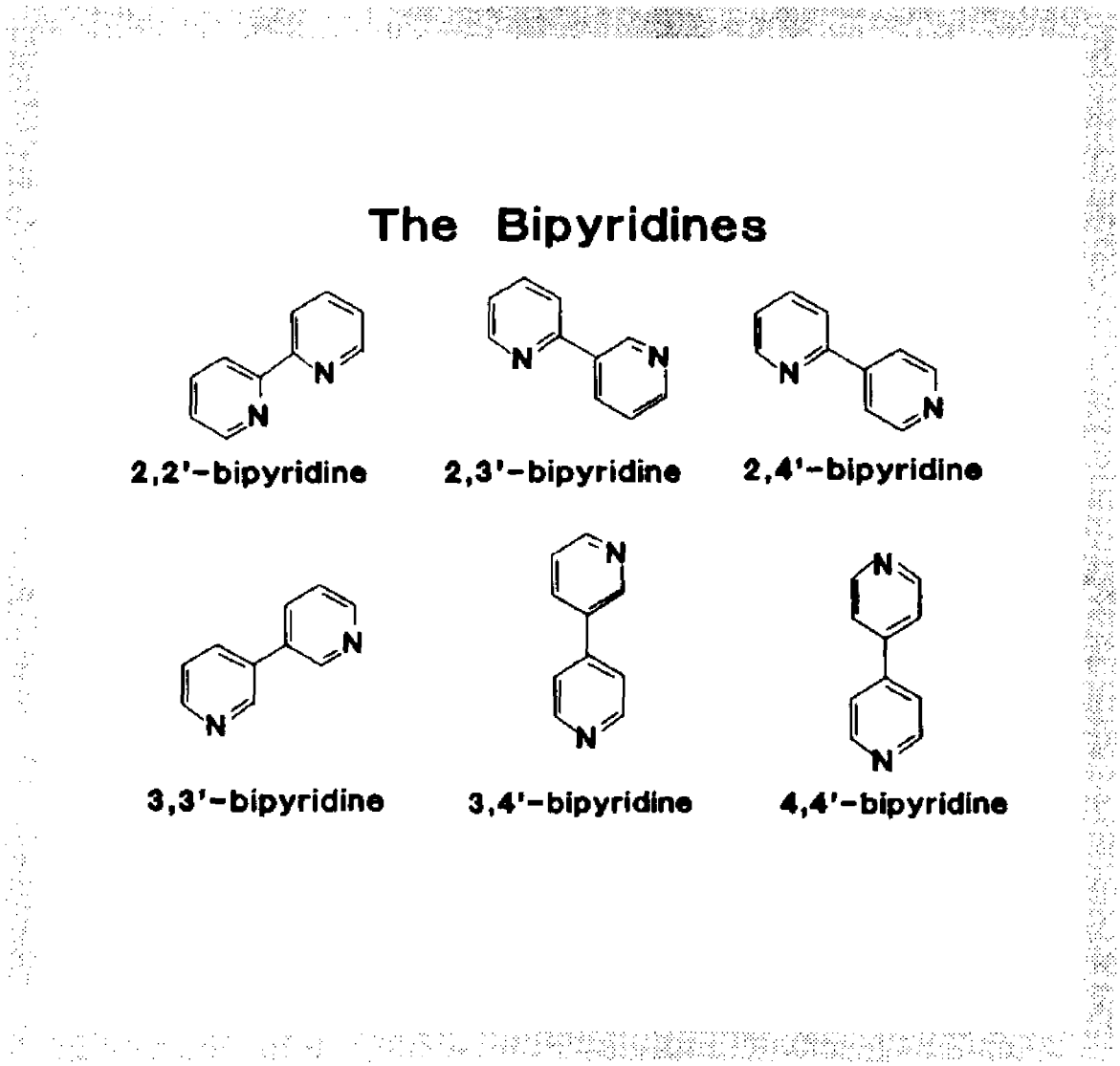

Introduction

The desirable photoredox properties of tris–(2,2'–bipyridine)ruthenium(II) cation (Chapter I), motivated the preparation of a wide variety of related diimine compounds. The aim has been to "fine tune" the photoredox properties of $[Ru(bpy)_3]^{2+}$ by substituting other diimine ligands for

2,2'–bipyridine. In this way, hundreds of complexes of the general formula $[Ru(bpy)_nL_{3-n}]^{2+}$ (where L is a bidentate diimine ligand) have been prepared, and investigated. The purpose of this chapter is to review the methods by which α–diimine compounds related to 2,2'–bipyridine can be prepared.

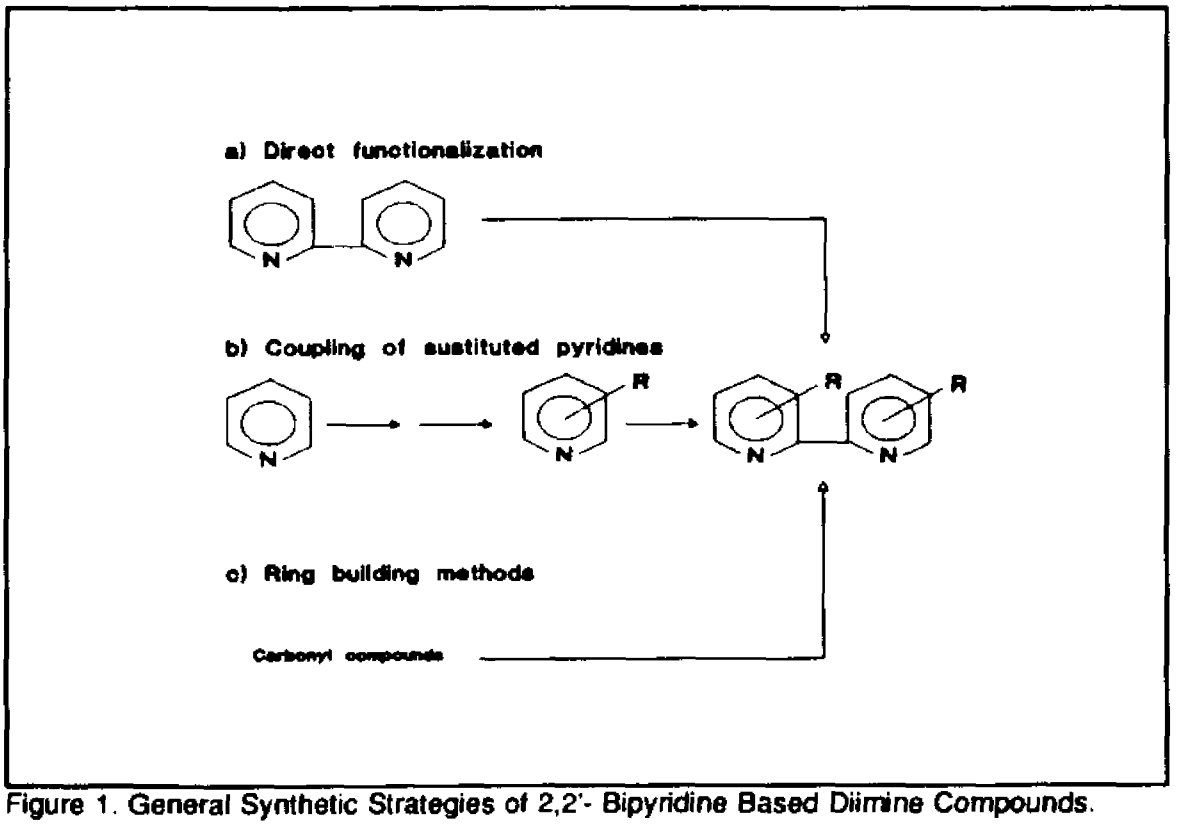

Figure 1. General Synthetic Strategies of 2,2'- Bipyridine Based Diimine Compounds.

There are three fundamental synthetic strategies leading to substituted 2,2'–bipyridines. (Figure 1).

a) Direct functionalization of 2,2'–bipyridine itself (Figure 1a) is the least common. 2,2'–Bipyridine, as is true of pyridines in general, is unreactive to most reagents useful in benzene chemistry. The most important reactions occur, instead, on the nitrogen atoms such as N–alkylation, and N–oxide formation. These procedures do activate the 2– and 4– positions of the pyridine ring toward certain useful procedures, but the synthetic possibilities are still limited[60a,b].

b) The two pyridines which compose the 2,2'– linkage are functionalized with pyridine chemistry[50a,b], and later coupled at the 2–positions to form the 2,2–bipyridine (Figure 1b). An important functionality to introduce is a halogen in the 2–position, as this provides a means of coupling the rings together. This method is the best way to prepare symmetrically substituted 2,2'–bipyridines from pyridines.

c) The pyridine rings are built from simpler starting materials (Figure 1c). For example, the condensation of 1,5–diketones with ammonium acetate is effective as in the Krohnke synthesis (below). This method is especially useful for highly substituted or unsymmetrical bipyridines.

The choice of which general method, or methods, to be used depends on the desired functionalities, symmetry, and the degree of substitution of the target polypyridyl.

Direct Coupling of Pyridines

Metal Catalysts

The action of a heterogeneous metal catalyst on pyridine, Raney nickel and palladium on carbon being the most common[51], produces 2,2'–bipyridine as the only isomeric bipyridine[52,53]. The procedure has been refined and remains the most important preparation of 2,2'–bipyridine[54–56]. Symmetrically substituted 2,2'–bipyridines have also been prepared[57–63]. Palladium on carbon usually gives lower yields of 2,2'–bipyridine than Raney nickel at low temperatures (Reflux temperature of the given pyridine)[64–73]. 2,2':6',2"–Terpyridine has been prepared with palladium on carbon[74–76] and is more effective than Raney nickel[77,78]. The coupling of pyridines with either Raney nickel or Pd/C remains the best way to prepare symmetrically substituted 2,2'–bipyridines. The pyridines which compose the 2,2'–bipyridine are prepared with pyridine chemistry, and are coupled as a final step.

The action of alkali metals on pyridines is used to prepare 4,4'–bipyridines, which can then be coupled to produce quaterpyridyl diimine compounds. Pyridine reacts with sodium to produce 1,1',4,4'–tetrahydro–4,4'–bipyridine (Figure 2)[79–82] which is easily oxidized to 4,4'–bipyridine under

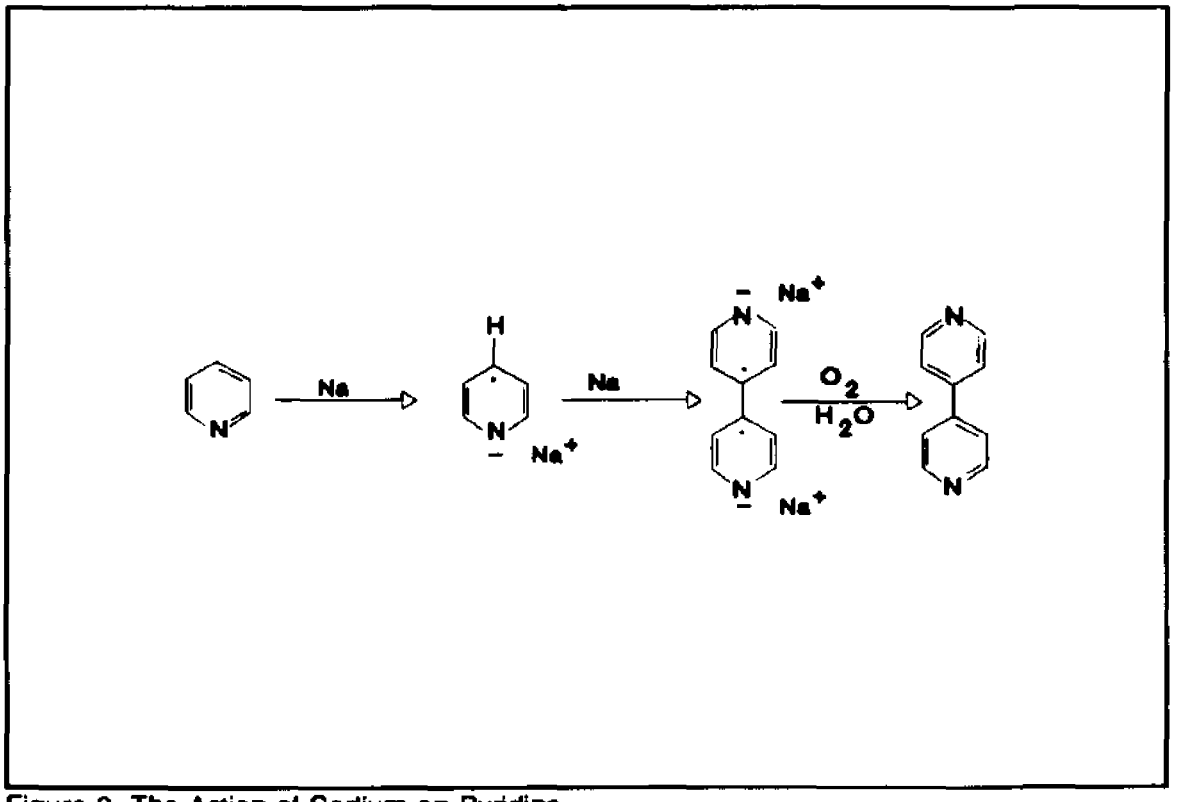

Figure 2. The Action of Sodium on Pyridine.

a variety of conditions[81,83,84]. With the proper choice of conditions, yields as high as 84% can be achieved[50c,85,86]. Symmetrically substituted 4,4'–bipyridines can be prepared with substituted pyridines[86–89]. Pyridine has also been found to react with zinc in acetic anhydride to give 1,1'–diacetyl–4,4'–tetrahydro–4,4'–bipyridine, and 4,4'–bipyridine results upon hydrolysis and oxidation[90–93]. Modifications in the procedure have improved the yield to as much as 50%[50c].

Organolithium Reagents

Treatment of pyridine with LDA (lithiumdiospropylamide) results in a 50% yield of 2,2'–bipyridine[94,95] and higher 2–pyridyl oligomers have also been prepared[96]. Kauffmann has done some elegant work with LDA and n–butyl lithium to produce a variety of polyheteroarenes[97,98].

Among the more interesting compounds reported by Kauffmann are the cycloheteroarenes based on π– deficient heterocycles. For example, the cyclotetrapyrimidine in Figure 3 was obtained

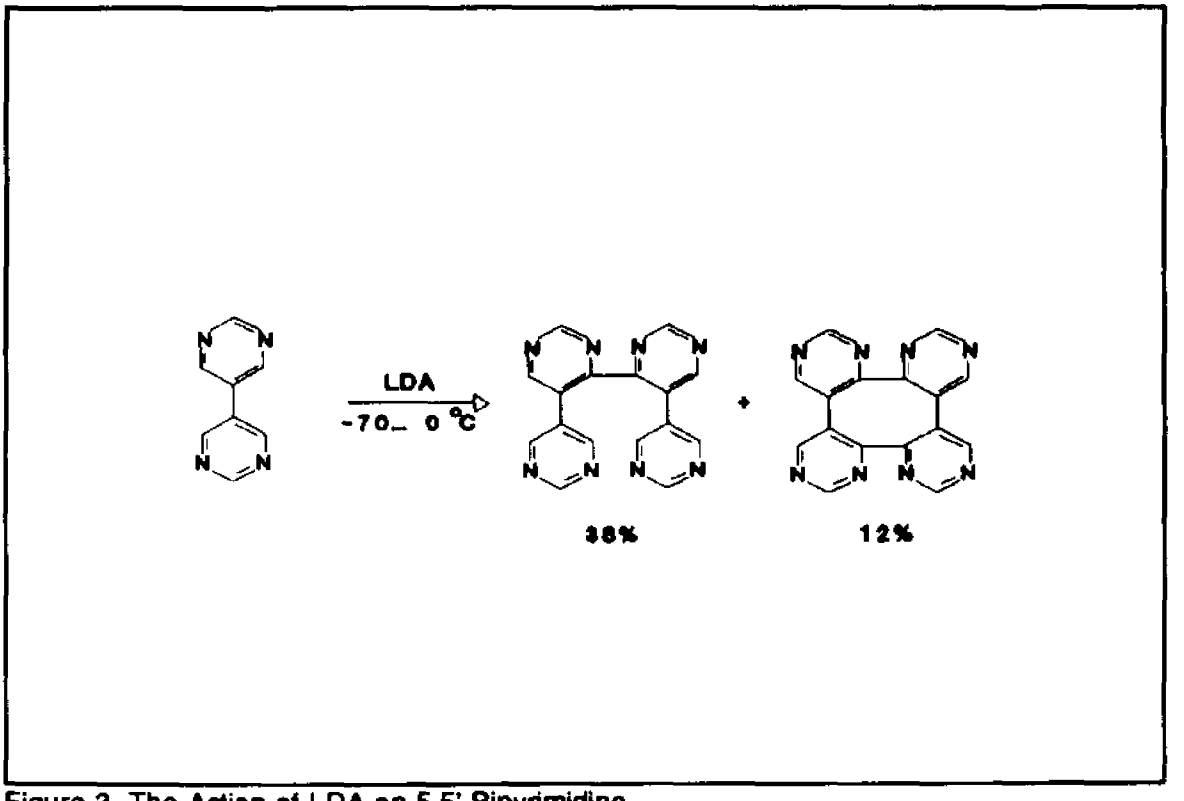

Figure 3. The Action of LDA on 5,5'-Bipyrimidine.

in 12% yield from the action of LDA on 5,5'–bipyrimidine. Figure 4 illustrates how a combined strategy of using the hindered base LDA combined with lithium–halogen exchange, using n–butyl lithium is used to couple π deficient heterocycles. In an attempt to synthesize the cycloheteroaromatic compound in Figure 5, Kaufmann obtained instead the quaterpyridyl and the hexapyridyl (in Figure 5) upon the treatment of 4,4'–bipyridine with LDA.

Other Metal Reagents

Organocopper reagents, made from the corresponding lithium compounds, have been used to prepare aza– crown ether type molecules[98]. The decomposition of 2–pyridyl gold, available from the corresponding lithium compound, results quantitatively in 2,2'–bipyridine (Figure 6). Methyl derivatives of 2,2'–bipyridine have been prepared by this method in 69– 77% yield[99]

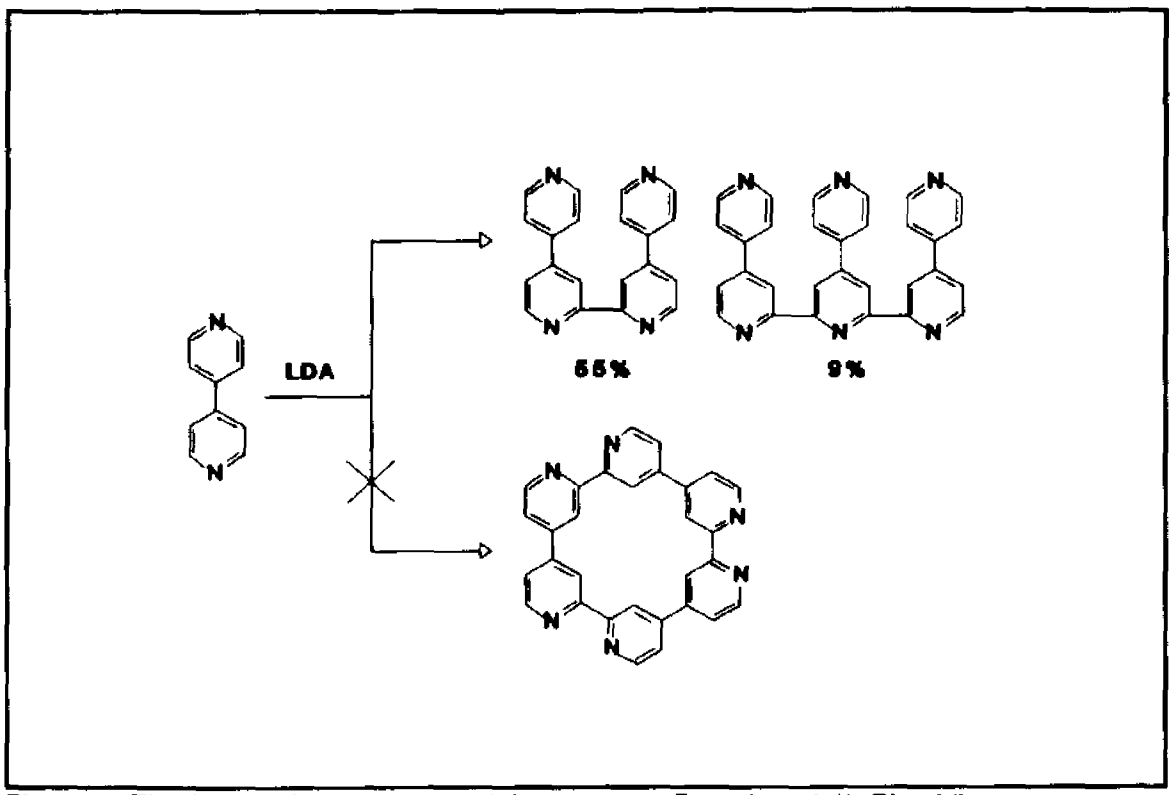

Figure 4. The Synthesis of a Tetracycloheteroarene Based on 4,4'- Bipyridine.

Coupling of Halogen Substituted Pyridines

Uhlmann Reaction

The classical method by which halogen containing pyridines are coupled is the Uhlmann reaction. Bipyridines can be prepared by heating a halopyridine, usually the bromo–, in a high boiling solvent in the presence of copper powder. The resulting bipyridine is coupled through the positions which contained the halogen. This method has been used to prepare 2,2'–bipyridine[100–109] as well as higher oligomers[101], 4,4'–bipyridine[110,111], 2,3'–bipyridine[111], 2,4'–bipyridine[111,112], 3,3'–bipyridine[111,113]. The yield of bipyridine is usually low, and the harsh conditions required limit the scope of the reaction. In addition, the reaction is useful only for the preparation of symmetrical bipyridines. However, recently, there has been work to improve the procedure. Thompson and Gaudino[114] have synthesized a series of 5–arylnicotinates by adding a palladium catalyst (Figure 7). With this method, they obtained good yields of unsymmetrical biaryls, and at lower temperatures

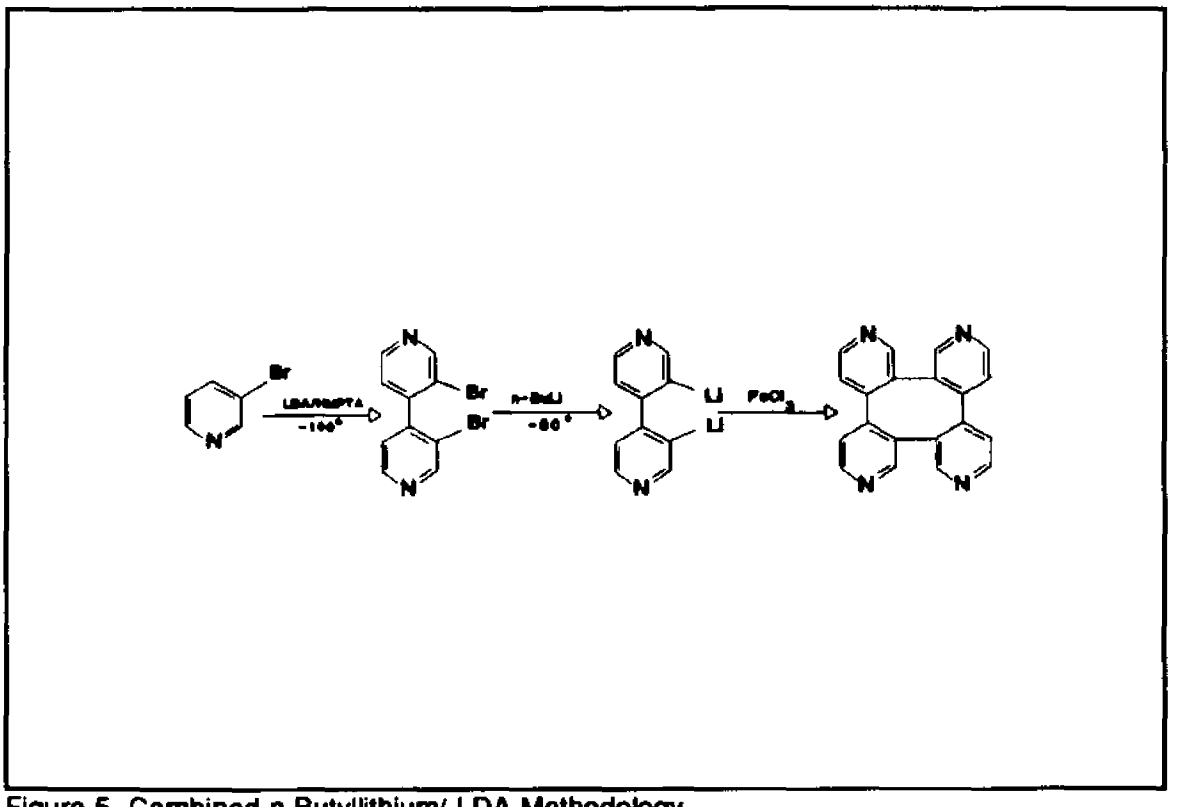

Figure 5. Combined n-Butyllithium/ LDA Methodology.

than with the traditional Uhlmann reaction. The 3–arylnicotinate illustrated in Figure 7 could not be prepared in the absence of the palladium catalyst.

Organoborane/Palladium Methods.

Developing methodology which uses palladium and organoborane chemistry is proving to be the most general way to form substituted π– deficient heteroarenes. Davidson and Triggs[115] observed that aryl boronic acids, available from the corresponding Grignard reagents, in the presence of sodium palladate, gave the corresponding biaryls in good yields under mild conditions. This observation has led other workers to explore the scope and limitations of the general procedure[116,117].

Various heteroarenes have been prepared using tetrakis [triphenylphosphine]palladium in a two phase system (Figure 8). The method has been applied to the of preparation

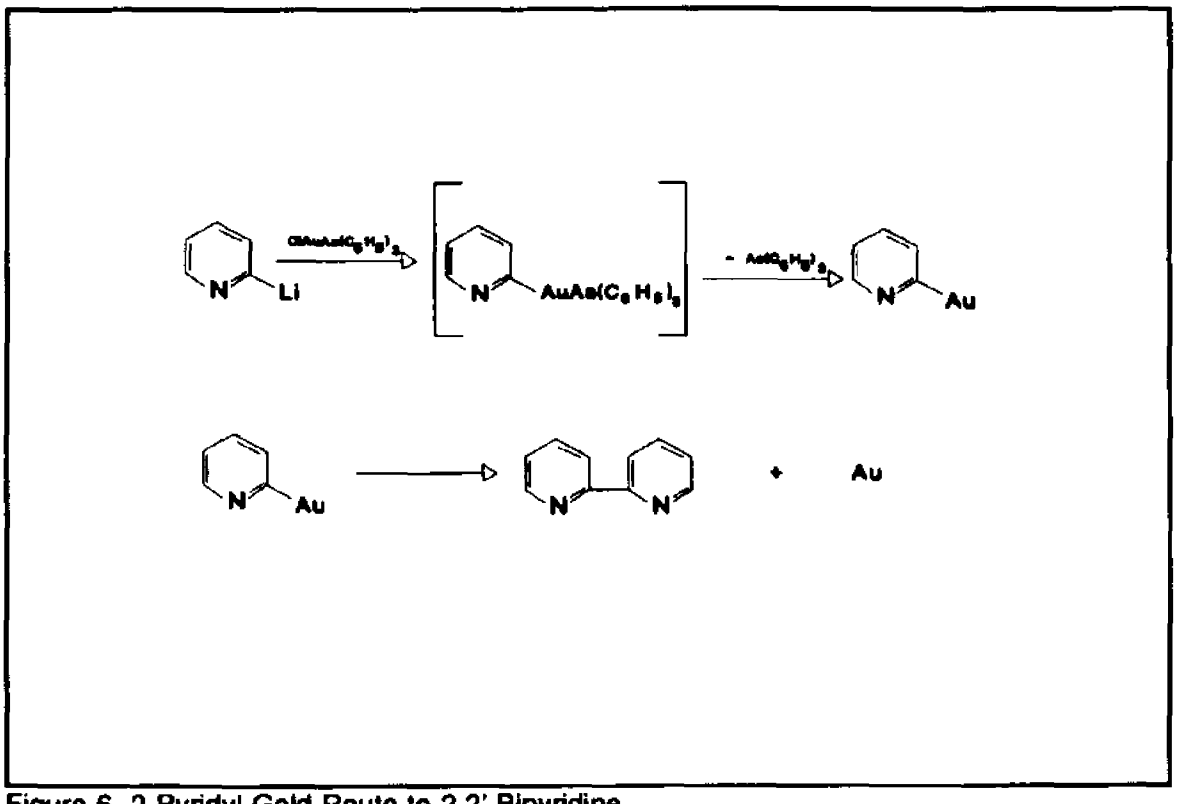

Figure 6. 2-Pyridyl Gold Route to 2,2'-Bipyridine.

3–heteroarylpyridines, that are inaccessible by other methods[118]. Some compounds which have been prepared are 3,3–bipyridine (82%), 2,3–bipyridine (85%), and 3–(3–pyridyl)quinoline (77%). With a tetrakis [triphenylphosphine]palladium or a palladium acetate catalyst the authors prepared, 5–arylnicotinates with a variation of this approach[114].

Thompson demonstrated the flexibility of this approach in the synthesis of a pyridine based pharmaceutical[119] (Figure 9). [1,1'–Bis(diphenylphosphino)–ferrocene]palladium[117,120] formed *in situ* is selective, and gives generally good yields of coupled products. This method promises to be extremely valuable in syntheses of heteroarenes which contain sensitive functionalities because the reaction is carried out under mild conditions[120] (90°C), and often results in excellent yields.

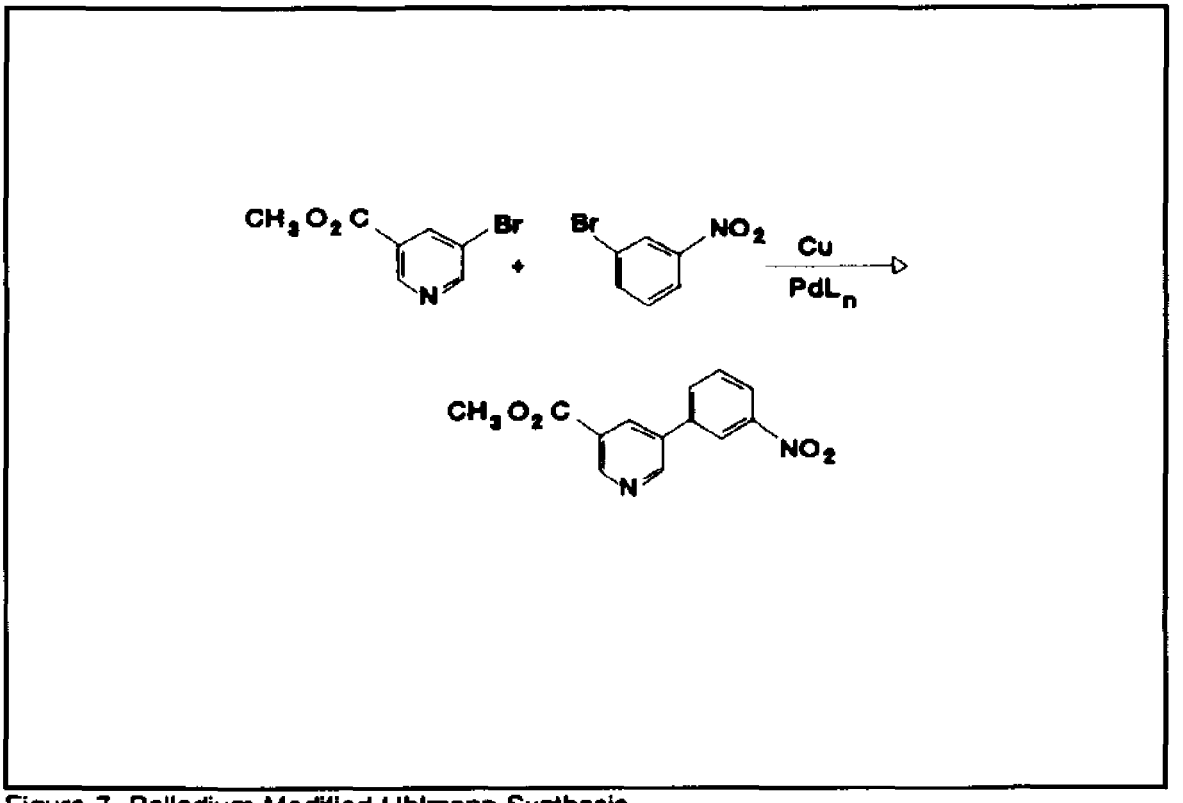

Figure 7. Palladium Modified Uhlmann Synthesis.

Other Methods

The Grignard reaction has been used to prepare 2,2'–bipyridine,[112,121] 2,3'–bipyridine,[112] and 4,4'–bipyridine[111,114]. The method has not been a popular one and the use of LDA or heterogeneous metal catalysts gives better results, and does not require a halogenated pyridine. 2,2'–and 4,4'–Bipyridines have also been prepared by treating bromopyridines with alkaline sodium formate, in the presence of a palladium on carbon catalyst[122].

Ring Building Methods

Ring building methods require more steps than the schemes which use coupling of pyridines, but allow access to unsymmetrical or highly substituted polypyridines.

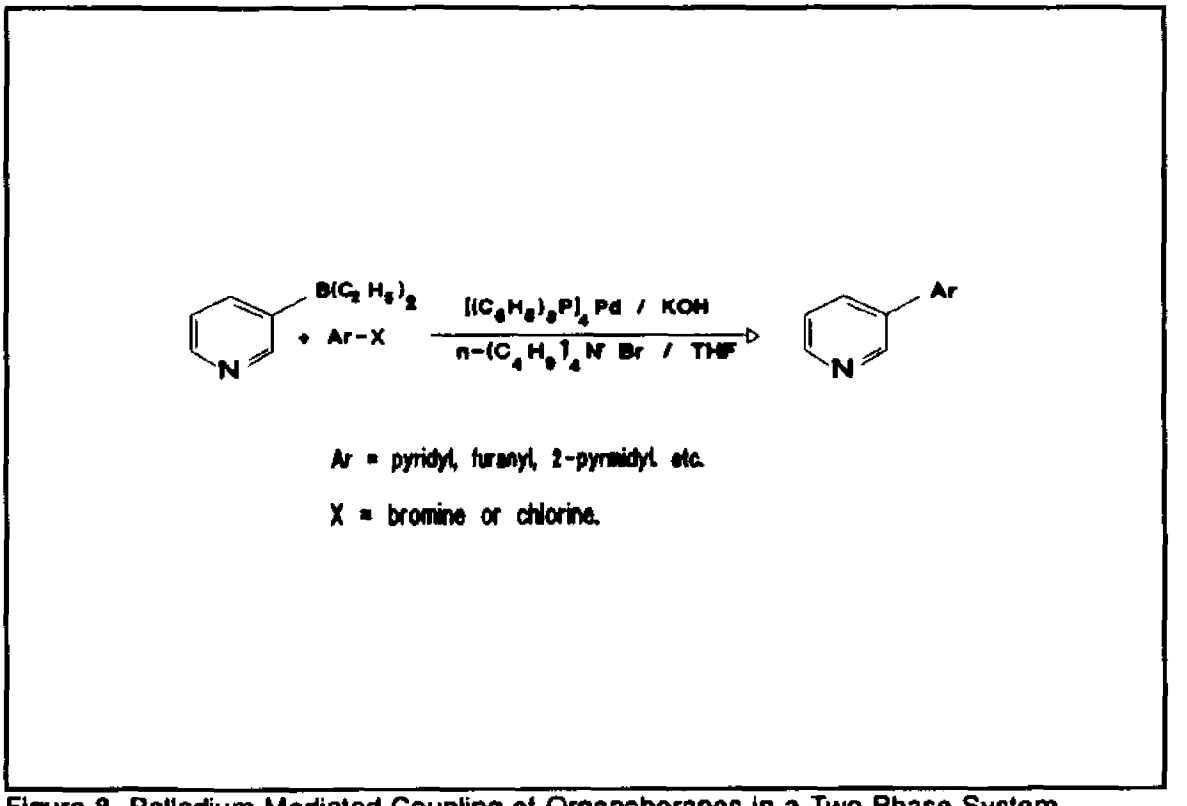

Figure 8. Palladium Mediated Coupling of Organoboranes in a Two Phase System.

Krohnke Synthesis

In a 1976 review[123], Krohnke discusses the approach to substituted pyridines in which pyridine rings are built from simpler components. The methodology (Figure 10) utilizes acylpyridinium salts, available from the corresponding bromoketones and pyridine, which undergo Michael addition with unsaturated ketones to form 1,5–diketones. The pyridine ring is formed via addition of ammonium acetate to the 1,5–diketones in glacial acetic acid. With a judicious choice of R– groups, a tremendous variety of substituted pyridines have been prepared[123]. The major advantage to the method is that it may be used to synthesize highly substituted polypyridines with sensitive functionalities. Figure 11 illustrates some polyheterocyclic compounds prepared by this procedure which could function as multi–dentate ligands.

Related Methods

Clever methodology was used by Newkome and Lee for the first synthesis of 18–[(2,6) pyridino$_5$coronand–6], "sexipyridine" (Figure 12)[124]. Cyano–substituted pyridines react with

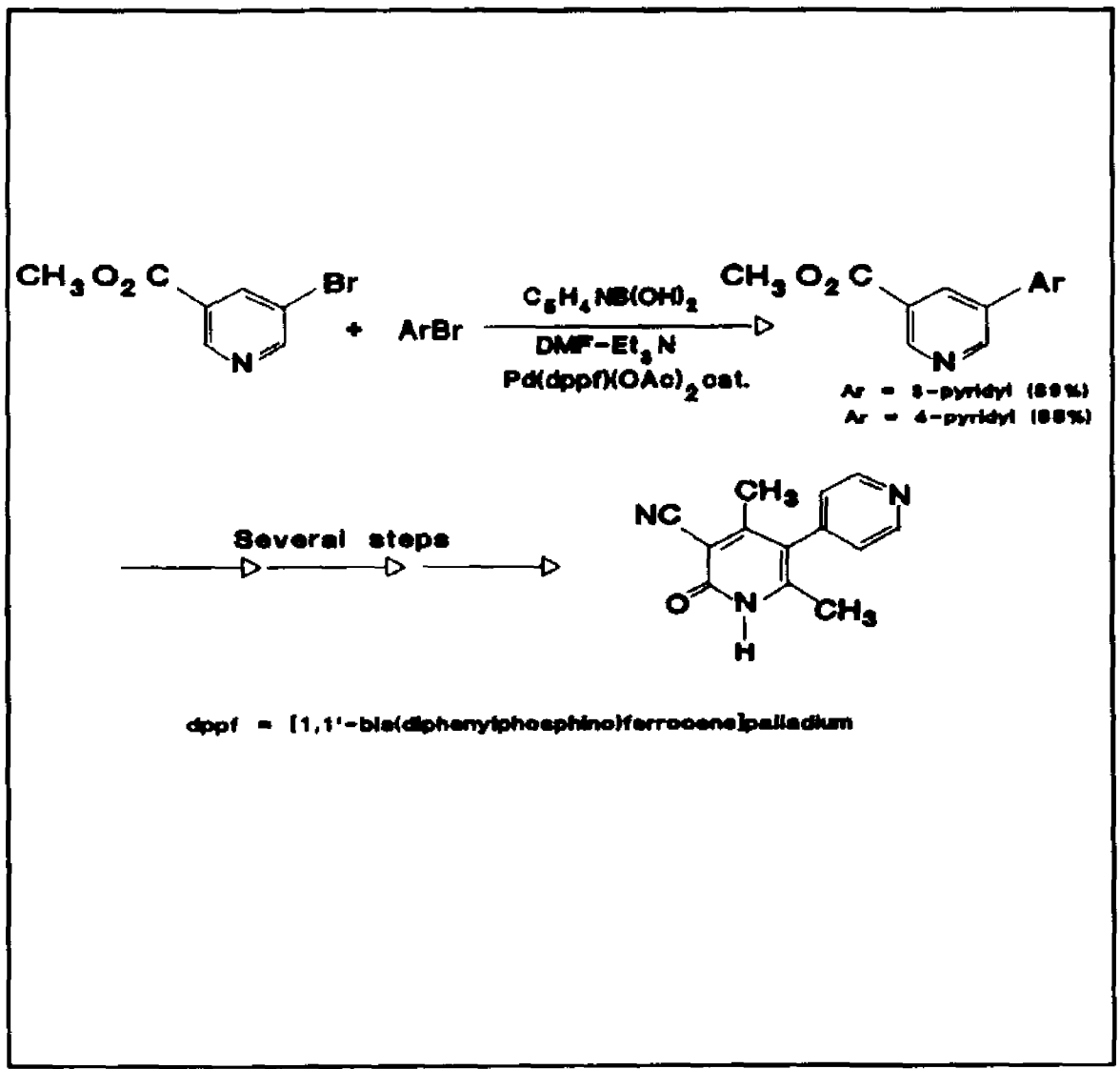

Figure 9. Synthesis of a 4-Methyl- Derivative of the Cardiotonic Milrone.

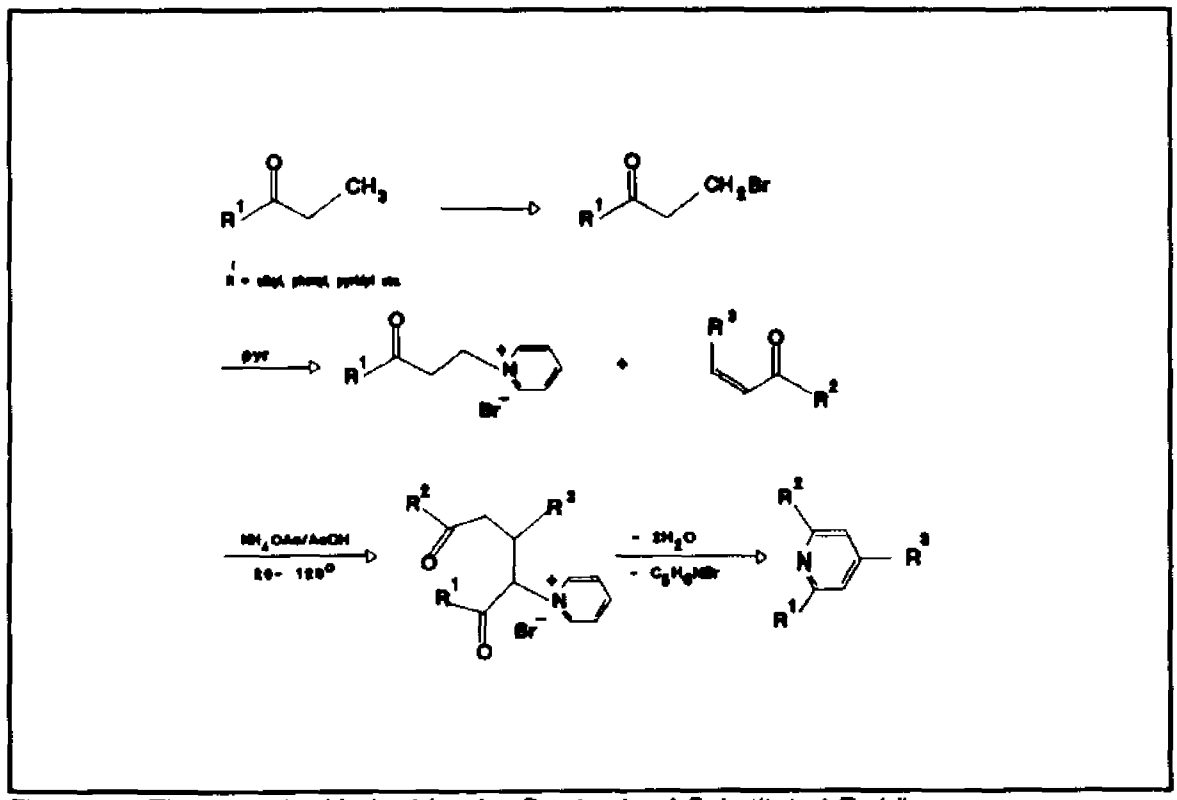

Figure 10. The Krohnke Method for the Synthesis of Substituted Pyridines.

acetylene in the presence of a cobalt catalyst to give 2–pyridylpyridines at 120°C with yields in excess of 90%[125]. In addition, pyridines bridged by methylene linkages were also prepared in excellent yields. The method has yet to be applied to the preparation of terpyridines, and routes to the required cyano–bipyridines are available (below).

Halogenation of Pyridines[80a]

A convenient and high yield method for the regioselective halogenation of pyridines is currently not available. Such a method is important, as it would allow pyridines to be used as building blocks in the preparation of polypyridines.

Direct Halogenation

Direct chlorination, or bromination, of pyridine requires several hundred degrees, and gives predominately the 3–isomer[50a]. 2,2'–Bipyridine chlorinates ortho to the nitrogen atoms to form a mixture of 6–chloro–2,2'–bipyridine and 6,6'–dichloro–2,2'–bipyridine[128]. Bromination gives similar results[50]. 4,4'–bipyridine gives mono–, di–, tri–, and tetrasubstituted chloro– derivatives, with chlorination occurring α to the nitrogen atoms[126–128]. Vapor phase bromination of 3,3'–bipyridine gives 5–bromo–3,3'–bipyridine as the major product[129]. The direct halogenation of 2,4'–bipyridine, and 3,4'–bipyridine has not been investigated. Direct halogenation is unsatisfactory for most applications because to the drastic conditions required, and the formation of isomeric mixtures.

Halogenation Via the 2–Pyridone

This method requires three steps (Figure 13). The pyridine is alkylated, usually with methyl iodide to form a pyridinium salt. Treatment of the salt with potassium ferricyanide gives the corresponding α–pyridone, which can be halogenated selectively in the 2–position[50a] with phosphorous pentabromide or phosphorous pentachloride. The disadvantages of this method are the required three steps, the use of the acidic phosphorous reagent as the halogen source, and it is limited to the preparation of α–bromopyridines.

Fluoropyridinium Salts

This method has just appeared in the literature, and promises to be an improvement over existing methods of halogenating of pyridines in the α–position. Acetyl hypofluoride[130–132] reacts with pyridines dissolved in methylene chloride to give an N–fluoropyridinium salt which then undergoes a substitution, in the α–position, to yield a mixture of 2–chloropyridine (70%) and 2–acetylpyridine (15%). The reaction is instantaneous at room temperature (Figure 14)[133]. Replacing the methylene chloride with methylene bromide, gives a 50–60% yield of 2–bromopyridine and 20% of 2–acetylpyridine. The reactivity of N–fluoropyridinium triflate has been

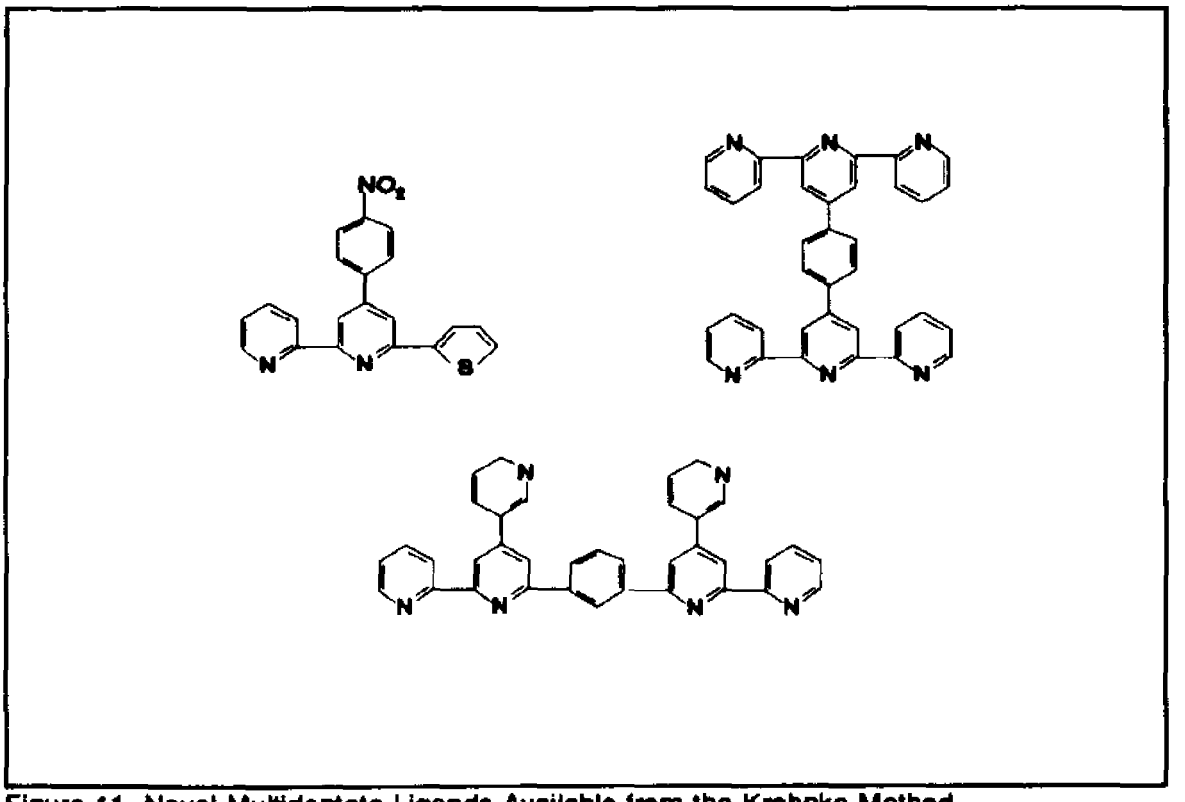

Figure 11. Novel Multidentate Ligands Available from the Krohnke Method.

investigated, and a carbene intermediate proposed[134].

Cyanopyridines

Cyanopyridines can be easily converted to acetylpyridines, which are useful in ring building methods of polypyridines, such as the Krohnke synthesis. In addition, treatment of cyanobipyridines with the above cobalt catalyst could be a valuable route to terpyridines. Alternatively, bis–(cyano)–bipyridines could be converted to quaterpyridines. 2–Cyanopyridines are prepared from pyridine N–oxides with KCN and benzoyl chloride[50a], and many N–oxides of the bipyridines are known[50c]. The mono–[50c,135,136] and di–[50c,137–139] N–oxides of 2,2'–bipyridine and both the N–oxides of 4,4'–bipyridine[50c] are available.

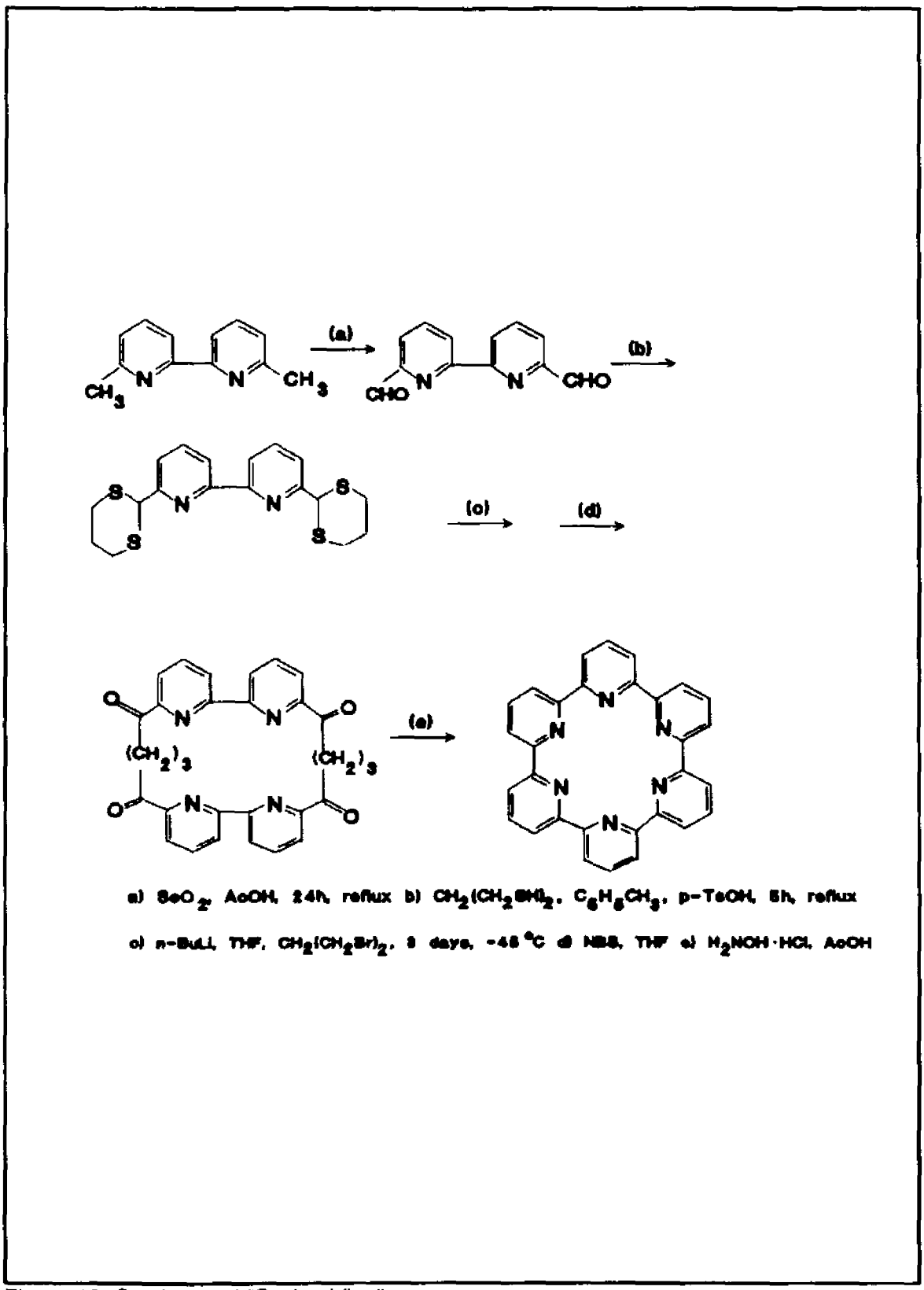

Figure 12. Synthesis of "Sexipyridine".

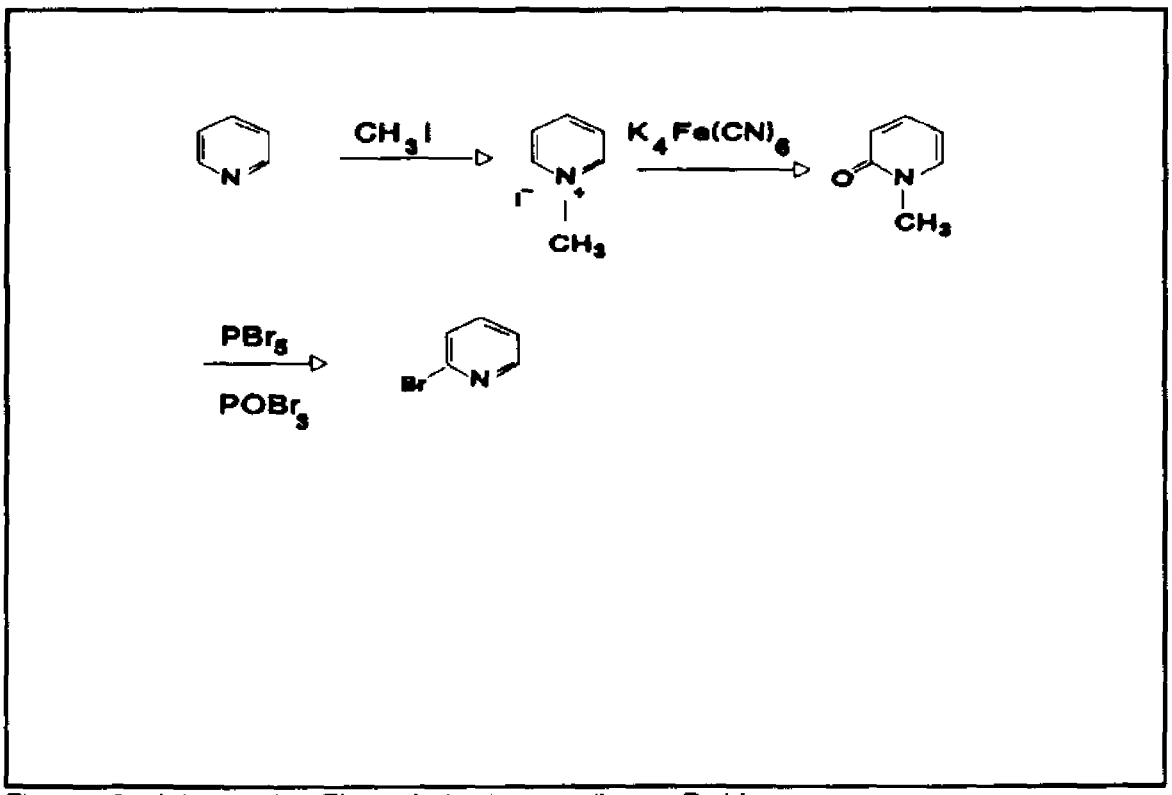

Figure 13. Halogenation Through the Intermediate α-Pyridones.

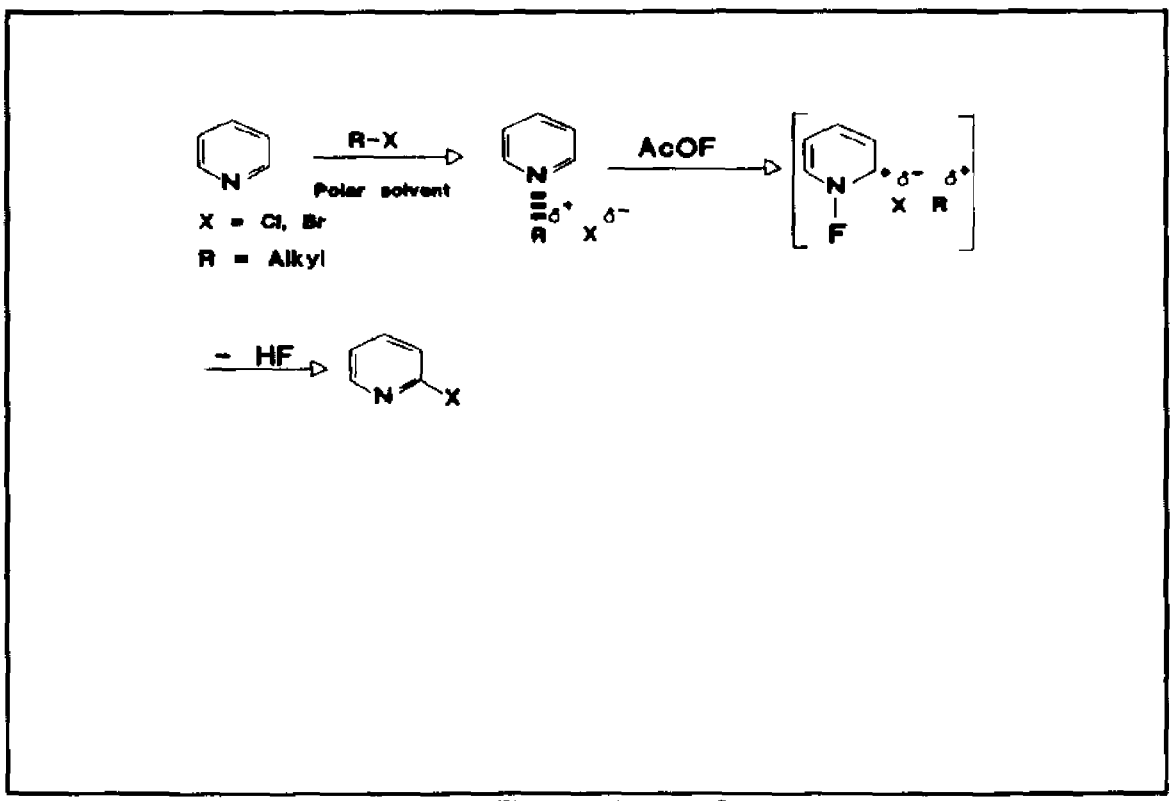

Figure 14. Halogenation Through a N-Fluoropyridinium Salt.

Part II: The Present Work

Chapter IV. 2,2':4,4'':4',4'''–Quaterpyridine

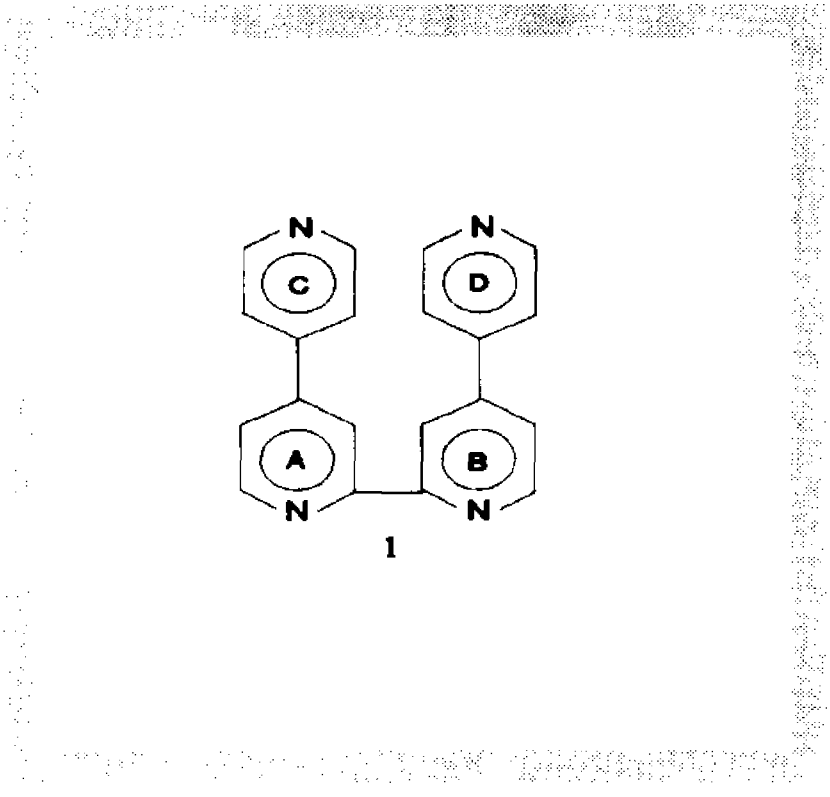

1

Introduction

There are currently two literature reports concerning the preparation of 2,2':4,4'':4',4'''–quaterpyridine (qpy). The first, over 50 years ago by Burstall[101] was a high temperature reaction of 4,4'-bipyridine with iodine that was reported to produce compound **1**. More recently, qpy had been reported by Kauffmann as a side product in the attempt to prepare a macrocyclic polypyridyl from 4,4'–bipyridine and LDA[97,98]. The Burstall method is unsuitable as a routine preparation of the quaterpyridyl, due to the drastic conditions and poor percentage conversion involved in the synthesis, while Kauffmann gave no details for his LDA procedure. This chapter presents a convenient method for the preparation of **1**, and its complete characterization.

Results and Discussion

Preparation of 2,2':4,4":4',4"'—Quaterpyridine

The simplest methods by which symmetrical substituted 2,2'—bipyridines can be prepared are those that involve the direct coupling of pyridines using a heterogeneous metal catalyst. The starting material for this approach to 2,2':4,4":4',4"'—quaterpyridine (Scheme 1) is the commercially available 4,4'—bipyridine. The most effective metal catalysts for the coupling of bipyridines are Raney nickel and palladium on activated carbon. Raney nickel generally affords higher yields, at the reflux temperature of the pyridine, but Pd/C is easier to handle and use because it does not have to be degassed. High temperatures are accessible because of the high boiling point of 4,4'—bipyridine (> 250 °C). Yields with palladium on carbon at higher temperature, rival those on Raney nickel. In the procedure described in the Experimental Section (Chapter XIII) the yield with Pd/C is 1—2 g quaterpyridyl/1 g catalyst. Palladium on carbon need not be degassed prior to its use, and a mixture of the catalyst and 4,4'—bipyridine may then be heated directly, without the difficulty of introducing a solid onto degassed Raney nickel.

The preparation of qpy with Pd/C (Scheme 1) was found to be a practical, routine method of preparing the quaterpyridyl in a single step. Any uncoupled starting material can easily be recovered and used again with no effect on the yield of subsequent preparations.

The catalyst, however, cannot be recycled. The yield of quaterpyridyl is diminished when a previously used sample of catalyst is employed. The yield is generally only 0.1—0.5 g quaterpyridyl/1 g of previously used catalyst. Traces of quaterpyridyl in the starting material also causes a drop in the yield, albeit a modest one. It is likely that the product quaterpyridyl bonds strongly to the catalyst, and causes it to be slowly poisoned during the reaction. It is not completely recovered during the work—up.

There are essentially no detectable side products if the reaction is carried out below 200 °C. However, higher temperatures result in small amounts of high melting (> 270 °C) side products. These account for at most 200 mg of the crude quaterpyridyl product. After the reaction is

completed, the problem is to separate the relatively small amount of the quaterpyridyl product from the 4,4'–bipyridine starting material, and the high melting side products. Fortunately there are large differences in the solubility properties of 4,4'–bipyridine and those of the products, and this forms the basis for the most effective isolation of the quaterpyridyl. Most significantly, only 4,4'–bipyridine has any appreciable solubility in acetone, so stirring a quaterpyridyl/4,4'–bipyridine mixture with acetone, as detailed in Chapter XIII, results in removing the bulk of 4,4'–bipyridine from the crude product. The amount of acetone is not critical, as the quaterpyridyl is almost completely insoluble. The crude quaterpyridyl may also be isolated by distilling off the 4,4'–bipyridine. This alternative is slower, but results in complete removal of 4,4'–bipyridine.

Scheme 1. Preparation of 2,2':4,4":4',4"'-Quaterpyridine.

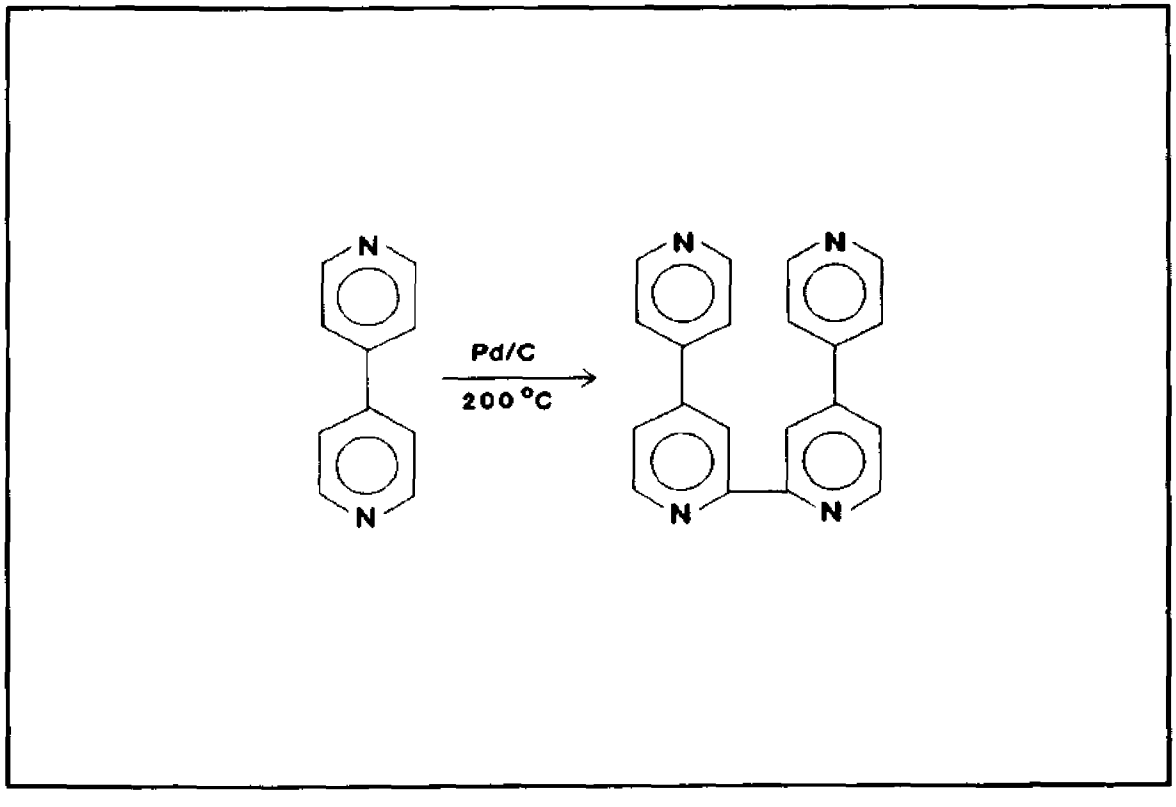

Small amounts of pure quaterpyridyl may be obtained by recrystallization from hot ethanol. The procedure works well for small amounts of quaterpyridyl (< 2g), but is awkward for larger samples as large volumes of the solvent are required. An alternative purification procedure is to dissolve

the crude quaterpyridyl in hot chloroform, then filter to remove the high melting impurities. Hexane can then be added to precipitate the quaterpyridyl, as the quaterpyridyl is quite soluble in chloroform, but insoluble in hexane. Quaterpyridyl isolated by this alternative purification route, appears to have increased ethanol solubility, and this makes possible a convenient recrystallization from ethanol. This may be because the higher melting products are insoluble and removed in the chloroform/hexane procedure. Ultra pure samples of the quaterpyridyl can be obtained by vacuum sublimation, but this was rarely used in practice, as it requires high temperatures, and there is more loss than in repeated crystallizations from ethanol.

Other methodologies were tried but with little or no success. No quaterpyridyl was detected from 4,4'–bipyridine with either Grignard reagents, n–butyllithium or LDA. Recently, however, an LDA method has been reported[97,98]. We also investigated the preparation of qpy via coupling of 2–bromo–4,4'–bipyridine, However this compound is accessible only in low yields, due to the number of steps in its preparation (Chapter III). The only feasible route to 2–bromo–4,4'–bipyridine is from the 2–pyridone (Chapter III). This three step route was difficult, and of low overall yield. The treatment of the 4–4'–(2–pyridyl)–2–pyridone with PBr_5/PBr_3 resulted in only a trace of the 2–bromo–4,4'–bipyridine. The overall yield of quaterpyridyl from the procedure would have been small, and result in the loss of all the 4,4'–bipyridine starting material.

Thus, heating 4,4'–bipyridine with palladium on carbon is the method of choice for the preparation of the quaterpyridyl. In a single step 10 g of pure quaterpyridyl can be prepared, and nearly all of the unreacted 4,4'–bipyridine is recovered.

^{13}C NMR.

The 75 MHz decoupled carbon 13 spectra of 2,2':4,4":4',4"'–quaterpyridine (qpy) is shown in Figure 1. The spectrum shows the expected eight resonances. The values for the resonances of some simpler, analogous, pyridines used as models to interpret the qpy spectrum, are listed in Table I. The ^{13}C resonances for the quaterpyridyl are listed in Table II. The numbering system used

in this discussion, and in Table I is illustrated in Figure 1.

In general, carbon atoms meta to the nitrogen atom in pyridines give signals in the range 118–124 ppm. In the spectrum of 2,2':4,4":4',4"'–quaterpyridine there are three resonances in this range, 119.0, 121.5, and 121.7, corresponding to meta carbons in the quaterpyridyl (C3(3'), C5(5'), C5"(C5"'), and C3"(C3"). Resonances in the 135–146 ppm range are indicative of carbons in the four positions of pyridine rings, carbons C4(4') and C4"(4"') in the quaterpyridyl. There are two resonances in the ^{13}C spectrum of the quaterpyridyl at 145.6, and 146.6 ppm. The carbon atoms ortho to the nitrogen atoms (C2(2'), C6(6') and C2"(2"', 6",6"'), are further downfield from 147 to 156 ppm, and there are three in the spectrum at 150.0, 150.6, and 156.6. The extreme downfield resonance is an indication that there is a 2,2'–bipyridine linkage in the molecule, since this compares well with the carbon C2(2') in 2,2'–bipyridine (155.7 ppm). Thus, the ^{13}C NMR is consistent with the structure 1 for the quaterpyridyl

^1H NMR.

The ^1H NMR spectrum of 2,2':4,4":4',4"'- quaterpyridine is shown in Figure 2. The protons on ring C (D) are of the type AA'XX'. Protons H3" and H6" form an apparent doublet (rel. area 4) at 7.65 δ. Values for the coupling constants are likely to be of the same order as in other pyridines (Table III). Coupling constants of adjacent protons, $J_{2,3}$ and $J_{5,6}$ are over three times the values for protons coupled across two nuclei ($J_{3,5}$ and $J_{4,6}$). Thus, $J_{3",2"}$ is expected to be large compared to $J_{3",5"}$, and the AA'XX' pattern closely resembles the A_2B_2 spectrum of 4,4'-bipyridine. The corresponding doublet expected for protons H2" and H6" in the quaterpyridyl is not resolved on our instrument, and appears under the multiplet (rel. area 6) at 8.68 δ. Analogous protons, H2(2') and H6(6'), in the spectrum of 4,4'-bipyridine appear at a similar δ value (8.70 δ).

The three protons on ring A produce a spectrum of the AMX type, similar to the AMXY spectrum of 2,2'-bipyridine. Protons H6(6') are the furthest downfield, ortho to the nitrogen atom on a disubstituted ring, and due to the large magnitude of $J_{6,5}$, compared to $J_{6,3}$, appear as a

doublet at 8.80 δ (rel. area 2). Proton H5 is assigned to the quartet (rel. area 2) at 7.65 δ. The assignment of protons H3(3') is based on the analogous protons in 2,2'-bipyridine. In the spectrum of 2,2'-bipyridine, protons H3(3') are further downfield than H5(5') at 8.40 and 7.23 δ respectively (Table IV). The larger than expected δ value for H3(3') is thought to be due to a transoid conformation[140], in which the lone pairs on the nitrogen atoms deshields protons H3(3') relative to H5(5'). The protons H3(3') on the quaterpyridyl are likely to be subject to the same effect, and we believe them to lie under the multiplet (rel. area 6) at 8.68 δ. The proton chemical shifts for qpy are summarized in Table IV. Based on the ^{13}C and ^{1}H NMR spectra, we assign the structure 1 quaterpyridyl.

Mass Spectrum

The dominant fragmentation pathways in 2,2'–bipyridine[141], and 4,4'–bipyridine[142] are the expulsion of H·, CN·, HCN, and to a lesser extent C_2H_2. The base peaks in both spectra are due to the molecular ion. Hydrogen atom expulsion from the molecular ion gives the largest fragments (M–1) in both 4,4'–bipyridine (44% of base peak) and 2,2'–bipyridine (42%). Expulsion of HCN from the molecular ion fragment is favored over the loss of CN· in both 4,4'–bipyridine (10% to 6%) and 2,2'–bipyridine (20% to 10%). The expulsion of HCN dominates the expulsion of H·, CN· and C_2H_2 from the M–1 ion. High resolution mass spectra was used to discriminate the loss of CN· from the loss of C_2H_2, and it was found that expulsion of CN· dominates in both 2,2'–bipyridine and 4,4'–bipyridine. Pyridine–pyridine bond fission was found to be an important pathway in the fragmentation of 2,2',2"–terpyridyl[143]. Doubley charged molecular ions are also significant in the spectra[143] of 4,4'–bipyridine (3.8%), 2,2'–bipyridine (4.0%), and 2,2',2"–terpyridyl (5.8%).

The 70 eV mass spectrum of 2,2':4,4":4',4"'–quaterpyridine (qpy, Compound 1) is shown in Figure 3, and the analysis of the fragmentation pattern in presented in Scheme 2. The base peak in the spectrum is the molecular ion at m/e 310. The largest fragment results from the loss of a hydrogen atom from the molecular ion, $C_{20}H_{13}N_4^+$, (25% of the base peak). Loss of HCN then

Scheme 2. Fragmentation Pattern of 2,2':4,4":4',4"'-Quaterpyridine.

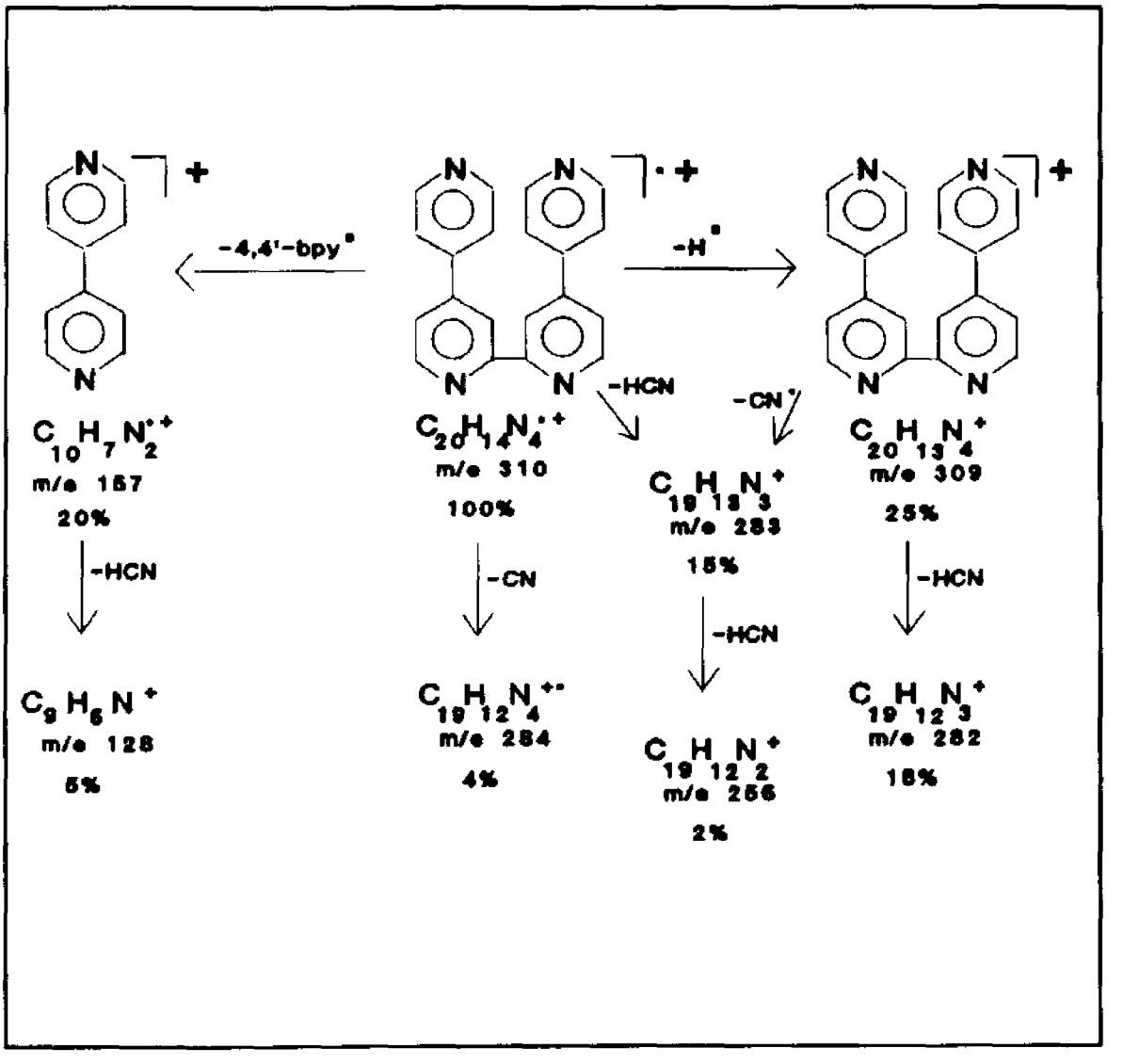

gives $C_{19}H_{12}N_3^+$, m/e 282 (18%). Expulsion of HCN from the molecular ion results in $C_{19}H_{13}N_3^+$, m/e 283 (15%). Expulsion of CN· from the molecular ion results in the $C_{19}H_{14}N_3^+$ at m/e 284. It is likely that loss of C_2H_2 from the molecular ion also contributes to this peak. The peak at m/e 155 (20%) results from C—C bond fission, giving 4,4'—bipyridinium cation $C_{10}H_7N_2^+$, and the M^{++} ion $C_{20}H_{14}N_4^{++}$. The bipyridinium cation then expels HCN to give the ion $C_9H_6N^+$, m/e 128 (5%).

Absorption Spectra.

The ultraviolet (UV) spectrum of qpy is given in Figure 4. Two strong $\pi \rightarrow \pi^*$ transitions at

290 nm (ε= 2.56 X10^4 M^{-1},cm^{-1}) and 238 nm (ε= 6.38X10^4 M^{-1},cm^{-1}) are shown in the spectrum.

Cyclic Voltammetry

The cyclic voltammogram at 500 mv/s of 2,2':4,4":4',4"'–quaterpyridine measured in acetonitrile contains two reductions on the anodic scan at E^a_p –1.69 V and –1.90 V (vs. SCE). There are two corresponding reductions on the cathodic scan at E_p^c –1.58 and –1.79 V. The 110 mv difference between the waves on the anodic scan and the corresponding cathodic waves for both reductions are higher than the predicted value of 59/n mv (where n is the number of electrons under the wave) in a reversible system (Reversibility is further discussed in the Experimental Section, Chapter XIII).

Conclusion

An improved preparation of the polypyridyl, 2,2':4,4":4',4"'–quaterpyridine have been presented. NMR and mass spectrometry have been used to confirm the structure.

Table I. ^{13}C Resonances of Bipyridines[144].

C#	Pyr	2,2-bpy	2,4'-bpy	4,4'-bpy
2	148.9	155.7	153.6	150.1
3	123.2	120.6	120.0	120.8
4	135.5	136.4	136.2	144.8
5	123.2	123.2	123.0	120.8
6	148.9	148.7	149.3	150.1
2'	---	155.7	149.6	150.1
3'	---	120.6	120.2	120.8
4'	---	136.4	145.5	144.8
5'	---	123.2	120.2	120.8
6'	---	148.7	149.6	150.1

$CDCl_3$ Solutions, measured in ppm relative to TMS.

Table II. ^{13}C Resonances for qpy.

Position[a]	ppm
β	119.1
β	121.5
β	121.7
γ	145.6
γ	146.6
α	150.0
α	150.6
α	156.6

[a]Relative position either α, β or γ to the pyridine nitrogen

[b]The carbons of the 2,2'- linkage.

Table III. Coupling Constants for Bipyridines[145].

J^a	2,2-bpy	3,3-bpy	4,4-bpy
$J_{2,2'}$	—	—	5.0[b]
$J_{3,4}$	8.0	—	—
$J_{4,5}$	7.6	7.8	—
$J_{5,6}$	4.8	4.9	5.0[b]
$J_{3,5}$	1.3	—	—
$J_{4,6}$	1.8	1.6	—

[a]Values given in Hertz, for samples in $CDCl_3$.
[b]Authors report only an approximate value.

Table IV. Proton NMR frequencies.

Proton	qpy	[qpyme]$^+$	[qpyme$_2$]$^{2+}$	2,2'-bpy[146]	4,4'-bpy[146]
H2	—	—	—	—	8.70
H3	8.68	8.71	8.91	8.40	7.49
H4	—	—	—	7.74	—
H5	7.66	8.00	8.20	7.23	7.49
H6	8.80	8.87	9.02	8.65	8.70
H2'	—	—	—	—	8.70
H3'	8.68	8.58	8.91	8.40	7.49
H4'	—	—	—	7.74	—
H5'	7.80	7.81	8.20	7.23	7.49
H6'	8.80	8.75	9.02	8.65	8.70
H2"	8.68	9.08	9.16		
H3"	7.65	8.60	8.71		
H4"	—	—	—		
H5"	7.65	8.60	8.71		
H6"	8.68	9.08	9.16		
H2"'	8.68	8.67	9.16		
H3"'	7.65	7.75	8.71		
H4"'	—	—	—		
H5"'	7.65	7.75	8.71		
H6"'	8.68	8.67	9.16		

Solutions in $CDCl_3$, 2,2'-bpy = 2,2'- bipyridine, 4,4'-bpy = 4,4'- bipyridine

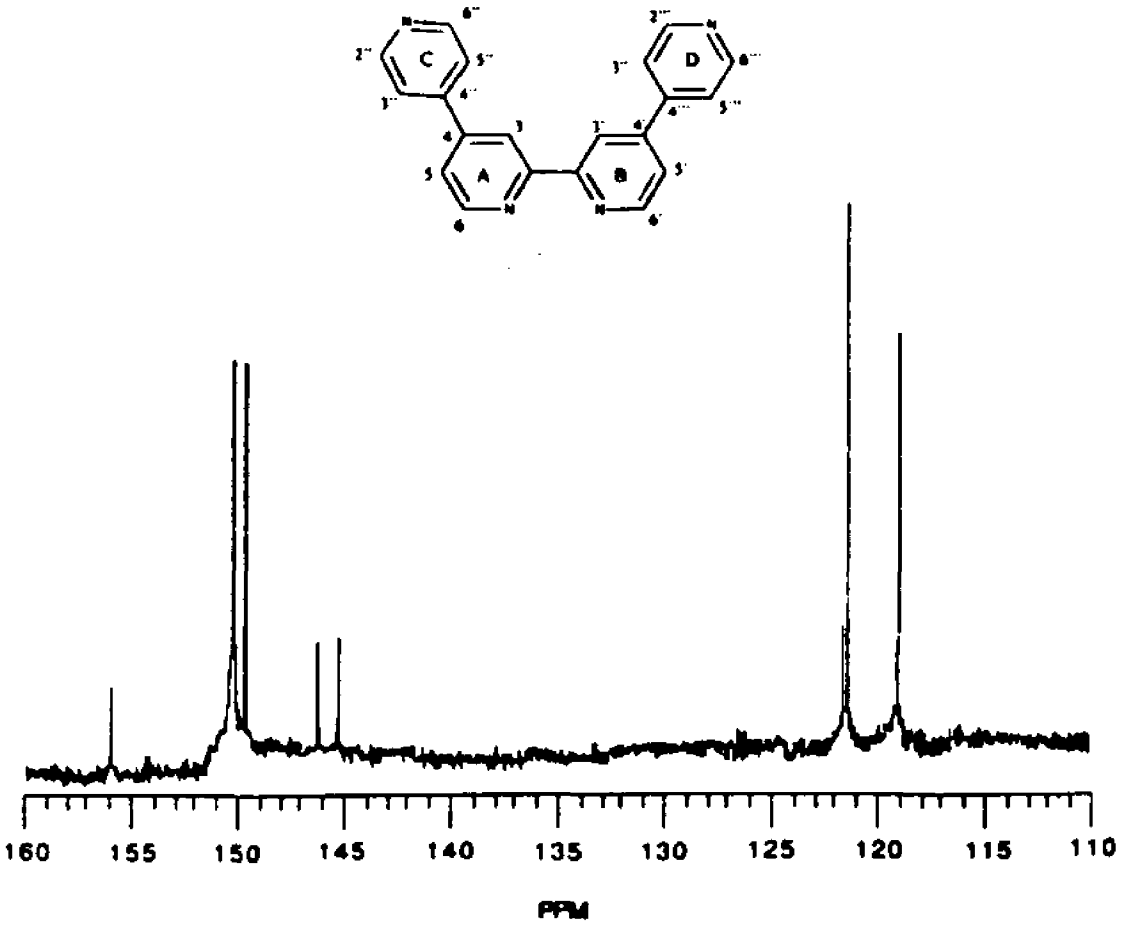

Figure 1. Decoupled ^{13}C Spectrum of 2,2':4,4":4',4"'-Quaterpyridine.

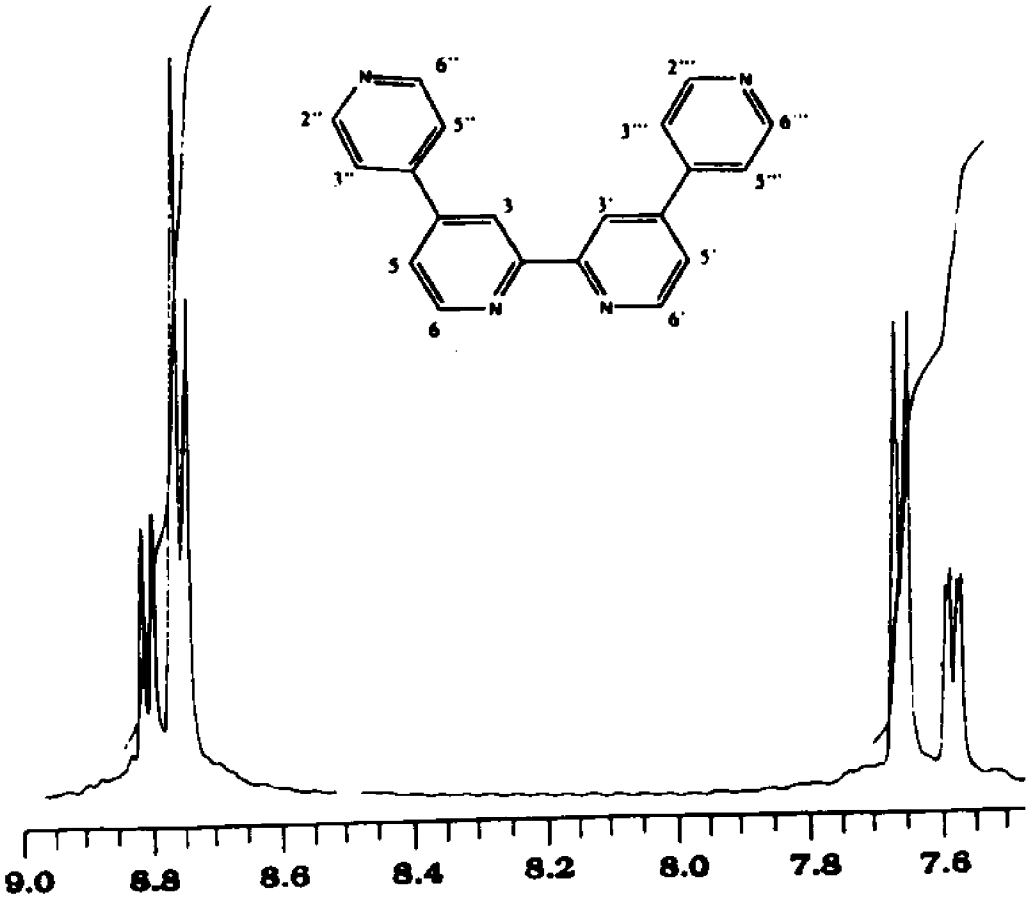

Figure 2. 300 Mhz ^{1}H Spectrum of 2,2':4,4'':4',4'''-Quaterpyridine.

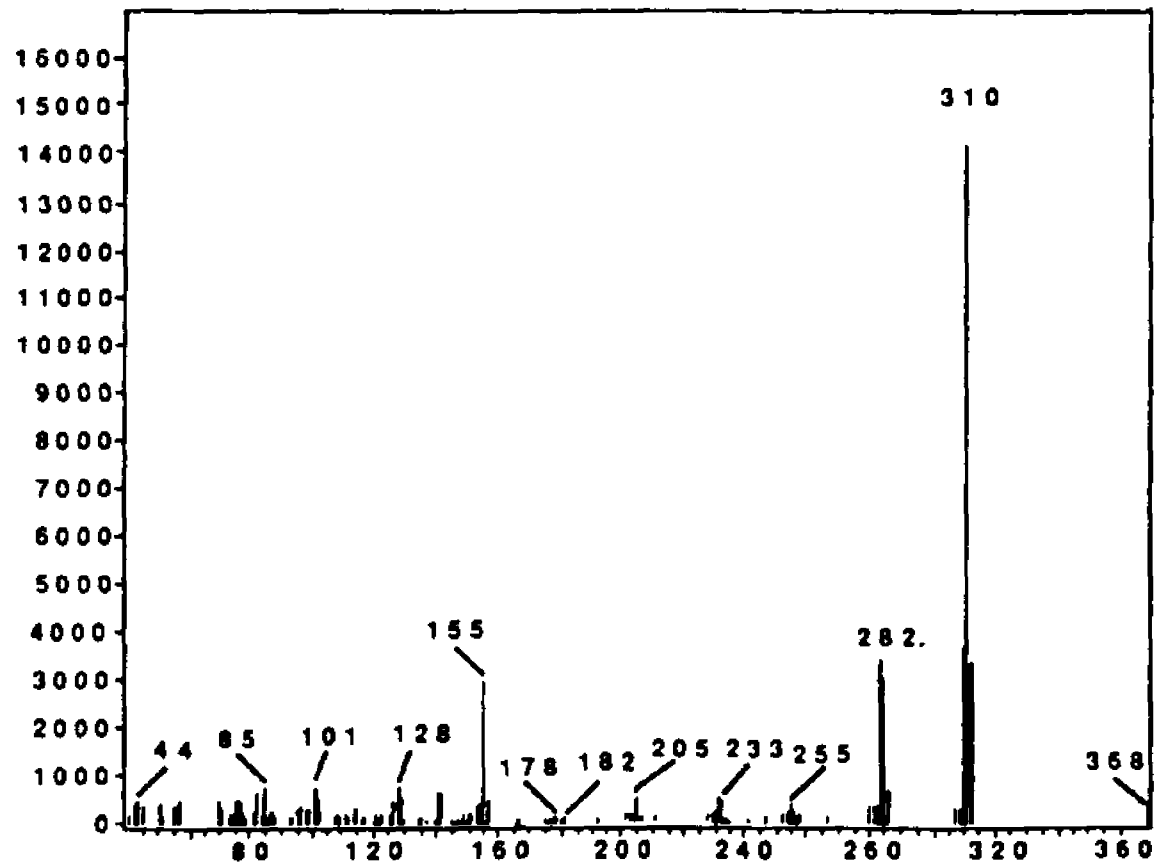

Figure 3.70 eV Electron Impact Mass Spectrum of 2,2':4,4'':4',4'''-Quaterpyridine.

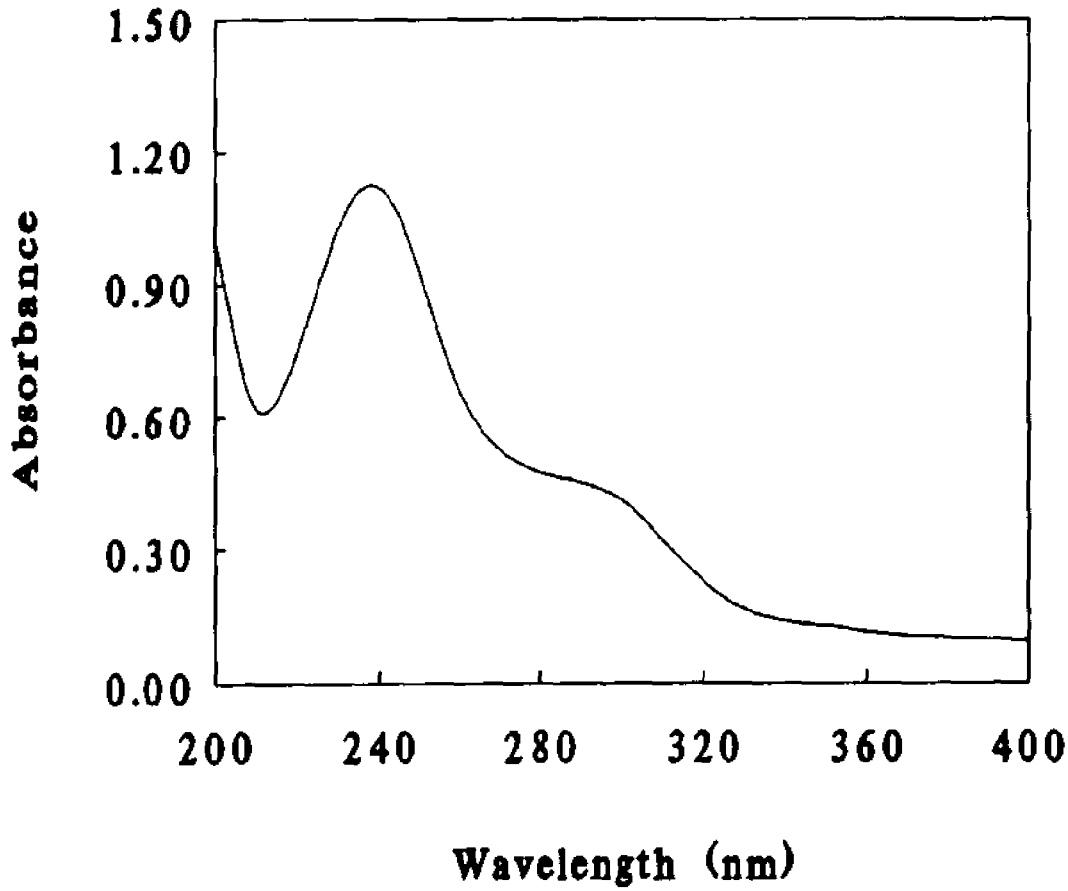

Figure 4. Absorption Spectrum of 2,2':4,4":4',4"'-Quaterpyridine.

Chapter V. Quaternization of 2,2':2,4'':2',4'''–Quaterpyridine

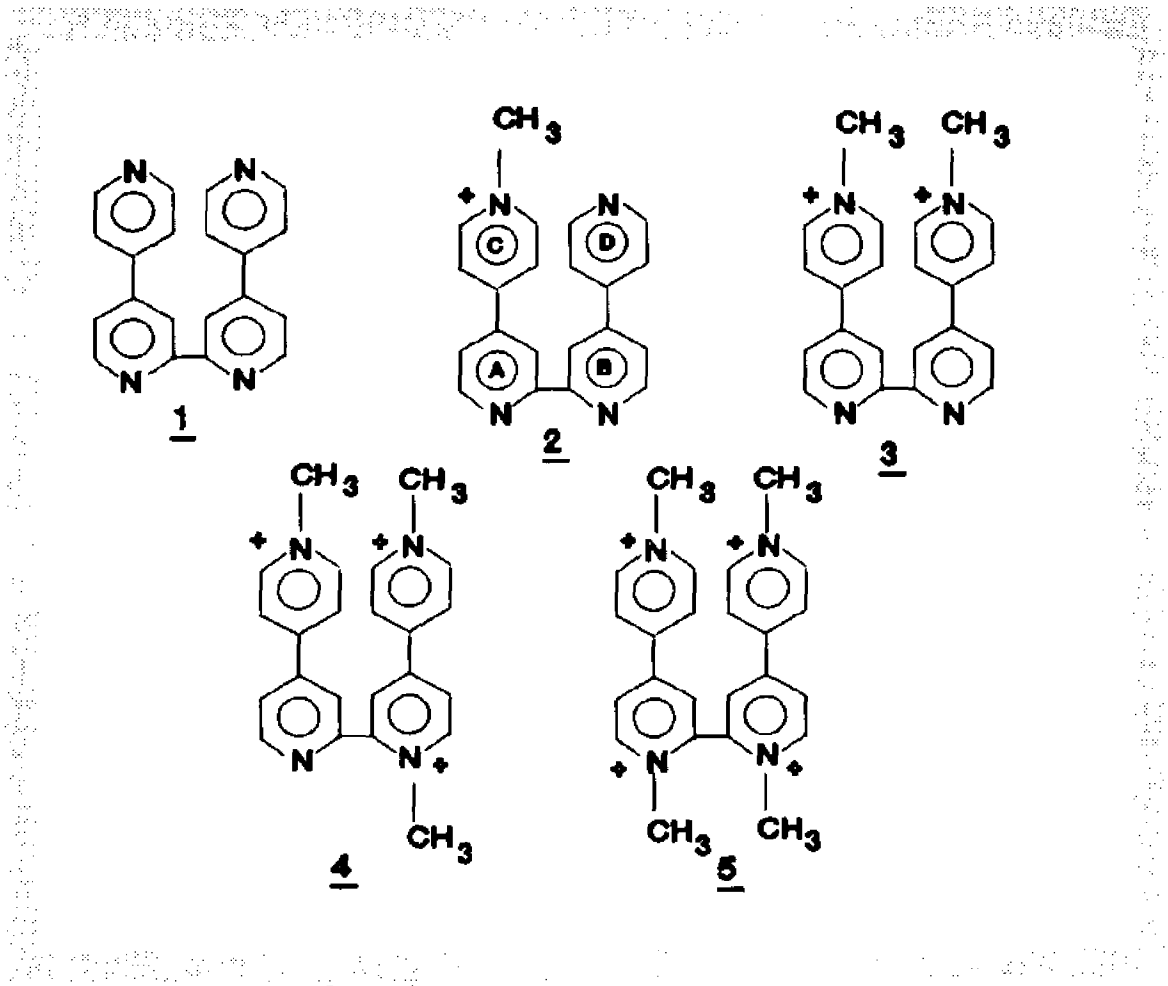

qpy and its Quaternized Derivatives.

Results and Discussion

Quaternization Methodology

The reactivity of the nitrogen atoms of the quaterpyridyl toward methylation was explored with different methylating agents. Under all conditions, with all methylating agents tested, the nitrogen atoms of rings C and D (Scheme 1) reacted first, and further alkylation on the nitrogen atoms in rings A and B could only be achieved under forcing conditions. In addition, quaternization

on all four nitrogen atoms was never observed. These conclusions were confirmed by proton and carbon 13 NMR spectroscopy.

The most selective alkylating agent of those tried is methyl iodide. Under the appropriate conditions it is possible to form mono–, di–, and tri– methyl iodide salts of the quaterpyridyl

Scheme 1. Quaternization of qpy

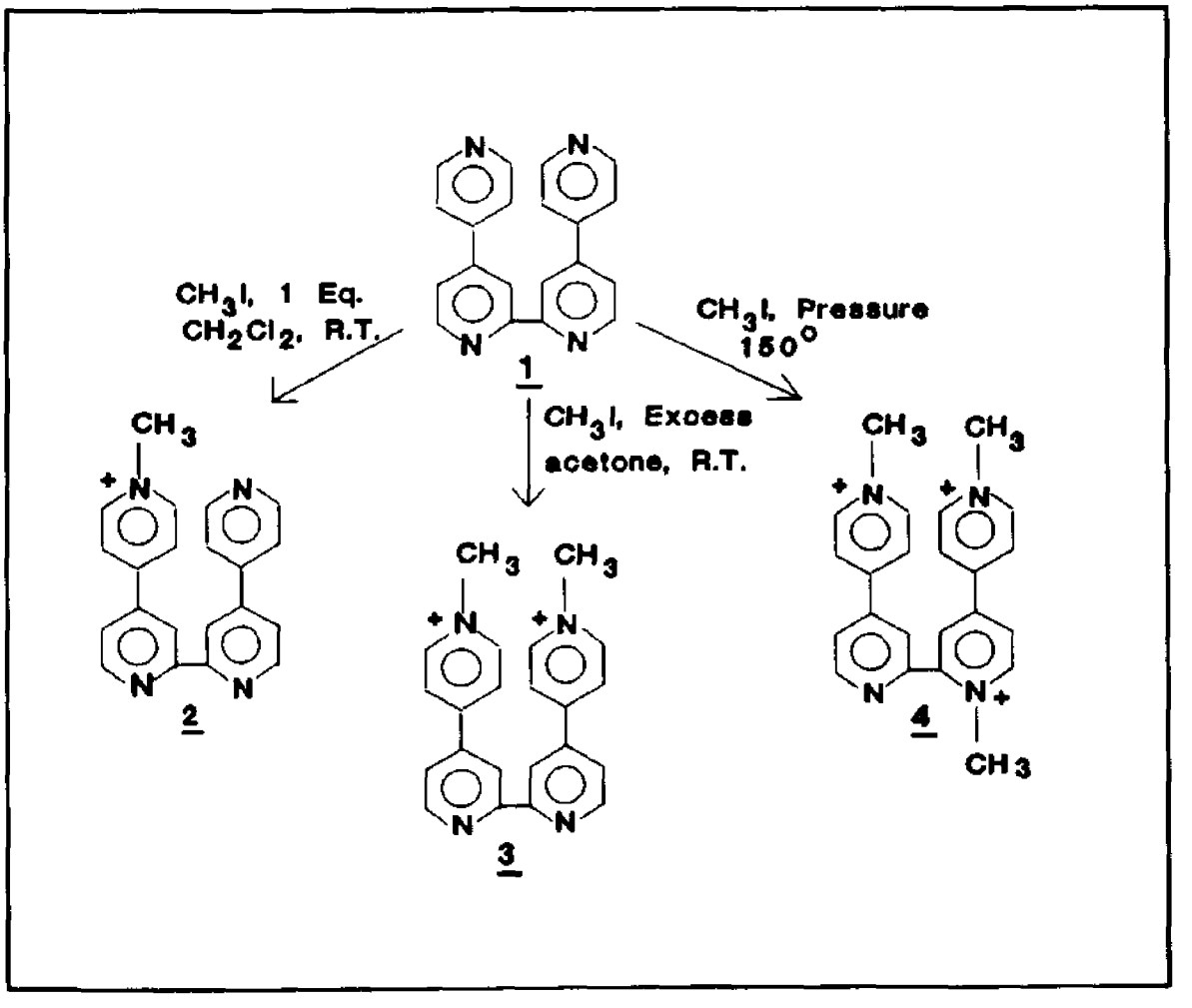

(Scheme 1). The dimethyl quaternary salt 3 was the first to be characterized. When acetone is used as the solvent with an excess of methyl iodide as the alkylating agent, only the single diquat 3 is formed. No higher quaternized products are formed, and there is no alkylation on rings A and B. The reaction is complete after 15 minutes under reflux or overnight at room temperature. As the iodide salt, the diquat is highly soluble in water, and highly insoluble in organic solvents such as chloroform, dichloromethane, and acetone. It is sparsely soluble in 95% ethanol, which can be used for the recrystallization of small samples. Increasing the water content of the ethanol raises its solubility, and can be used to crystallize larger amounts, but the addition of water also decreases the quantity of the recovered diquat. The iodide of 3 forms yellow platelets following this crystallization procedure.

Conversion of the iodide to a hexafluorophosphate salt is effected by adding an aqueous solution of the iodide to a saturated solution of ammonium hexafluorophosphate. The reaction is nearly quantitative, and completely changes the solubility properties of the salt. As the hexafluorophosphate salt, the diquat is appreciably soluble in acetone and acetonitrile, but is highly water insoluble. The best purification method is to dissolve the salt in acetone, followed by precipitation with diethyl ether. For most applications the iodide salt was found to be suitable, and the hexafluorophosphate salt was used only in the electrochemical studies.

The monoquaternary salt 2 is best prepared using one equivalent of methyl iodide in methylene chloride. From acetone, nearly equal amounts of the monoquat, diquat, and starting quaterpyridyl are isolated. No quaternization is observed in less polar solvents, such as hexane or ether. As the iodide salt, the monoquat has excellent solubility properties. It is sufficiently polar to have appreciable water solubility, but is also soluble in organic solvents such as chloroform. The iodide salt is isolated as the monohydrate and is a pale yellow solid. The hexafluorophosphate salt can be prepared in the same manner as the diquat.

To proceed past the dimethylated stage with methyl iodide, harsh conditions are required.

When a mixture of the quaterpyridyl and methyl iodide is heated to 100– 150 °C in a sealed tube, a greenish solid is obtained. The solid has unusual properties. For example, it forms a purple solution in water, and a green solution in alcohols. Earlier work on other highly quaternized salts[146] had revealed similar peculiarities. It was suspected that this behavior resulted from the formation of radicals, but our salt gave no EPR signal in the absence of a reducing agent. It is highly hygroscopic, and extremely difficult to dry. If left in the air, it forms a green oil. Crystals can be obtained by grinding thoroughly with acetone or THF. The salt will not crystallize out of any solvent in which it will dissolve (polar aprotic solvents, alcohols, or water). NMR of the crude product (DMSO–d_6, 60 MHz) gives two methyl singlets (rel. area 2:1), and a broad aromatic region (rel. area 14). From this data, and the established reactivity pattern of the quaterpyridyl, methylation on rings C and D in preference to A and B, the structure **4** is assigned for the product.

More powerful methylating agents were used in an attempt to prepare the tetramethylquaterpyridinium ion **5**. This is an interesting ion, as it is a dimer of methyl viologen, and a potential two electron carrier. Using trimethyloxonium tetrafluoroborate in 1,2–dichloroethane in a sealed tube, only the triquat ion **4** was isolated. Dimethyl sulfate gave similar results. We conclude that the tetramethyl salt cannot be formed in any simple quaternization procedure. From this point on **2** will be referred to as [qpyme]$^+$, and **3** as $[qpyme_2]^{2+}$.

^{13}C NMR of $[qpyme_2]^{2+}(I^-)_2$

The decoupled carbon 13 spectrum of $[qpyme_2]^{2+}(I^-)_2$ is shown in Figure 1. Table I summarizes the ^{13}C chemical shifts for qpy, $[qpyme]^+(I^-)$, and $[qpyme_2]^{2+}(I^-)_2$. In the spectrum of $[qpyme_2]^{2+}(I^-)_2$, there are the expected nine resonances. These include one for the methyl group (48.1 ppm), three in the range (118– 124 ppm) for carbons in a meta relation to a pyridine nitrogen atom, three ortho (147–156 ppm), and two para (135–146). The presence of nine resonances is consistent with structure **3**, but does not confirm that bis– methylation occurs on rings C and D.

Definitive assignment as to the position of methylation will be made after the analysis of the proton NMR.

^{1}H NMR of $[qpyme_2]^{2+}(I^-)_2$

The proton NMR of $[qpyme_2]^{2+}(I^-)_2$ is shown in Figure 2. The numbering system used for the following discussion is also illustrated in the Figure, and Table III (Chapter IV) summarizes the δ values and assignments for the signals. Integration indicates that there are six aliphatic (4.41 δ) and 14 aromatic protons. The position of the singlet at 4.41 δ confirms the presence of methyl groups on quaternized nitrogen atoms, because methyl groups on ring carbons would appear further upfield.

The protons on ring C(D) are of type AA'XX', and those on ring A(B) are AMX. Protons on ring C form apparent doublets at 8.71 δ (rel. area 4) and 9.16 δ (rel. area 4). The farthest downfield of these doublets, is assigned to protons H2" and H6" and protons H3" and H5" in the upfield doublet.

In contrast to the spectrum of the parent quaterpyridyl, that of $[qpyme_2]^{2+}(I^-)_2$ shows a clear resolution of the three protons on ring A. The farthest protons downfield are H6(6') (doublet, rel. area 2) at 9.02 δ. The protons farthest upfield in the aromatic region are H5(5') at 8.20 δ. The signal is broadened in comparison to that for H6(6'), and the spitting in the AMX quartet is more evident. This is because the meta coupling constant $J_{3,5}$ is larger than the para $J_{3,6}$. The final proton of the trio H3 is nearly a singlet (rel. area 2) at 8.91 δ, due to the extremely small magnitude of both $J_{3,5}$ and $J_{3,6}$, little splitting is evident in the signal.

As discussed above, the ^{13}C NMR indicates that the ion contains two equivalent methyl groups, on either rings A and B, or on C and D.

The most important protons in the spectrum, regarding the assignment of the position of methylation, are those ortho to the nitrogen atoms, protons H6(6') on rings A and B, and H2" (2"'), H6"(6"') on rings C and D. In the spectrum of the quaterpyridyl the ortho protons associated with

rings A and B (protons H6(6') are the furthest downfield in the spectrum at 8.80 δ, with the ortho protons on rings C and D at 8.68 δ. If quaternization were to occur on rings A and B, the protons, in the spectrum of the diquat, on disubstituted rings A and B (protons H6(6')) would be the farthest downfield. Instead ortho protons on rings C and D are shifted past those on rings A and B, and are the furthest signals downfield. Thus, from the combination of proton and carbon 13 NMR, we assign the structure **3** to the dication

^{13}C NMR of [qpyme]$^+$(I^-).

The decoupled carbon 13 spectrum of [qpyme]$^+$(I^-) is shown in Figure 3, and the chemical shifts for qpy, [qpyme]$^+$(I^-), and [qpyme$_2$]$^{2+}$(I^-)$_2$ are summarized in Table I. In the spectrum of [qpyme]$^+$(I^-) there are seventeen expected resonances: one for the methyl group (48.128 ppm), six in the range (118– 124 ppm) assigned to carbons in a meta relation to a pyridine nitrogen, six ortho (147–156 ppm), and four para (135–146). The spectrum confirms that there is a single methyl group in the molecule. The pattern of seventeen resonances could not be produced in any di– , tri, or tetra– quaternized species. The spectrum is consistent with the structure **2**, but by itself does not exclude the possibility that the methyl group is positioned on ring A and not C.

^{1}H NMR of [qpyme]$^+$ I^-.

The ^{1}H spectrum of [qpyme]$^+$(I^-) is shown in Figure 4. Integration of the spectrum indicates the presence of three aliphatic protons (singlet 4.40 δ) and 14 pyridine protons. The position of the singlet is in the range expected for protons on a methyl quaternized pyridine ring. Figure 4 illustrates the numbering system used in the following discussion. Protons on rings C and D are of type AA'XX', and rings A and B contain protons of type AMX. Protons H2"(6") are the farthest downfield at 9.08 δ (rel area 2). The corresponding doublet (rel. area 2) for the protons H3"(5") is at 8.60 δ.

The protons on ring D, H"'(6"') and H3"'(5"'), appear as the pair of doublets (rel. area 2)

at 8.67 and 7.75 δ. The splitting of the doublet, into a quartet is more obvious in the protons on ring D than in those on C, and allows the assignments of the quartets at 8.67 and 7.75 δ to be coupled to one another, and independent of the doublets at 9.08 and 8.60 δ due to protons on ring C.

The H6 signal in the spectrum of the monoquat is the farthest downfield of any signal on rings A and B at 8.87 δ (rel. area 2). Protons H3 and H3' are likely to appear as singlets, by analogy to protons H3(3') in the spectrum of the diquat, and H3 will be farthest downfield at 8.71 δ (rel. area 1). The signal for H6' is at 8.57 δ (rel. area 1). Finally, the distorted doublets at 8.00 and 7.81 δ are assigned to H5 and H5', respectively.

Based on an argument similar to that presented above for the interpretation of the diquat spectrum (i.e. ortho protons on ring C (H2"(6") are further downfield than ortho protons on ring A due to quaternization occurring on rings C and D) the same is true in the spectrum of the monoquat. The downfield position of protons H2"(6") relative to H6' is evidence that the methyl group is positioned on ring C, as in structure **2**.

Ultra Violet Absorption Spectra

Ultra Violet spectra of qpy and its two methylated derivatives are presented in Figure 5. The major transition in the spectrum of the parent quaterpyridyl is the $\pi \rightarrow \pi^*$ centered at 238 nm. The corresponding transition in the dimethyl cation occurs at 257 nm. The spectrum of the monomethyl cation shows a band 238 nm with a low energy shoulder at 257 nm. To a close approximation, the spectrum of the monomethyl cation is the sum of the spectrum of the parent quaterpyridyl and that of the dimethyl cation. The spectrum in Figure 6 was generated by summing, on a point by point basis, the spectrum of the dimethyl quaternary cation, and that of the quaterpyridyl. The spectra shows maxima at 257 nm and 238 nm, and closely resembles the spectrum of the monomethyl cation.

A simple interpretation of the spectral data is that the π^* orbitals responsible for the two transitions are localized largely on different halves of the monomethyl cation. In this view, the

monomethyl cation can be considered as being composed of two units– one consisting of 4,4'–bipyridine, and the other N–methyl–4,4'– bipyridinium cation. The transition at 257 nm is to a π^* localized on the N–methyl–4,4'–bipyridine unit, and the transition at 238 nm is terminated on the 4,4'– bipyridine unit.

Complexation

In order to test the chelating properties of qpy and its methylated derivatives, as well as to confirm the availability of diimine nitrogen atoms for complexation, ferrous complexes of **1**, **2**, and **3** were prepared. All three quaterpyridyls (parent, mono– and dimethyl derivatives) form deeply purple colored complexes upon addition of ferrous ammonium sulfate to methanolic solutions of the quaterpyridyls. The visible absorption spectra, which consist of MLCT bands, show a shift to lower energy with the addition of each methyl group (Figure 7).

Cyclic Voltammetry of $[qpyme]^+(I^-)$ and $[qpyme_2]^{2+}(I^-)_2$ as their Hexafluorophosphate Salts

The Electrochemical behavior of $[qpyme]^+(I^-)$ and $[qpyme_2]^{2+}(I^-)_2$ are summarized in Scheme 2. The voltammogram of $[qpyme]^+(I^-)$ in Figure 8a shows one reversible couple at $E^{o'}$ = --0.79 V if the scan is performed from 0 to -1.2 V. The position of the wave is independent of scan rate, and the ratio of the current for the cathodic half wave to the anodic is 0.98. In addition, there are no changes to the voltammogram after 20 scans at 100 mv/s. Extending the lower scan boundary to -2.1 V reveals several additional waves. The first on the anodic scan occurs at -1.66 V. The voltammogram, with these scan limits, quickly decomposes after a few scans at 100 mv/s. The ratio of the cathodic current to the anodic on the first wave ($E^{o'}$ = -0.79 V) decreases with each scan.

The diquaternary salt **3** shows two anodic and two corresponding cathodic reductions when scanned from 0.0 to -1.2 V (Figure 8b). The cathodic waves occur at -0.84 and –0.92 V, and the

Scheme 2. Electrochemical Behavior of 2 and 3.

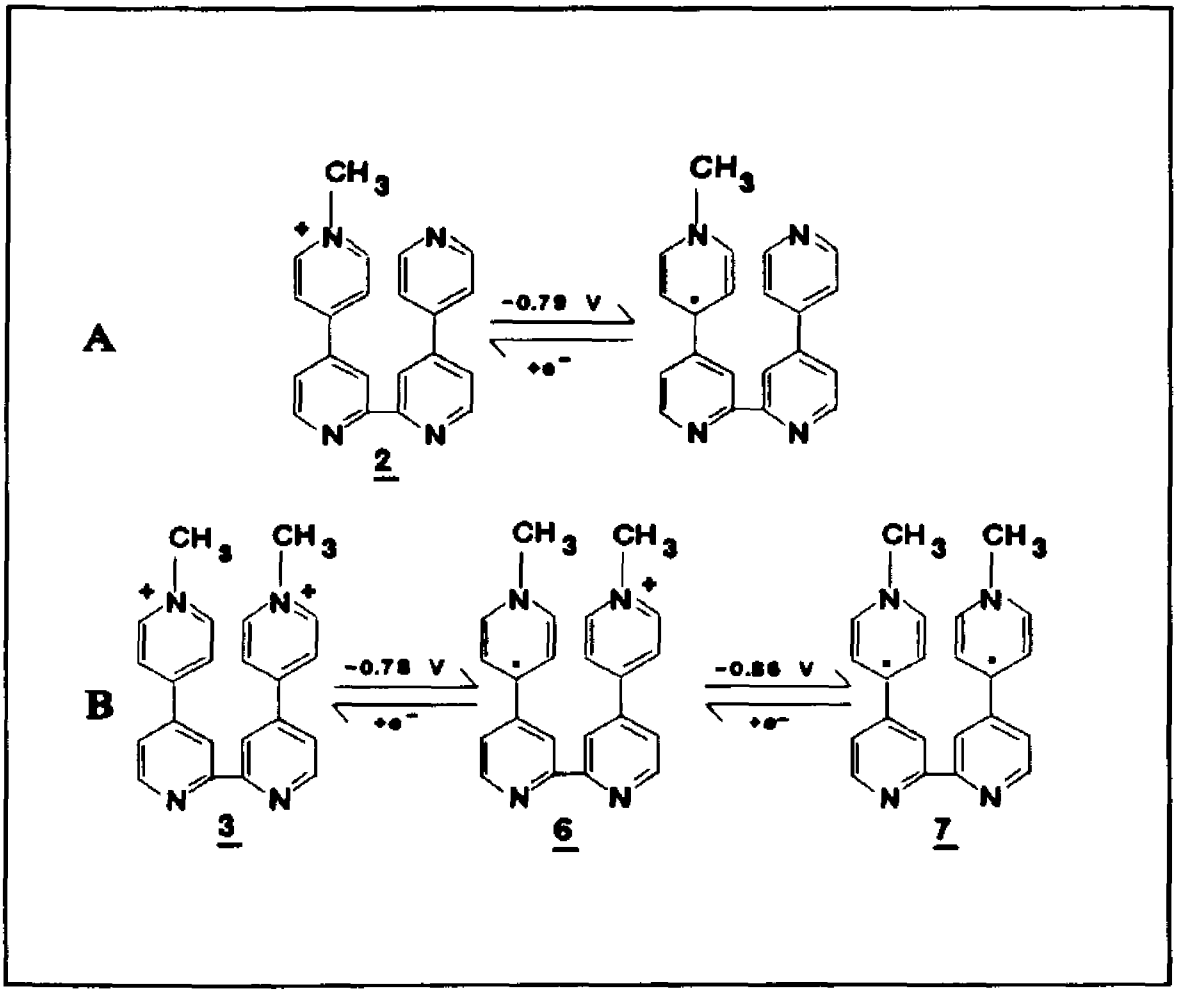

anodic portions are approximately -0.85 and -0.71 V. Because of the close spacing of these waves there is some uncertainty in the calculation of their half wave (E°) potentials. The ratios of the currents (anodic to cathodic) on both the waves is in excess of 0.98, indicative of a reversible process. E° values for the waves are -0.78 and -0.86 V respectively. Peak potentials are independent of scan rate, and multiple scans produce no changes in the voltammogram. Scanning from 0.0 to -2.1 V gives similar results to that of the monomethyl salt. The current on the cathodic scan decreases, eventually falling into the baseline, upon multiple scans at 100 mv/s. The electrochemical behavior of the monoquat ion 2, is similar to that for N--methyl--4,4'--bipyridinium cation (not shown), in which the first reduction occurs at --0.84 V (measured vs the SCE). This

potential is, within experimental error, the same as the first reduction in the monoquat (Scheme 2).

The diquat, ion **3**, contains two reductions in this potential region, at –0.84 and –0.92 V (Scheme 2). The first reduction in the diquat forms the radical cation **6**, which can be further reduced to species **7**. Based on simple resonance considerations, the species **7** must exist as a diradical (no reasonable resonance structure can be drawn in which the two unpaired electrons are paired in a bond). The electrochemical behavior of **2** is in contrast to that of other viologens, such as methyl viologen (Scheme 3). In the cyclic voltammogram (CV) of methyl viologen, the two reduction waves are well spaced, and fully reversible. The diquat **3** behaves as if it were two independent N–methyl–4,4'–bipyridinium units.

Conclusion

The reactivity of qpy toward methyl iodide has been explored, and has resulted in selective procedures for the preparation of the iodide salts of **2** and **3**. The ions have been characterized using proton and carbon 13 NMR, and UV spectroscopy. They both readily form complexes with Fe(II), and may be used as ligands to other metals as well.

Scheme 3. Electrochemical Behavior of Methyl Viologen

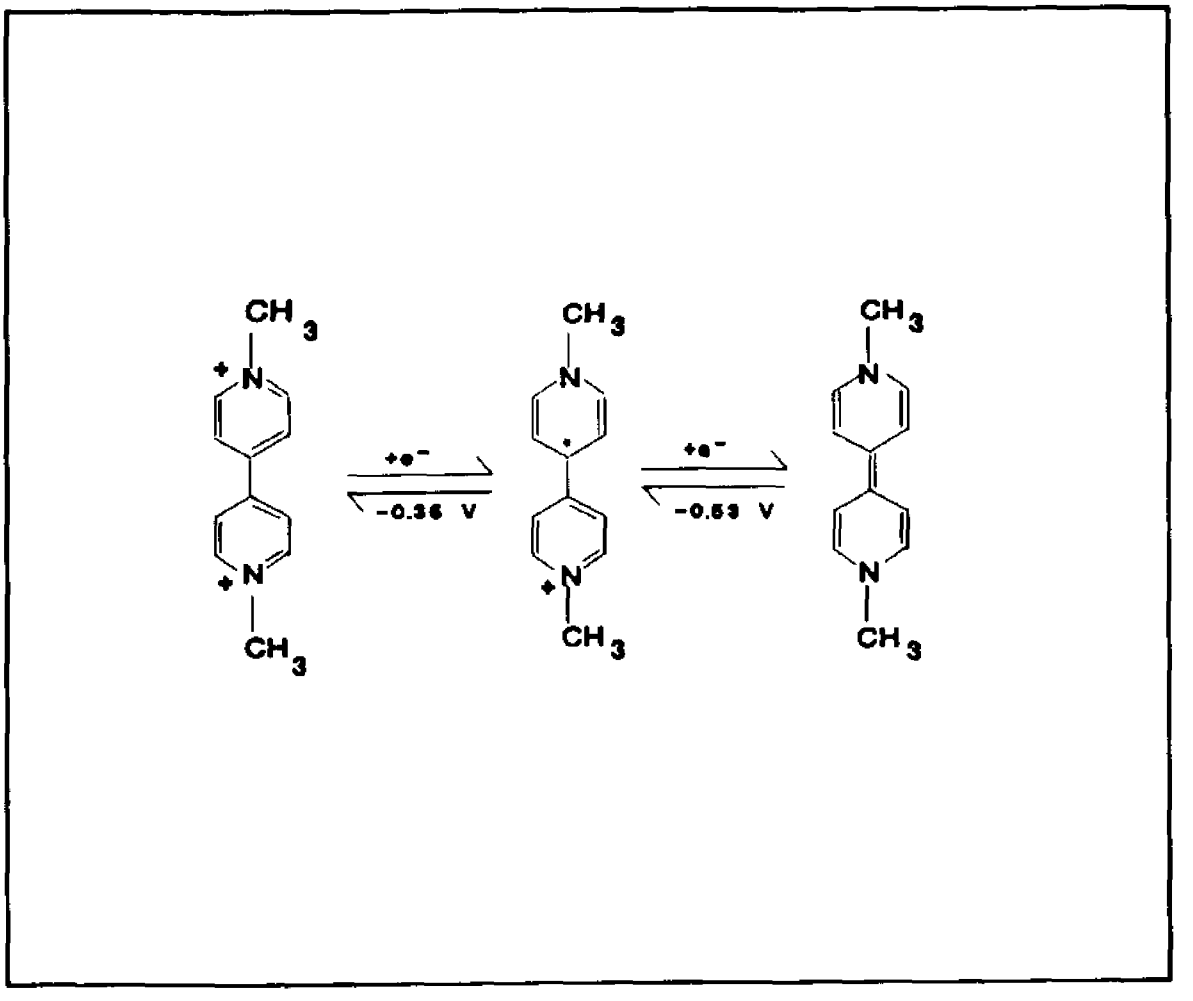

Table I. ^{13}C Resonances[a] for qpy[b], $[qpyme]^+(I^-)$[c] and $[qpyme_2]^{2+}(I^-)_2$[c]

#	qpy	$[qpyme]^+(I^-)$	$[qpyme_2]^{2+}(I^-)_2$
1	119.1	48.1	48.1
2	121.5	118.3	119.3
3	121.7	118.8	123.3
4	145.6	121.6	125.7
5	146.6	122.4	143.0
6	150.0	122.5	146.8
7	150.6	125.5	151.3
8	156.7	142.4	152.2
9		144.5	156.3
10		145.9	
11		146.5	
12		150.7	
13		151.0	
14		151.1	
15		152.1	
16		155.6	
17		156.4	

[a]Measured relative to TMS. [b]Sat. Solution in $CDCl_3$.
[c]Sat. Solution in DMSO-d_6

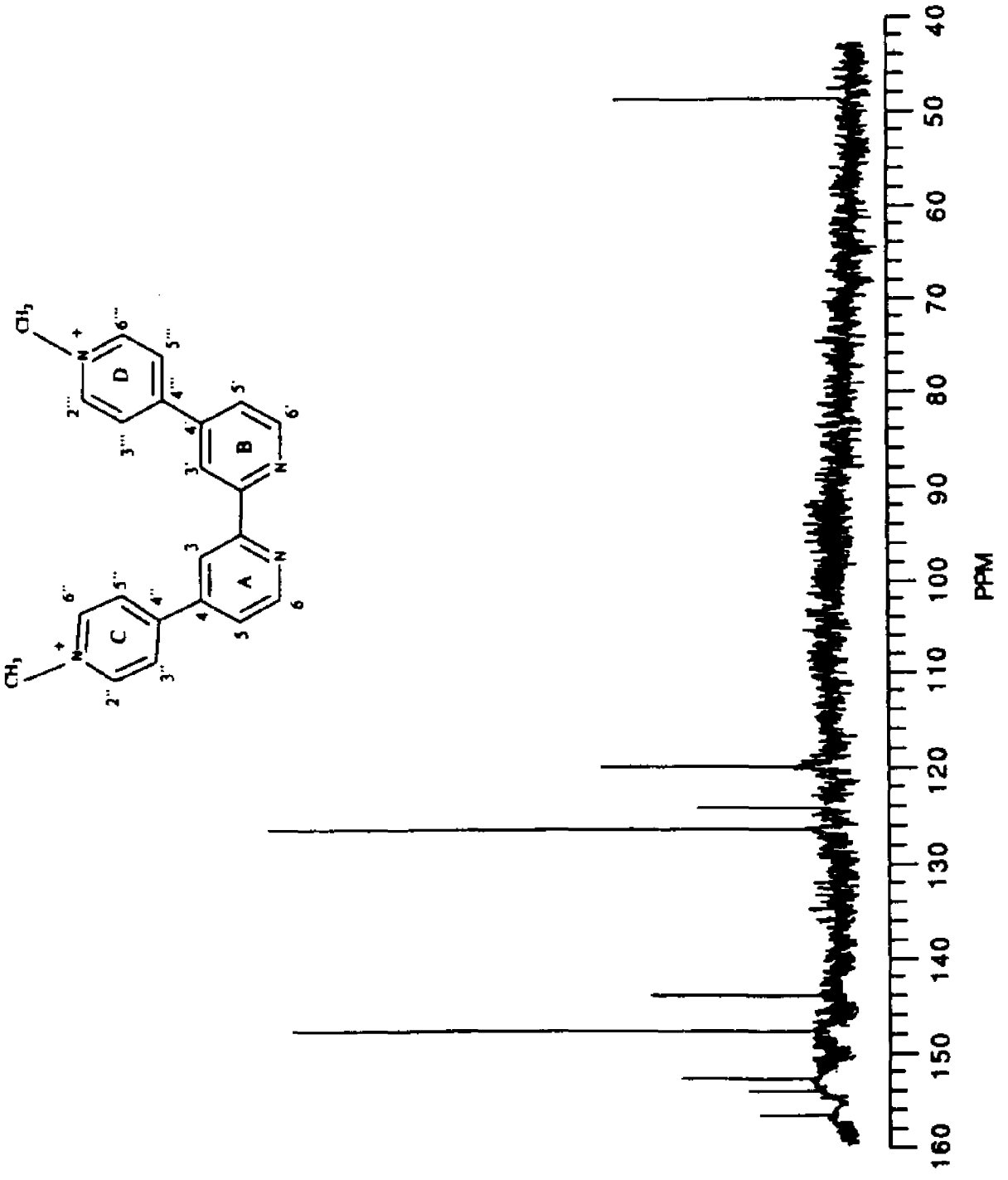

Figure 1. 75 MHz ^{13}C NMR Spectrum of $[qpyme_2]^{2+}(I^-)_2$.

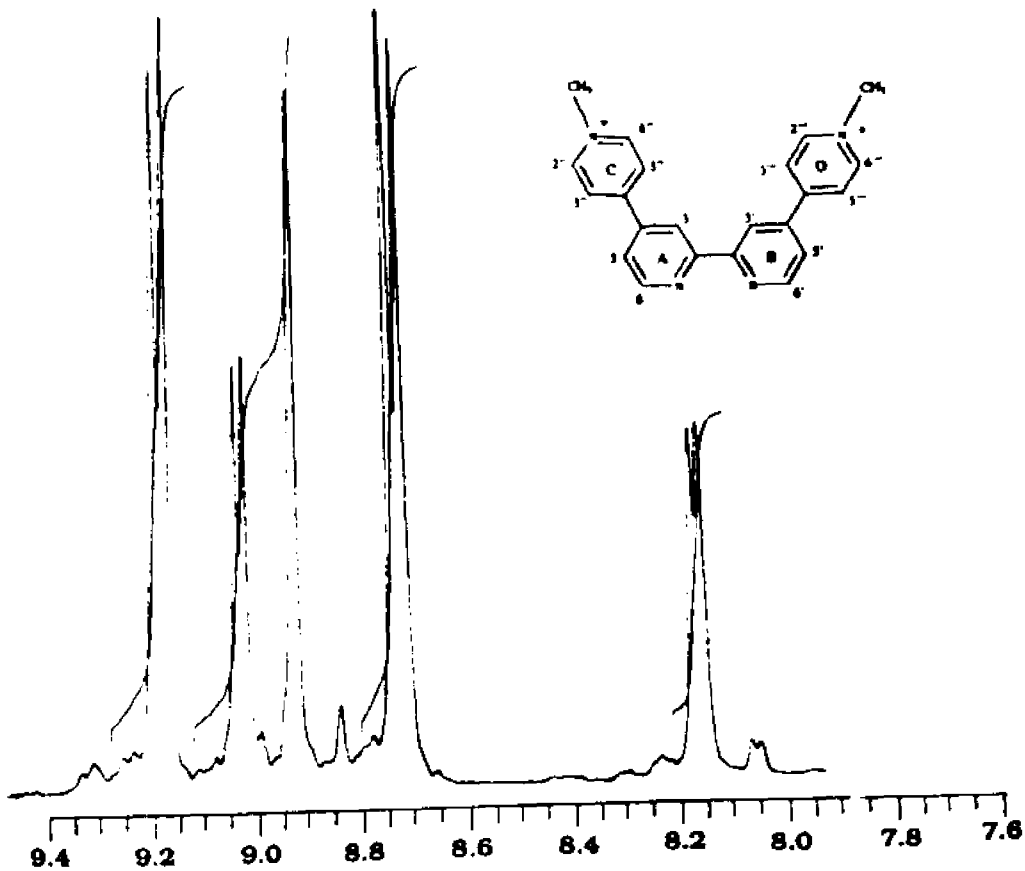

Figure 2. 300 MHz ^{1}H NMR of $[qpyme^2]^{+}(I^-)_2$

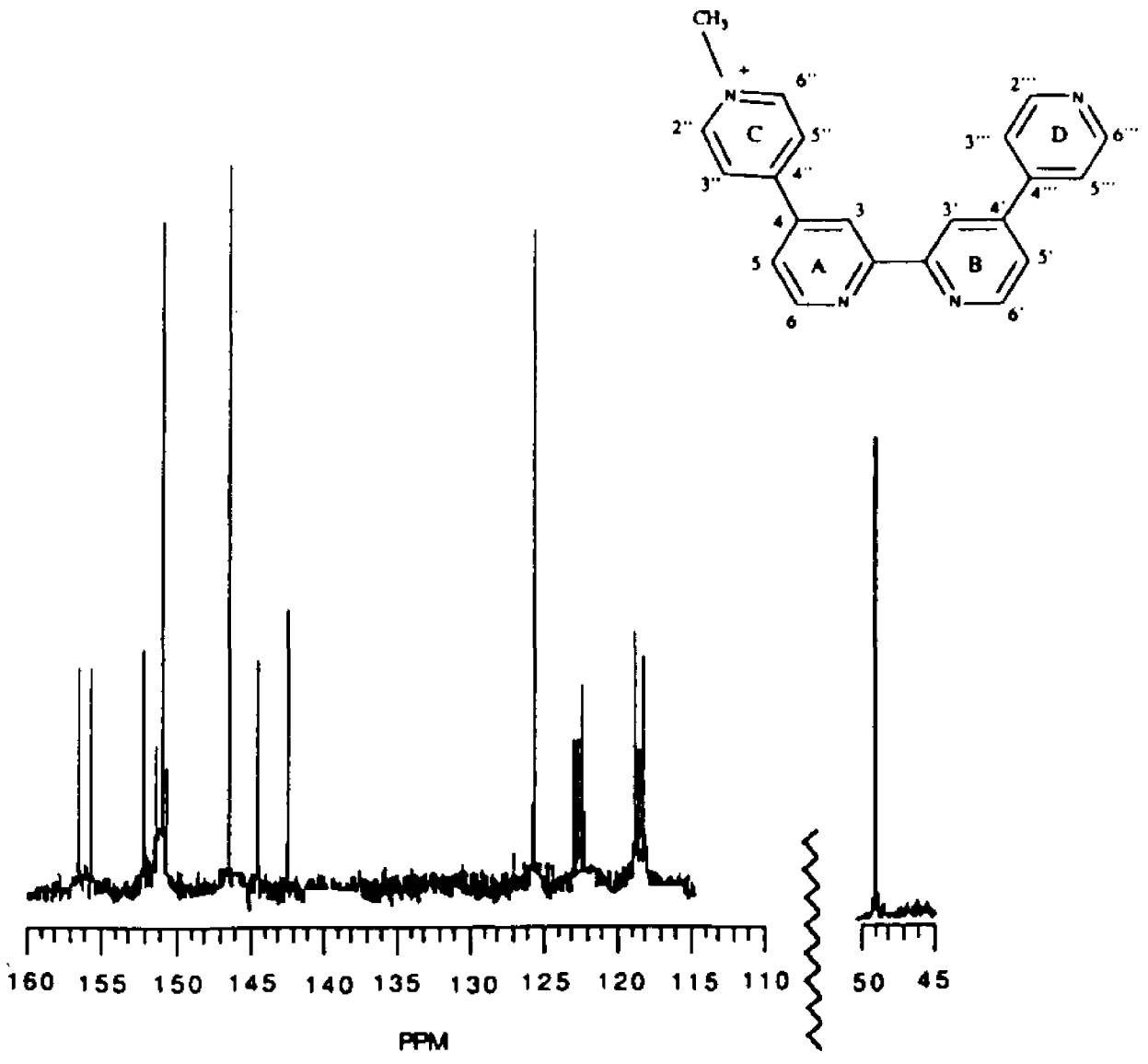

Figure 3. 300 MHz ^{13}C NMR Spectrum of [qpyme]$^{+}$(I^{-}).

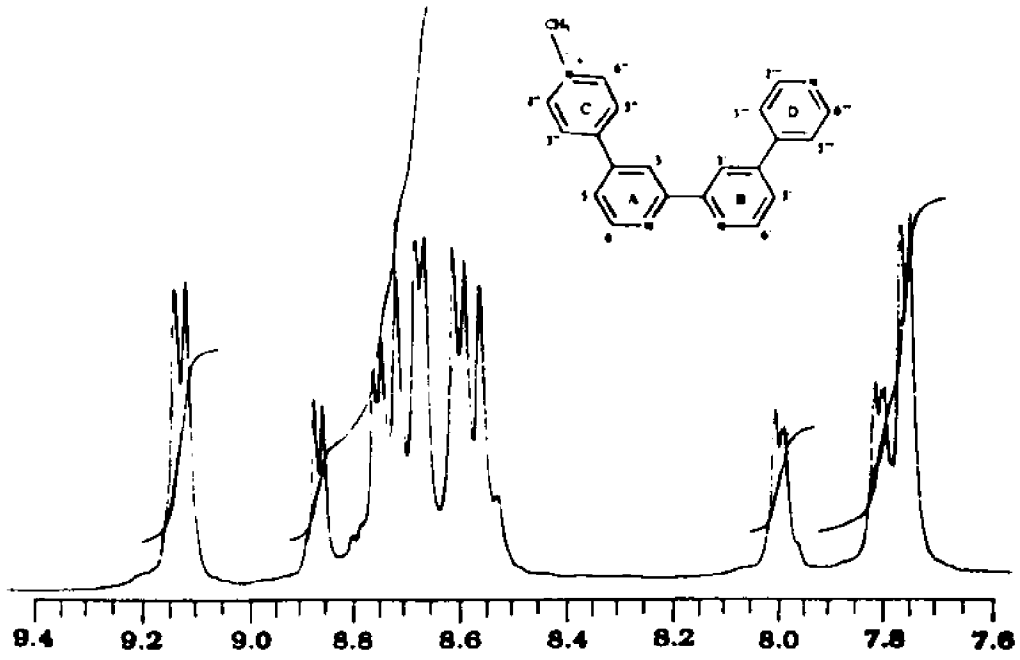

Figure 4. 300 MHz ^{1}H NMR Spectrum of [qpyme]$^+$(I^-).

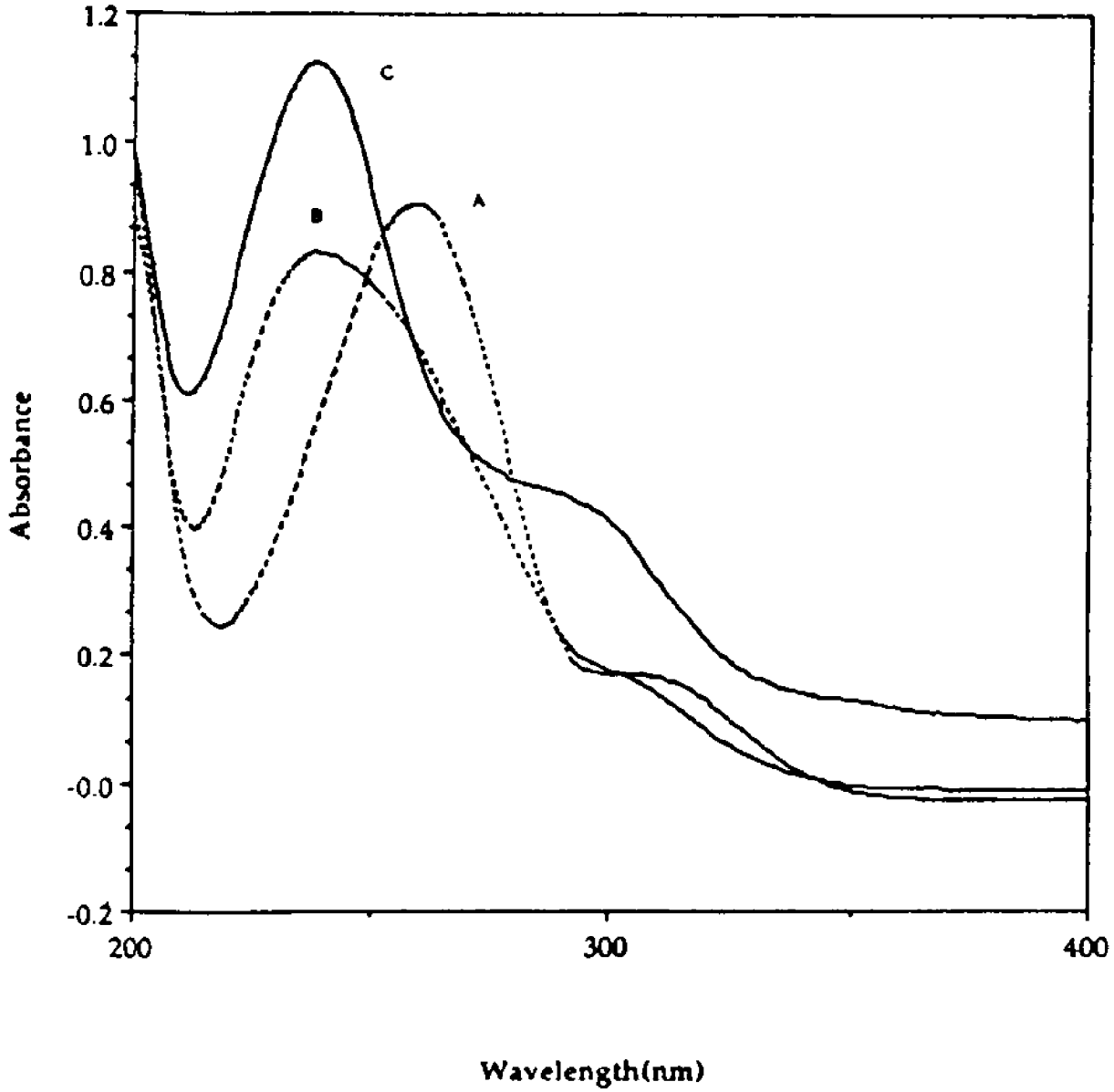

Figure 5. UV Spectra of a) qpy, b) $[qpyme]^{+}(I^{-})$, and c) $[qpyme_2]^{2+}(I^{-})_2$.

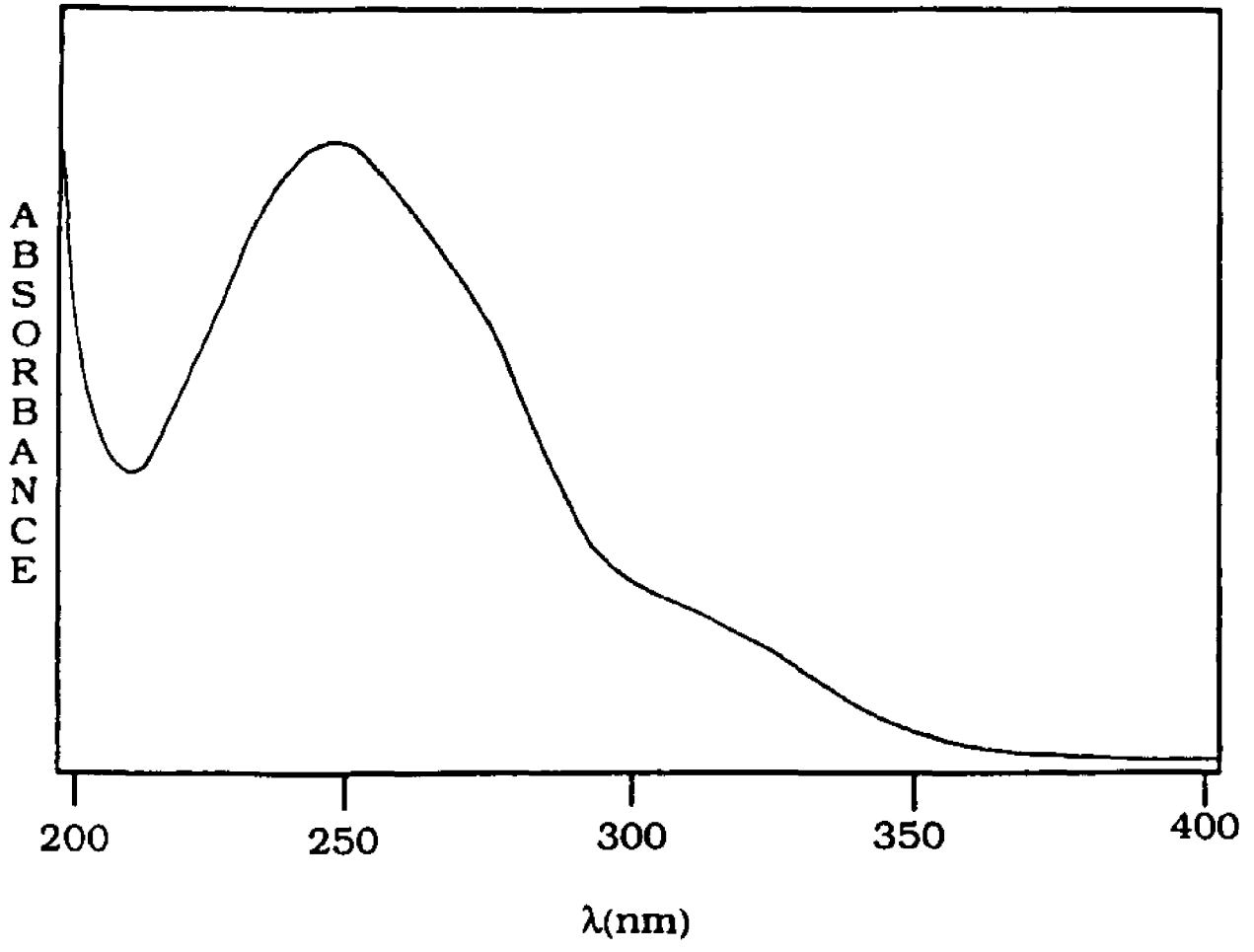

Figure 6. Spectral Summation of qpy and $[qpyme_2]^{2+}(I^-)_2$.

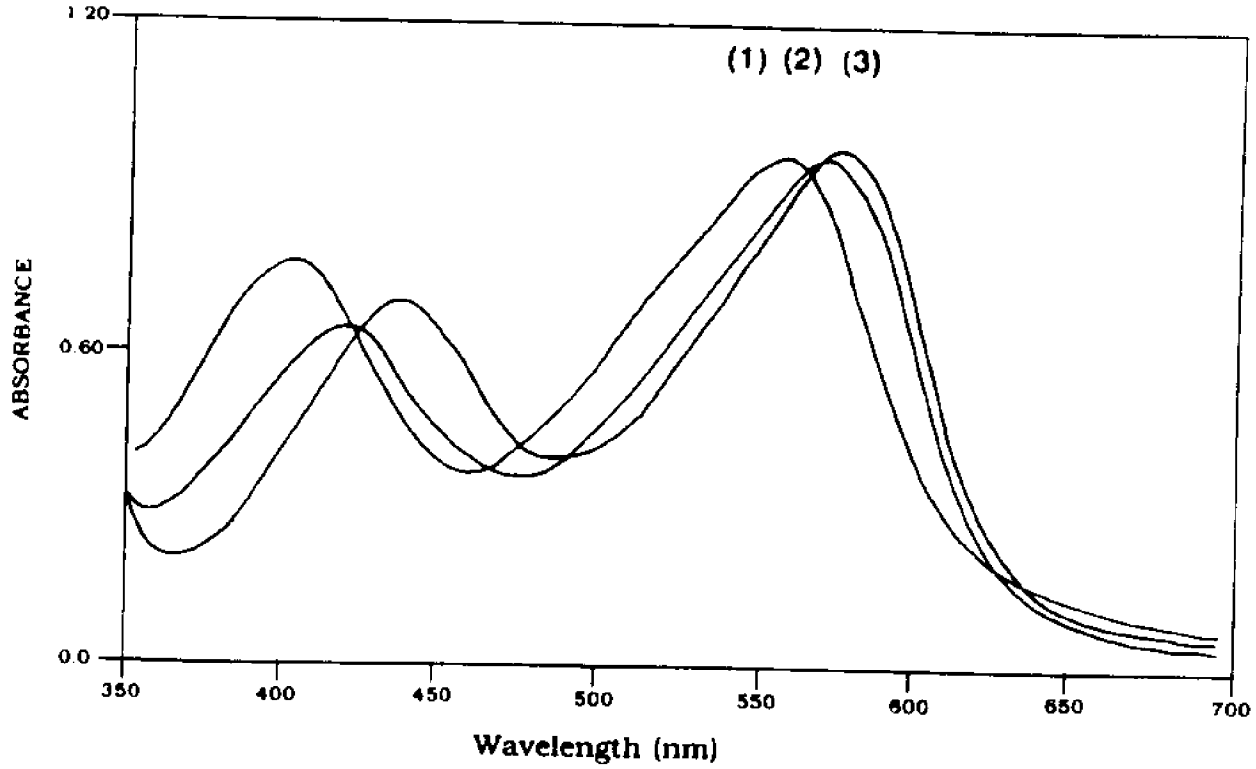

Figure 7. Visible Spectra of Ferrous Complexes of Ligands qpy (1), $[qpyme]^{+}(I^{-})$ (2) and $[qpyme_2]^{2+}(I^{-})_2$(3).

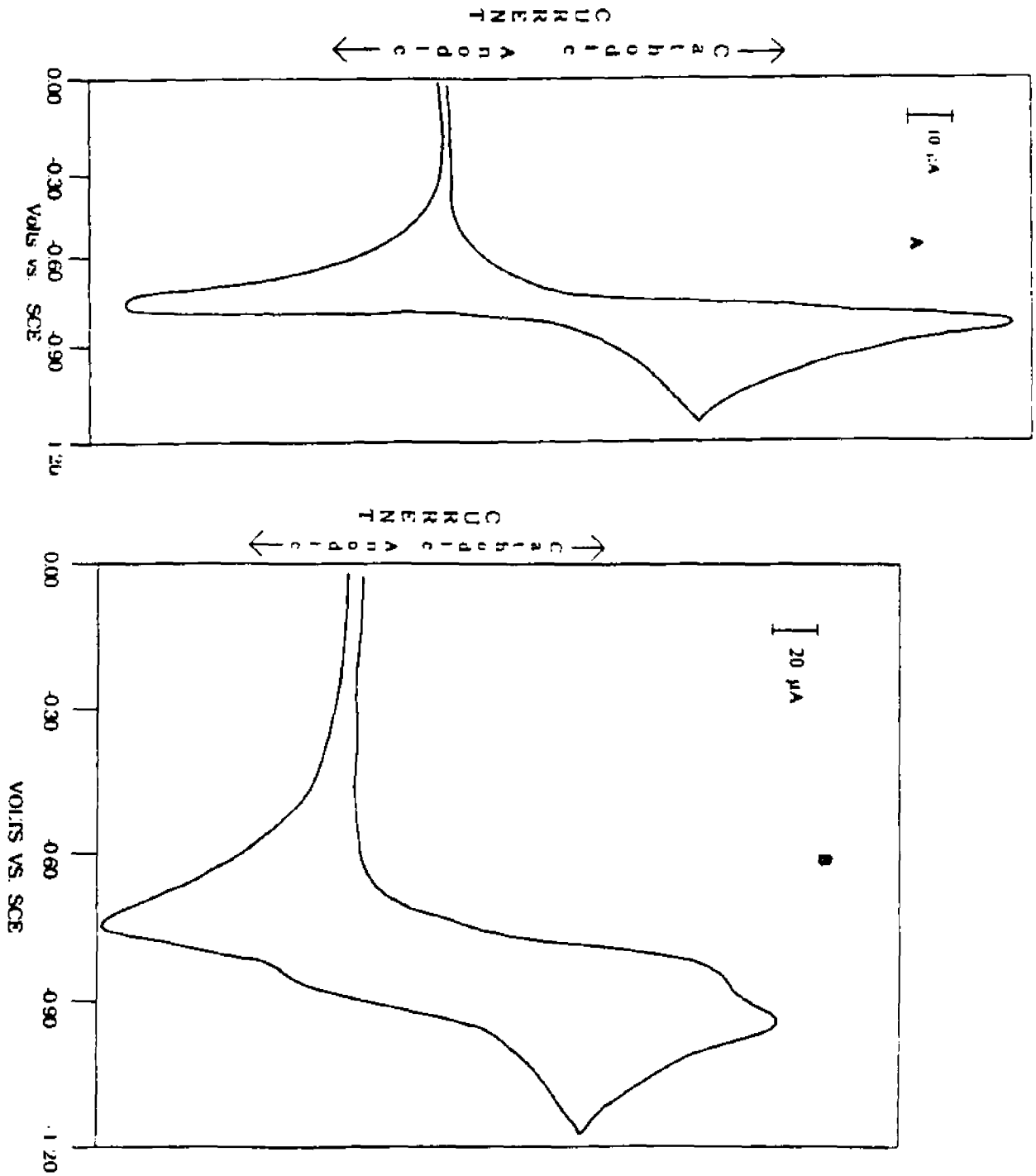

Figure 8. Cyclic Voltammograms of a) $[qpyme]^{+}(I^{-})$ and b) $[qpyme_2]^{2+}(2I^{-})$. at 200 mv/s, Glassy Carbon Anode in 0.1 M Tetra-n-Butyltetrafluoroborate Acetonitrile Solution.

Chapter VI. Bis-Bipyridine Ru(II) Complexes Based on 2,2':4,4'':4',4'''-Quaterpyridine.

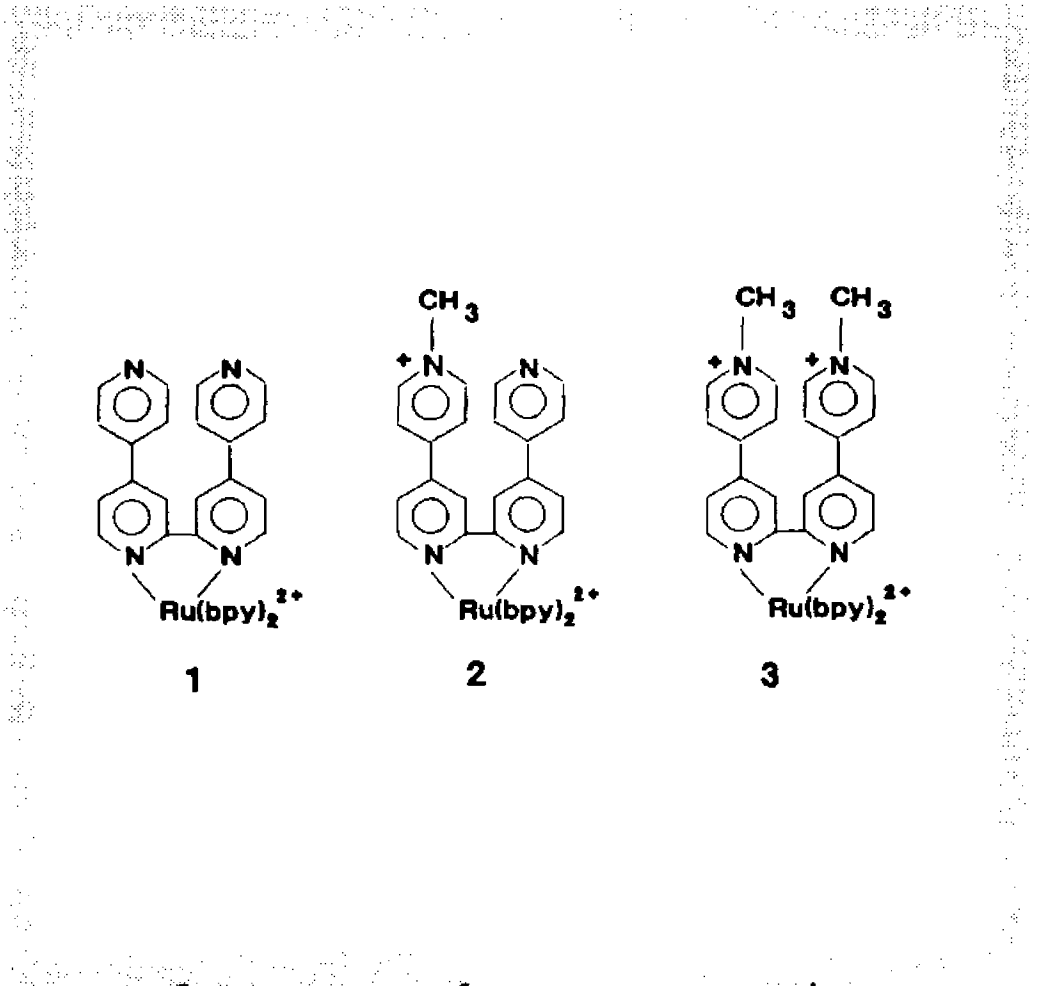

$[Ru(bpy)_2qpy]^{2+}$ 1 ,$[Ru(bpy)_2qpyme]^{3+}$ 2, and $[Ru(bpy)_2qpyme_2]^{4+}$ 3

Results

Synthesis and Characterization

The bis-bipyridine complexes based on 2,2':4,4'':4',4'''-quaterpyridine, $[Ru(bpy)_2L^{n+}]^{(n+2)+}$ (where L = qpy, [qpyme]$^+$, or $[qpyme_2]^{2+}$) are prepared by refluxing $Ru(bpy)_2Cl_2$ with one equivalent of the respective ligand in 50% ethanol. Characterization of complexes **1**, **2** and **3** was done by NMR and elemental microanalysis. Important in confirming that the methyl groups on ligands

[qpyme]$^{+}$ and [qpyme$_2$]$^{2+}$ survived the complexation procedure is ^{13}C NMR. The 75 MHz decoupled ^{13}C spectrum of [Ru(bpy)$_2$qpyme]$^{3+}$ is shown in Figure 1a, and the frequencies of the resonances are summarized in Table I. Shown in the spectrum is the expected 22 resonances, five for carbons on the two equivalent coordinated bipyridines, 17 on the methylated quaterpyridyl, including one for the methyl group at 49.6 ppm. Integration of the ^{1}H spectrum of [Ru(bpy)$_2$qpyme]$^{3+}$ (not shown), indicates that there are three methyl protons (singlet 4.44 δ, 3H) compared to 30 pyridine protons. Thus the ^{13}C and ^{1}H spectra are consistent with the structure proposed for [Ru(bpy)$_2$qpyme]$^{3+}$.

The ^{13}C spectrum of [Ru(bpy)$_2$qpyme$_2$]$^{4+}$ is shown in Figure 1b, and the frequencies of the resonances are summarized in Table I. The spectrum shows a total of 14 resonances, one for the two equivalent methyl groups (49.6 ppm), five for the bipyridine carbons, and eight for the aromatic carbons on the bis-methylated quaterpyridyl. The ^{1}H NMR spectrum (not shown) shows 6 aliphatic protons, in a singlet (4.45 δ, 6H), and a 30 H multiplet in the aromatic region. The ^{13}C and the ^{1}H NMR spectra are in agreement with the structure [Ru(bpy)$_2$qpyme$_2$]$^{4+}$. Micro analyses of all three complexes fall within acceptable limits (See Experimental section).

Absorption Spectra

All three complex ions, [Ru(bpy)$_2$qpy]$^{2+}$, [Ru(bpy)$_2$qpyme]$^{3+}$, and [Ru(bpy)$_2$qpyme$_2$]$^{4+}$, absorb strongly in the visible and the ultraviolet regions of the spectrum. Their spectra are shown in Figure 2, and their spectral data are summarized in Table II. As the number of quaternary methyl groups on the coordinated quaterpyridyl is increased the low energy band undergoes a shift to the red. The maximum occurs at 473 nm for [Ru(bpy)$_2$qpy]$^{2+}$, at 487 nm for [Ru(bpy)$_2$qpyme]$^{3+}$, and 492 nm for [Ru(bpy)$_2$qpyme$_2$]$^{4+}$. All three complexes have an additional band in the visible at approximately 430 nm. The band is better resolved in the spectra of [Ru(bpy)$_2$qpyme]$^{3+}$ and [Ru(bpy)$_2$qpyme$_2$]$^{4+}$ than that of [Ru(bpy)$_2$qpy]$^{2+}$, where it overlaps the band at 473 nm.

Emission Spectra

All three complexes are luminescent in methanol/ethanol glass at 77 K (Figure 3), and in fluid solution at room temperature (Figure 4). The emission data are summarized in Table III. $[Ru(bpy)_2qpy]^{2+}$ luminesces strongly with a maximum at 660 nm in water and the emission maximum is slightly blue shifted in acetonitrile solution, characteristic of the stabilization of a ^{3}(MLCT) state by the more polar solvent. The emission quantum yield is 0.078 in acetonitrile and 0.053 in water, both higher than those observed for $[Ru(bpy)_3]^{2+}$ under the same conditions (ϕ_{em}=0.062[147] and ϕ_{em}=0.042[148]). $[Ru(bpy)_2qpyme_2]^{4+}$ shows a weak emission in both acetonitrile (ϕ_{em}=0.0054) and water (ϕ_{em}=0.0013), and the maximum occurs at 728 nm in both solvents. We are currently unable to report with confidence the quantum yield and excited state lifetime values for $[Ru(bpy)_2qpyme]^{3+}$. Samples which satisfy all the normal criteria for analytical purity are found to emit very weakly, on the order of that observed for $[Ru(bpy)_2qpyme_2]^{4+}$. However, the emission does not decay exponentially in either acetonitrile or water. Since luminescence is such a sensitive technique, we are unable to rule out the possibility that traces of the highly emissive $[Ru(bpy)_2qpy]^{2+}$ are present. For example, the possibility exists that a certain fraction of the $[Ru(bpy)_2qpyme]^{3+}$ sample self-reacts to give $[Ru(bpy)_2qpy]^{2+}$ and $[Ru(bpy)_2qpyme_2]^{4+}$, which could be facilitated by laser excitation. The presence of even minute quantities of $[Ru(bpy)_2qpy]^{2+}$ could introduce large errors in quantum yield and lifetime measurements- the problem being more severe in the latter.

Excited State Lifetimes

Excited state lifetimes in acetonitrile are given in Table IV. The lifetime of $[Ru(bpy)_2qpy]^{2+}$ in acetonitrile is 1418 ns, and that for $[Ru(bpy)_2qpyme_2]^{4+}$ is 63 ns. The traces obtained for $[Ru(bpy)_2qpyme]^{3+}$ are non-exponential in acetonitrile, having two components of 1453 and 75 ns. These values are reported with the reservations stated above. Traces measured in water for both $[Ru(bpy)_2qpy]^{2+}$ and $[Ru(bpy)_2qpyme]^{3+}$ are also non-exponential. This is likely due to the presence

of the free pyridine nitrogen atoms on the coordinated quaterpyridyl, which allow the possibility of acid-base equilibria in aqueous solution. For example, the lifetime of $[Ru(bpy)_2qpy]^{2+}$ at pH 2 is markedly shorter than that obtained at pH 7 (on the order of 200 ns and 600 ns respectively).

Electrochemical Measurements

Cyclic voltammograms for the three complexes are shown in Figures 5 and 6. Both the reduction and oxidation waves of the three complexes were determined to be one electron events using the criteria of Polcyn and Shain[149]. The electrochemical data are summarized in Table V. The first reduction of $[Ru(bpy)_2qpy]^{2+}$ occurs at -1.09 V. The free quaterpyridyl has a lower reduction potential than that of bpy, and this reduction at -1.09 V can therefore be assigned to be localized on the coordinated qpy. The second reduction in Figure 5 is assigned to the first reduction of a bpy in $[Ru(bpy)_2qpy]^{2+}$. Since the free ligand does not undergo oxidation below +2 V, the oxidation wave at +1.24 V is inferred to be metal centered.

The cyclic voltammogram of $[Ru(bpy)_2qpyme]^{3+}$ is shown in Figure 6a. The first two reduction waves occur at -0.73 and -0.91 V. Since both values are of lower potential than the first reduction of $[Ru(bpy)_3]^{2+}$ (Table V), as well as the second reduction of $[Ru(bpy)_2qpy]^{2+}$, both occur on the coordinated dimethylquaterpyridyl, as the reduction of a bipyridine would occur at considerably lower (more negative) potential. It is uncertain whether the third wave at -1.20 V represents a further reduction of the methylquaterpyridyl or the first reduction of a bipyridine. The Ru(II)/Ru(III) couple at +1.37 V occurs at slightly higher potential than in $[Ru(bpy)_2qpy]^{2+}$.

The cyclic voltammogram of $[Ru(bpy)_2qpyme_2]^{4+}$ is shown in Figure 6b. The first two reductions occur at -0.70 and -0.82 V, and both waves represent reductions of the coordinated methylquaterpyridyl. While the first reductions of $[Ru(bpy)_2qpyme]^{3+}$ and $[Ru(bpy)_2qpyme_2]^{4+}$ occur at the same potential, the second reduction in $[Ru(bpy)_2qpyme_2]^{4+}$ occurs at a lower potential than the corresponding reduction in $[Ru(bpy)_2qpyme]^{3+}$. The presence of the second quaternized pyridine ring in $[Ru(bpy)_2qpyme_2]^{4+}$, lowers the second reduction potential by providing another viologen-like

reduction site. Again, the assignment of waves at higher (more negative) potential is uncertain. The Ru(II)/Ru(III) couple occurs at $E^{o'}$ = +1.48 V.

Resonance Raman Spectra

Resonance Raman spectra at two different excitation wavelengths are shown in Figure 7. Excitation of $[Ru(bpy)_2qpyme_2]^{4+}$ at 457.9 nm (at approximately the midpoint between the absorptions bands at 430 and 492 nm), results in enhancement of bpy[150] vibrations at 1562, 1490, 1323, and 1177 cm^{-1}. For excitation at 488.0 nm, bands at 1648, 1619, 1542, 1339 and 1260 cm^{-1} are enhanced and can be inferred to be vibrations of chelated $qpyme_2^{2+}$. A similar result is obtained for $[Ru(bpy)_2qpyme]^{3+}$. Excitation at 457.9 nm enhances bpy vibrations at 1564, 1490, 1324, and 1175 cm^{-1}, as compared to the spectrum that results from 488.0 nm excitation. The $[qpyme]^+$ vibrations are assigned to bands occurring at 1648, 1619 1543, 1339, 1287, and 1256 cm^{-1}. The resonance Raman spectrum of $[Ru(bpy)_2qpy]^{2+}$ is very similar to that of $[Ru(bpy)_3]^{2+}$, with only minor bands at 1617 and 1254 cm^{-1} and a medium intensity band at 1534 cm^{-1} assignable to coordinated qpy. The resonance Raman spectrum of $[Ru(qpy)_3]^{2+}$ indicates that a strong band at about 1481 cm^{-1} is due to qpy, only 9 cm^{-1} below an equally strong bpy band, seen in resonance Raman spectra of all bpy complexes. The 1490 cm^{-1} bpy band is notable in the 457.9 nm spectra, reported here whereas the 1481 cm^{-1} (substituted qpy) band is notable in the 488 nm spectra (i.e. the 9 cm^{-1} difference is consistently observed). Enhancement of the bpy pattern of vibrations upon excitation of $[Ru(bpy)_2qpyme]^{3+}$ and $[Ru(bpy)_2qpyme_2]^{4+}$ at 457.9 nm, in conjunction with the enhancement of $[qpyme]^+$ and $[qpyme_2]^{2+}$ vibrations with 488.0 nm excitation, allows the assignment of the long wavelength transitions in the absorption spectra of $Ru(bpy)_2qpyme]^{3+}$ and $[Ru(bpy)_2qpyme_2]^{4+}$ as transitions which terminate on orbitals located on $[qpyme]^+$ and $[qpyme_2]^{2+}$ ligands respectively. The absorption bands at 430 nm in $[Ru(bpy)_2qpyme]^{3+}$, and at 429 nm in $[Ru(bpy)_2qpyme_2]^{4+}$ is assigned to the a MLCT transition to a coordinated 2,2'-bipyridine.

Discussion

Absorption Spectra

Absorption bands in the visible region (λ> 400 nm) of ruthenium(II) diimine complexes are due to spin allowed ^{1}(MLCT) transitions. In tris- α-diimine heteroleptic complexes of the type $[Ru(bpy)_2L]^{2+}$, MLCT transitions to both ligands can be observed if the energy difference of the bands is large enough to permit their resolution. The band for the coordinated bpy can usually be observed between 420- 430 nm. The two bands are hardly resolved in the spectrum of $[Ru(bpy)_2qpy]^{2+}$, as they are nearly equal in intensity, and merge into a broad band with two barely resolved maxima at 473 and 429 nm. Quaternization on the remote quaterpyridyl lowers the energy of the transition to that ligand, producing an increased resolution of the bands in the spectra of $[Ru(bpy)_2qpyme]^{3+}$ and $[Ru(bpy)_2qpyme_2]^{4+}$.

Electrochemistry

The single reversible oxidation wave for $[Ru(bpy)_3]^{2+}$ has been assigned to the removal of an electron from a metal centered t_2 orbital[151,152]. The oxidation wave for $[Ru(bpy)_2qpy]^{2+}$ is at a similar potential to the accepted value for $[Ru(bpy)_3]^{2+}$ (1.28 V vs. SCE in acetonitrile). This suggests that the energies of the metal d orbitals are not significantly perturbed by the additional pyridine functionalities of the quaterpyridyl. The oxidation potentials of $[Ru(bpy)_2qpyme]^{3+}$, and $[Ru(bpy)_2qpyme_2]^{4+}$ are shifted to more positive values (+1.37 and +1.48 V respectively).

It has been generally observed that the electrochemical potentials of related $[Ru(bpy)_2L]^{2+}$ complexes[3b] shift to the positive as the electron withdrawing character of the ligand L is increased. Electrochemical studies on the free ligands suggest that the LUMOs of the free ligands are lowered as a result of quaternization. The free diquaternary salt shows two reduction waves at -0.78 and -0.86 V, the monoquaternary salt a single wave at -0.79 V, and the free quaterpyridyl cannot be reduced below -1.7 V. These results closely parallel the results for the bis-bipyridine complexes 1-3. The first two reductions in $[Ru(bpy)_2qpyme_2]^{4+}$ (-0.70 and -0.82 V) and the first in

$[Ru(bpy)_2qpyme]^{3+}$ (-0.73 V) all occur on the quaterpyridyl ligands, and because their potentials are very similar to those obtained on the free ligands, we conclude that the viologen sites in $[Ru(bpy)_2qpyme]^{3+}$ and $[Ru(bpy)_2qpyme_2]^{4+}$ remain largely undisturbed by the metal center.

Excited State Behavior

The lowest excited state of $[Ru(bpy)_3]^{2+}$ is considered to be composed of four closely spaced states which are considered to be of triplet multiplicity ^{3}(MLCT). The spacing of these ^{3}(MLCT) states is small, and they require low temperatures to be resolved[153]. At room temperature they may be considered to be a single state. The decay from this manifold of ^{3}(MLCT) states[154] can occur by luminescence (k_r), non-radiatively (k_{nr}) or through a temperature dependent surface crossing to metal centered, ^{3}(MC), state or states. Experimentally k_r and k_{nr} can be obtained from lifetime and quantum yield measurement, and the contribution of decay through a ^{3}(MC) from a temperature dependence of the lifetime study.

The radiative rate constants for $[Ru(bpy)_2qpy]^{2+}$, $[Ru(bpy)_3]^{2+}$, and $[Ru(bpy)_2qpyme_2]^{4+}$ are similar in acetonitrile. The non-radiative rate constants for $[Ru(bpy)_2qpy]^{2+}$ and $[Ru(bpy)_3]^{2+}$ are again similar, while that for $[Ru(bpy)_2qpyme_2]^{4+}$ is considerably larger.

It is imprudent to compare the excited state decays of these complexes too closely. The charges on the periphery of $[Ru(bpy)_2qpyme_2]^{4+}$ present several difficulties. The resonance Raman results of these and related Ru(II) heteroleptic α- diimine complexes indicate the excited state has enhanced electron density on the ligand with the lowest LUMO energy, e.g. in the case of $[Ru(bpy)_2qpyme_2]^{4+}$ the enhanced electron density would lie on the N,N'– dimethylquaterpyridinium ligand. The MLCT transition to this ligand will result in an excited state which has a Ru(III) core and a singly *positive* acceptor ligand. To our knowledge all other excited Ru(II) α-diimine complexes studied to date are composed of a Ru(III) core and a *negative* or *neutral* acceptor ligand. It is interesting that the values of k_{nr} for $[Ru(bpy)_2qpyme_2]^{4+}$ are very similar in both water and acetonitrile. Coupling to the O-H vibration of water apparently does not significantly alter the

mechanism of excited state decay in the protic solvent. The mechanism by which a cationic excited state would dissipate energy through the solvent is likely to be different, and this difference could manifest itself in atypical values of k_{nr}, compared to other excited Ru(II) α-diimine complexes.

Excited state Potentials

Excited state potentials of the three complexes are listed in Table 5. Those of $[Ru(bpy)_2qpy]^{2+}$ are high enough to make the complex a viable candidate for participation in excited state redox schemes. In addition, the complex possesses two free pyridine rings which could be used to modify the rates of electron transfer using the free nitrogen atoms to interact with a suitable quencher. For the series of bis-bipyridine complexes **1- 3**, the complex ions become progressively poorer excited state reductants, but more potent excited state oxidants. The excited state redox potentials of $[Ru(bpy)_2qpyme]^{3+}$ and $[Ru(bpy)_2qpyme_2]^{4+}$ indicate the complexes are poorer reductants in the excited state than $[Ru(bpy)_3]^{2+}$, but more potent excited state oxidants.

Conclusion

We report the preparation of a series of ruthenium complexes based on the quaterpyridyl ligand. The complex, $[Ru(bpy)_2qpy]^{2+}$ is strongly luminescent, has excited state properties similar to $[Ru(bpy)_3]^{2+}$, and is an excellent candidate for use in energy conversion schemes. The complexes $[Ru(bpy)_2qpyme]^{3+}$ and $[Ru(bpy)_2qpyme_2]^{4+}$ demonstrate how simple modifications of the ground state structure, quaternization on the remote pyridine nitrogen atoms of $[Ru(bpy)_2qpy]^{2+}$, can substantially reduce emission quantum yields, excited state oxidation potential, and lifetimes.

Table I. ^{13}C NMR Resonances.

#	$[Ru(bpy)_2qpyme]^{3+}$	$[Ru(bpy)_2qpyme_2]^{4+}$
1	49.6	49.6
2	124.0	------
3	124.2	------
4	124.3	------
5	124.4	------
6	125.8	125.9
7	127.0	127.3
8	127.3	127.3
9	129.2	129.2
10	139.6	139.8
11	143.7	143.8
12	146.8	147.5
13	150.4	------
14	152.7	------
15	152.8	152.7
16	153.0	------
17	153.2	153.3
18	153.8	154.4
19	158.1	------
20	158.2	158.0
21	158.8	158.2
22	159.7	159.4

[a]Sat. Solutions in CD_3CN. Values measured relative to TMS.

Table II. Absorption Spectral Data

Complex	$\lambda_{max.}$	$\epsilon \times 10^4$	Solvent
$[Ru(bpy)_2qpy]^{2+}$			
	473	2.3	MeOH
	429	—	
	357	2.1	
	306(Sh.)	—	
	289	7.8	
	252	11	
$[Ru(bpy)_2qpyme]^{2+}$			
	486	1.3	MeOH
	430	1.3	
	310(Sh.)	—	
	286	6.4	
	248	6.6	
$[Ru(bpy)_2qpyme_2]^{4+}$			
	492	1.4	MeOH
	430	1.5	
	330	1.9	
	285	6.1	
	253	5.2	

Table III. Luminescence Data

Complex	λ_{max} (nm)	ϕ_{max}	Conditions[a]
$[Ru(bpy)_2qpy]^{2+}$			
	650	0.078	25°C, CH_3CN
	660	0.053	25°C, H_2O
	615 (Sh. 660)		77K, MeOH/EtOH
$[Ru(bpy)_2qpyme]^{2+}$			
	685 (Sh. 715)	[0.0025][b]	25°C, CH_3CN
	670	[0.0020][b]	25°C, H_2O
	650		77K, MeOH/EtOH
$[Ru(bpy)_2qpyme_2]^{2+}$			
	728	0.0054	25°C, CH_3CN
	728	0.0013	25°C, H_2O
	655		77K, MeOH/EtOH
$[Ru(bpy)_3]^{2+}$	608	0.062[26]	25°C, CH_3CN
	608	0.042[26]	25°C, H_2O

[a]Dearated solutions unless otherwise stated. [b]The values are uncertain, see text.

Table IV. Excited State Lifetimes

Complex	τ(ns)	$10^{-6}k_r(s^{-1})$	$10^{-6}k_{nr}(s^{-1})$	$10^{-6}(k_r+k_{nr})(s^{-1})$	Conditions[a]
$[Ru(bpy)_2qpy]^{2+}$	1418	5.5	71	76	CH_3CN
$[Ru(bpy)_2qpyme_2]^{4+}$	63	4.0	1600	1600	CH_3CN
	68	1.9	1500	1500	H_2O
$[Ru(bpy)_3]^{2+}$ [b]	860	7.2	110	117	CH_3CN

[a] All solutions are degassed and at 25°C unless otherwise stated.
[b] Values taken from reference 3b.

Table V. Electrochemical data

	Oxidation			Reductions			Excited State		
Complex	$E_{1/2}$	ΔE_p[a]	$E_{1/2}(1)$	ΔE_p	$E_{1/2}(2)$	ΔE_p	$E(A^+/A)^*$	$E(A^+/A^-)^*$	E^{00}
$[Ru(bpy)_2(qpy)]^{2+}$	1.24	0.13	-1.09	0.14	-1.44	0.24	-0.67	0.82	1.91
$[Ru(bpy)_2qpyrne]^{2+}$	1.37	0.10	-0.73	0.11	-0.91	0.12	-0.49	1.13	1.86
$[Ru(bpy)_2qpyrne_2]^{2+}$	1.46	0.10	-0.70	0.11	-0.82	0.13	-0.38	1.00	1.70
$[Ru(bpy)_3]^{2+}$	1.29[b]	.095[c]	-1.33[d]	0.10[e]			-0.81[b]	0.84[f]	2.1

[a]All potentials in Volts vs. SCE. [b]Difference in peak potentials for forward and reverse scan are not corrected for cell resistance. [c]Excited state potentials. [d]Reference 153. [e]As measured on our experimental setup. [f]Reference 154. [g]Reference 155.

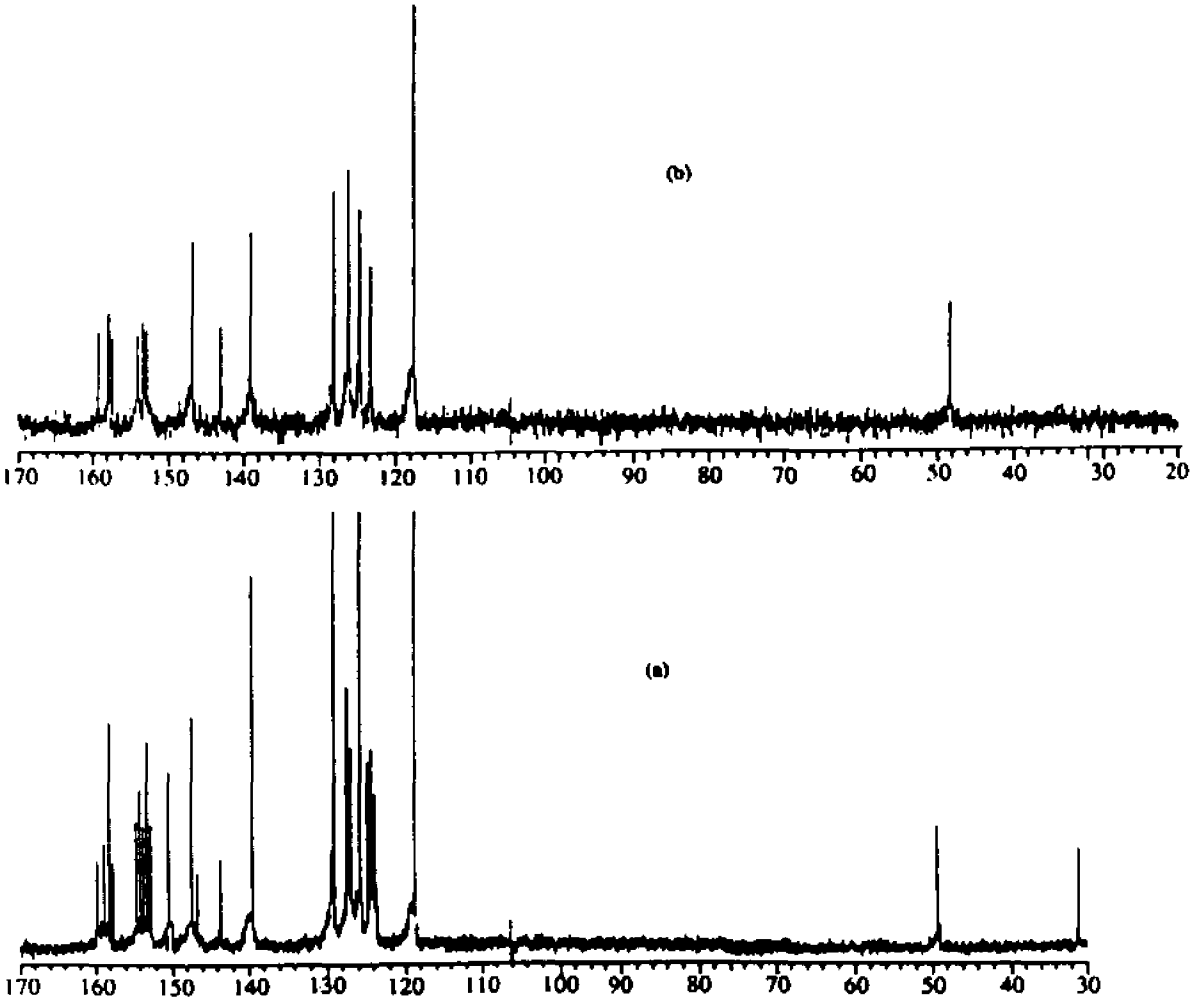

Figure 1. ^{13}C Spectra of a) $[Ru(bpy)_2qpyme]^{3+}$ and b) $[Ru(bpy)_2qpyme_2]^{4+}$ in CD_3CN. The peaks at 120 ppm in both spectra are due to the solvent.

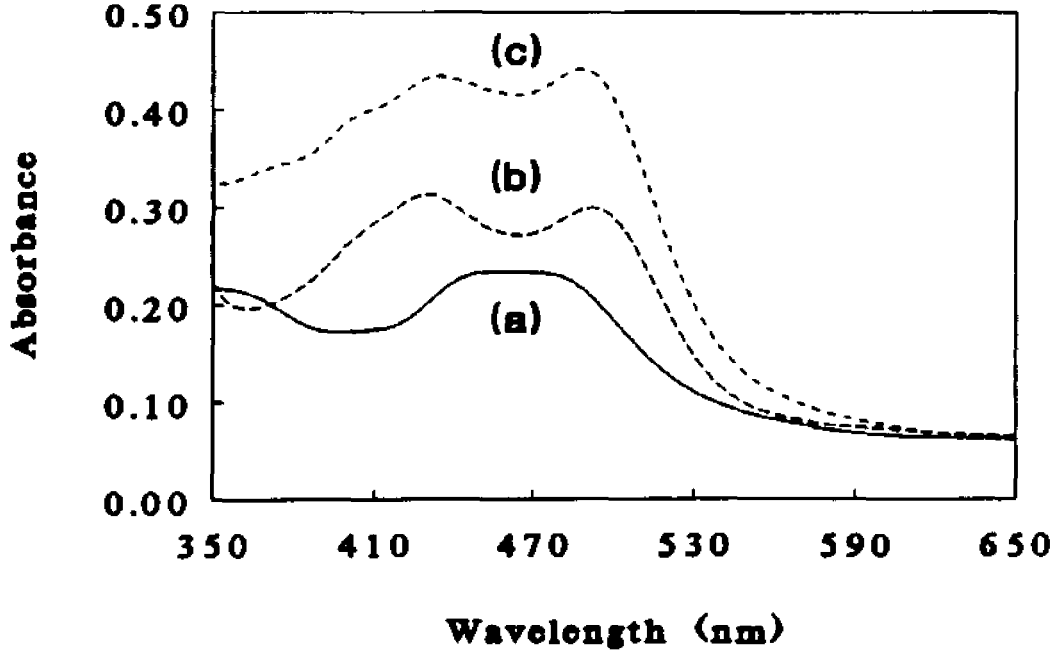

Figure 2. Absorption Spectra of a) $[Ru(bpy)_2qpy]^{2+}$, b) $[Ru(bpy)_2qpyme_2]^{4+}$ and c) $[Ru(bpy)_2qpyme]^{3+}$.

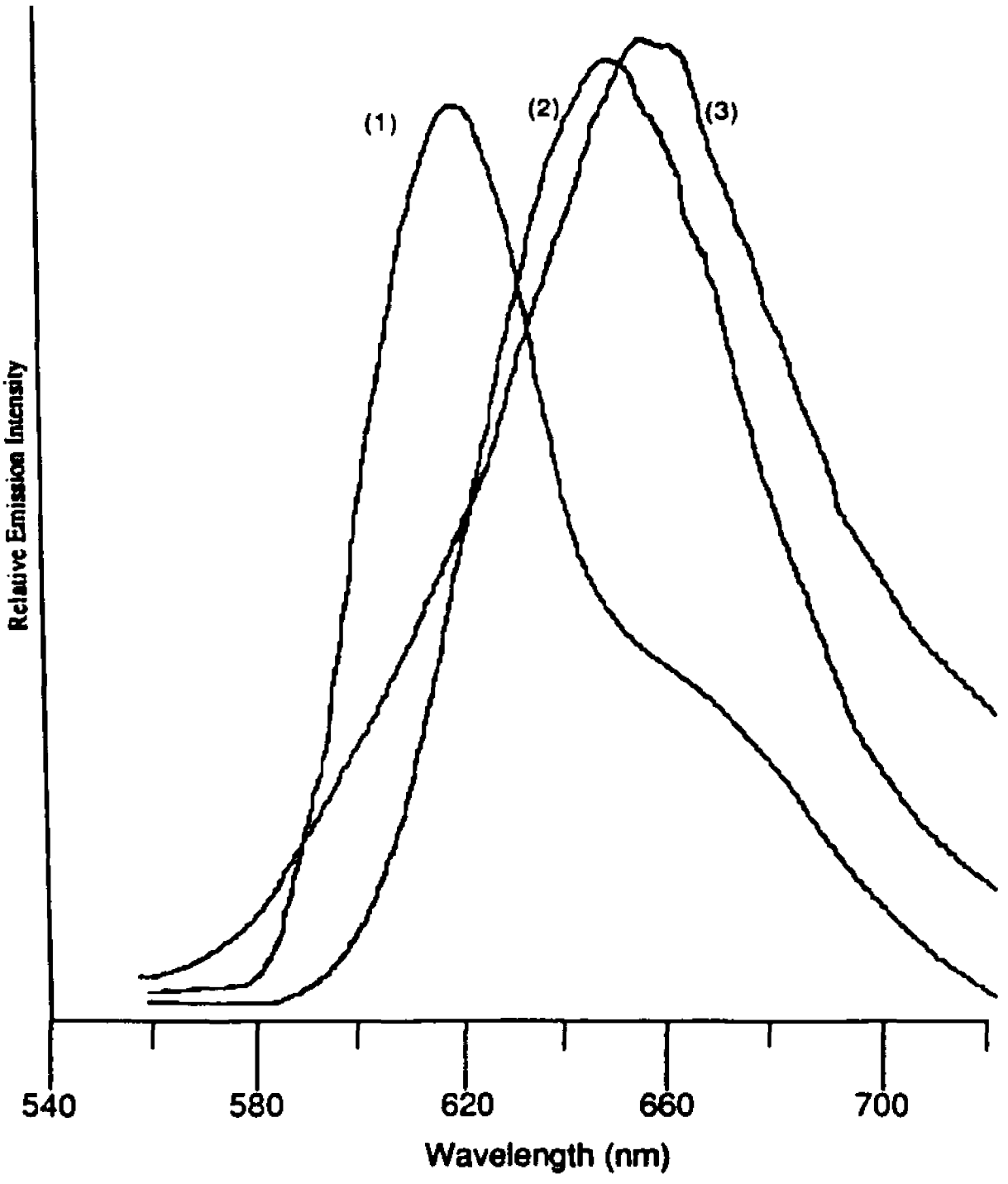

Figure 3. Emission Spectra of 1, 2 and 3 in 4:1 Methanol/Ethanol Glass at 77 K, λ_{exc} = 500 nm.

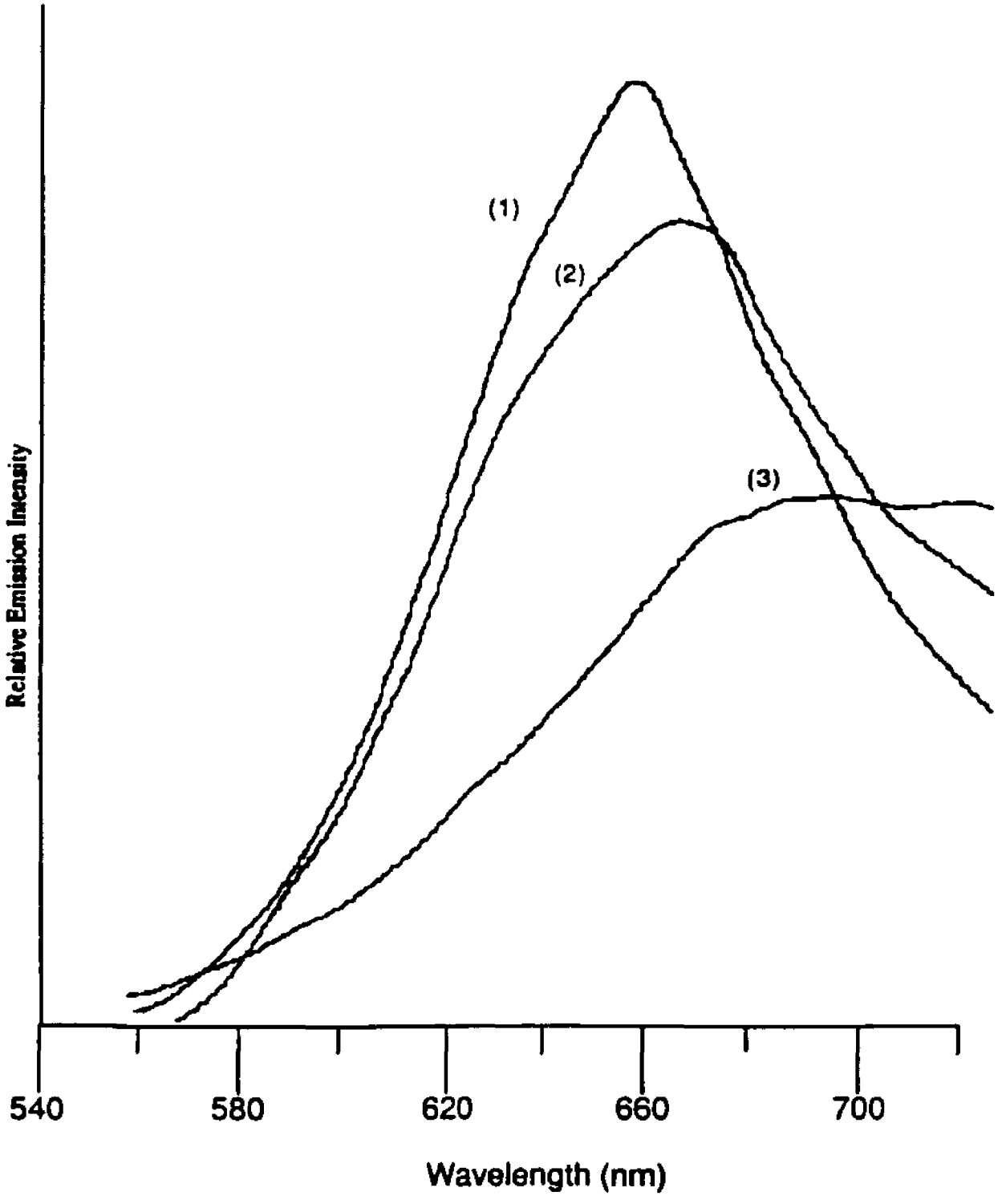

Figure 4. Emission Spectra of 1, 2 and 3 in Water at 25°, λ_{exc} = 500 nm.

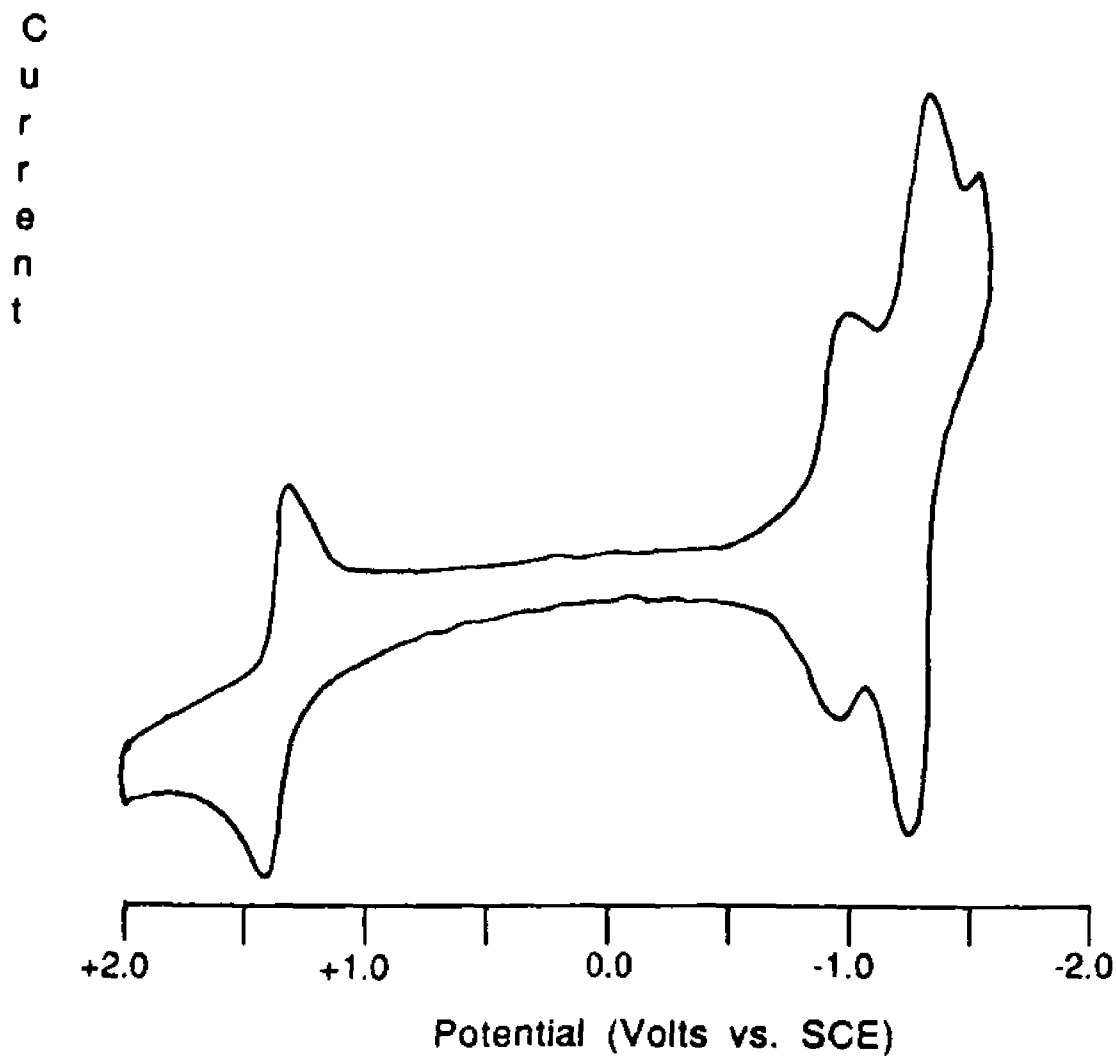

Figure 5. Cyclic Voltammogram of $[Ru(bpy)_2qpy]^{2+}$ in 0.1 M Tetra-n-Butylammoniumtetrafluoroborate CH_3CN vs SCE, 200 mv/s, Glassy Carbon Anode.

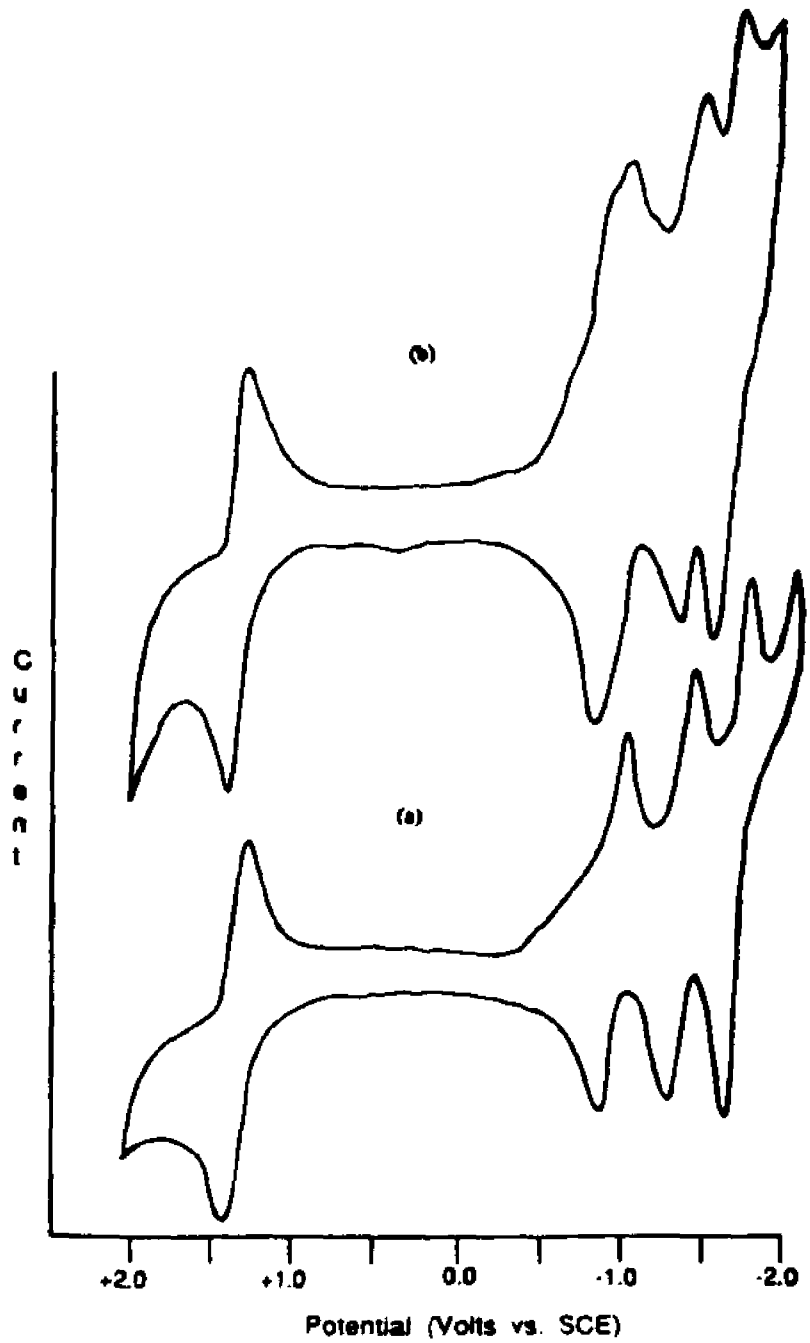

Figure 6. Cyclic Voltammograms of a) $[Ru(bpy)_2qpyme]^{3+}$ and b) $[Ru(bpy)_2qpyme_2]^{4+}$ in 0.1 M Tetra-n-Butylammoniumtetrafluoroborate CH_3CN vs. SCE, Glassy Carbon Anode, 200 mv/s.

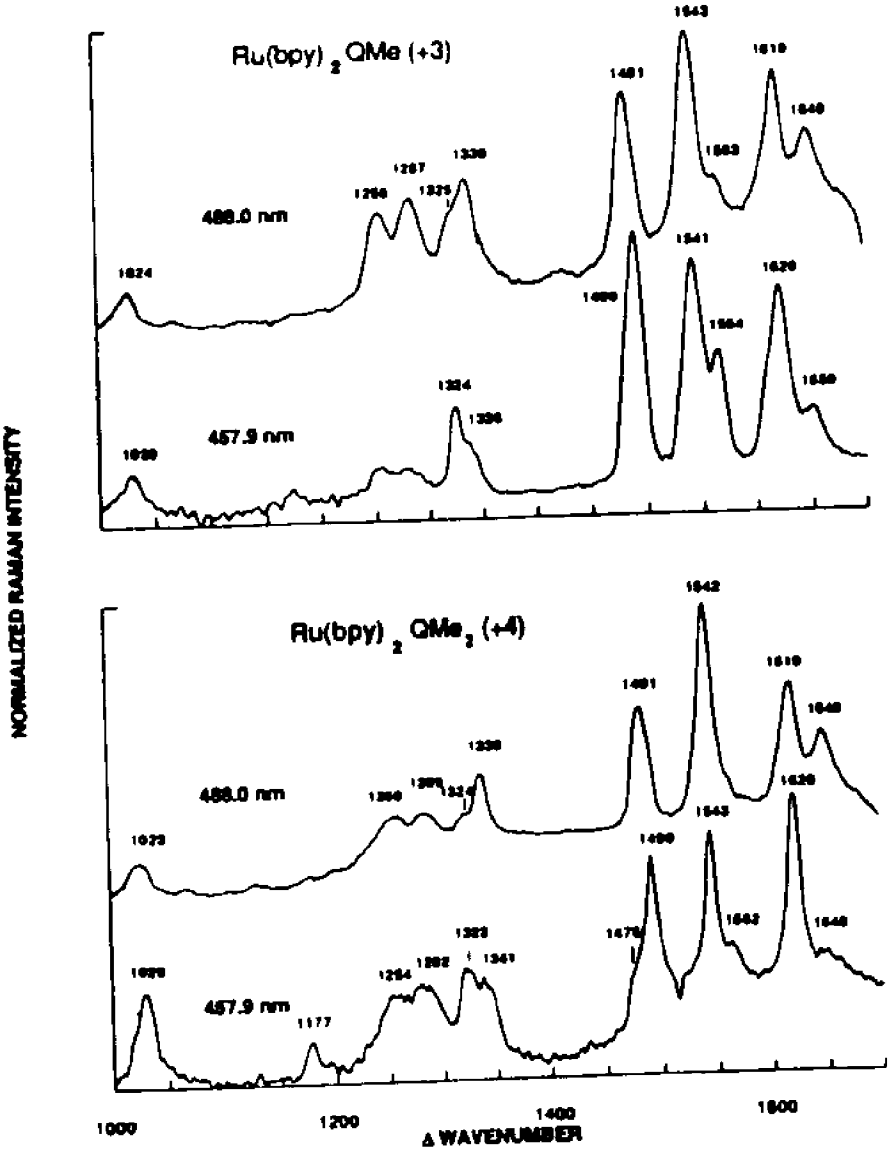

Figure 7. Resonance Raman Spectra of $[Ru(bpy)_2qpyrme]^{3+}$ and $[Ru(bpy)_2qpyrme_2]^{4+}$.

Chapter VII. Ground and Excited State pK_a's of $[Ru(bpy)_2qpy]^{2+}$ and $[Ru(bpy)_2qpyme]^{3+}$

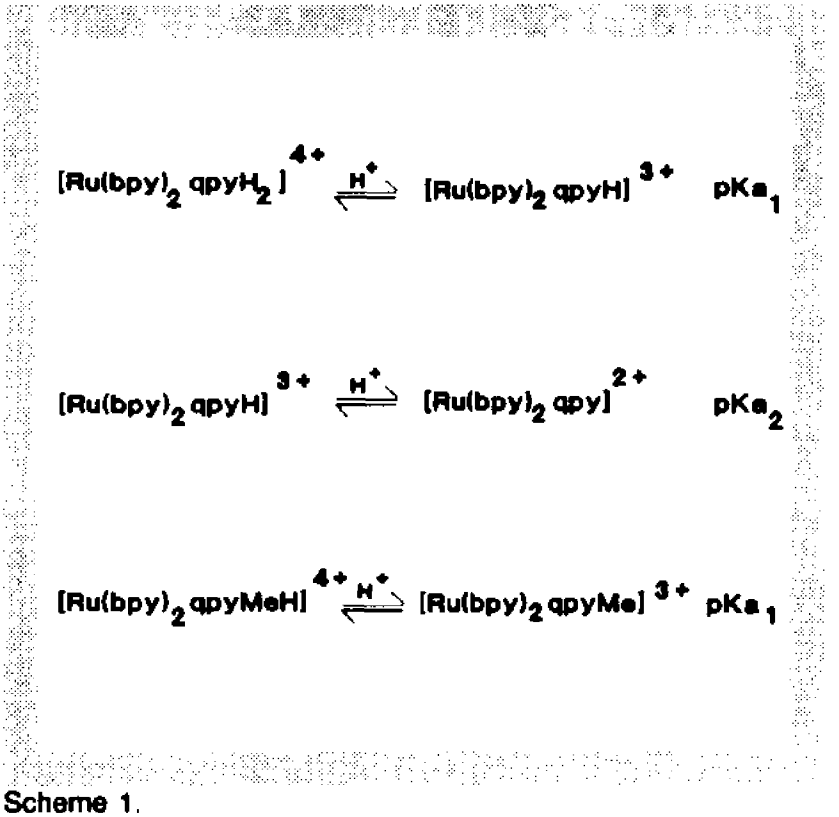

Scheme 1.

Introduction

The complex $[Ru(bpy)_2qpy]^{2+}$ has two basic sites located on the non-coordinating pyridines of the chelated quaterpyridyl, and the complex $[Ru(bpy)_2qpyme]^{3+}$ has a single basic site. Each of these basic sites has an acidity constant associated with it, which in principle can be measured by a spectrophotometric titration technique (detailed in Chapter XIII).

For symmetrical diacids in which the acidic sites are spatially isolated from one another (i.e. non-interacting) the values for the two acidity constants can not equal one another, for statistical reasons. In fact Equation 1 restricts the value for pK_{a2} relative to pK_{a1}.

$$pK_{a2} = pK_{a1} + Log_{10}(4) \qquad (1)$$

Thus the two pK_a's will differ by at least $\log_{10}(4)$ even if the two acid sites are symmetrically equivalent and completely non-interacting (See the Experimental Section for a derivation of Equation 1). Similar statistical arguments can be applied to polyprotic acids. Table I gives the values calculated for the di- to hex- acid cases.

An excited state acidity constant represents the loss of a proton by a species while in the excited state. In order to permit measurement of an excited state pK_a, at least one of the conjugate acid-base pair should be luminescent, and *must* be sufficiently long lived. Luminescence, if present, permits the simplest method for the determination of excited state acidity constants. Decrease or increase of luminescence intensity is plotted as a function of solution acidity and the pK_a is calculated from the resulting titration curve. The excited state, however, must be sufficiently long lived so as to permit the establishment of true acid-base equilibria. Fortunately, most Ru(II) polypyridine complexes satisfy both these criteria, and their excited state acidity constants can be measured by the spectrophotometric titration experiment. Some excited state acidity constants have been determined for Ru(II) complexes, including those of $[Ru(bpz)_3]^{2+}$ (where bpz = 2,2'-bipyrazine)[158], $[Ru(bpy)_2bpz]^{2+}$ [159], and $[Ru(bpy)_2dpp]^{2+}$ (where dpp = 2,3-bis(2-pyridyl)pyrazine)[160]. This chapter is concerned chiefly with the study of the acid-base behavior of $[Ru(bpy)_2qpy]^{2+}$, in both the ground and excited state. These measurements are a necessary prelude to any studies of the complexes as a photoredox reagent.

Results and Discussion

Ground State Pk_a of $[Ru(bpy)_2qpyme]^{3+}(PF_6^-)_3$

Visible absorption spectra of $[Ru(bpy)_2qpyme]^{3+}$ from pH 6.85 to 2.29 are shown in Figure 1. The spectrum shifts noticeably to the red as the acidity of the solution is increased, and isobestic points occur at 340 and 390 nm. In addition, throughout the entire pH range, the band at 429 nm increases in intensity. The largest changes in the spectrum in particular the band at 429 nm, occur between pH 3.11 and pH 4.92. Absorption spectra in this narrow region of pH are shown in

Figure 2. Plotting the absorbance at 429 nm vs pH gives the titration curve in Figure 3. The Gran plot (Δabs/ΔpH vs. pH) of the experimental data has a broad maximum at approximately pH 3.8 (not shown). In order to obtain a better value of the pK_a, the titration experiment was digitally simulated. Using a difference of 0.7 between the molar absorptivities of $[Ru(bpy)_2qpyme]^{3+}$ and $[Ru(bpy)_2qpymeH]^{3+}$ at 429 nm, and a pK_a 3.9 gave the best fit (solid line in Figure 3). Because 3.9 is also on the maximum of the Gran plot, this value is assigned as the pK_a of $[Ru(bpy)_2qpyme]^{3+}$.

Ground State pK_a's of $[Ru(bpy)_2qpy]^{2+}(PF_6^-)_2$

Absorption spectra of the ion $[Ru(bpy)_2qpy]^{2+}$ in neutral and weakly acidic aqueous solution are shown in Figure 4. The spectrum remains constant as the solution is acidified until a pH of approximately 4.0 is reached. Between pH 4.06 and 3.00, there are significant spectral changes, and a set of isobestic points at 483, 445, 378 nm develop (Figure 5). Between pH 3.00 and 98% sulfuric acid, the spectrum gradually shifts to the red, and decreases in intensity, but no new isobestic points develop. The set of spectra from pH 2 to pH 3 are shown in Figure 6

Because isobestic points are observed only between pH 3 and pH 4, it is our assertion that both pK_a's of the diacid $[Ru(bpy)_2qpyH_2]^{4+}$ occur in this region of acidity. If only *one* acidity constant is in this region, one would have to conclude that the complex resists di-protonation even in 98% sulfuric acid. However, since the pK_a of $[Ru(bpy)_2(qpyme)H]^{3+}$ is 3.9, the acidity constant for $[Ru(bpy)_2qpyH_2]^{4+}$ is thought to have a similar value.

Figure 7 gives the titration curve for $[Ru(bpy)_2qpy]^{2+}$ at 360 nm. The Gran plot indicates a single inflection point at 3.9 pH units. There are two distinct interpretations of this value. The first is that it represents a single pK_a at 3.9, and the second that it represents the average of two acidity constants centered at 3.9 pK units. In the case of two acidity constants closer than ≈ 2 pK units, two distinct protonation steps will not be resolved on the titration curve. Yet the titration curve will be qualitatively different than in the single pK_a case. Digital simulations indicate that the presence of the second acidity constant causes the titration curve to be steeper. The data in Figure 7 cannot

be adequately fitted assuming there is only a single pK_a at 3.9 pK units, but can be fitted by assuming closely spaced pK_a's (the solid line in the Figure). The pK_a values chosen for the fit were 4.2 and 3.5. Equation 1 does not permit the values for the two pK_a's to be closer than 0.65 pH units. The two pK_a values for $[Ru(bpy)_2qpyH_2]^{4+}$ should be separated by *at least* 0.65 pK units, and the values for the pK_a's satisfy this criterion.

The analysis of the titration curve at 500 nm in Figure 8 gives a different result, indicating the dependence of the titration curve on wavelength. The value obtained for the Gran plot is 4.0, which is similar to that obtained for the plot at 360 nm, but the data *can* be fitted with a single pK_a rather than with two. The solid line in the Figure resulted from fitting with a single pK_a at 4.0 pK units; only pK_{a1} is observed. At 500 nm, spectral changes are associated with either the *second* protonation or the first deprotonation, but both are not observed. The difference in the extinction coefficients for the free base, $[Ru(bpy)_2qpy]^{2+}$ and the monoacid, $[Ru(bpy)_2qpyH]^{2+}$ are too close to one another to be resolved. Only the second protonation produces significant spectral changes, and the resulting titration curve.

In the normal pH range three species are present, the free base $[Ru(bpy)_2qpy]^{2+}$ and its two conjugate acids, $[Ru(bpy)_2qpyH]^{3+}$ and $[Ru(bpy)_2qpyH_2]^{4+}$ (Scheme 1). The spectrum of the free base occurs in neutral solution and the lowest energy MLCT transition occurs at 476 nm. The spectrum of the diacid, $[Ru(bpy)_2qpyH_2]^{4+}$, occurs below pH 3, and contains two clearly resolved bands at 429 and 497 nm. As expected, the absorption spectrum of $[Ru(bpy)_2qpyH_2]^{4+}$, $[Ru(bpy)_2qpymeH]^{3+}$, and $[Ru(bpy)_2qpyme_2]^{4+}$ are virtually indistinguishable from one another. In the narrow region of pH in which the mono-acid dominates, the spectrum is considerably broadened. Spectral broadening has also been observed in the pH dependent spectrum of $[Ru(bpz)_3]^{2+}$, and has been reported to result from lifting the degeneracy from the π^* orbital of the mono protonated acceptor ligand in the MLCT transition[158]. In the case of $[Ru(bpy)_2qpy]^{2+}$, the spectrum of the mono-protonated species is also broadened relative to the spectrum of $[Ru(bpy)_2qpyme]^{3+}$, which has a similarly non-degenerate acceptor π^*. The dominant factor determining spectral broadening in the

case of $[Ru(bpy)_2qpyH]^{3+}$ is the existence of multiple species in solution, giving superimposed spectra. The lifting of degeneracy of the acceptor orbital plays only a minor role in the qpy complexes.

Excited State pK_a of $[Ru(bpy)_2qpy]^{2+}$

At pH 7, the complex shows a bright red-orange emission with a maximum at 660 nm. As the pH of the solution is decreased the emission intensity declines, shifts to the red, and finally becomes undetectable at pH values less than 2. The luminescence seen in the range 2< pH <7 is attributed to a mix of that due to $[Ru(bpy)_2qpy]^{2+}$ and that due to $[Ru(bpy)_2qpyH]^{3+}$; emission from the latter is weaker than that of the former. Figure 9 shows the decrease in intensity of the luminescence at 660 nm as a function of pH, and the corresponding titration curve is shown in Figure 10. The latter permits an excited state pK_a to be calculated as 5.0. Because no emission is observed below pH 2 the diacid is concluded to be non-emissive. The complex is a stronger base in the excited state than in the ground state, which is consistent with the character of the emissive state in that there is more electron density on the quaterpyridyl following excitation.

Conclusion

The complexes $[Ru(bpy)_2qpy]^{2+}$ and $[Ru(bpy)_2qpyme]^{2+}$ are strong bases, compared to other Ru(II) complexes with free nitrogen atoms. The complex $[Ru(bpy)_2qpy]^{2+}$ is a stronger base in the excited state, comparable to that of free pyridine. The acidity constants of the two complex ions imply that the free nitrogen atoms are readily available to be coordinated to additional metals or to interact with heterogeneous substrates such a porous Vycor glass or DNA. The complexes are well suited as probes of these materials because their photophysical properties are sensitive to environmental changes in a predictable manner.

Table I.

# Sites	ΔPka				
	1-2	2-3	3-4	4-5	5-6
2	0.85	—	—	—	—
3	0.48	0.48	—	—	—
4	0.43	0.38	0.43	—	—
5	0.40	0.30	0.30	0.40	—
6	0.38	0.27	0.24	0.27	0.38

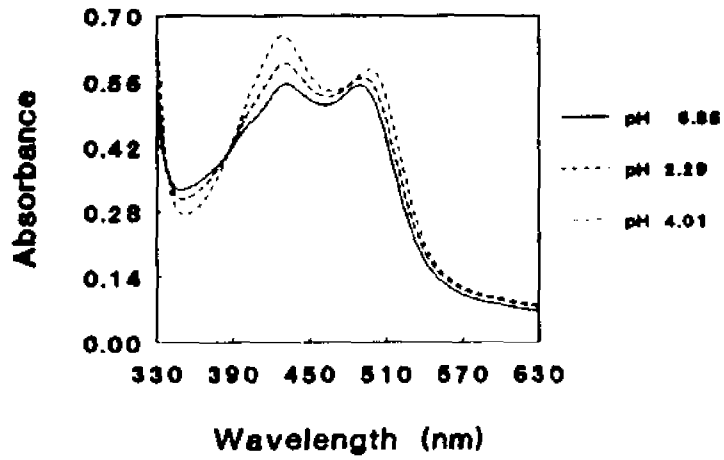

Figure 1. Absorption Spectra of $[Ru(bpy)_2qpyme]^{3+}$

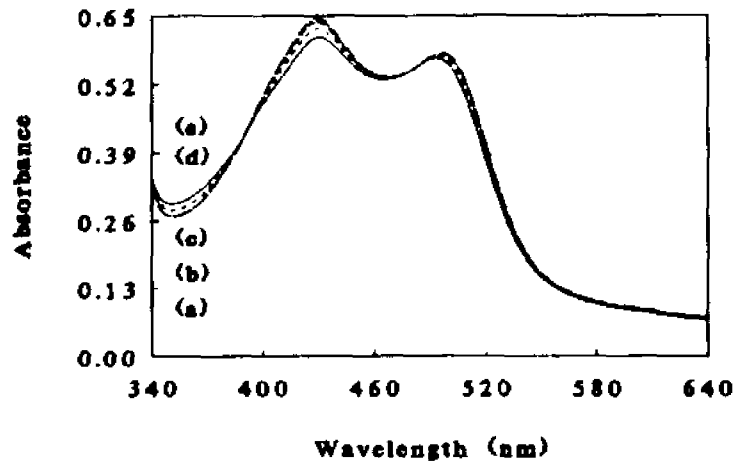

Figure 2. Absorption Spectra of $[Ru(bpy)_2qpyme]^{3+}$ at pH a)4.01 b) 3.70 c) 3.37 d) 3.24 e) 3.11.

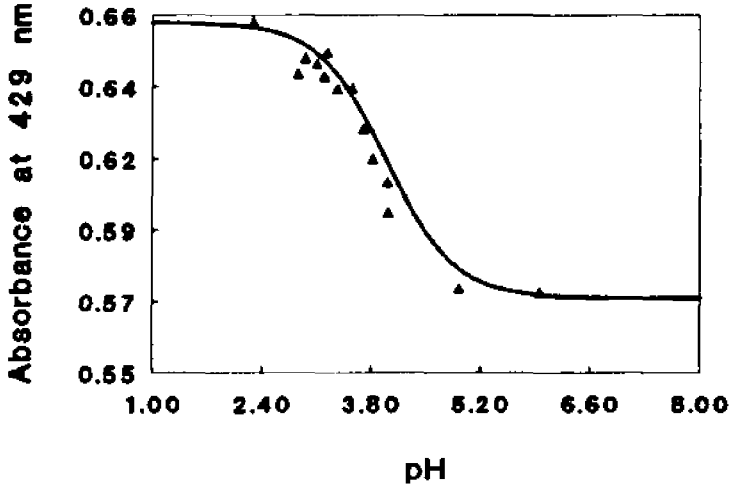

Figure 3. Titration Curve for $[Ru(bpy)_2qpyme]^{3+}$.

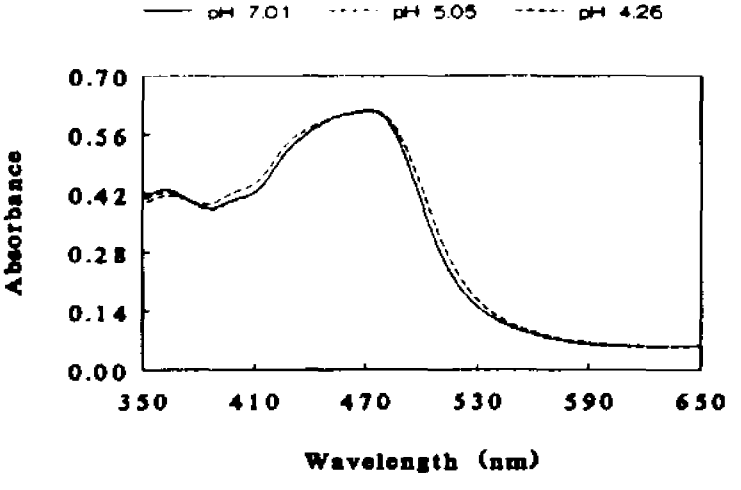

Figure 4. Absorption Spectra of $[Ru(bpy)_2qpy]^{2+}$ at pH 7.01, 5.05, and 4.26.

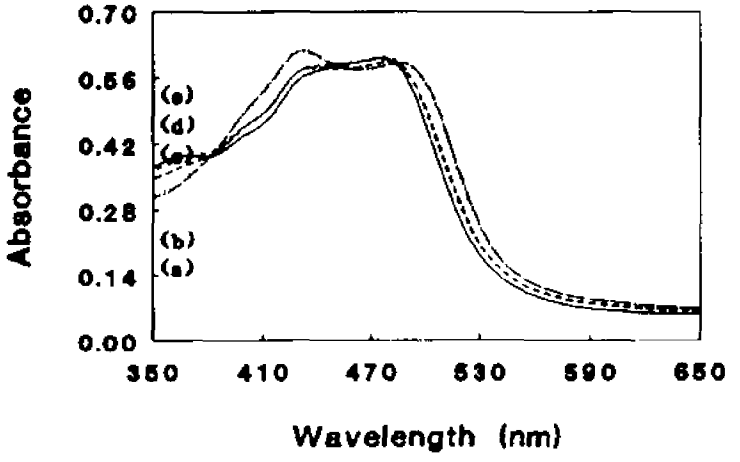

Figure 5. Absorption Spectra of $[Ru(bpy)_2qpy]^{2+}$ at pH a) 4.01 b) 3.85 c) 3.67 d) 3.28 e) 3.17.

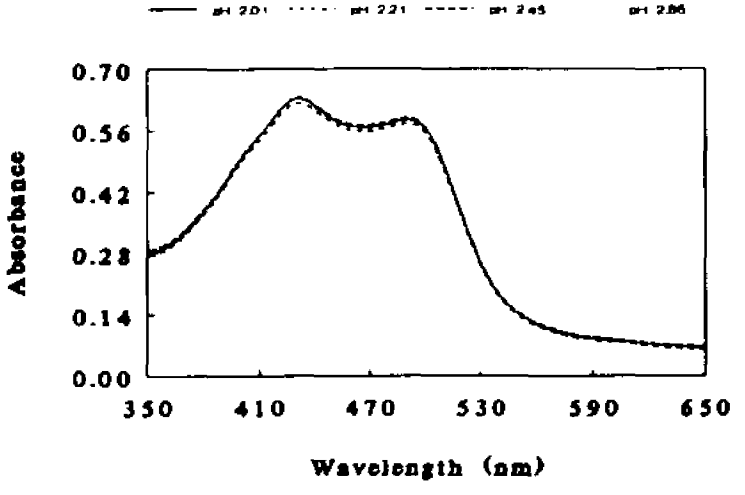

Figure 6. Absorption Spectra of $[Ru(bpy)_2qpy]^{2+}$

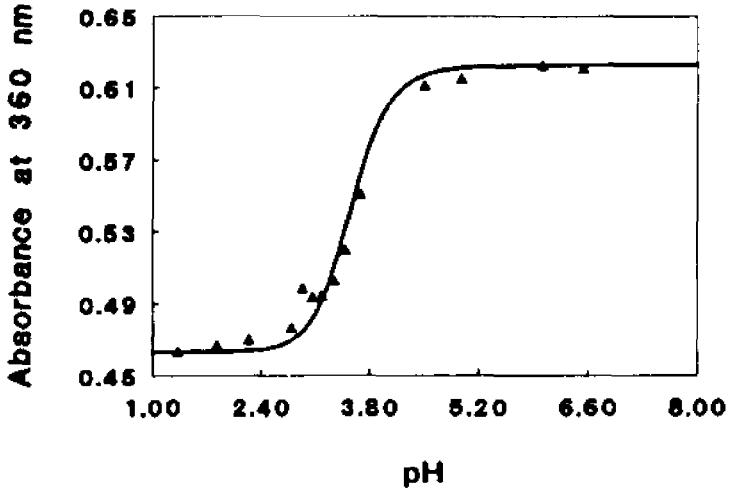

Figure 7. Plot of Absorbance at 360 nm vs. pH for $[Ru(bpy)_2qpy]^{2+}$.

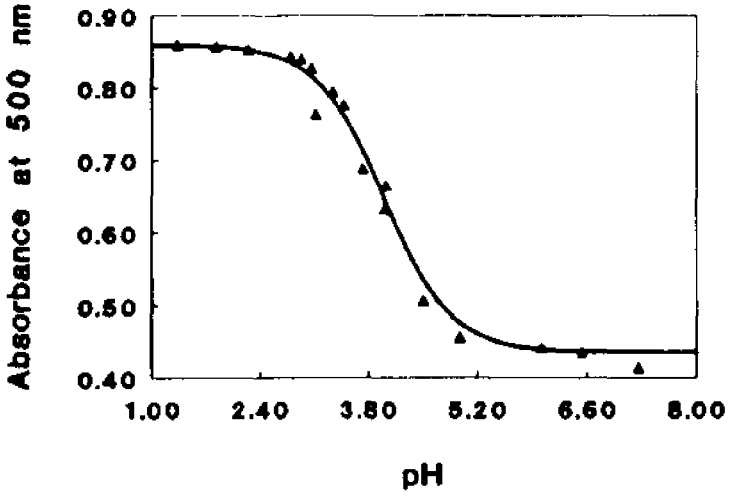

Figure 8. Plot of Absorbance at 500 nm vs. pH for $[Ru(bpy)_2qpy]^{2+}$.

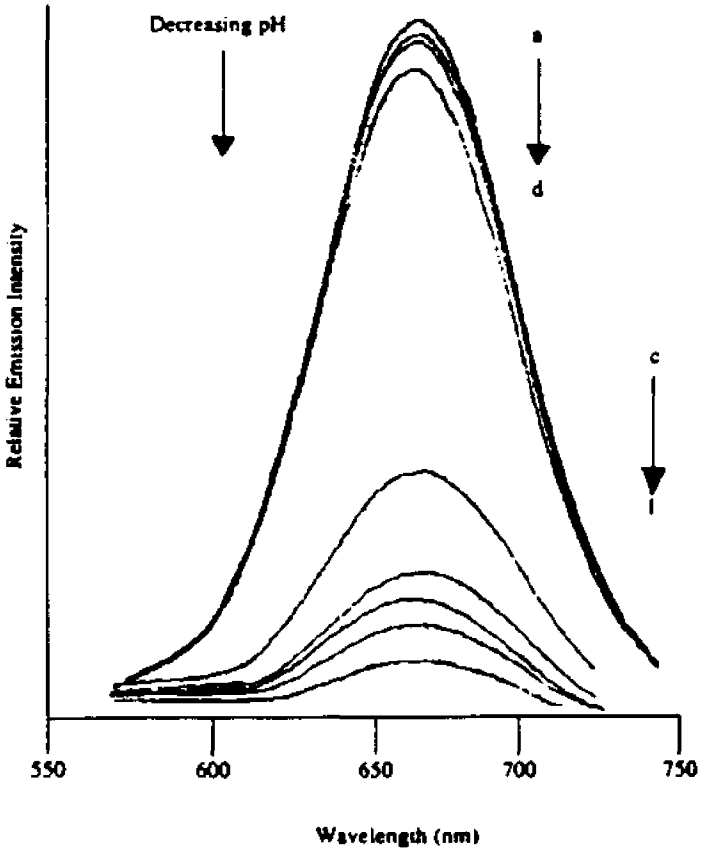

Figure 9. Emission Spectra of $[Ru(bpy)_2qpy]^{2+}$ at pH a) 7.01 b) 6.02 c) 5.50 d) 5.00 e) 4.30 f) 4.12 g) 3.53 h) 2.56 and i) 1.97.

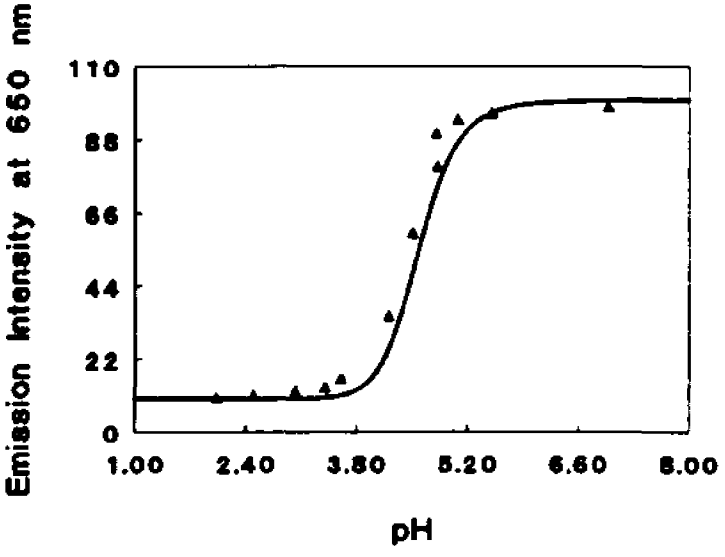

Figure 10. Plot of Emission Intensity at 660 nm vs. pH for $[Ru(bpy)_2qpy]^{2+}$.

Chapter VIII. Tris- Quaterpyridyl Ruthenium(II) Complexes

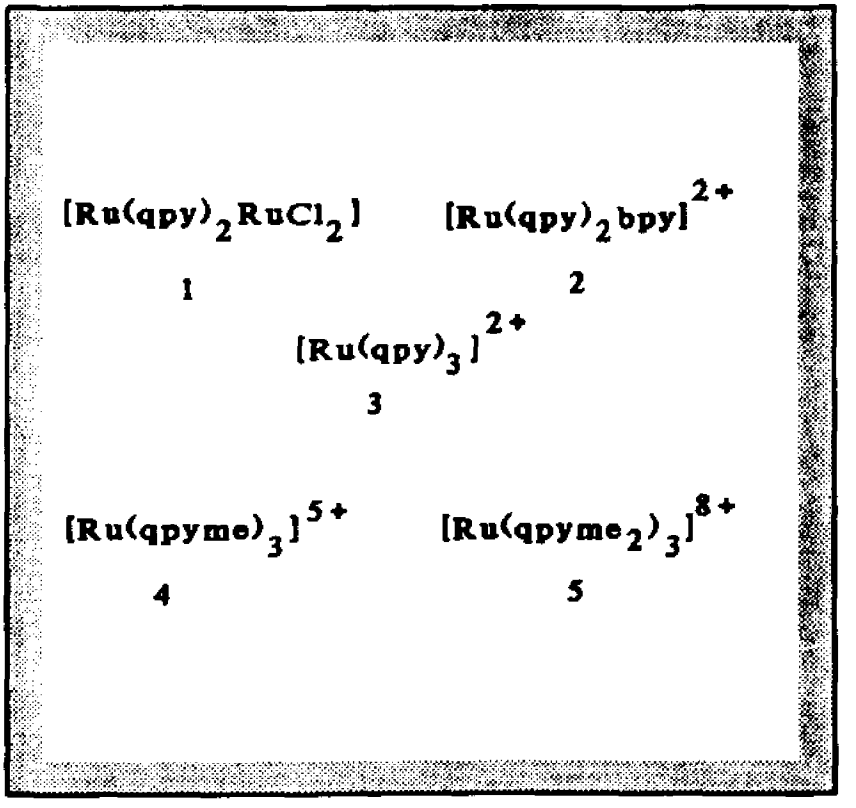

Results and Discussion

Preparation

The general methodology for the preparation of ruthenium(II) complexes with three identical diimine ligands requires the initial preparation of a complex of the type $Ru(L)_2Cl_2$, where L represents the diimine ligand (Scheme 1). This complex is then isolated, treated with a further equivalent of L to form $[Ru(L)_3]^{2+}(Cl^-)_2$. This two step method presents some difficulties when applied to the preparation of $[Ru(qpy)_3]^{2+}$. Refluxing two equivalents of qpy with $RuCl_3$ in dimethylformamide (DMF), conditions similar to those used to prepare $Ru(bpy)_2Cl_2$, does *not* result in the expected product bis-quaterpyridyl complex, $Ru(qpy)_2Cl_2$. Instead, the major product is a brown solid insoluble material, the elemental analysis of which is inconsistent with a bis-quaterpyridyl complex. The material also gives a purple color in the presence of ferrous ion. These observations suggest that the material is polymeric, and contains free diimine sites. Thus, it is

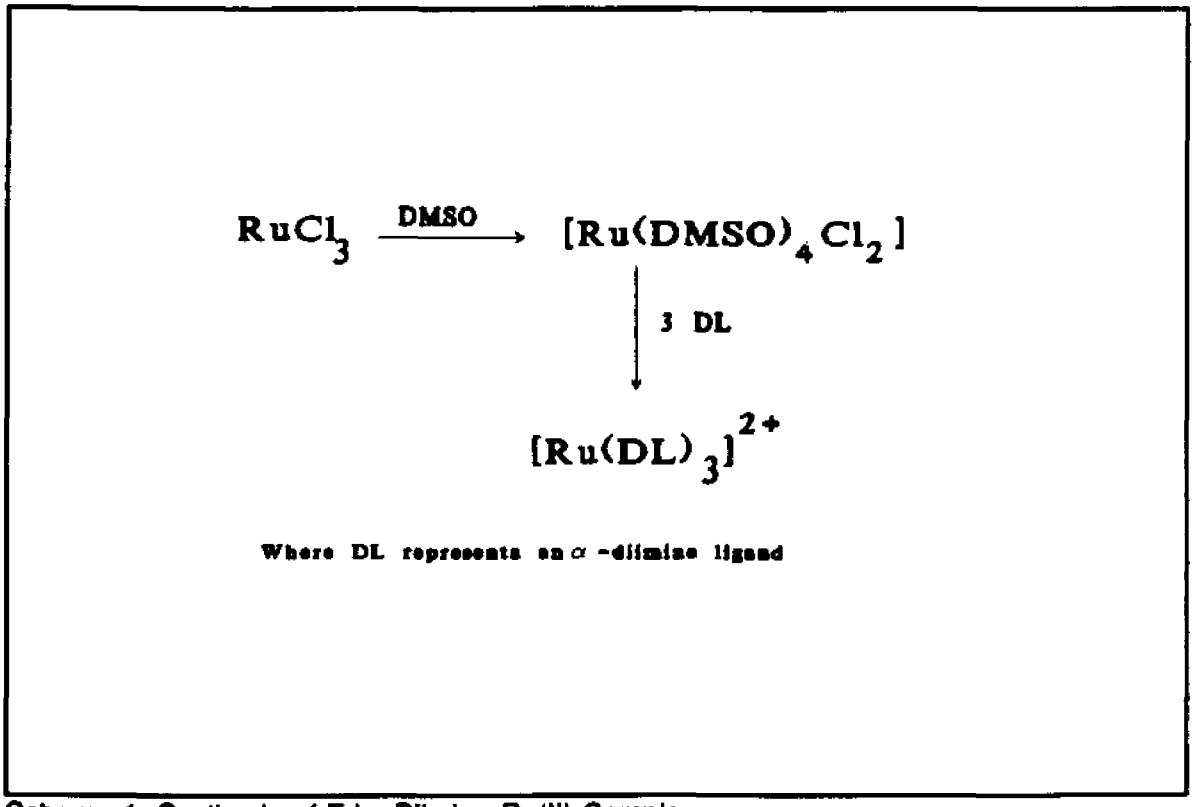

Scheme 1. Synthesis of Tris -Diimine Ru(II) Complexes.

probable that both the diimine nitrogen atoms *and* the "remote" nitrogen atoms, of the quaterpyridyl readily coordinate to ruthenium(II), and as a result there are diimine sites in the material, available for coordination to ferrous ion (ferrous ion does not give a purple color in the presence of simple, "non-diimine", pyridines). However, refluxing the brown material with a small excess of qpy in ethylene glycol does give a low yield of $[Ru(qpy)_3]^{2+}$, in which there is coordination to Ru(II) only through the diimine site. Apparently, coordination through the remote (non-diimine) nitrogen atoms is labile compared to coordination through the diimine site. This rapid ligand substitution renders the material useless in the preparation $[Ru(qpy)_2L]^{2+}$ type complexes. For example, refluxing the material with one equivalent of 2,2'-bipyridine gives several products, including $[Ru(qpy)_3]^{2+}$, $[Ru(bpy)_2qpy]^{2+}$, $[Ru(bpy)_3]^{2+}$ and $[Ru(qpy)_2bpy]^{2+}$.

We discovered a superior method for the preparation of $[Ru(qpy)_3]^{2+}$. This requires an initial preparation of $[Ru(DMSO)_4Cl_2]^{2+}$, by warming ruthenium trichloride in DMSO and collecting the

precipitate[161]. The complex is obtained pure, and the method results in an effective purification of commercial ruthenium chloride. $[Ru(qpy)_3]^{2+}$ is then prepared by refluxing $[Ru(DMSO)_4Cl_2]^{2+}$ with three equivalents of qpy in water/ethanol. The brown polymeric substance discussed above is again formed, but the yield of $[Ru(qpy)_3]^{2+}$ is greatly improved. The methylated complex 4, is prepared under the same conditions. The tris Ru(II) complex of bis-methylated quaterpyridyl 5, seems to form under the same conditions used in the preparations of 3 and 4, but NMR and microelemental analysis are inconsistent with the structure 5. Purification of the complex is difficult, and it is not stable in solution over time.

Characterization

The 60 MHz ^{1}H NMR spectrum of $[Ru(qpy)_3]^{2+}$ has only pyridine resonances. The spectrum of $[Ru(qpyme)_3]^{2+}$ has a singlet for the nine equivalent methyl protons and the expected 42 pyridine resonances. Microelemental analysis for both 3 and 4 are within acceptable limits (see Chapter XIII for these results).

Absorption Spectra

The absorption spectra of $[Ru(qpy)_3]^{2+}$ and $[Ru(qpyme)_3]^{2+}$ are shown in Figure 1, and their spectral data are summarized in Table I. The spectrum of $[Ru(qpyme_2)_3]^{6+}$ also shown in the Figure 1, is of a crude reaction product, and is included only for completeness. The spectral maximum of $[Ru(qpy)_3]^{2+}$ occurs at 476 nm, and $[Ru(qpyme)_3]^{2+}$ at 487 nm. The red shift in the spectra of $[Ru(qpyme)_3]^{2+}$ reflects the lowering of the π^* acceptor orbital of the MLCT transition in the quaternized quaterpyridyl.

Luminescence

In aqueous solution at room temperature, $[Ru(qpy)_3]^{2+}$ has a bright orange– red emission

centered at 635 nm (Figure 2a). The quantum yield of emission in air equilibrated and degassed methanol are 0.055 and 0.14 respectively. The emission from $[Ru(qpy)_3]^{2+}$ is stronger than for most other α-diimine Ru(II) complexes. For example, $[Ru(bpy)_3]^{2+}$ has a quantum yield of only 0.043 in degassed methanol. At 77 K, in methanol or PVA (polyvinylalcohol/water/ethanol) glass, the emission maximum of $[Ru(qpy)_3]^{2+}$ occurs at 617 nm (16,207 cm^{-1}), with a well resolved low energy shoulder at 667 nm (14,992 cm^{-1}, Figure 3a). The excited state lifetime of $[Ru(qpy)_3]^{2+}$ in degassed aqueous solution is 991 ns, which places it among the longest lived Ru(II) polypyridine complexes; $[Ru(bpy)_3]^{2+}$ has a lifetime of 599 ns under the same conditions.

$[Ru(qpyme)_3]^{2+}$ is also emissive, but its luminescence maximum is red shifted relative to that of $[Ru(qpy)_3]^{2+}$ (Figure 2b). In fluid solution the maximum occurs at 680 nm, accompanied by a shoulder at 715 nm. The quantum yield of emission in air equilibrated methanol is 0.0074, and in degassed methanol is 0.010. At 77 K in methanol/ethanol glass, the emission maximum occurs at 650 nm (Figure 3b). The emission data for $[Ru(qpy)_3]^{2+}$ and $[Ru(qpyme)_3]^{2+}$ are summarized in Table II. As was observed for the bis-bipyridine complexes, $[Ru(bpy)_2qpy]^{2+}$ and $[Ru(bpy)_2qpyme]^{2+}$ (Chapter VI), methylation of the remote pyridine rings of the quaterpyridyl decreases the quantum yield and shifts the maximum to the red.

Ground State Acidity Constants of $[Ru(qpy)_3]^{2+}$

$[Ru(qpy)_3]^{2+}$ has six basic sites, located on the non- coordinating pyridine nitrogen atoms, and each has a pK_a associated with it (Scheme 2). The complex, as its hexafluorophosphate salt, can be dissolved in 70% sulfuric acid, and be subsequently isolated without any observable change in its spectroscopic properties. Beyond 70%, there is evidence that the complex undergoes oxidative decomposition; the solution turns green, and its visible absorption spectrum no longer contains strong MLCT bands. All acidity measurements in the normal pH range are reversible. There is no difference in the results, whether the titration begins in acid, and base is added, or if the original solution was neutral and made acidic. The titration technique is discussed in Chapter

$$[Ru(qpy)_3]^{2+} \underset{pKa_6}{\overset{H^+}{\rightleftharpoons}} [(qpyH)Ru(qpy)_2]^{3+}$$

$$[(qpyH)Ru(qpy)_2]^{3+} \underset{pKa_5}{\overset{H^+}{\rightleftharpoons}} [(qpyH)_2 Ru(qpy)]^{4+}$$

$$[(qpyH)_2 Ru(qpy)]^{4+} \underset{pKa_4}{\overset{H^+}{\rightleftharpoons}} [(qpyH)_3 Ru]^{5+}$$

$$[(qpyH)_3 Ru]^{5+} \underset{pKa_3}{\overset{H^+}{\rightleftharpoons}} [(qpyH)_2 Ru(qpyH_2)]^{6+}$$

$$[(qpyH)_2 Ru(qpyH_2)]^{6+} \underset{pKa_2}{\overset{H^+}{\rightleftharpoons}} [(qpyH)Ru(qpyH_2)_2]^{7+}$$

$$[(qpyH)Ru(qpyH_2)_2]^{7+} \underset{pKa_1}{\overset{H^+}{\rightleftharpoons}} [Ru(qpyH_2)_3]^{8+}$$

Scheme 2. Protonation of $[Ru(qpy)_3]^{2+}$.

XIII.

As expected, the absorption spectrum of $[Ru(qpy)_3]^{2+}$ is pH dependent (Figure 4). The band positions and intensities in the absorption spectrum of $[Ru(qpy)_3]^{2+}$, remain constant as the acidity of the solution is increased until a pH of 4.0 is reached. Between pH 4.0 and 3.0 there are significant spectral changes (Figure 5 and 6). Isobestic points develop at 205, 239, 285, 317, 377 and 450 nm, and the entire spectrum shifts to lower energy.

Figure 7 shows the titration curve at 360 nm for this region of pH. A Gran plot (Δabs/ΔpH

vs. pH) has a broad maximum, and does not yield an accurate value for an acidity constant(s). However, when the experimental data were digitally simulated assuming pK_a values of 4.2 and 3.6, an excellent fit was obtained (the solid line in Figure 7). The data could not be adequately fitted with a single pK_a, and fitting with more than two acidity constants was not attempted. Titration curves using other wavelengths were constructed, and gave similar results. For example plotting absorbance at 310 nm gave a well defined Gran plot with an inflection point at 3.9 pK units. This value is also the midpoint of the two pK_a values calculated using absorbance at 360 nm.

Thus, the spectral changes in this region of pH reveal the values of the acidity constants. The pK_a at 4.2 pK units is assigned to be pK_{a6}, the first protonation of $[Ru(qpy)_3]^{2+}$. This value is similar to pK_{a2} of $[Ru(bpy)_2qpy]^{2+}$ and to pK_{a1} of $[Ru(bpy)_2qpyme]^{2+}$ (Table III). As described in the previous Chapter, it is possible to predict the values of subsequent acidity constants using a statistical method, which presumes all the acidic sites are equivalent and non– interacting. Inspection of Table I in Chapter VII indicates that the maximum value for pK_{a5}, using 4.2 pK units as the value of pK_{a6}, is 3.9 pK units (see Chapter VII for the application of Table I). Similarly, pK_{a4} would occur at 3.7 pK units. It is expected from the results outlined in Chapter VII that there would be little interaction between the basic sites of $[Ru(qpy)_3]^{2+}$, and the acidity constants for at least the first three protonations would closely parallel the statistically predicted values, as was observed for $[Ru(bpy)_2qpy]^{2+}$. Thus, the *fourth* pK_a is assigned as 3.6, and the *fifth* as 3.9 pK units. Unfortunately, below pH 3.0, no new isobestic points were detected (Figures 8 and 9), which prohibits determination of the final three acidity constants. This result could be anticipated from the results for $[Ru(bpy)_2qpy]^{2+}$, in which spectral changes due to the second protonation of a quaterpyridyl are small compared to those of the first.

There have been few studies of this type for comparative purposes, but Lever's[158] spectrophotometric study of tris-(2,2'-bipyrazine)ruthenium(II) complex, which also has two protonation sites on each of the three bpz ligands, merits some comment. In the case of $[Ru(bpz)_3]^{2+}$, each of the first three protonation steps occur on different bipyrazine ligands, and each

causes the spectrum to red shift. With the fourth protonation, the first to occur on a previously protonated bpz, the absorption spectrum blue shifts.

As opposed to the case of $[Ru(bpz)_3]^{2+}$, all the spectral changes in the region of pH 3.0 to 4.0 for $[Ru(qpy)_3]^{2+}$ result in shifting the spectra to lower energy - no blue shift is observed. Because the emission spectrum *does* blue shift (see below), it is a further indication that the spectral changes leading to the final three protonations of $[Ru(qpy)_3]^{2+}$ are not observed. This, of course, assumes that shifts in the absorption and emission spectra will occur in the same direction. The contrary has not been observed in all the Ru(II) tris-diimine complexes prepared to date.

Excited State Acidity Constants of $[Ru(qpy)_3]^{2+}$

In aqueous solution above pH 6, $[Ru(qpy)_3]^{2+}$ is strongly luminescent with the maximum residing at 635 nm. The intensity of the emission remains nearly constant as the solution acidity is increased until a pH of 5.5 is reached. Between pH 5.5 and 4.3, there is a loss of emission intensity, but no detectable shift of the emission maximum. (Figure 10). Plotting the emission intensity at 635 nm vs pH through this pH range gives the titration curve in Figure 11. From the plot an inflection point at 4.4 can be calculated. The experimental data can be fitted assuming two pK_a's at 5.2 and 4.1. Between pH 4.2 and 3.1, the spectrum shifts to the red, and at approximately pH 3.7 the spectral maximum reaches its lowest energy at 657 nm (Figure 12). From pH 3.4 to 68% sulfuric acid, the spectral maximum continually shifts to higher energy (Figures 13, 14, 15 and 16), and in 68% sulfuric acid the maximum occurs at 637 nm (Figure 16). The spectral changes at 310 nm and between pH 3.43 and 2.00 were analyzed. From the titration curve, a single inflection point at 3.4 pK units is calculated. Because the curve could not be successfully fitted, this value may, or may not, represent a single acidity constant.

These results closely parallel those obtained by Lever[168] for the protolytic equilibria of $[Ru(bpz)_3]^{2+}$. In neutral solution, $[Ru(bpz)_3]^{2+}$ emits at 595 nm. As the solution acidity is increased, the intensity of the emission decreases and broadens. From the decrease in emission intensity,

the first excited state pK_a is calculated to be 3.80. As the emission at 595 nm is quenched, a new emission at 717 nm begins to appear. From this emission a second pK_a^* is calculated as –2.2. Increasing the solution acidity further results in a rapid increase in emission intensity, which reaches a maximum in 96% sulfuric acid. Accompanying this growth of emission intensity is a shift to higher energy of the maximum to 620 nm. A third pK_a^* is calculated to be –8.6, which is assigned as pK_{a1}^* (the equilibrium between the pentaprotonated and the hexaprotonated complexes). In their study it was only possible to calculate these three excited state acidity constants for the $[Ru(bpz)_3]^{2+}$ cation.

It is significant that for both $[Ru(bpz)_3]^{2+}$ and $[Ru(qpy)_3]^{2+}$, only three different emission maxima are observed: 595, 717 and 620 nm for $[Ru(bpz)_3]^{2+}$ and 635, 657 and 637 nm for $[Ru(qpy)_3]^{2+}$.

All known ruthenium tris diimine complexes emit from the lowest excited state, and in heteroleptic complexes, from the MLCT state associated with the ligand bearing the lowest energy π^* orbital. On this basis it is reasonable to expect that all possible species resulting from protonation of complexes of the type $[Ru(L)_3]^{2+}$ (where L is an α-diimine ligand, having two basic sites) would show a maximum of only *three* distinct emission maxima. Species possessing a di-protonated L would show an emission associated with this ligand, having the lowest π^*. Those having a mono- but no di-protonated L would show an emission associated with mono-protonated L. Only in the free base, $[Ru(L)_3]^{2+}$, would an emission associated with free L be observed. The myriad of observed emission maxima would then simply be weighted sums of these three wavelengths.

The quenching of the emission from $[Ru(qpy)_3]^{2+}$ at 635 nm allows the calculation of two pK_a^*'s as 5.2 and 4.1. In agreement with the results for $[Ru(bpz)_3]^{2+}$, the last two excited state acidity constants (first two protonations) are greater than their ground state counterparts. This is expected, due to the increased electron density on the ligand following MLCT excitation. Decreasing the pH further increases the concentration of species containing a mono-protonated

quaterpyridyl. The emission spectrum red shifts and increases in intensity, but the intensity remains far weaker than that associated with the free base, $[Ru(qpy)_3]^{2+}$. At pH 3.7, the spectrum is at its lowest energy point (657 nm), and then begins to blue shift with decreasing pH. Emission from species containing di-protonated quaterpyridyl ligands start to dominate. In this interpretation, the inflection point at 3.4 pK units is not a distinct pK_a, but rather the point where concentration of mono–protonated quaterpyridyl containing species is equal to the concentration of di-protonated species. The blue shift of the ligand to metal charge transfer (LMCT) emission in diprotonated species, also observed by Lever[158] with $[Ru(bpz)_3]^{2+}$, is a curious result, that at present eludes a satisfying explanation.

Cyclic Voltammetry

Oxidation and reduction potentials for $[Ru(qpy)_3]^{2+}$ and $[Ru(qpyme)_3]^{6+}$ were measured by cyclic voltammetry in 0.1 M tetrabutylammonium tetrafluoroborate DMF at a Pt disk working electrode. Their electrochemical potentials, as well as potentials for some other complexes, are given in Table IV. All waves were found to be reversible as defined by the criteria described in the experimental section (Chapter XIII).

The oxidation potentials of $[Ru(qpy)_3]^{2+}$ and $[Ru(qpyme)_3]^{6+}$ (1.49 and 1.44 V respectively) are higher than that of $[Ru(bpy)_3]^{2+}$ (1.26[3b]), but less than those of other tris-diimine Ru(II) complexes containing π deficient heterocycles such as $[Ru(bpm)_3]^{2+}$ (1.69[3b]) and $[Ru(bpz)_3]^{2+}$ (1.86[3b]), where bpm = 2,2'-bipyrimidine and bpz = 2,2'-bipyrazine. This suggests that the t_2 orbitals of these two quaterpyridyl complexes are stabilized relative to $[Ru(bpy)_3]^{2+}$, and destabilized relative to $[Ru(bpm)_3]^{2+}$ and $[Ru(bpz)_3]^{2+}$.

The first reduction potential of $[Ru(qpy)_3]^{2+}$ occurs at –0.96 V, which is less negative than the first reduction in $[Ru(bpy)_3]^{2+}$ (-1.27[3b]). As expected the π^* of the coordinated quaterpyridyl is lower in energy than that of 2,2'-bipyridine in $[Ru(bpy)_3]^{2+}$, but higher than that of bpm in $[Ru(bpm)_3]^{2+}$ (first reduction potential = -0.91[3b] V) and that of bpz in $[Ru(bpz)_3]^{2+}$ (–0.80[3b] V). The

first reduction of [qpyme]$^{+}$ in [Ru(qpyme)$_3$]$^{2+}$ is lower than that of qpy in [Ru(qpy)$_3$]$^{2+}$, due to the lowering of the ligand π^{*} as a result of quaternization.

Excited State Potentials

Excited state potential diagrams for [Ru(qpy)$_3$]$^{2+}$, [Ru(bpy)$_3$]$^{2+}$, and [Ru(qpyme)$_3$]$^{2+}$ are given in Figures 17 and 18. The strongest excited state oxidant, and weakest excited state reductant is [Ru(qpyme)$_3$]$^{2+}$. [Ru(qpy)$_3$]$^{2+}$ is a stronger excited state oxidant, but a weaker excited state reductant than [Ru(bpy)$_3$]$^{2+}$.

Table I. Absorption Spectral Data.

Complex	$\lambda_{max.}$
$[Ru(qpy)_3]^{2+}$	476 (Sh. 440)
	358
	308
$[Ru(qpyme)_3]^{2+}$	492
	410
	320
$[Ru(qpyme_2)_3]^{2+}$	496
	417
	324

All spectra recorded in aqueous solution.

Table II. Emission Data.

Complex	$\lambda_{Max.}$ (nm)	ϕ	Conditions
$[Ru(qpy)_3]^{2+}$	635	0.055	MeOH, Air, 25°
	635	0.14	MeOH, N_2, 25°
	617		MeOH, 77 K
$[Ru(qpyme)_3]^{2+}$	680(Sh. 715)	0.0074	MeOH, Air, 25°
	650(Sh. 715)	0.055	MeOH, N_2, 25°
	650		MeOH, 77 K

Table III. pK_a Data for Ruthenium Quaterpyridyl Complexes.

Complex	pKa	pKa*
$[Ru(qpy)_3]^{2+}$	4.2, 3.9, 3.7	5.2, 4.0
$[Ru(bpy)_2qpy]^{2+}$	4.2, 3.5	5.0
$[Ru(bpy)_2qpyme]^{2+}$	3.9	-- [a]

[a] Not measured

Table IV. Electrochemical Data

Complex	Oxidation	Reduction(s)
	$E^{\circ}_{1/2}$ [a]	$E^{\circ}_{1/2}$ [a]
$[Ru(qpy)_3]^{2+}$	1.49	-0.96, -1.14, -1.36
$[Ru(qpyme)_3]^{2+}$	1.44	-0.69, -0.96, -1.28
$[Ru(bpy)_3]^{2+}$ [b]	1.26	-1.31
$[Ru(bpz)_3]^{2+}$ [b]	1.86	-0.80
$[Ru(phen)_3]^{2+}$ [b]	1.40	-1.41
$[Ru(bpm)_3]^{2+}$ [b]	1.69	-0.91

[a] All potentials in Volts vs. SCE in 0.1 M tetra-n-butylammoniumtetrafluoroborate DMF, with a glassy carbon anode.

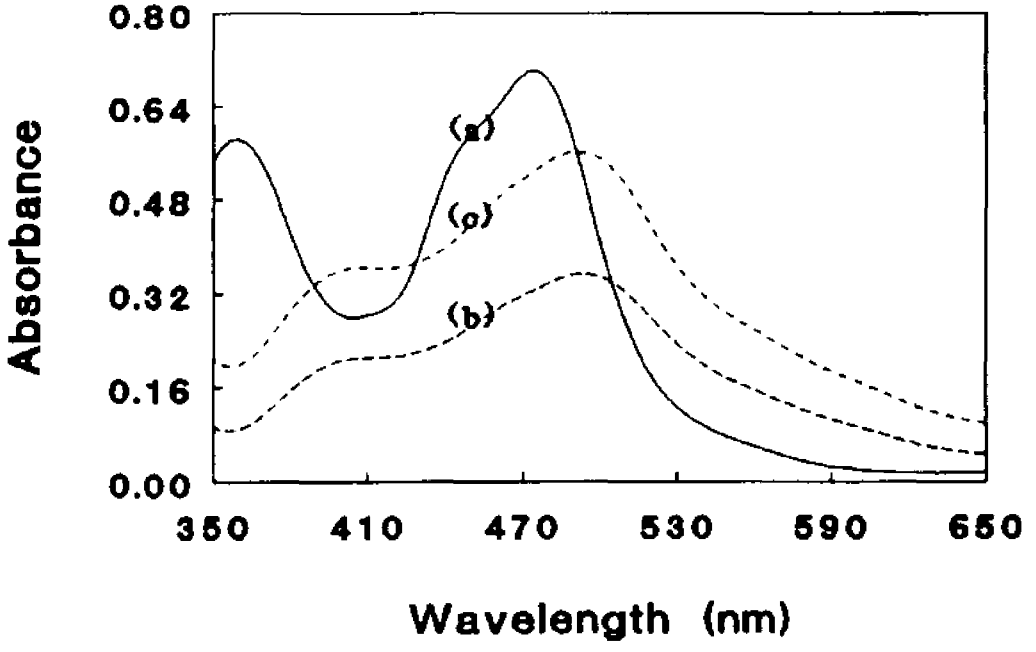

Figure 1. Absorption Spectra of a) $[Ru(qpy)_3]^{2+}$ b) $[Ru(qpyme)_3]^{5+}$ and c) $[Ru(qpyme_2)_3]^{8+}$ in Acetonitrile.

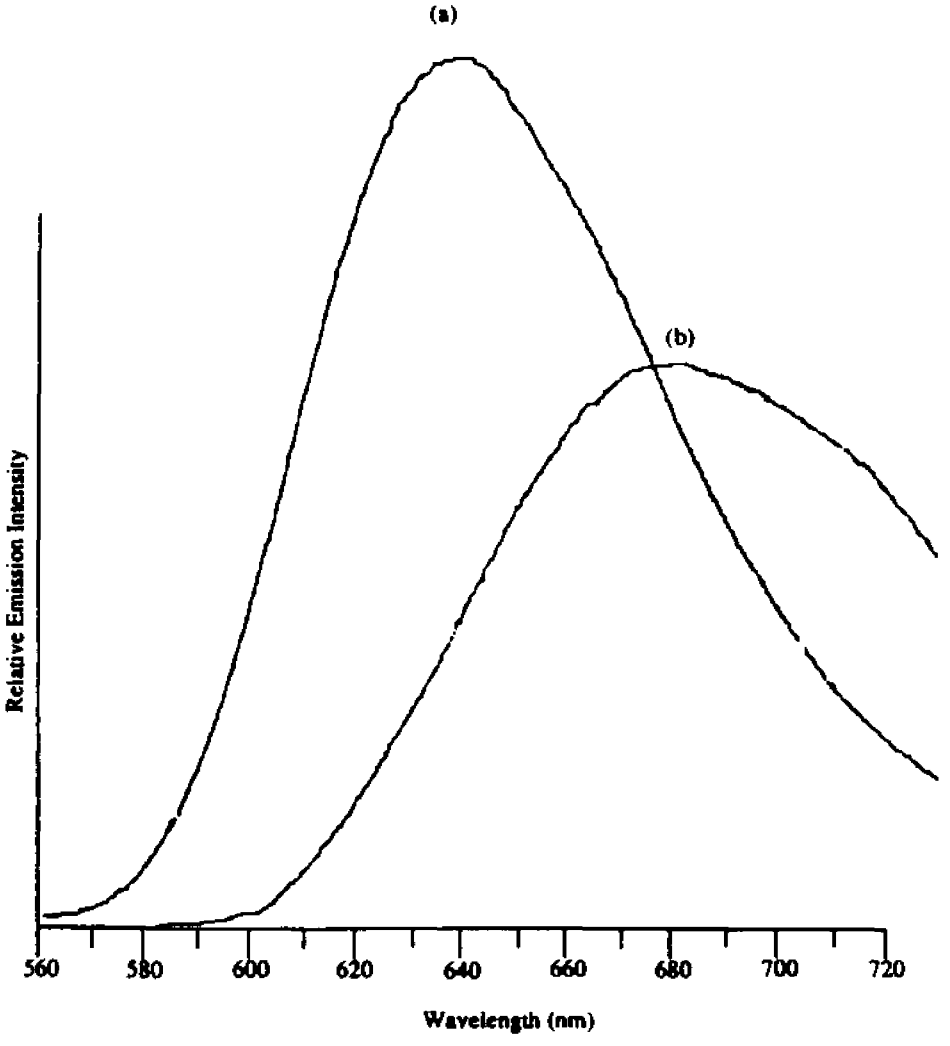

Figure 2. Emission Spectra of a) $[Ru(qpy)_3]^{2+}$ and b) $[Ru(qpyme)_3]^{5+}$ in Water, λ_{exc} = 450 nm (Intensities Do not Reflect Quantum Yields).

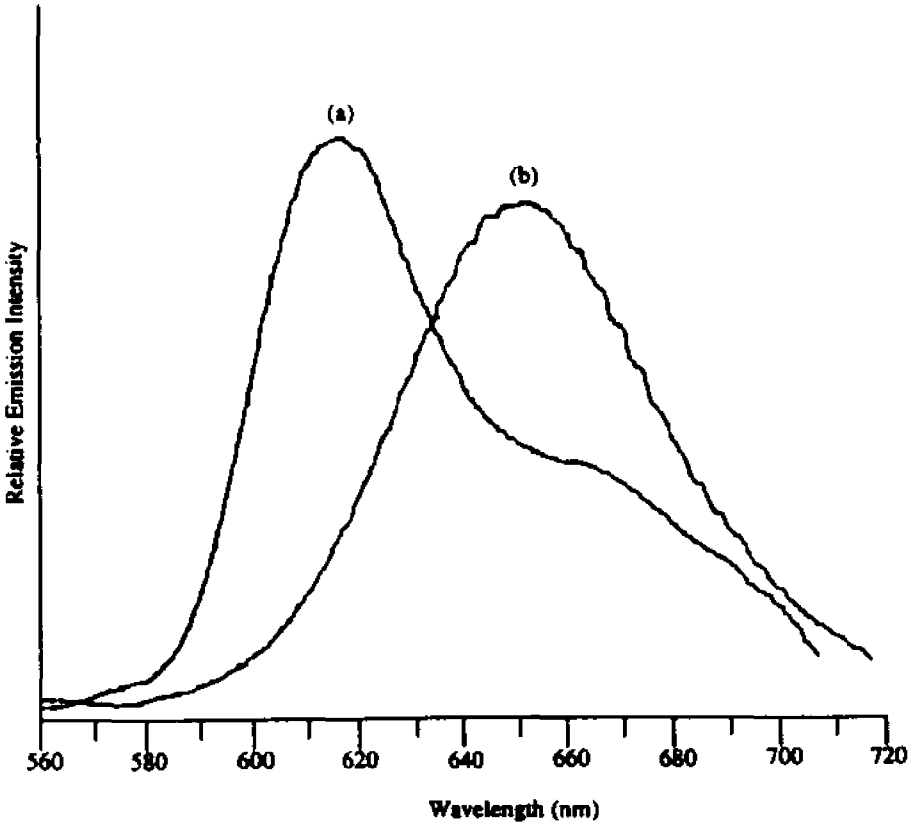

Figure 3. Emission Spectra of a) $[Ru(qpy)_3]^{2+}$ and b) $[Ru(qpyme)_3]^{5+}$. λ_{ext} = 450 nm, at 77 K (Intensities Do not Reflect Quantum Yields).

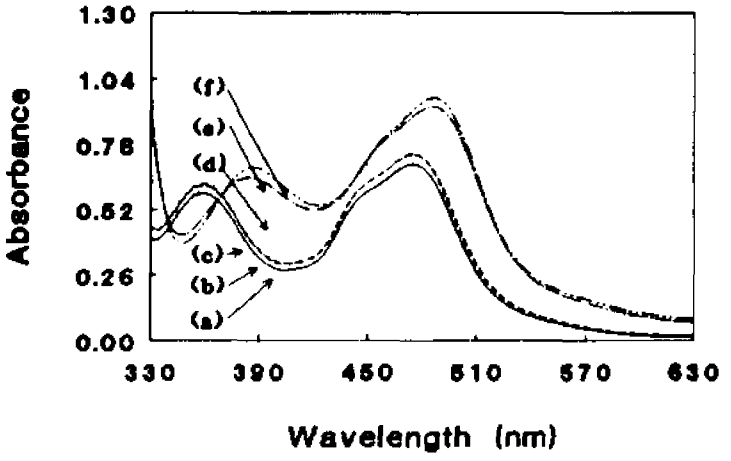

Figure 4. Absorption Spectra of $[Ru(qpy)_3]^{2+}$ at pH a) 7.26 b) 6.02 c) 4.98 d) 4.02 c) 3.06 and d) 1.83.

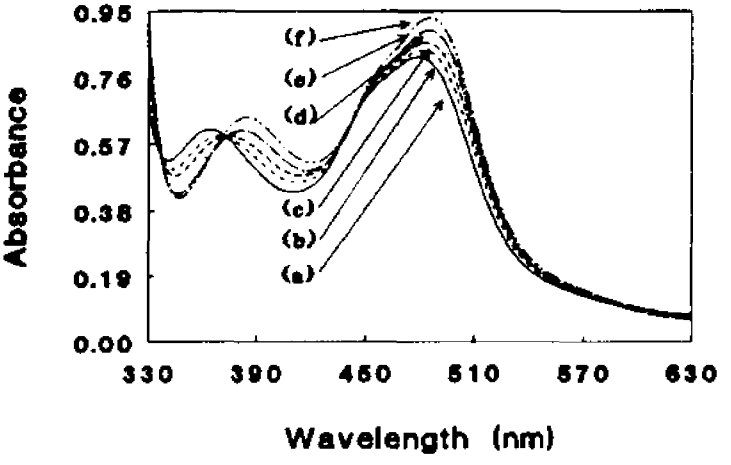

Figure 5. Absorption Spectra of $[Ru(qpy)_3]^{2+}$ at pH a) 4.02 b) 3.82 c) 3.67 d) 3.48 e) 3.34 and f) 3.06.

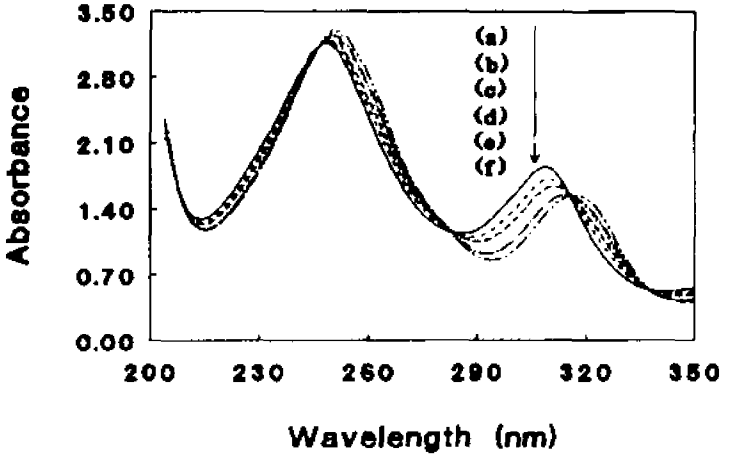

Figure 6. Absorption Spectra of $[Ru(qpy)_3]^{2+}$ at pH a) 4.02 b) 3.82 c) 3.67 d) 3.48 e) 3.34 and f) 3.06.

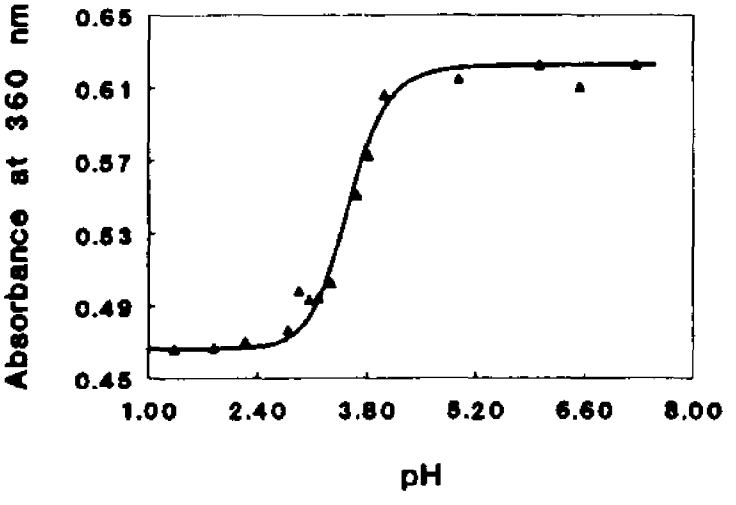

Figure 7. Titration Curve for $[Ru(qpy)_3]^{2+}$.

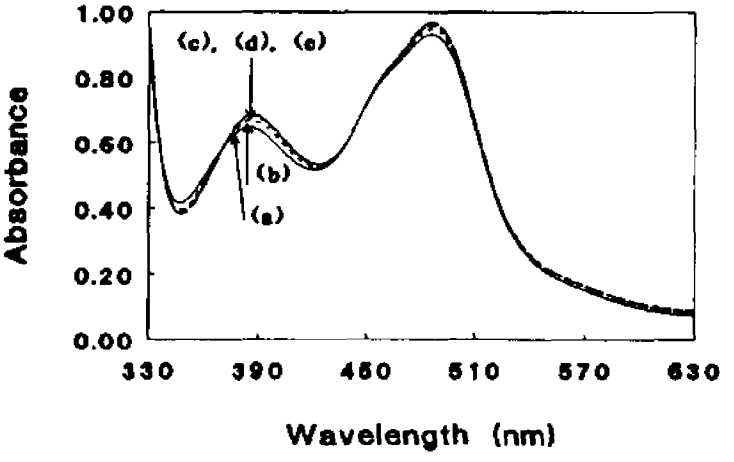

Figure 8. Absorption Spectra of a) $[Ru(qpy)_3]^{2+}$ at pH a) 2.93 b) 2.79 c) 2.24 d) 1.83 and e) 1.33

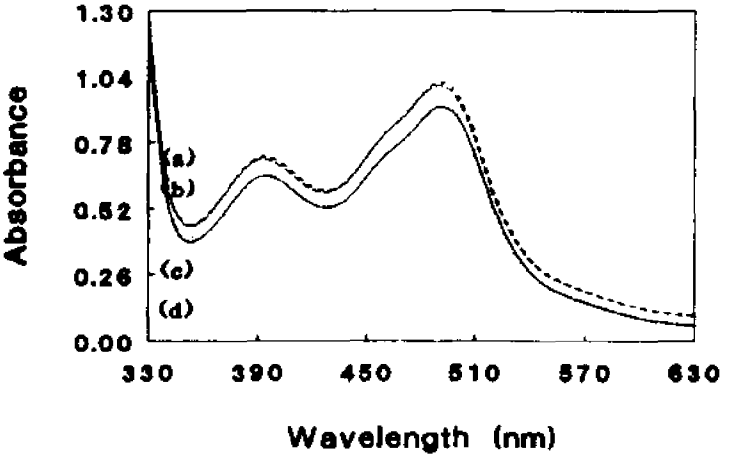

Figure 9. Absorption Spectra of $[Ru(qpy)_3]^{2+}$ in a) 14.4 b) 29.4 c) 39.2 and d) 49.0 %Sulfuric Acid.

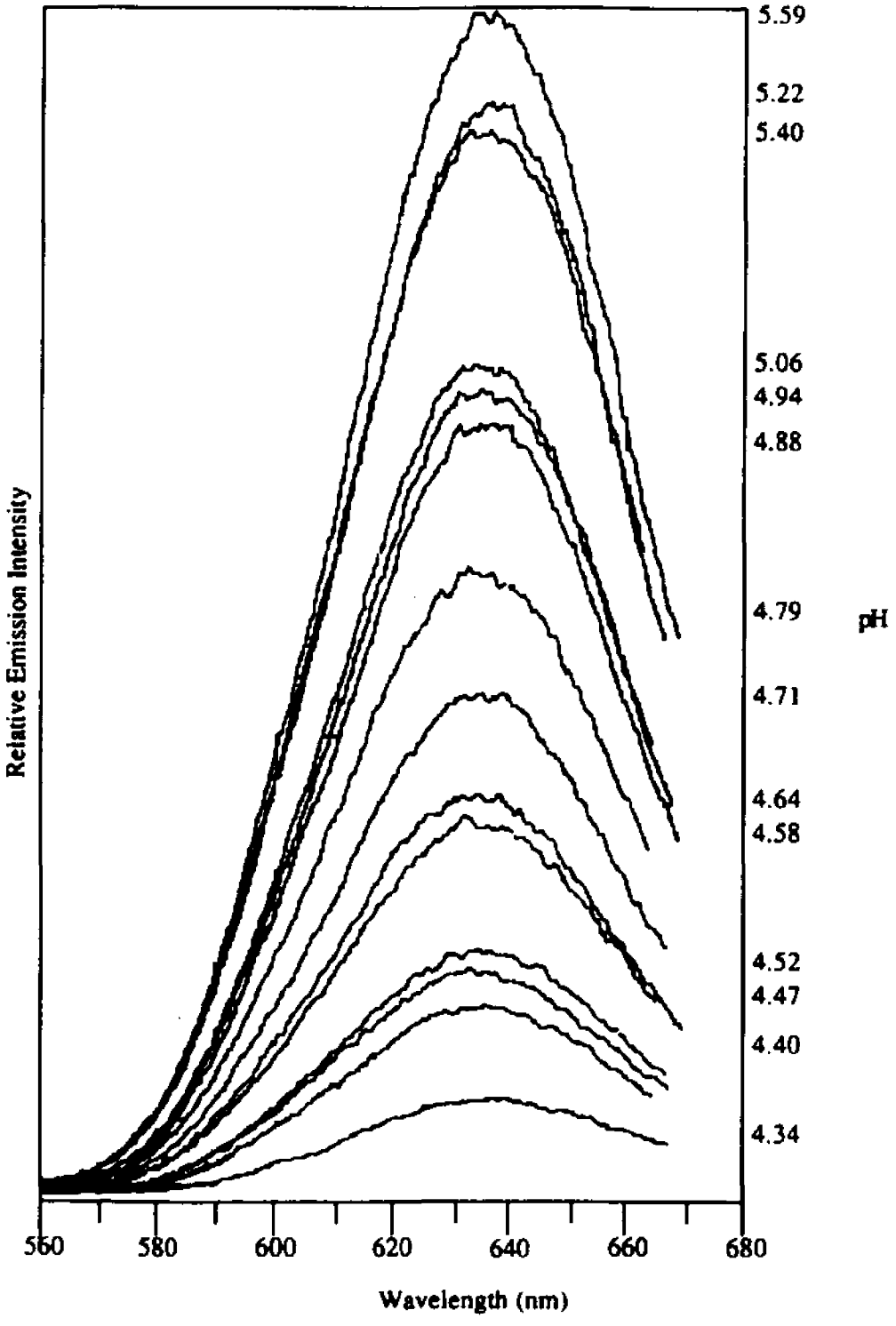

Figure 10. Luminescence Spectra of $[Ru(qpy)_3]^{2+}$ (pH Values Given on Figure).

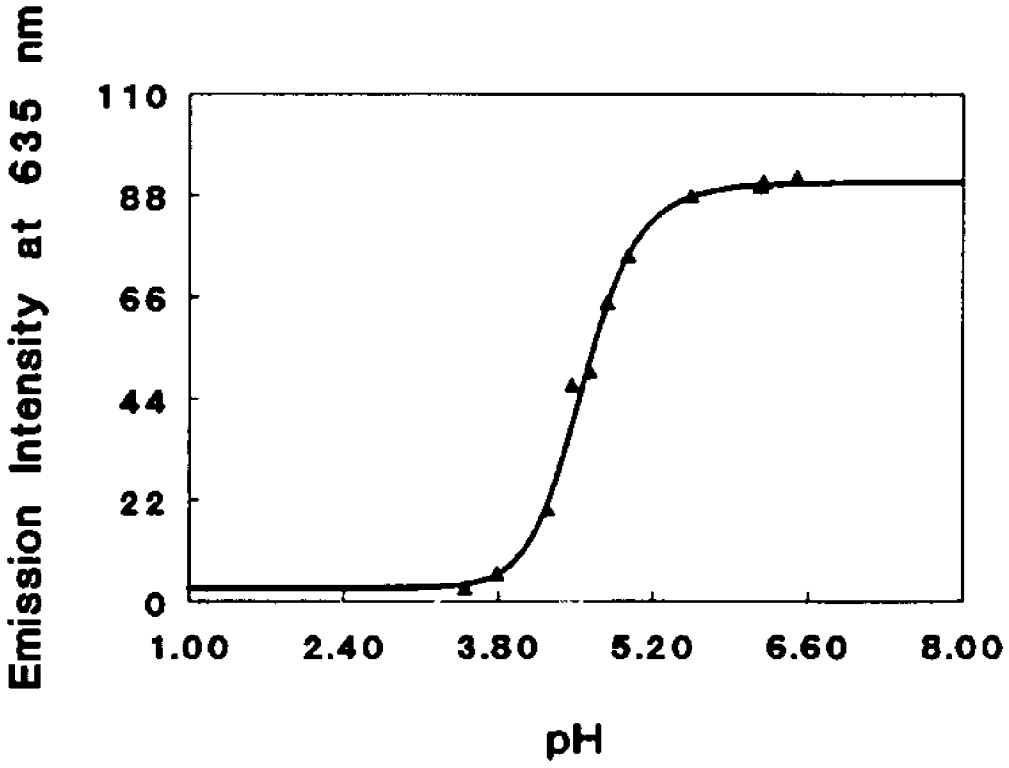

Figure 11. Luminescence Titration Curve for $[Ru(qpy)_3]^{2+}$.

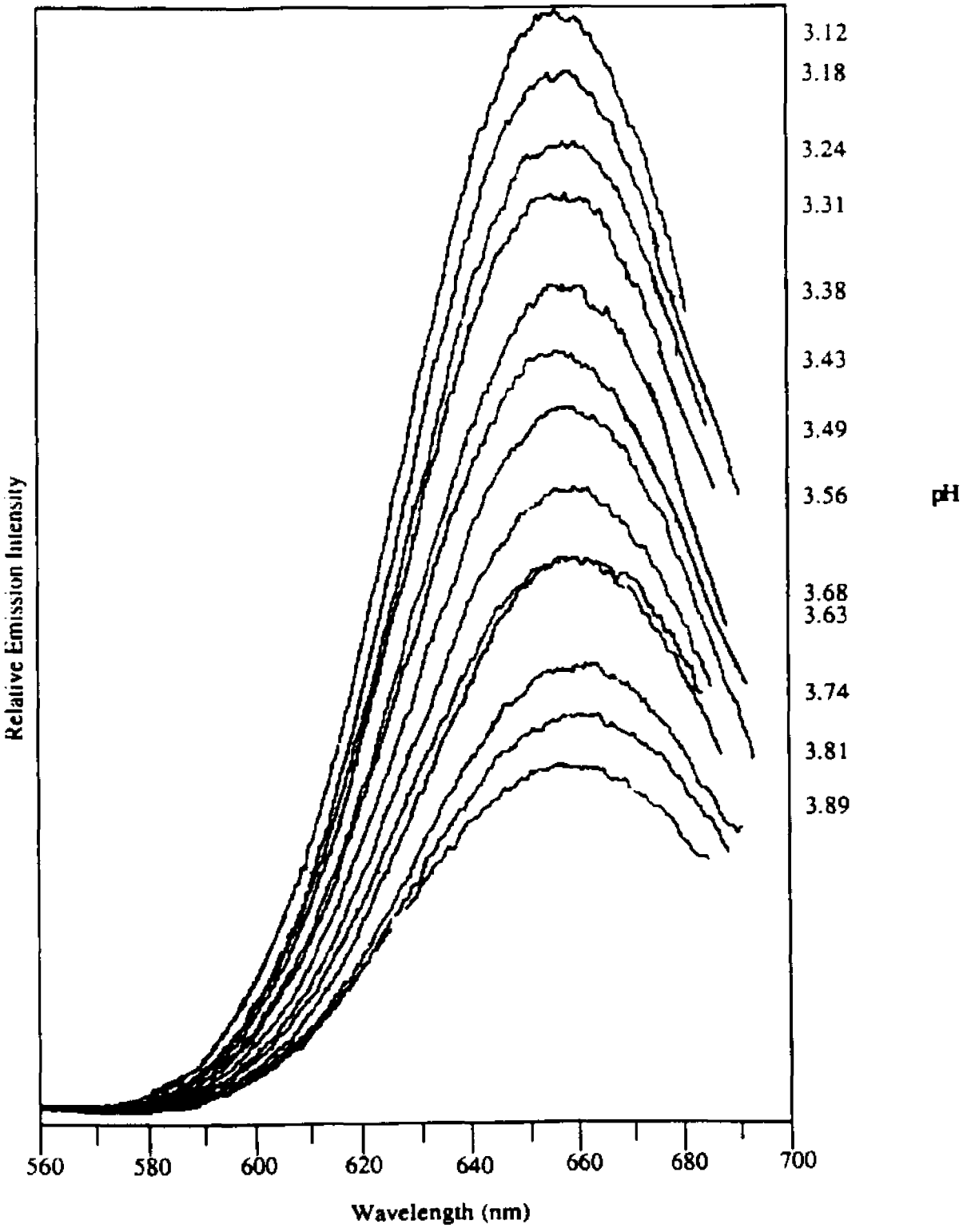

Figure 12. Luminescence Spectra of $[Ru(qpy)_3]^{2+}$ (pH Values Given on Figure).

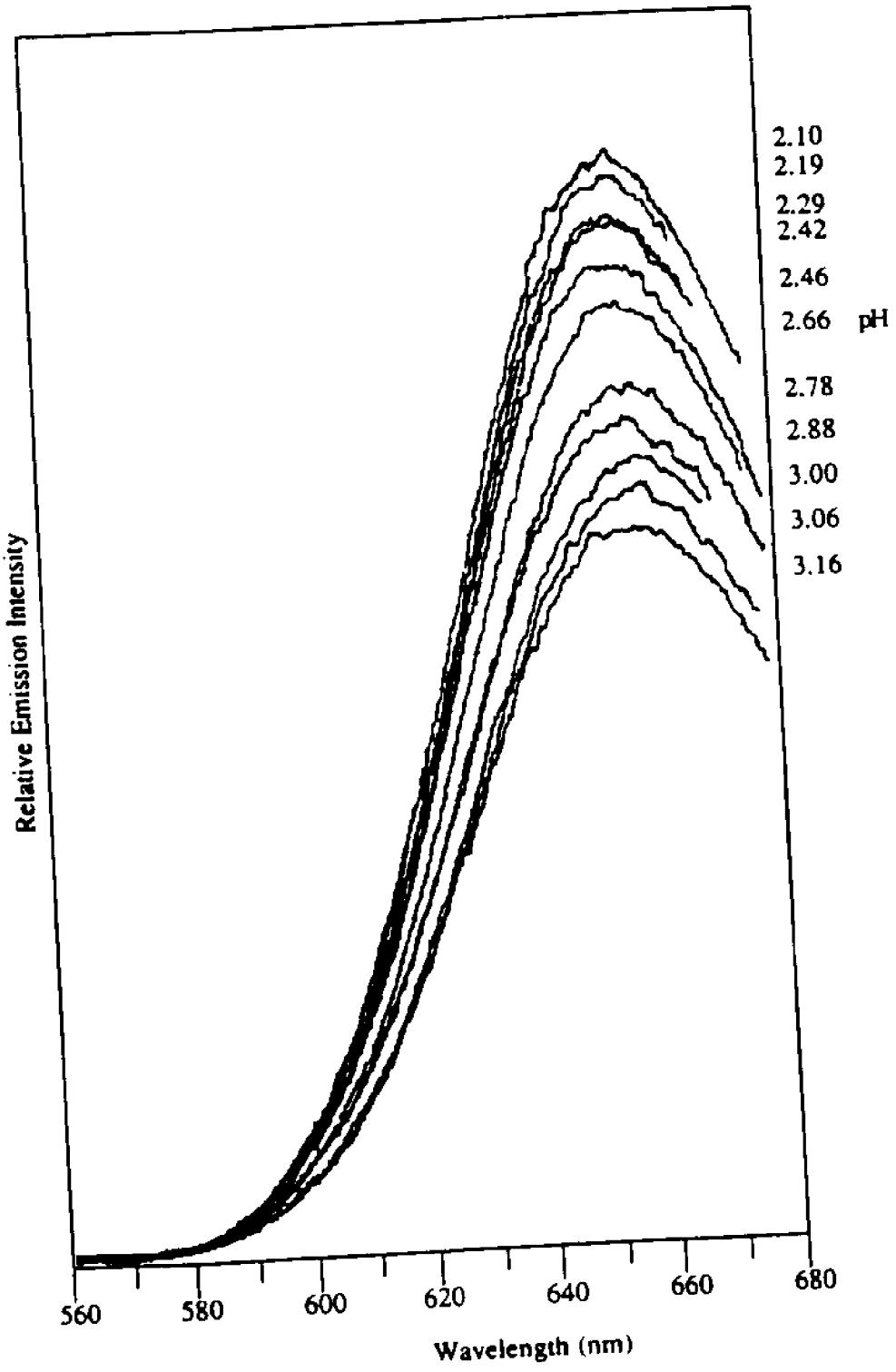

Figure 13. Luminescence Spectra for $[Ru(qpy)_3]^{2+}$.

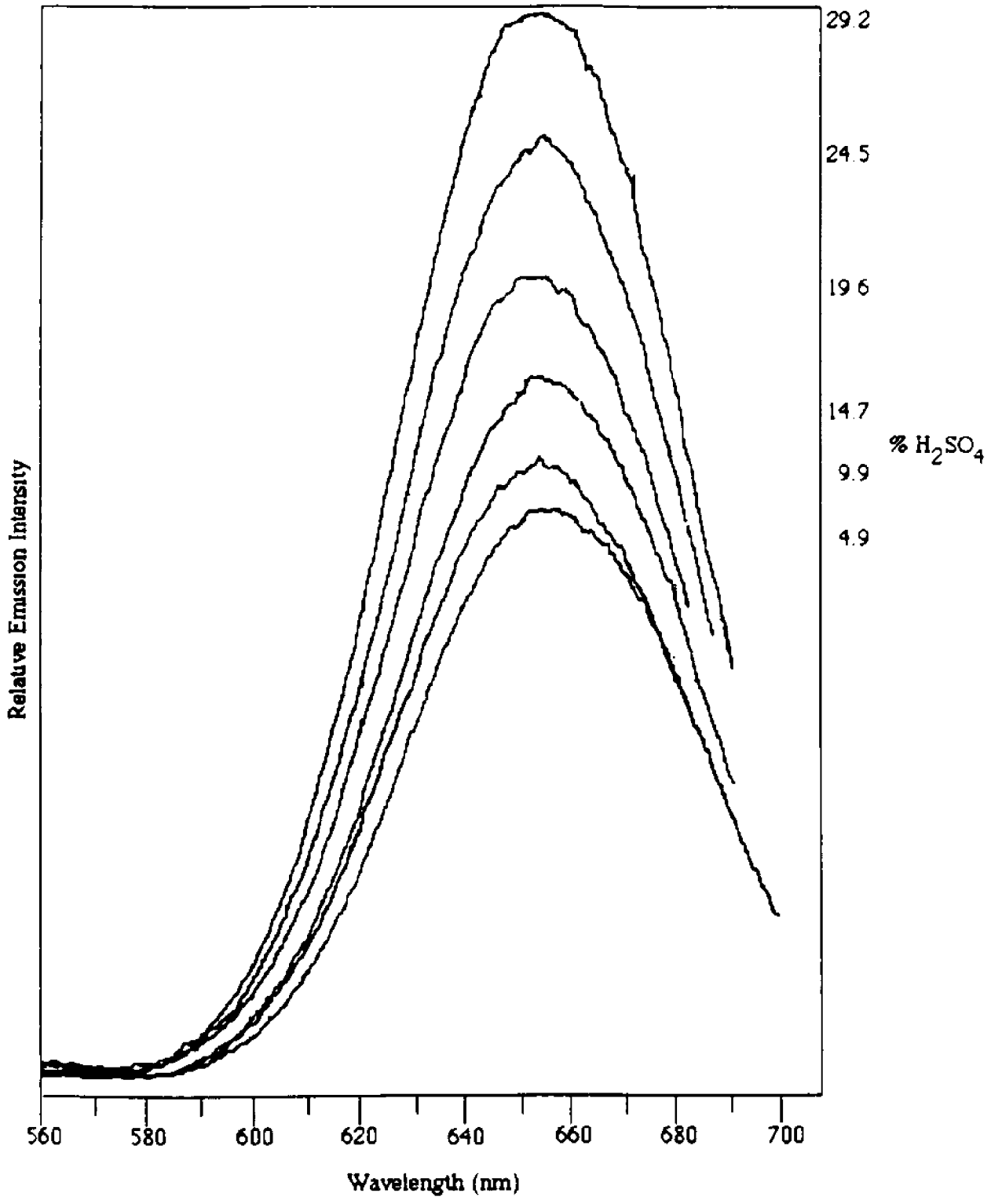

Figure 14. Luminescence Spectra of $[Ru(qpy)_3]^{2+}$ (pH Values Given on Figure).

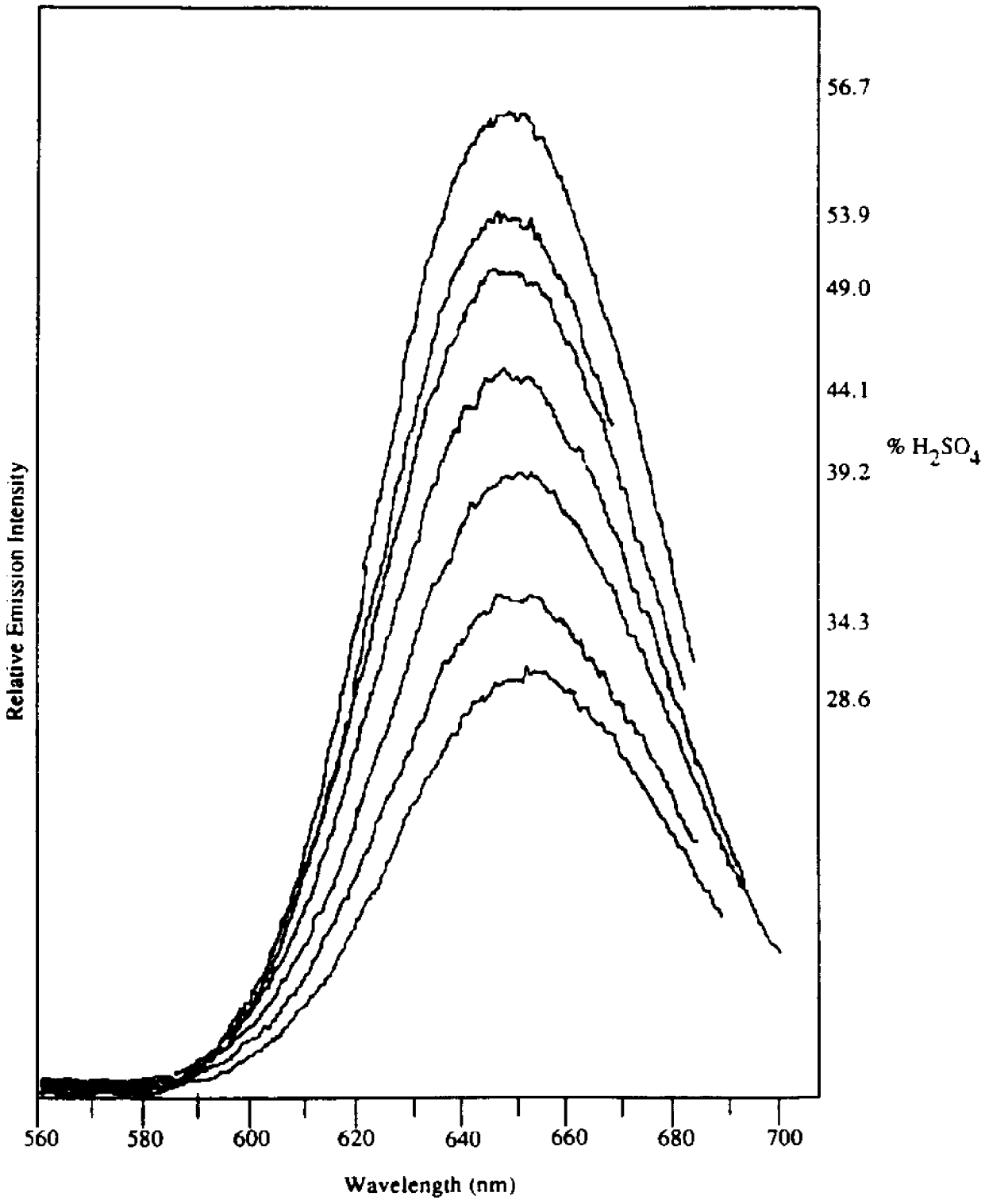

Figure 15. Luminescence Spectra of $[Ru(qpy)_3]^{2+}$ (pH Values Given on Figure).

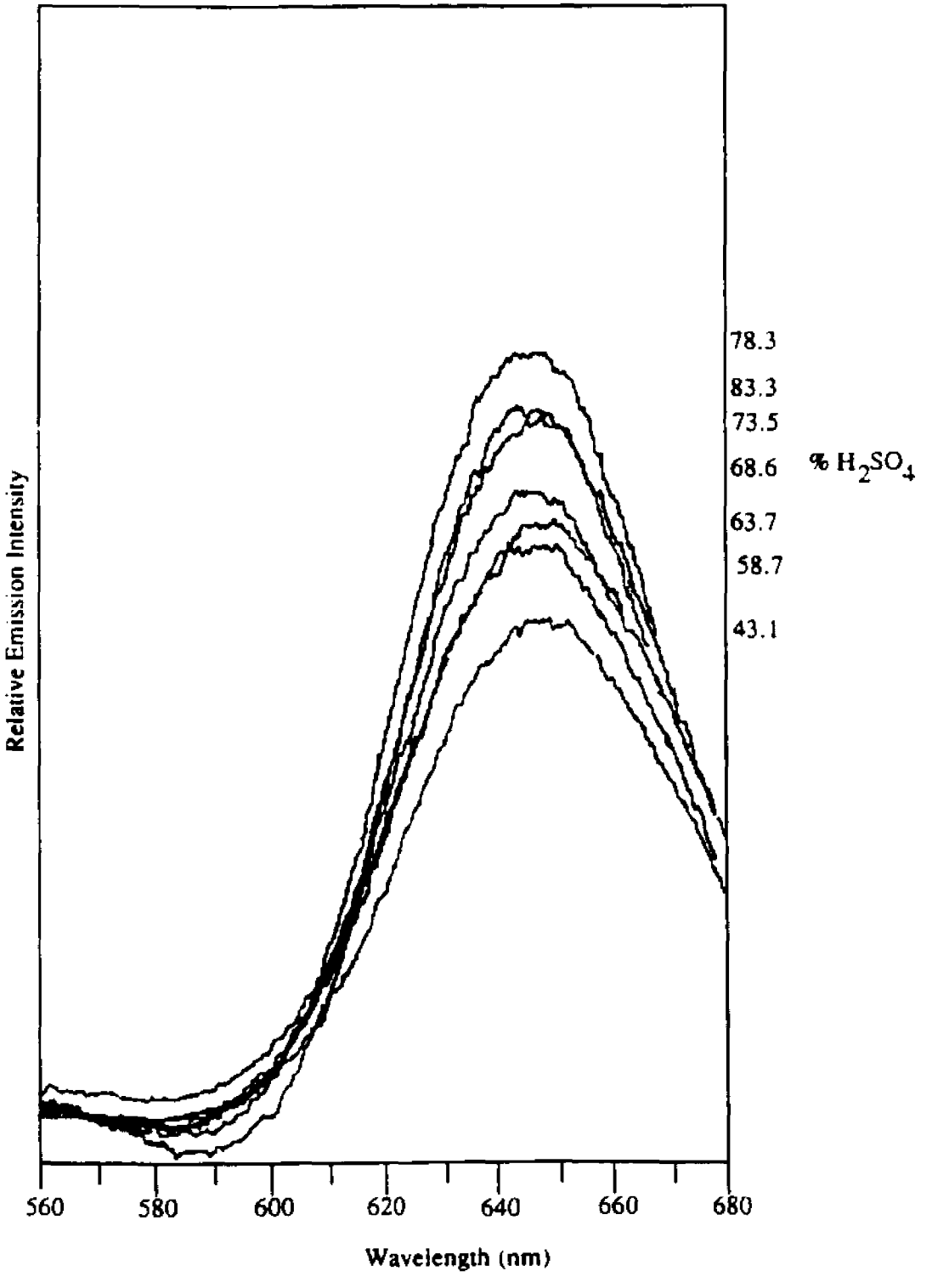

Figure 16. Luminescence Spectra of $[Ru(qpy)_3]^{2+}$ (pH Values Given on Figure).

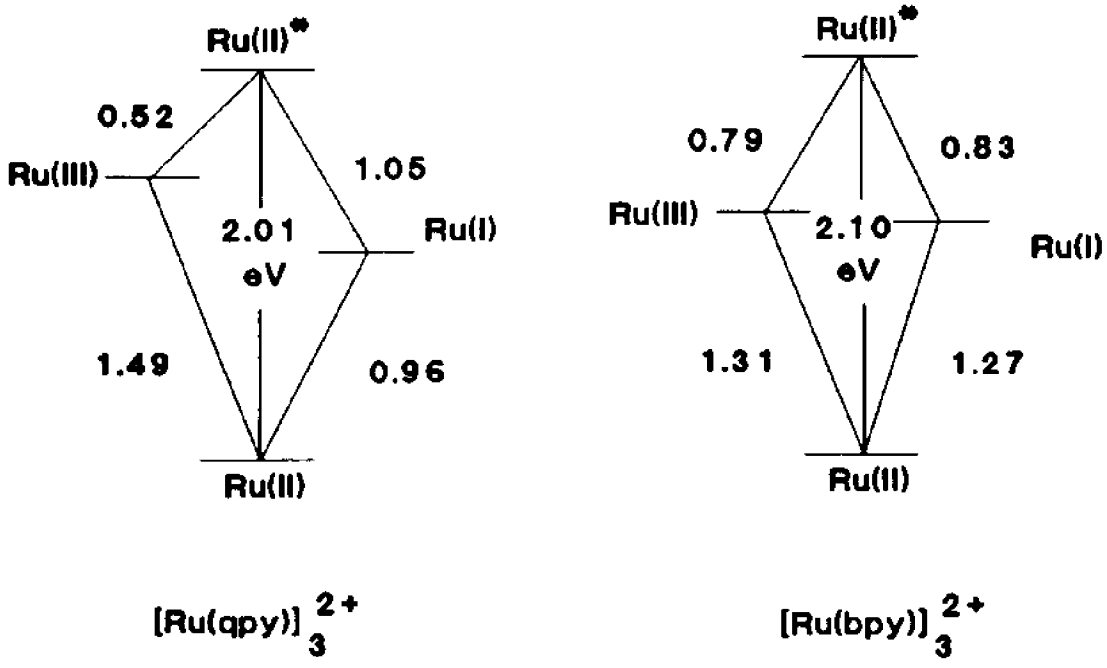

Figure 17. Excited State Potential Diagrams.

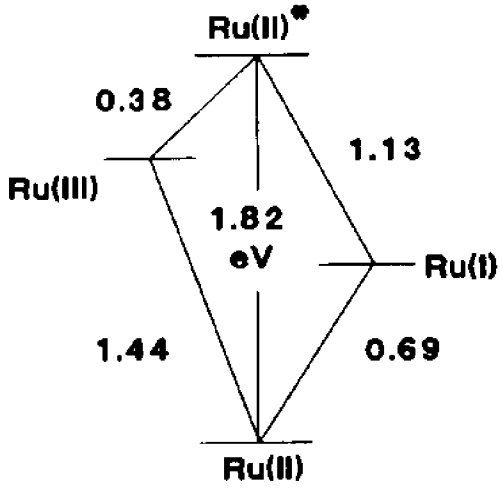

$[Ru(qpyme)]_3^{5+}$

Figure 18. Excited State Potential Diagram.

Chapter IX. Monomeric and Homonuclear Dimeric Ru(II) Complexes Containing 4,7'-Phenanthrolino-5',6':5,6-Pyrazine (ppz)

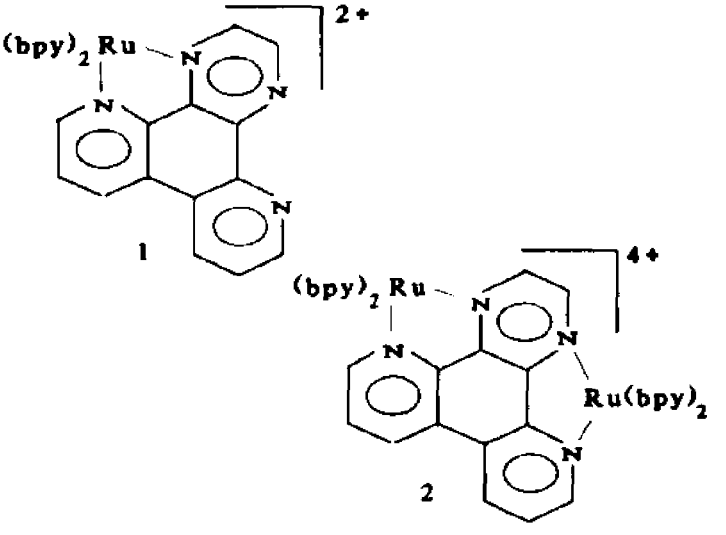

Introduction

Many important redox schemes are multi-electron processes, and a theme in current ruthenium chemistry is the development of systems capable of converting photoinduced single electron transfer events into multielectron transfer reactions. A limitation in the use of the ruthenium(II) tris-2,2'-bipyridine cation, $[Ru(bpy)_3]^{2+}$ as an excited state redox reagent, is its inability to transfer more than one electron in a single encounter with a quencher. One approach is to replace a bpy on $[Ru(bpy)_3]^{2+}$ with a bridging ligand (Chapter II cites several examples), which can bind a second $[Ru(bpy)_2]$ moiety. Because "dimers" of this type contain two Ru(II) chromophores,

they could, in principle, participate in two-photon, two-electron events. This chapter is concerned with the preparation, characterization, photophysics, and electrochemistry of the homonuclear Ru(II) monomeric and dimeric complexes of (1 and 2), including the evaluation of their excited state redox properties.

Results and Discussion

Preparation of compounds

The preparation of the 2,3-di-(2-pyridyl)-pyrazine (dpp) series of complexes has been previously reported[30]. 4,7'-Phenanthrolino-5',6':5,6-pyrazine used in the preparation of the ppz based complexes, was prepared from 4,7'-phenanthroline-5,6-dione (obtained as a gift from Ciba Geigy). The dimeric homonuclear complex, $[(bpy)_2RuppzRu(bpy)_2]^{4+}$, is prepared by refluxing one equivalent of the bridging ppz, with two equivalents of $Ru(bpy)_2Cl_2$ in 50% ethanol. The chloride salt can be prepared directly by column chromatography on the reaction mixture. The column is packed and developed using acetonitrile. After the addition of several volumes of acetonitrile, a red/yellow band, containing $Ru(bpy)_2Cl_2$ elutes first. The monomer $[Ru(bpy)_2ppz]^{2+}$ is eluted next, as a broad yellow band, by adding a small amount of 95% ethanol to the mobile phase. The dimer (a deep purple–blue band) is eluted with 95% ethanol. The hexafluorophosphate salt of the dimer $[(bpy)_2RuppzRu(bpy)_2]^{4+}$ can be prepared by filtering the reaction mixture into saturated ammonium hexafluorophosphate, and using column chromatography as above for the chloride salt. When pure, the dimer is a blue crystalline solid. It is stable for extended periods of time (samples several years old show no signs of decomposition) as a crystalline solid, in solution and when adsorbed onto porous Vycor glass. As the hexafluorophosphate salt, the dimer is soluble in polar aprotic solvents, including acetonitrile, DMF, and acetone; the chloride salt is highly water soluble.

The monometallic complex $[Ru(bpy)_2ppz]^{2+}$ is best prepared by refluxing an excess of the ppz ligand with one equivalent of $Ru(bpy)_2Cl_2$ in aqueous ethanol. Without an excess of the

bridging ligand, as much as 80% dimer is isolated. Varying the reaction time does not improve the monomer/ dimer ratio. The progress of the reaction can be followed by thin layer chromatography (Alumina, ethanol or acetonitrile). Spots due to both the dimer, and the monomer appear almost immediately upon reflux. The monomer/dimer ratio can be maximized by slowly adding an ethanolic solution of $Ru(bpy)_2Cl_2$ to ppz (in 95% ethanol) at reflux. The work-up used for the monomer is identical to that for the dimer. The solubility and stability of $[Ru(bpy)_2ppz]^{2+}$ is similar to its dimeric analog.

Absorption Spectra

Complexes of the type $[Ru(bpy)_2L]^{2+}$ (where L is an α-diimine ligand) generally give two bands in the visible region of the spectrum, one of which is usually between 410 and 430 nm. The independence of the energy of this band through a wide range of L, leads to the conclusion that the band is due to a transition terminated on a bipyridine. This assignment has often been confirmed by resonance Raman spectroscopy (see reference 31, for an example). The other band is a MLCT transition terminated on the L ligand, and is usually observed at lower energy than the bipyridine band, as most L studied have a lower LUMO energy than does bipyridine. The absorption spectra of $[Ru(bpy)_2ppz]^{2+}$ and $[(bpy)_2RuppzRu(bpy)_2]^{4+}$ are shown in Figure 1. Both complex ions have a transition in the bipyridine region (420 and 418 respectively). The transition in the monomer to a π^* orbital on ppz occurs at 474 nm, and appears as a shoulder to the 420 nm absorption. In the dimer, the low energy band, terminated on ppz occurs at 573 nm, and both bands are well resolved in the spectrum. In the dimer the π^* of the bridging ligand is 3600 cm^{-1} lower in energy than in the monomer. This is not a large drop when compared with other bridging ligands in complexes of the type $[(bpy)_2Ru–BL–Ru(bpy)_2]^{4+}$. For example, when BL = 2,2'-bipyrimidine[27] or 4,4'-dimethyl-2,2'-bipyrimidine[28], the π^* orbitals of these bridging ligands are lowered 8290 cm^{-1} and 6780 cm^{-1}, respectively. The 3600 cm^{-1} value is similar to that obtained for the complex, $[(bpy)_2RudppRu(bpy)_2]^{4+}$ (2230 cm^{-1})[30].

Cyclic Voltammetry

Half wave potentials for the ppz monomer **1** and dimer **2**, as well as some other related complexes are given in Table I. The voltammogram of $[(bpy)_2RuppzRu(bpy)_2]^{4+}$ is shown in Figure 2. From the criteria discussed in the experimental section (Chapter XIII), all waves in the ppz and dpp voltammograms, both oxidations and reductions, involve a single electron. Because the free ppz and dpp ligands have no oxidations below +2.0 V, the oxidations in the all the complexes are assigned to the removal of an electron from a metal centered t_2 orbital. $[(bpy)_2RuppzRu(bpy)_2]^{4+}$ and $[(bpy)_2RudppRu(bpy)_2]^{4+}$, each with two metal centers, have two oxidation waves; $[Ru(bpy)_2ppz]^{2+}$ has one. The potentials for the first oxidations of these dimers, and the single oxidation of their respective monomers are similar, indicating there is no significant perturbation imposed on the metal t_2 orbitals by the addition of another $[Ru(bpy)_2]$ unit to the monomer to form the dimer. That is, in both $[(bpy)_2RuppzRu(bpy)_2]^{4+}$ and $[(bpy)_2RudppRu(bpy)_2]^{4+}$ the metal centers are only weakly coupled. In comparison, the extent of coupling in the dimers of bipyrimidine[27] (bpym) and 4,4′-dimethyl–bipyrimidine[28] (dmbpm) is large. The first oxidation of $[(bpy)_2RubpmRu(bpy)_2]^{4+}$ occurs at +1.50 V and its monomer at +1.33 V; those of the monomer/dimer of dmbpm occur at 1.22 and 1.40 V respectively.

Reduction waves in ruthenium polypyridine complexes represent the addition of electrons into ligand centered π^* orbitals. Typically, a single reversible couple for each ligand is observed. In the case of $[Ru(bpy)_2dpp]^{2+}$, the first reduction occurs on the dpp ligand, having a lower energy LUMO than bipyridine, and occurs at -1.14 V. The second and third reductions are assigned to the sequential reductions of the coordinated bipyridines (-1.53 and -1.74 V). The first reduction of the dpp dimer occurs at -0.71 V. Appending the second metal center, significantly lowers the LUMO of the bridging dpp. The same trend can be observed for the monomers and dimers of ppz. The first reduction potentials of the monomer and dimer are -1.11 and -0.71 V respectively.

These electrochemical results indicate that the second metal center in both

$[(bpy)_2RudppRu(bpy)_2]^{4+}$ and $[(bpy)_2RuppzRu(bpy)_2]^{4+}$ behaves as a simple electron withdrawing group. The lowering of the first reduction potential (to more negative values) in each dimer, relative to the monomer, indicates that the LUMO of the bridging ligand is stabilized by the presence of the second metal center. Because there is little difference in the monomer/dimer oxidation potentials, there is only minimal communication between the metal centers in both dimers.

Luminescence Spectra

Monometallic $[Ru(bpy)_2ppz]^{2+}$ is luminescent in fluid solution at room temperature. Excitation between 300 and 500 nm results in a red emission at 700 nm (Figure 3a). Bimetallic $[(bpy)_2RuppzRu(bpy)_2]^{4+}$ also shows a luminescence in fluid solution at approximately 820 nm (Figure 3b). Because, the emission is in a spectral region where the sensitivity of the photomultiplier (RCA C31034) declines rapidly with increasing wavelength, the true maxima may be farther to the red.

It has been generally observed that most bimetallic Ru(II) complexes are not luminescent in fluid solution at room temperature, and $[(bpy)_2RudppRu(bpy)_2]^{4+}$ prepared in our laboratories[30] was in fact the first emissive bimetallic Ru(II) species to be reported. However, it may in fact be the case that earlier dimers that were reported to be non-luminescent emit in a region which is outside the detection limits of most commercial emission spectrophotometers. Figure 4 shows the correlation between emission energy, and the energy of the lowest lying MLCT transition in some bimetallic α-diimine Ru(II) complexes. As the MLCT band shifts to lower energy the emission does the same. This supports the notion that earlier Ru(II)/Ru(II) dimers reported in the literature may emit in a region that is out of the range of most commonly used detectors. Metal-metal interaction plays an important role in the luminescence properties of bimetallic complexes. The bimetallic complex containing dmbpym[28] has its low energy absorption at 578 nm, which is nearly the same as the luminescent ppz dimer, and yet no solution emission has been detected. The presence of another $Ru(bpy)_2$ in a bimetallic species offers an additional pathway for non-radiative decay. The

efficiency of this pathway is dependent on the extent of coupling which exists between the metal atoms. The difference in the first oxidation potentials in the mono- and bi- metallic dmbpym complexes is 180 mv. This difference in the ppz and dpp complexes is 20 and 10 mV respectively. As previously stated, the difference in the first oxidation potential of the dimer and that of the monomer directly reflects the extent of metal-metal interaction. The metal atoms in the bipyrimidine series interact strongly with one another, while the interaction is a minimum in the ppz and dpp dimers. Thus, this pathway for non-radiative decay is less important in the ppz and dpp dimers than it is with those of bpm and dmbpm.

Resonance Raman Spectra

Resonance Raman spectra of $[Ru(bpy)_2ppz]^{2+}$ and $[(bpy)_2RuppzRu(bpy)_2]^{4+}$ are similar to the spectra previously reported for the dpp complexes[30] (not shown). As the excitation wavelength is varied, selective frequencies in the spectra are enhanced. The enhanced vibrations occur on the ligand(s) in the complex which are involved in the MLCT transition closest to the excitation wavelength.

The visible absorption bands in bimetallic $[(bpy)_2RuppzRu(bpy)_2]^{4+}$, are well resolved and with a 488 nm excitation (approximately midway between the bands), the characteristic vibrations of bpy at 1563, 1492, 1317, and 1175 cm^{-1} are evident in the spectrum. With a 562 nm dye laser, the frequencies at 1619, 1582, 1480, 1457, 1252, 1220, and 1196 cm^{-1} are enhanced. The latter set of vibrations, which are within the region of diimine stretching frequencies, are not present in the resonance Raman spectrum of $[Ru(bpy)_3]^{2+}$, and thus can, be assigned to be vibrations of ppz. With 457.9 nm excitation, the bpy vibrations are approximately equal in intensity to those of ppz. The wavelength dependence of the diimine vibration pattern allows an unambiguous assignment of the absorption bands. The low energy band terminates on ppz, and the high energy band on bpy.

Excitation of $[Ru(bpy)_2ppz]^{2+}$ with the 457.9 nm line produces clear enhancement of the bpy

vibration at 1491 cm^{-1}, relative to the ppz vibration at 1532 cm^{-1}. With the 488.0 nm argon laser, ppz vibrations at 1532, 1482, 1257, and 1194 cm^{-1} are enhanced. The absorption bands are not well resolved in $[Ru(bpy)_2ppz]^{2+}$. With 457.9 nm excitation, vibrations due to ppz still dominate the spectrum. As in the case of bimetallic $[(bpy)_2RuppzRu(bpy)_2]^{4+}$, the low energy transition in the absorption spectrum of monometallic $[Ru(bpy)_2ppz]^{2+}$ is an MLCT transition terminated on a ppz, and the high energy band is terminated on a bpy.

Excited state potentials

Excited state potential diagrams for $[(bpy)_2RuppzRu(bpy)_2]^{4+}$ and $[Ru(bpy)_2ppz]^{2+}$ are shown in Figure 5. The method by which the values were calculated is described in the experimental section (Chapter XIII). The bimetallic complexes are weaker excited state reductants than are their monometallic counterparts. Because the energies of the metal t_2 orbitals remain constant, as evidenced by the similarity of monomer and dimer first oxidation potentials, the difference in the $2+^{*}/3+$ for the monomers, as compared to the dimers, is chiefly due to the decrease in energy of the ligand π^* acceptor orbital. However, the dimers of both dpp and ppz are stronger excited state oxidants than are their respective monomers. The decrease of the π^* orbital in the dimers is more than offset by the decrease in their reduction potentials.

Conclusion

Luminescence is a highly useful probe of excited state properties of metal complexes. While Ru(II) monometallic diimine complexes are usually luminescent, there are only a few luminescent bimetallic species. Both monometallic $[Ru(bpy)_2ppz]^{2+}$ and bimetallic $[(bpy)_2RuppzRu(bpy)_2]^{4+}$ are luminescent in fluid solution at room temperature, allowing the simple determination of their excited state redox potentials. Bimetallic $[(bpy)_2RuppzRu(bpy)_2]^{4+}$ is a weak excited state reductant, but a surprisingly strong oxidant.

Table I. Electrochemical data.

	Oxidations	Reductions
Complex	$E^{o'}$	$E^{o'}$
$[Ru(bpy)_2ppz]^{2+}$	1.37	-1.11,-1.67
$[(bpy)_2RuppzRu(bpy)_2]^{4+}$	1.35, 1.52	-0.67, -1.34, -1.57
$[(bpy)_2RuppzPtCl_2]^{2+}$	1.58	-0.43, -1.20, -1.50, -1.70
$[(bpy)_2RudppRu(bpy)_2]^{4+}$	1.33, 1.55	-0.71, -1.16, -1.55
$[Ru(bpy)_2dpp]^{2+}$	1.34	-1.14, -1.53, -1.74

All potentials for 10^{-3} M solutions in acetonitrile containing 0.10 M tetra-n-butylammonium tetrafluoroborate as the supporting electrolyte. Potentials in Volts vs. the SCE.

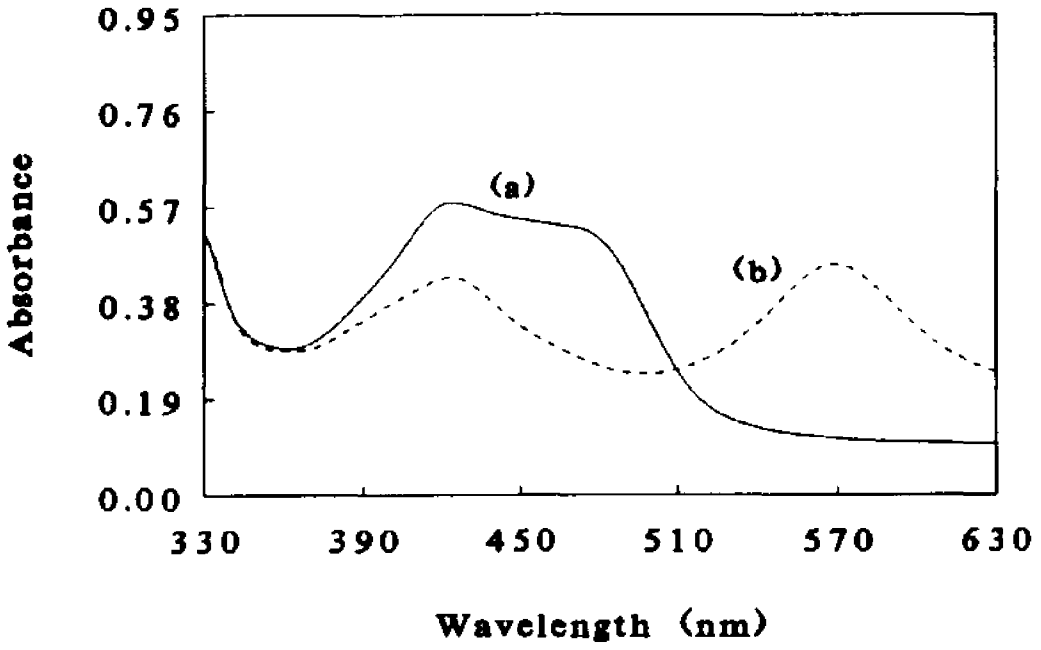

Figure 1. Absorption Spectra of a) $[Ru(bpy)_2ppz]^{2+}$ and b) $[(bpy)_2RuppzRu(bpy)_2]^{4+}$ in Acetonitrile Solution.

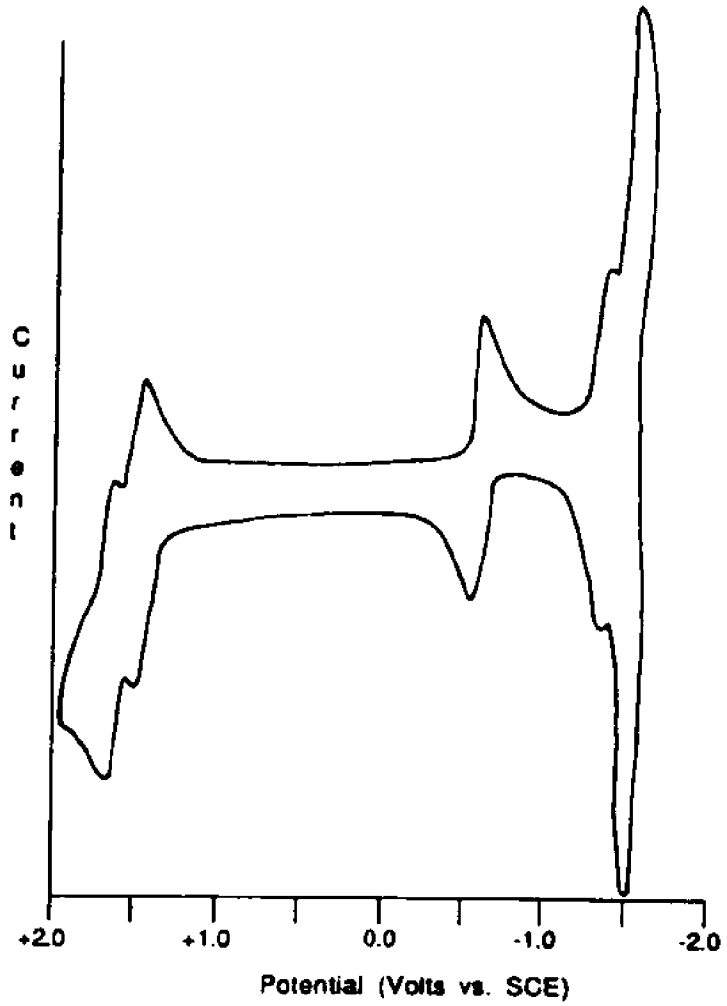

Figure 2. Cyclic Voltammogram of $[(bpy)_2RuppzRu(bpy)_2]^{4+}$ at 200 mv/s Pt Working Electrode in Acetonitrile/ 0.0 M TBAF.

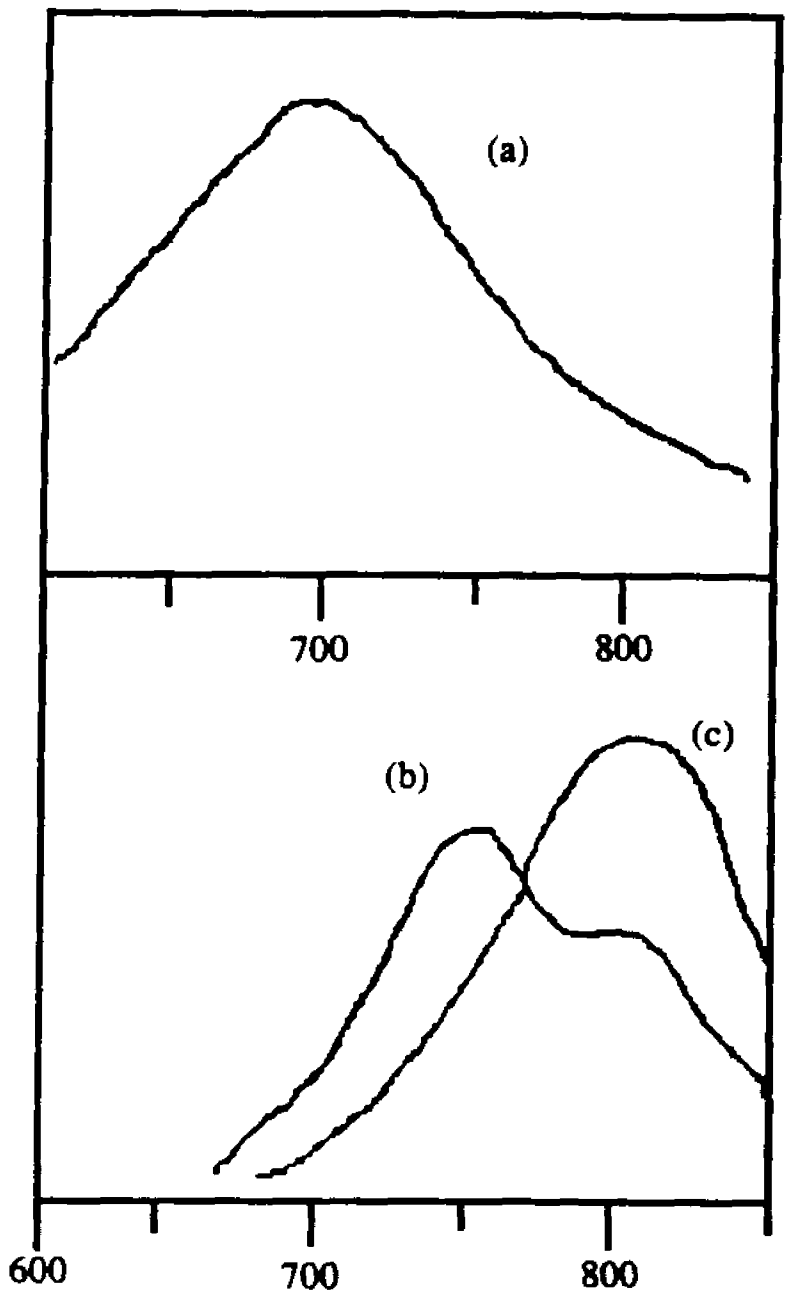

Figure 3. Emission Spectra of a) 1 25°C and b) 2 at 77K in Methanol Glass, and c) 2 at 25°C

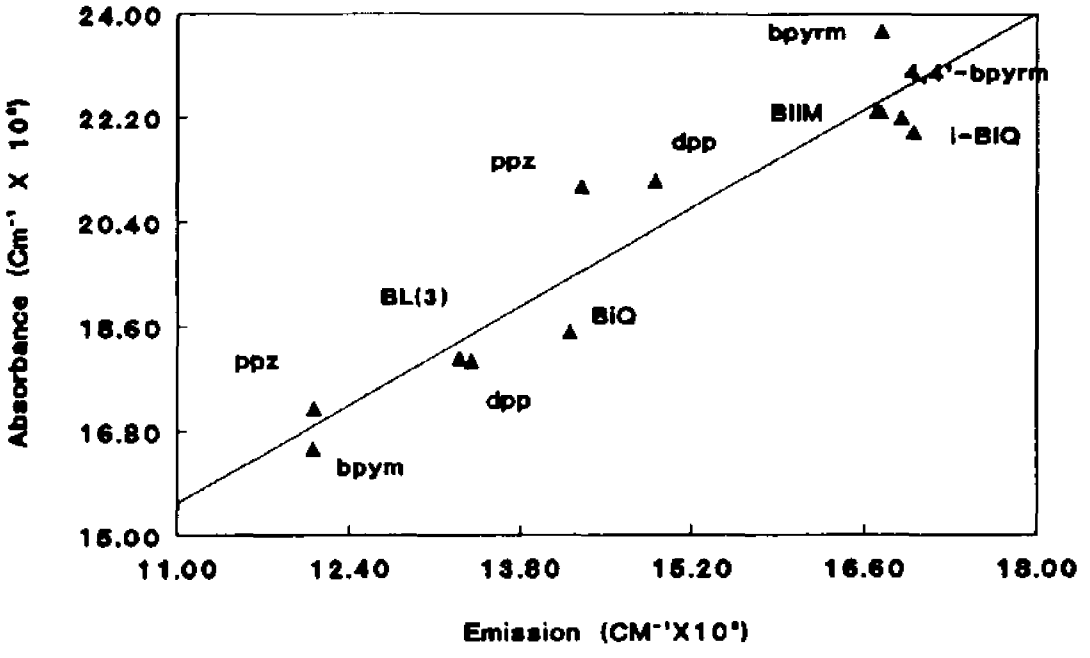

Figure 4. Correlation Between Emission and Absorption Energies for Ru(II) Polypyridine Complexes.

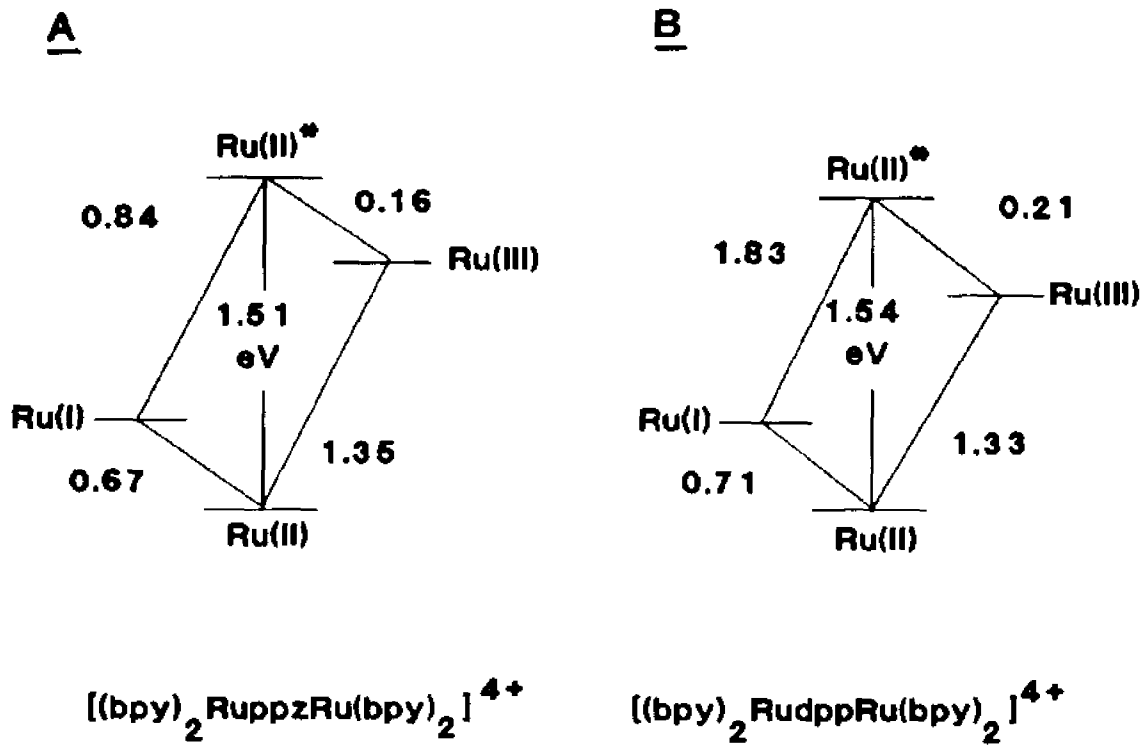

Figure 5. Excited State Potential Diagrams for a) $[(bpy)_2RuppzRu(bpy)_2]^{4+}$ and b) $[(bpy)_2RudppRu(bpy)_2]^{4+}$

Chapter X. Ru/Pt Heterodinuclear Dimers Containing 4,7'-Phenanthrolino-5',6':5,6-Pyrazine, or 2,3-di-(2-Pyridyl)Pyrazine

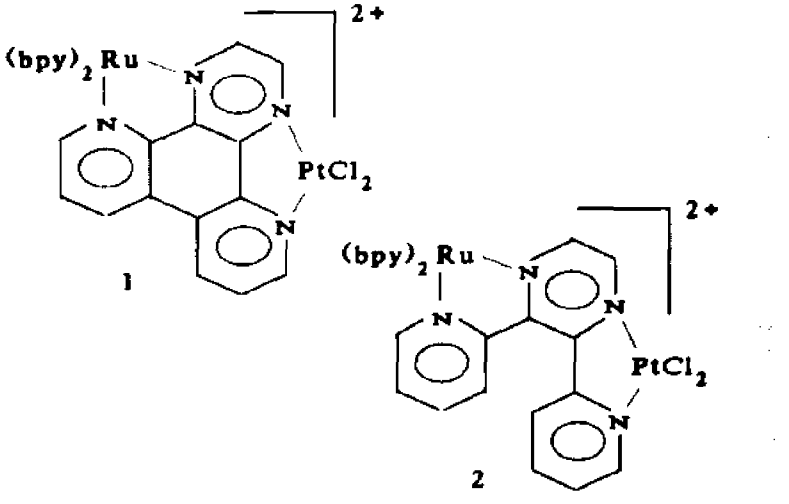

Introduction

Since the discovery that the excited state of the cation $[Ru(bpy)_3]^{2+}$ can be quenched oxidatively and reductively, a tremendous amount of research has been devoted to utilizing the cation in the photochemical production of chemicals and fuels. Schemes aimed toward the photochemical "splitting" of water in fluid solution are riddled with difficulties, and there is doubt that such a catalytic cycle will ever be developed. These difficulties include: sensitizer instability, rapid back electron transfer from the quencher to the sensitizer, and mechanistic problems associated with applying single electron steps to net multi-electron processes.

One approach, to solving these problems is the synthesis of "supermolecules" that contain sensitizer, quencher, and catalyst all in a single molecule. In principle this supermolecule can then be diffused onto a suitable surface and cleaved into its components. If the diffusion of the individual components can be limited or regulated during cleavage, then the possibility exists that their spatial distribution is controlled on the surface, and, thereby, control the kinetics of the catalytic cycle. In this chapter the first steps in this approach are discussed. Complex ions of the type, $[(bpy)_2Ru(BL)PtCl_2]^{2+}$ (where BL = 4,7'–phenanthrolino-5',6':5,6-pyrazine (ppz) or 2,3–di–(2–pyridyl)pyrazine (dpp) have been prepared. They contain a sensitizer, $[(bpy)_2RuBL]^{2+}$ and a catalyst, the platinum atom. Several systems by which these "supermolecules" can be cleaved both in solution and on PVG (porous Vycor glass) are explored.

Results and Discussion

Preparation of $[(bpy)_2RuppzPtCl_2]^{2+}$ and $[(bpy)_2RudppPtCl_2]^{2+}$

The preparation of $[Ru(bpy)_2ppz]^{2+}$ is discussed in Chapter IX, and the preparation of $[Ru(bpy)_2dpp]^{2+}$ has been previously reported[30]. These monometallic species comprise the ruthenium source in the synthesis of the two title heterobinuclear complexes. The platinum source is $Pt(DMSO)_2Cl_2$, which is prepared in two steps from commercial chloroplatinic acid (H_2PtCl_6)[162,163]. Equimolar amounts of either $[Ru(bpy)_2ppz]^{2+}$ or $[Ru(bpy)_2dpp]^{2+}$ and $Pt(DMSO)_2Cl_2$ are then heated in ethylene glycol, giving either $[(bpy)_2RuppzPtCl_2]^{2+}$ or $[(bpy)_2RudppPtCl_2]^{2+}$. The stability of the two heterobinuclear complexes are vastly different. Samples of $[(bpy)_2RuppzPtCl_2]^{2+}$ may be stored indefinitely, either as a crystalline solid or in solution, without any visible signs of decomposition. On the other hand, $[(bpy)_2RudppPtCl_2]^{2+}$ does not even survive purification using column chromatography. Obviously, this instability causes difficulties in its structural proof.

The absorption spectrum of freshly prepared $[(bpy)_2RudppPtCl_2]^{2+}$ is exactly as expected. In comparing the absorption spectra of $[Ru(bpy)_2dpp]^{2+}$ and $[(bpy)_2RudppRu(bpy)_2]^{4+}$ it has been shown that the band at 470 nm in the spectrum of $[Ru(bpy)_2dpp]^{2+}$ splits into two bands at 425 and

525 nm in the spectrum of the homonuclear dimer[30]. The same trend is observed in the ppz complexes; the band at 474 nm in $[Ru(bpy)_2ppz]^{2+}$ is split into bands at 418 and 570 nm. The high energy bands in the spectra of both these complexes were assigned to transitions terminated on a bipyridine, and the low energy transitions terminated on the respective bridging ligands. It is similarly observed that substituting $PtCl_2$ for $Ru(bpy)_2$ in $[(bpy)_2RuppzPtCl_2]^{2+}$ (see below) splits the band in the monomer into bands at 550 and 420 nm. The low energy transition is 20 nm higher in energy than that in the homobinuclear dimer.

From the above trends one would expect two bands in the visible spectrum of $[(bpy)_2RudppPtCl_2]^{2+}$, one at approximately 430 nm, by analogy to the spectrum of $[(bpy)_2RudppRu(bpy)_2]^{4+}$, and the other 20 nm less than the low energy band in the spectrum of $[(bpy)_2RuppzPtCl_2]^{2+}$. Thus, the two bands at 430 nm and 510 nm observed in the spectrum of freshly prepared $[(bpy)_2RudppPtCl_2]^{2+}$ are close to what one would predict. In addition, one could even assign the high energy band to be terminated on a bipyridine, and the low energy band terminated on the bridging dpp.

It is acknowledged that the positions of bands in an absorption spectrum constitute, at best, a weak structural proof, but due to the nature of the studies presented below, the instability of $[(bpy)_2RudppPtCl_2]^{2+}$ relative to $[(bpy)_2RuppzPtCl_2]^{2+}$ is an *advantageous* quality; it allows the ion to be cleaved *selectively and under mild conditions*.

Absorption Spectra

Absorption spectra of $[(bpy)_2RuppzRu(bpy)_2]^{4+}$ and $[(bpy)_2RuppzPtCl_2]^{2+}$ are shown in Figure 1. As described in Chapter IX, the lowest energy MLCT bands of $[Ru(bpy)_2ppz]^{2+}$ and $[(bpy)_2RuppzRu(bpy)_2]^{2+}$ can be assigned to result from MLCT transitions to orbitals localized on the ppz ligand. The red shift of the low energy band of $[(bpy)_2RuppzRu(bpy)_2]^{4+}$ is largely due to the lowering of the ppz π^*, induced by the presence of the second ruthenium center. The same shift to lower energy is observed in the heterobinuclear dimer $[(bpy)_2RuppzPtCl_2]^{2+}$. The band appears

at higher energy than in the homonuclear dimer (550 nm and 570 nm respectively). In contrast to $[Ru(bpy)_2ppz]^{2+}$ and $[(bpy)_2RuppzRu(bpy)_2]^{4+}$, no luminescence has been observed for $[(bpy)_2RuppzPtCl_2]^{2+}$ in neither fluid solution, nor at 77 K. Apparently, the excited state is efficiently quenched by the presence of the Pt(II) center.

Absorption spectra taken on freshly prepared samples of $[(bpy)_2RudppPtCl_2]^{2+}$ show two bands in the visible at 510 and 430 nm. Again the band at 510 nm is at higher energy than the analogous band in the homonuclear dimer, $[(bpy)_2RudppRu(bpy)_2]^{4+}$ (525 nm). As with the heterobinuclear ppz complex, no emission has been observed.

Electrochemical Behavior of $[(bpy)_2RuppzPtCl_2]^{2+}$

The cyclic voltammogram of $[(bpy)_2RuppzPtCl_2]^{2+}$ is given in Figure 2, and Table I contains electrochemical data for $[Ru(bpy)_2ppz]^{2+}$, $[(bpy)_2RuppzRu(bpy)_2]^{4+}$ and $[(bpy)_2RuppzPtCl_2]^{2+}$. The first oxidation in $[(bpy)_2RuppzRu(bpy)_2]^{4+}$ was found to occur at a similar potential to that in the monomer $[Ru(bpy)_2ppz]^{2+}$, indicating that there is little perturbation of the metal t_2 orbitals induced by the second Ru(II) center. The oxidation potential of $[(bpy)_2RuppzPtCl_2]^{2+}$ is 203 mV positive to the first oxidation of $[(bpy)_2RuppzRu(bpy)_2]^{4+}$. The first reduction potential of the heterobinuclear dimer is also shifted positive compared to that of $[(bpy)_2RuppzRu(bpy)_2]^{4+}$. By analogy to the cyclic voltammogram of $[(bpy)_2RuppzRu(bpy)_2]^{4+}$, this wave is assigned to be the single electron reduction of the bridging ppz. This indicates that the LUMO of the bridging ppz has increased stability when bonded to Pt(II) as compared to Ru(II). This reflects the decreased ability of Pt(II), as compared to Ru(II), to undergo back-bonding. Similar observations have been made with another Ru(II)/Pt(II) dimeric species[181]. The lower first reduction potential of $[(bpy)_2RuppzRu(bpy)_2]^{4+}$ compared to that of $[Ru(bpy)_2ppz]^{2+}$, combined with the similarity of their first oxidation potentials, indicate that the second Ru(II) center behaves as a simple electron withdrawing group, and there is little interaction between the metal centers in the dimer. The disparity between the oxidation potentials of $[(bpy)_2RuppzRu(bpy)_2]^{4+}$ and $[(bpy)_2RuppzPtCl_2]^{2+}$ indicate that the Ru(II) and Pt(II) are strongly

coupled to one another. This strong interaction between the metal centers offers an efficient pathway for the deactivation of the excited state, and is one reason why no luminescence can be observed in the complex.

Resonance Raman Spectra of $[(bpy)_2RuppzPtCl_2]^{2+}$

The resonance Raman spectra of $[(bpy)_2RuppzPtCl_2]^{2+}$ using 514.5 nm excitation (Figure 3) and that of $[(bpy)_2RuppzRu(bpy)_2]^{4+}$ using 562 nm excitation (Chapter IX) closely resemble one another. Based on the assignments made to the bands in the spectrum of $[(bpy)_2RuppzRu(bpy)_2]^{4+}$ (Chapter IX), vibrations at 1260, 1467, 1495, 1620, and 1589 cm^{-1} are assigned to ppz.

Cleavage of $[(bpy)_2RuppzPtCl_2]^{2+}$ and $[(bpy)_2RudppPtCl_2]^{2+}$

A promising approach to the selective cleavage of $[(bpy)_2RuppzPtCl_2]^{2+}$ and $[(bpy)_2RudppPtCl_2]^{2+}$, seemed to lie in the reduction of the Pt(II) functionality to Pt^0. It was hoped that Pt^0 would not remain coordinated, and the complex would fall apart. Toward this end, two reducing systems: sodium borohydride in methanol and aqueous sodium dithionite were tested. Both the solution and PVG results are given below.

Reduction with Sodium Borohydride in Methanol

Solutions of either $[(bpy)_2RudppPtCl_2]^{2+}$, $[(bpy)_2RuppzPtCl_2]^{2+}$ or $[(bpy)_2Ruppz]^{2+}$ (50 mL, 1.0 O.D. in methanol) were treated with ca. 100 mg of solid sodium borohydride. The addition of sodium borohydride to monomeric $[Ru(bpy)_2ppz]^{2+}$ results in a deep purple solution. The absorption spectrum has two well resolved bands at 549 and 420 nm. After approximately 10 min in air the solution returned to the original yellow color. The absorption spectrum of this solution was found to be identical with that obtained prior to the borohydride addition. The reducing power of borohydride is -1.24 V in basic aqueous solution, which is sufficient to reduce $[Ru(bpy)_2ppz]^{2+}$. Spectroelectrochemical results[165] for the related $[Ru(bpy)_2dpp]^{2+}$ ion, indicate that the addition of

a single electron to coordinated dpp results in red shifting its visible absorption spectrum. Addition of a second electron gives bands at 530 and 495 nm, which are characteristic of a singly reduced bipyridine[165,166]. Because these bands are absent in the spectrum of $[Ru(bpy)_2ppz]^{2+}$, following treatment with sodium borohydride, it is likely that borohydride reduction of the complex results in the reversible addition of a single electron to the coordinated ppz. It is important that the reduction is 100% reversible, and $[Ru(bpy)_2ppz]^{2+}$ is stable under these reaction conditions.

Immediately following the addition of sodium borohydride to $[(bpy)_2RuppzPtCl_2]^{2+}$, the solution changed from light purple to deep green. The absorption spectra, before and after the borohydride addition, are given in Figure 4. The absorption band at 549 nm is replaced by a strong band at 650 nm. The band at 420 nm remained relatively unchanged. After approximately 10 min in air the green solution turned pale yellow with a maximum absorbance at 487 nm, and there were no further spectral changes. The emission spectrum after two hours shows a single well-shaped band at 630 nm. A grayish -black precipitate is evident from concentrated reaction mixtures. A band at 630 nm is also present in the doubly reduced spectrum of $[(bpy)_2RudppRu(bpy)_2]^{4+}$, in which the first two reductions occur on the bridging dpp[166]. This indicates that borohydride reduction of $[(bpy)_2RuppzPtCl_2]^{2+}$ gives doubly reduced ppz. This doubly reduced species in not stable in air and decomposes, giving a product which absorbs at 460 and emits at 630 nm. As opposed to the case of monomeric $[Ru(bpy)_2ppz]^{2+}$, borohydride addition to $[(bpy)_2RuppzPtCl_2]^{2+}$ results in a chemical change. Because the same grayish black precipitate is formed from borohydride reduction of $Pt(DMSO)_2Cl_2$, we believe it to be platinum black. The spectral properties of the ruthenium product are inconsistent with simple cleavage, resulting in monomeric $[Ru(bpy)_2ppz]^{2+}$ (λ_{max}= 474, λ_{em}= 700 nm), but they are consistent with the formation of a tris-diimine ruthenium(II) complex (strong luminescence, and visible absorption). Similar results can be obtained by reducing $[(bpy)_2RudppPtCl_2]^{2+}$ with sodium borohydride. After borohydride addition, the spectrum rapidly and irreversibly blue shifts (Figure 5) with a maximum at 485 nm. The solution shows an emission at 648 nm, and a black precipitate is formed. There is no intermediate spectrum as

is observed in the case of $[(bpy)_2RuppzPtCl_2]^{2+}$.

Chemical Reduction in Aqueous Sodium Dithionite

A solution of $[(bpy)_2RudppPtCl_2]^{2+}$ (4 mL, 1.0 O.D. in water) was treated with 20 mg of sodium dithionite. After 20 min, the solution gave an absorption spectrum with two bands at 424 and 477 nm, and also an emission spectrum consisting of a single band at λ_{em} = 680 nm (Figure 6). These values agree well with those obtained for authentic samples of $[Ru(bpy)_2dpp]^{2+}$ in ethanol[30] (λ_{max} = 430 nm, sh. 470 nm λ_{em} = 675 nm), but there is no visual evidence of the formation of platinum black. Either aqueous dithionite is unable to further reduce the platinum(II) product or the platinum metal is too finely divided to be seen. Under the same conditions, there are no changes in the spectral characteristics of $[(bpy)_2RuppzPtCl_2]^{2+}$. Apparently, it cannot be irreversibly reduced under these conditions.

Chemical Reduction of $[(bpy)_2RuppzPtCl_2]^{2+}$ and $[(bpy)_2RudppPtCl_2]^{2+}$ on PVG

The absorption spectrum of $[(bpy)_2RuppzPtCl_2]^{2+}$ adsorbed on to PVG is shown in Figure 7a. The MLCT transition terminated on the bridging ligand occurs at 570 nm, which is red shifted in comparison to the value measured in solution, but the low energy band remains at approximately the same position. Treatment of the deep purple glass with sodium borohydride, changes the color of the glass to a dirty orange. The absorption spectrum of the glass so treated is given in Figure 7b, and its absorption spectrum is similar to the spectrum obtained in methanol solution following borohydride treatment. The spectrum of $[Ru(bpy)_2ppz]^{2+}$ recorded on PVG is shown in Figure 8, and is qualitatively different than that of the borohydride reduction product, indicating the reduction of $[(bpy)_2RuppzPtCl_2]^{2+}$ is not simple cleavage.

The results of $[(bpy)_2RudppPtCl_2]^{2+}$ reduction with dithionite on PVG closely parallel those obtained in solution. Figure 9 shows the absorption spectrum before and after addition of sodium dithionite to PVG impregnated with $[(bpy)_2RudppPtCl_2]^{2+}$. The spectrum of the reduction product

indicates that the product is $[Ru(bpy)_2dpp]^{2+}$.

Conclusion

The first steps in testing the feasibility of placing a reaction site on PVG have been carried out. Conditions by which $[(bpy)_2RuppzPtCl_2]^{2+}$ could be selectively cleaved were not found. However, $[(bpy)_2RudppPtCl_2]^{2+}$ can be reductively cleaved with sodium dithionite to generate $[Ru(bpy)_2dpp]^{2+}$, both in solution and on PVG.

Table I. Electrochemical Data

	Oxidations	Reductions
Complex	$E^{o'}$	$E^{o'}$
$[Ru(bpy)_2ppz]^{2+}$	1.37	-1.11,-1.67
$[(bpy)_2RuppzRu(bpy)_2]^{4+}$	1.35, 1.52	-0.67, -1.34, -1.57
$[(bpy)_2RuppzPtCl_2]^{2+}$	1.58	-0.43, -1.20, -1.50, -1.70

All potentials for 10^{-3} M solutions in acetonitrile containing 0.10 M tetra-n-butylammonium tetrafluoroborate as the supporting electrolyte. Potentials in Volts vs. the SCE.

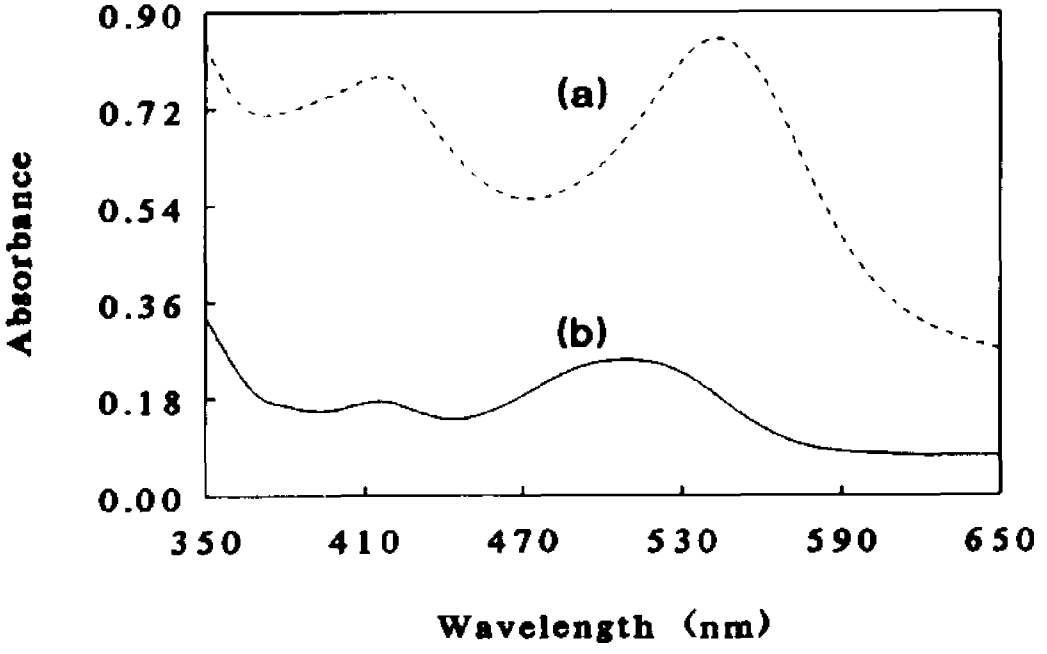

Figure 1. Absorption Spectra of a) $[(bpy)_2RuppzRu(bpy)_2]^{4+}$ and b) $[(bpy)_2RuppzPtCl_2]^{2+}$. Absorbance Values do not Reflect Molar Absorptivities.

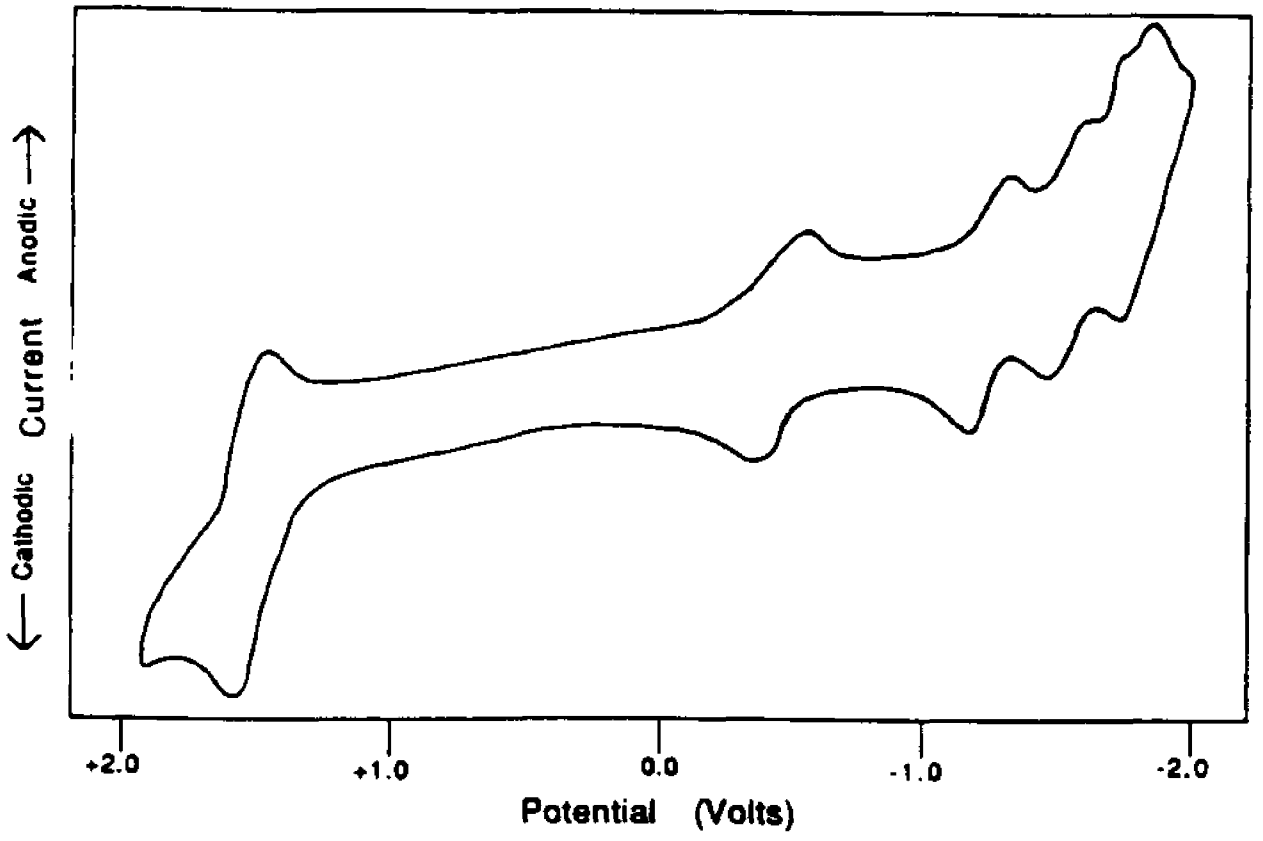

Figure 2. Cyclic Voltammogram of $[(bpy)_2RuppzPtCl_2]^{2+}$ 200 mv/s vs SCE, in 0.1 M Tetra-n-Butylammoniumtetrafluorborate Acetonitrile, at a Glassy Carbon Anode.

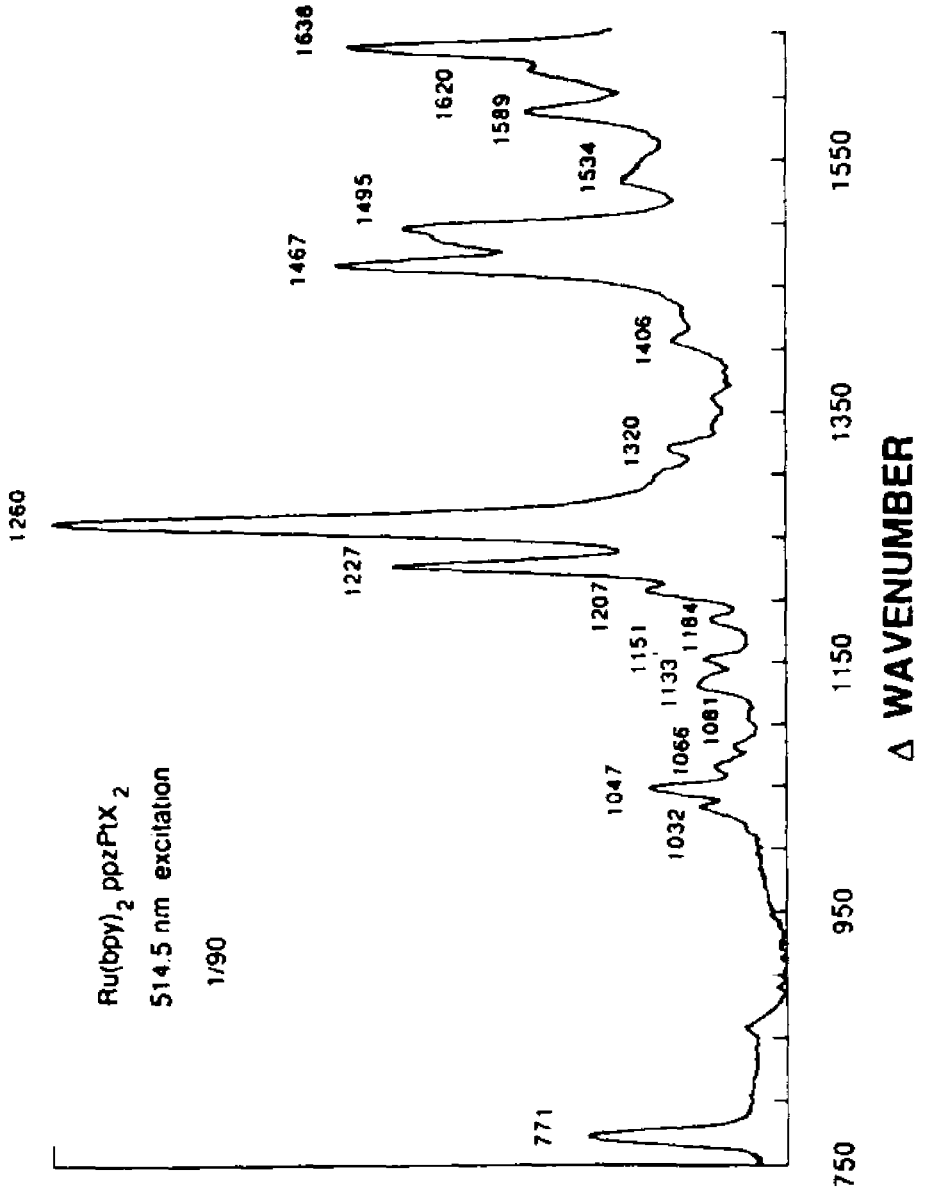

Figure 3. Resonance Raman Spectrum of $[(bpy)_2RuppzPtCl_2]^{2+}$. λ_{exc}= 514.5 nm

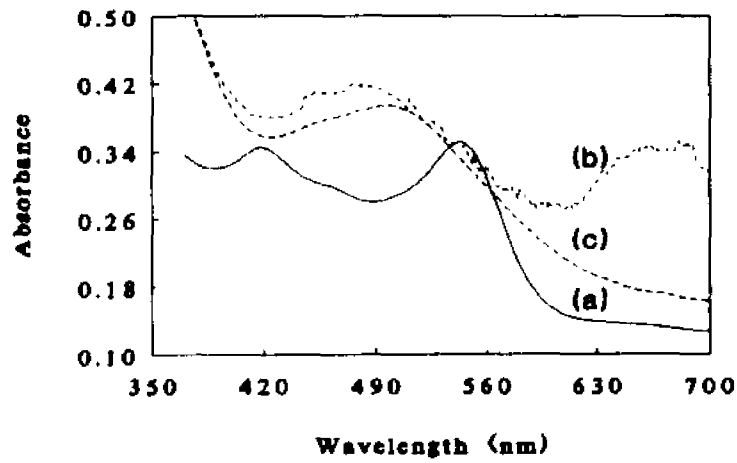

Figure 4. Absorption Spectra of a) 1 in Methanol b) Immediately Following $NaBH_4$ Treatment. c) Two Hours After Treatment With $NaBH_4$ (Absorbances do not Reflect Molar Absorptivities).

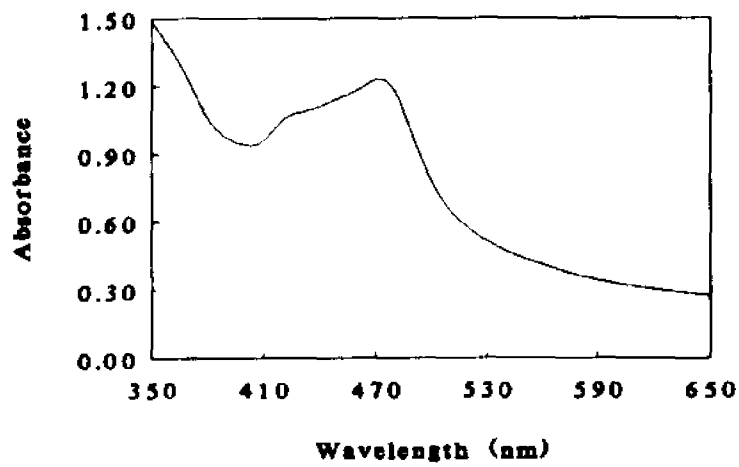

Figure 5. Absorption Spectra of $[(bpy)_2RudppPtCl_2]^{2+}$ Following Treatment With $NaBH_4$.

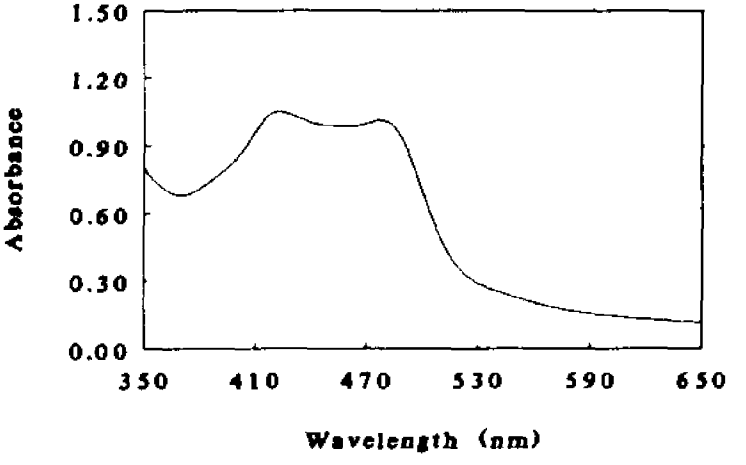

Figure 6. Absorption Spectrum of $[(bpy)_2RudppPtCl_2]^{2+}$ Following Treatment With Sodium Dithionite.

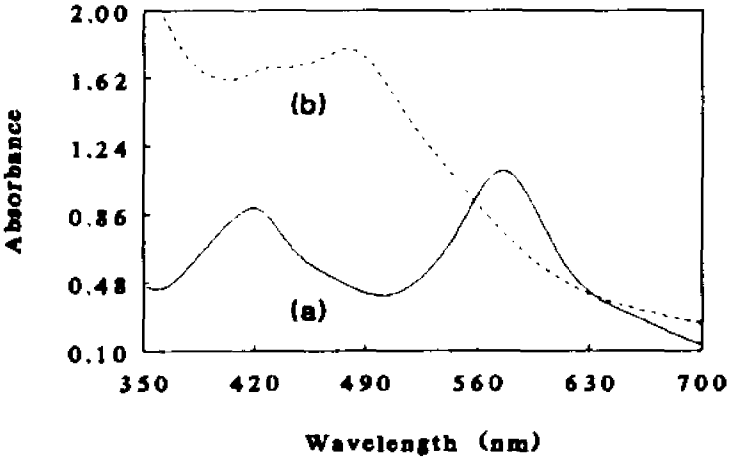

Figure 7. Absorption Spectra on PVG of a) 1 and b) Product of 1 and $NaBH_4$ (Absorbances do not Reflect Molar Absorptivities).

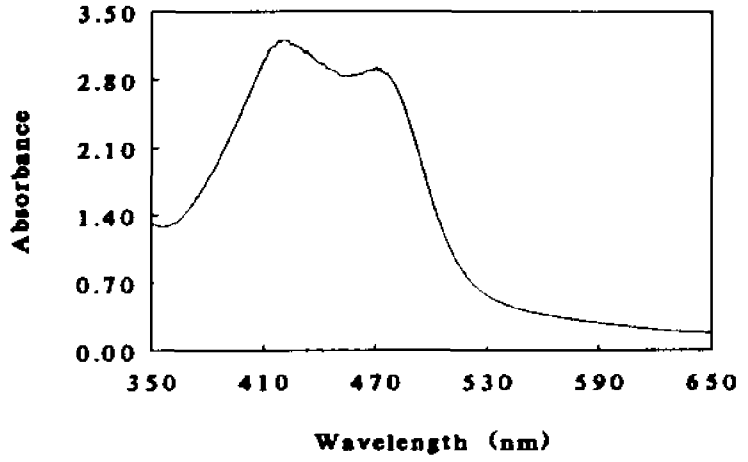

Figure 8. Absorption Spectra of $[Ru(bpy)_2ppz]^{2+}$ Recorded on PVG Glass.

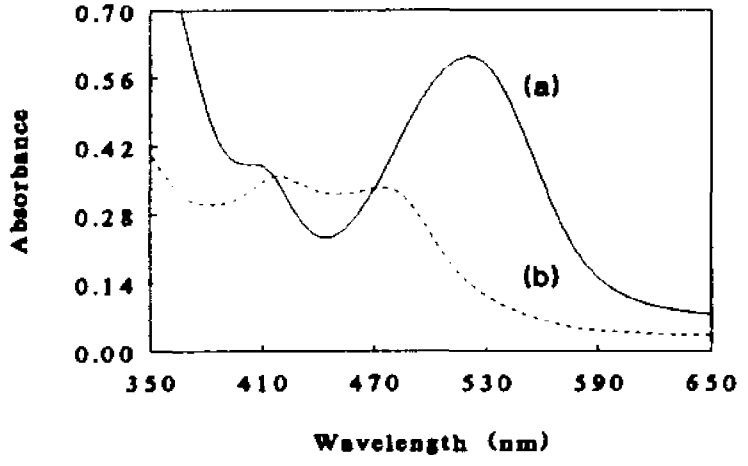

Figure 9. Absorption Spectra of a) 2 and b) 2 Following Treatment With Dithionite, Both Recorded on PVG.

Chapter XI. Effect of Ligand Planarity and Peripheral Charge on Intercalative Binding of $[Ru(bpy)_2L]^{2+}$ to B-DNA

Introduction

This is the first chapter of two detailing our investigation of the interaction of some of the complexes, described in this dissertation, with calf thymus DNA. This chapter investigates the effect of peripheral charge and ligand planarity on intercalative binding to B-DNA.

$[Ru(bpy)_2ppz]^{2+}$ and $[Ru(bpy)_2dpp]^{2+}$ have structures which differ from one another by a single chemical bond. The consequence of this is that the ppz ligand is completely planar, and the dpp is not. Comparing the interaction of the two complexes with B-DNA gives valuable insight into the effect of ligand planarity on the interaction of B-DNA with $[Ru(bpy)_2L]^{2+}$ type complexes.

The heteroleptic qpy complexes discussed in Chapter VI namely, $[Ru(bpy)_2qpy]^{2+}$, $[Ru(bpy)_2qpyme]^{3+}$ and $[Ru(bpy)_2qpyme_2]^{4+}$ have similar geometries and spatial characteristics, but differ by the charge on their periphery. Examination of this series of complexes allows the exploration of peripheral charge on the interaction of metal complexes with B-DNA.

Finally, comparison of $[Ru(bpy)_2ppz]^{2+}$ and $[(bpy)_2RuppzPtCl_2]^{2+}$ allow the investigation of bulk on the intercalating ligand.

Results

Effects of Binding to DNA on Visible MLCT Transitions

Visible spectra for each of the complexes studied, in buffer alone, and in the presence of calf thymus DNA are presented in Figures 1 and 2. All visible spectra are for solutions in 5 mM Tris buffer, pH 7.4, with 50 mM NaCl. For the complex $[Ru(bpy)_2ppz]^{2+}$, the MLCT band at 475 nm shifts to a final value of 485 nm as the DNA phosphate to ruthenium ratio ([P]/[Ru]) increases. At the same time, this transition shows a decrease in intensity with a maximal value of 20%. This band

has been assigned, based on resonance Raman studies, as a charge transfer terminating on the ppz ligand (Chapter IX). The MLCT band at 422 nm, which is assigned to a transition terminating on bpy, shows no wavelength shift and only modest intensity changes as the [P]/[Ru] ratio increases. Visible spectra of the complex $[Ru(bpy)_2dpp]^{2+}$ show no change in intensity or wavelength with increasing [P]/[Ru] ratio over the same range of values (spectra not shown).

For the complex in which $PtCl_2$ has been added to the periphery of the ppz ligand, the spectra in Figure 1 are notable for the red shift of the MLCT transition to the ppz ligand (shifted to 556 nm from 475 nm in $[Ru(bpy)_2ppz]^{2+}$). This shift is similar in magnitude to that observed for binuclear complexes in which a $[Ru(bpy)_2]^{2+}$ unit has been added, or in which the ppz is protonated. In the presence of DNA, this band shows a further red shift to 570 nm and a maximal decrease in intensity of 20%. Again, the transition at 408 nm, associated with bpy, shows little change.

For the complex $[Ru(bpy)_2qpy]^{2+}$, the spectra in Figure 2 show a larger decrease in intensity near 475 nm in the presence of DNA, with a lesser decrease near 430 nm. In this case, the MLCT transitions to bpy and qpy are not completely resolved, but resonance Raman studies indicate that the transition to qpy is red shifted compared to the bpy centered transition. For $[Ru(bpy)_2qpyme]^{3+}$, the shoulder at 475 nm undergoes no intensity decrease(<3%) in the presence of DNA, and no wavelength shift is evident. The complex $[Ru(bpy)_2qpyme_2]^{4+}$ presents a unique result for the series. The MLCT transition to $[qpyme_2]^{2+}$ at 500 nm undergoes a red shift to 520 nm in the presence of DNA, and in addition show a slight increase in intensity (~5%). To our knowledge, this is the first recorded *hyper*chromic effect for such a complex in the presence of DNA. For the series of complexes based on the qpy (or methylated qpy) ligand, the MLCT band (or region) associated with the qpy ligand alone shows significant changes. The region associated with bpy shows much smaller changes.

Effects of Binding to DNA on Fluorescence Spectra

The fluorescence spectra for the complexes with ligands ppz, dpp, qpy, $[qpyme]^+$ and $[qpyme_2]^{2+}$, with and without DNA, are shown in Figure 3. All spectra were run at [P]/[Ru] ratios >60. Table I summarizes the maximum wavelengths for emission and I/I_o values (for [P]/[Ru] ratios >60) for the complexes studied. Only the ppz and $[qpyme_2]^{2+}$ complexes show emission maximum wavelength shifts upon binding to DNA. The ppz complex shows a blue shift of 28 nm (595 cm^{-1}), while the $[qpyme_2]^{2+}$ complex shows a red shift of 15 nm (281 cm^{-1}). Emission intensities are essentially unchanged for the complexes with dpp, qpy and $[qpyme]^+$ upon binding to DNA. The complex with ppz shows the largest increase among the complexes in this study, and the $[qpyme_2]^{2+}$ complex once again shows results unique to the qpy series, with a modest increase in intensity. The complex in which platinum(II) has been added to the coordinated ppz shows no luminescence, either alone in solution, or in the presence of DNA.

Equilibrium Dialysis Binding Studies

Equilibrium dialysis experiments provide parameters K_b, the binding constant, and l, the average binding site size, from a fit to the McGhee and von Hippel equation as adapted by Barton et al.[38,43,44]:

$$r/C_f = (K_b/2)(1-2lr)\,[(1-2lr) / (1-2(l-1)r)]^{l-1}$$

where r is the fraction of DNA phosphate 'sites' occupied and C_f is the free solution concentration of ruthenium complex. Comparison of typical best fit curves and the associated experimental data for the complexes studied are shown in Figure 4. Table II summarizes the average K_b and l values obtained using at least two sets of data for each complex.

The ppz complex gives a binding constant of $5.5 \pm 0.5 \times 10^3$ (l=3-4). While the addition of a platinum site ($PtCl_2$) to the ppz periphery does not diminish the binding constant ($6.5 \pm 0.5 \times 10^3$),

this value is obtained only by fitting with a greatly increased parameter for the binding site size, l=16 to 18.

For the series of complexes with the ligands based on qpy, the highest K_b is found for $[qpyme_2]^{2+}$ ($2.8 \pm 0.6 \times 10^4$), with qpy ($1.3 \pm 0.2 \times 10^4$) and $[qpyme]^+$ ($1.4 \pm 0.3 \times 10^4$) only about a factor of 2 lower. The binding site size for this series is 2 to 3.

Enantioselectivity of Binding to DNA

Dialysates of experiments in which racemic solutions of the complexes studied were dialyzed against 1.6 mM calf thymus DNA for 48 hours were subjected to circular dichroism analysis. The results reported here (Figure 5) are qualitative, but indicate that the mixed ligand complexes with ppz, as well at its $PtCl_2$ adduct, and with $[qpyme_2]^{2+}$ all interact enantioselectively with DNA. The dialysate for the dpp complex, as well as the complexes with qpy and $[qpyme]^+$ show no circular dichroism signal.

Discussion

Effect of Ligand Planarity on Intercalative Binding to DNA

Our equilibrium dialysis results show that the complex $[Ru(bpy)_2ppz]^{2+}$ binds to DNA with a binding constant comparable[38,45] to that of $[Ru(phen)_3]^{2+}$ under similar conditions. Furthermore, the combination of fluorescence, circular dichroism and visible absorption data provides evidence that the major interaction with DNA is likely intercalative in nature and occurs within the major groove of β-form DNA, as has been demonstrated.[37-49,169,170] for $[Ru(phen)_3]^{2+}$. The hypochromicity observed specifically for the MLCT transition which has been assigned as terminating on the ppz ligand indicates that this ligand is reasonably assumed to intercalate between base pairs accessible via the major groove. This interaction would then have the effect of pulling the remaining structure, including the two additional bipyridine ligands coordinated to the ruthenium, into the major groove

to interact via van der Waals contacts with the atoms of DNA lining the groove. It is noteworthy that this effect is capable of enantioselectivity, as evidenced by the circular dichroism signal of the dialysate, despite the presence of only two bipyridines as ancillary ligands. It may be recalled that the complex $[Ru(bpy)_3]^{2+}$ shows little or no enantioselectivity[38] in its binding to DNA.

When $PtCl_2$ is coordinated to the periphery of the ppz ligand, most aspects of the binding are not seriously affected. Hypochromicity is significant for the MLCT transition upon binding to DNA, and the binding is still enantioselective. Though the binding constant remains comparable to that of the ppz complex, a reasonable fit to the McGhee and von Hippel equation requires an average site size of 16 to 18 base pairs, as compared to 2 to 4 base pairs for the other complexes studied here. Because of the similarity of the platinum substituted complex to the unsubstituted one in most other respects, we propose that this drastic increase in average site size is indicative of more significant disruption of the DNA structure as complex binds. The raw data alone show that the fraction of total sites which are occupied by the platinum containing complex is drastically reduced, as indicated by the intercept with the r axis. This effect may be due to the larger size of the coordinated platinum which must be accommodated between the base pairs of DNA to effect intercalation. It is interesting to note that one of the earliest examples of intercalation of a transition metal containing complex was a terpyridyl complex of platinum (II). The crystal structure[170] of this complex with a dinucleotide shows that the platinum penetrates the region between the base pairs involved in the intercalative binding.

A most interesting result from our study is the lack of evidence for intercalative binding of the dpp complex to DNA. The overall size and shape of the two complexes differs only in the lack of planarity of the dpp ligand. The ppz ligand is of course completely planar. For coordinated dpp, the pyrazine and one of the pyridyl substituents would be closest to coplanar, with the remaining pyridyl substituent rotated out of plane due primarily to the interaction between the 3 and 3' hydrogens. The crystal structure for a binuclear complex of dpp has been reported[170] to show the

pyridyl-pyrazine twist angle is 19.5° when both diimine sites are coordinated to a metal center. It would appear from these comparative results that the ability of such complexes to bind intercalatively is sensitively influenced by the inability of the intercalating ligand to assume a completely planar conformation.

For the case of the mixed ligand complex with qpy, where the absorption evidence suggests an intercalative mode of binding, the steric constraint to coplanarity of the pyridyl substituents and the coordinated bipyridyl is far less severe.

The above observations can be contrasted to the results for $[Ru(DIP)_3]^{2+}$, where the interpretation[44,49] has called for an intercalative mode of binding (involving opening up of the DNA structure). Despite the reported non-coplanarity of the phenyl substituents with the phenanthroline system due to hydrogens which interact in a fashion similar to those at the 3' and 3" positions of the dpp ligand. For the DIP ligand, however, the interaction between analogous hydrogens are somewhat less direct, and, therefore, probably less severe. The phenyl rings may be able to approach more closely to coplanarity with the phen system in this case than in the case of dpp. This difference may be enough to allow for the intercalation of the DIP, but not the dpp ligand.

Effect of Ligand Peripheral Charge on Binding to DNA

As evidenced by the absorption, circular dichroism and equilibrium dialysis results, there is an apparent discontinuity in the series of complexes with ligands based on qpy. While the complex containing qpy shows some hypochromicity associated with the qpy ligand near 475 nm, the $[qpyme]^+$ complex shows none. The visible spectrum of the $[qpyme_2]^{2+}$ complex shows a red shift for the MLCT transition assigned as terminating on this ligand, and, in contrast to other complexes studied to date, a small hyperchromic effect. This intensification of the MLCT transition is not consistent with intercalation of the $[qpyme_2]^{2+}$ ligand, and indeed, suggests some other specific orientation with respect to the aromatic base pairs of DNA.

Likewise, the fluorescence maximum and intensities for the qpy and [qpyme]$^+$ complexes are unaffected by binding to DNA, while the [qpyme$_2$]$^{2+}$ complex shows a red shift and intensity increase.

Finally, enantioselectivity is observed only for the [qpyme$_2$]$^{2+}$ complex, but not for the other two members of the series. The binding constant is about the same for the complexes with qpy or [qpyme]$^+$, but increases by about a factor of 2 for the [qpyme$_2$]$^{2+}$ complex. All three are, however, quite large and indicate strong binding to DNA.

The only difference in the members of the series is the increase in positive charge at the periphery of the ligand, as one, then two pyridyl substituents are methylated. Aqueous solubility increases with each methyl substituent added, as the overall charge on the complex ion rises from +2 to +4. This demonstrates that the hydrophilicity of the complexes, specifically the region associated with the qpy ligand, increases along the series with increasing charge. As a result, one might anticipate[36] binding based primarily on an intercalative interaction within the hydrophobic major groove, to decrease along the series. The qpy and [qpyme]$^+$ complexes show comparable binding constants, as well as modest (or no) hypochromism for the MLCT region associated with these ligands. Space filling models suggest that, because of the size of these ligands, they would not be accommodated symmetrically within the major groove of DNA. Rather, one of the pyridyl substituents could intercalate, leaving the other facing out of the groove and exposed to solvent. This model would allow that the qpy and [qpyme]$^+$ complexes interact in a somewhat similar way, with a pyridyl group partially intercalated, and the other pyridyl, or the methylated pyridyl on [qpyme]$^+$ then free to remain in the more hydrophilic environment outside the major groove. In the case of [qpyme]$^+$, the positively charged quaternary methyl could also associate with a DNA phosphate. This exposure to solvent could explain the lack of change in fluorescence. For these complexes, the emission arises from a π^* orbital on the L ligand. Because the overall binding constant in fact increases for the [qpyme$_2$]$^{2+}$ complex, we infer that the dominant mode of binding

is no longer intercalative, but based on electrostatic attraction. Space-filling models of the complexes show that the two positive charges on the $[qpyme_2]^{2+}$ ligand are the right distance apart (~12 angstroms) to interact electrostatically with a pair of phosphates, one on each of the strands of DNA in the double stranded β-form. The result is a binding which bridges the two strands, but is not intercalative in nature. In fact, such models show that the two ancillary bipyridine ligands can only be accommodated facing away from the major groove, with the $[qpyme_2]^{2+}$ ligand facing in, bridging the phosphates. This mode of binding would be more rigid, and result in alignment of the $[qpyme_2]^{2+}$ parallel with adjacent base pairs within the major groove, but not intercalating between them. The $[qpyme_2]^{2+}$ ligand would be more shielded from solvent, providing a rationale for the emission shift and intensity increase, as well as the observed shift in the MLCT band.

Table I. Fluorescence Data

L	λ_{max} w/o DNA	w DNA	Δλ(nm)	I/I_o
$[Ru(bpy)_2ppz]^{2+}$	700	762	+28	9.2
$[Ru(bpy)_2dpp]^{2+}$	685	685	0	1
$[(bpy)_2RuppzPtCl_2]^{4+}$	No Emission Observed			
$[Ru(bpy)_2qpy]^{2+}$	665	665	0	1
$[Ru(bpy)_2qpyme]^{2+}$	655	655	0	1
$[Ru(bpy)_2qpyme_2]^{2+}$	723	738	+15	1.8

Table II. Binding Parameters

L	K_b	I
$[Ru(bpy)_2ppz]^{2+}$	$5.5\pm 0.5 \times 10^3$	3-4
$[(bpy)_2RuppzPtCl_2]^{4+}$	$6.5\pm 0.5 \times 10^4$	16-18
$[Ru(bpy)_2qpy]^{2+}$	$1.3\pm 0.2 \times 10^4$	2-3
$[Ru(bpy)_2qpyme]^{2+}$	$1.4 \pm 0.3 \times 10^4$	2
$[Ru(bpy)_2qpyme_2]^{2+}$	$2.8 \pm 0.6 \times 10^4$	3

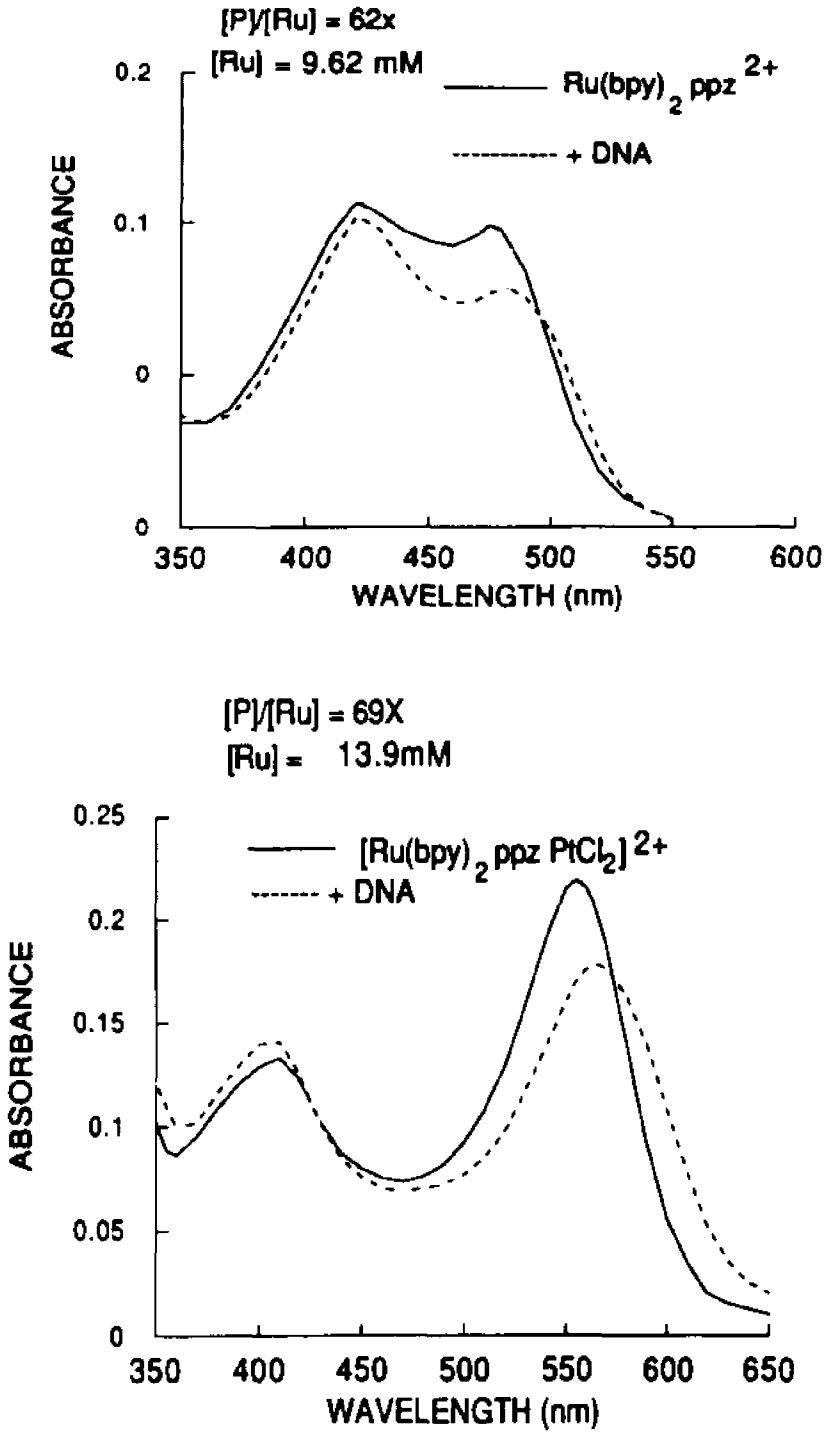

Figure 1. Absorption Spectra All Solutions in 5mM TRIS, pH 7.4, 50 mM NaCl.

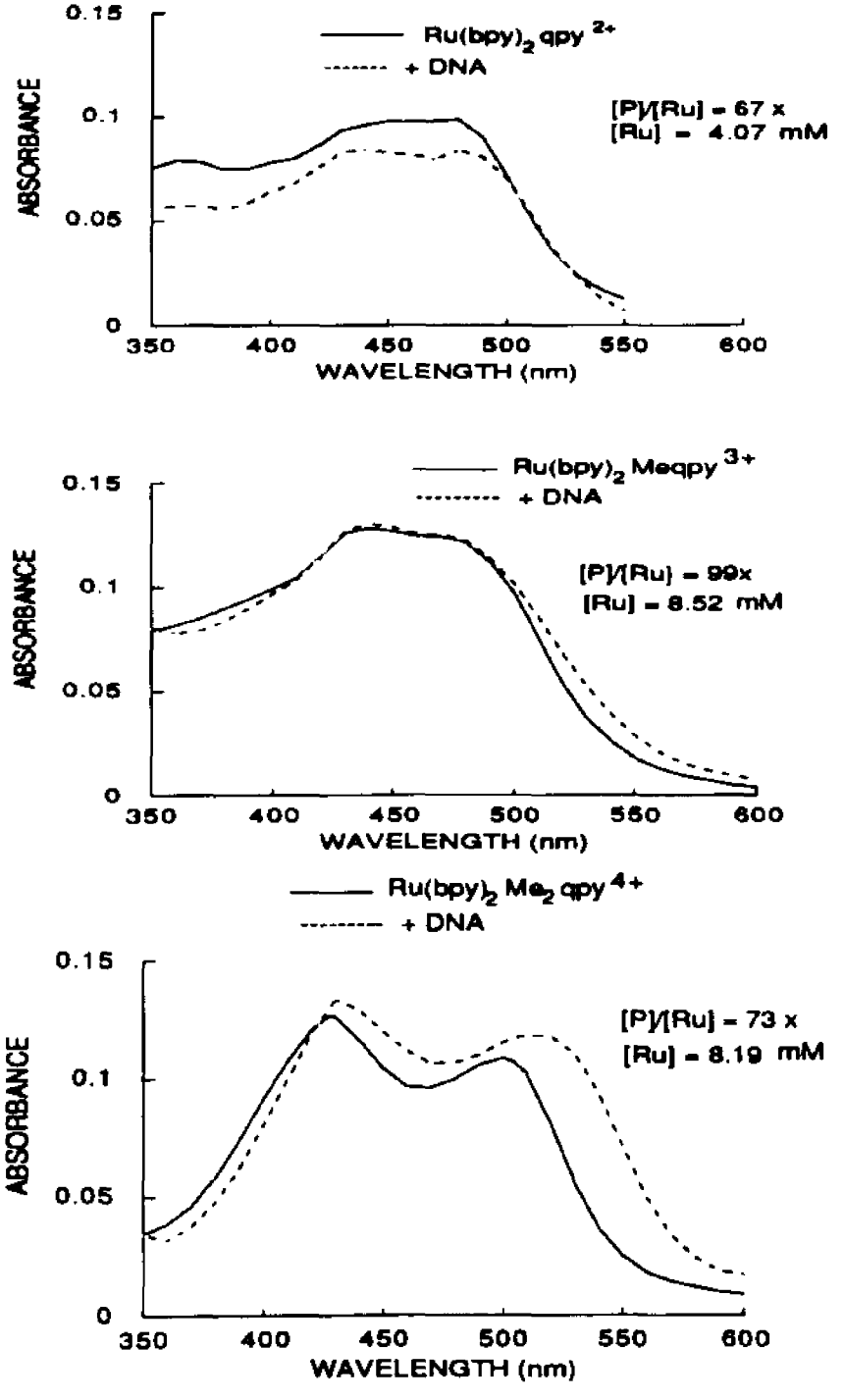

Figure 2. Absorption Spectra. All Solutions in 5mM TRIS, pH 7.4, 50 mM NaCl.

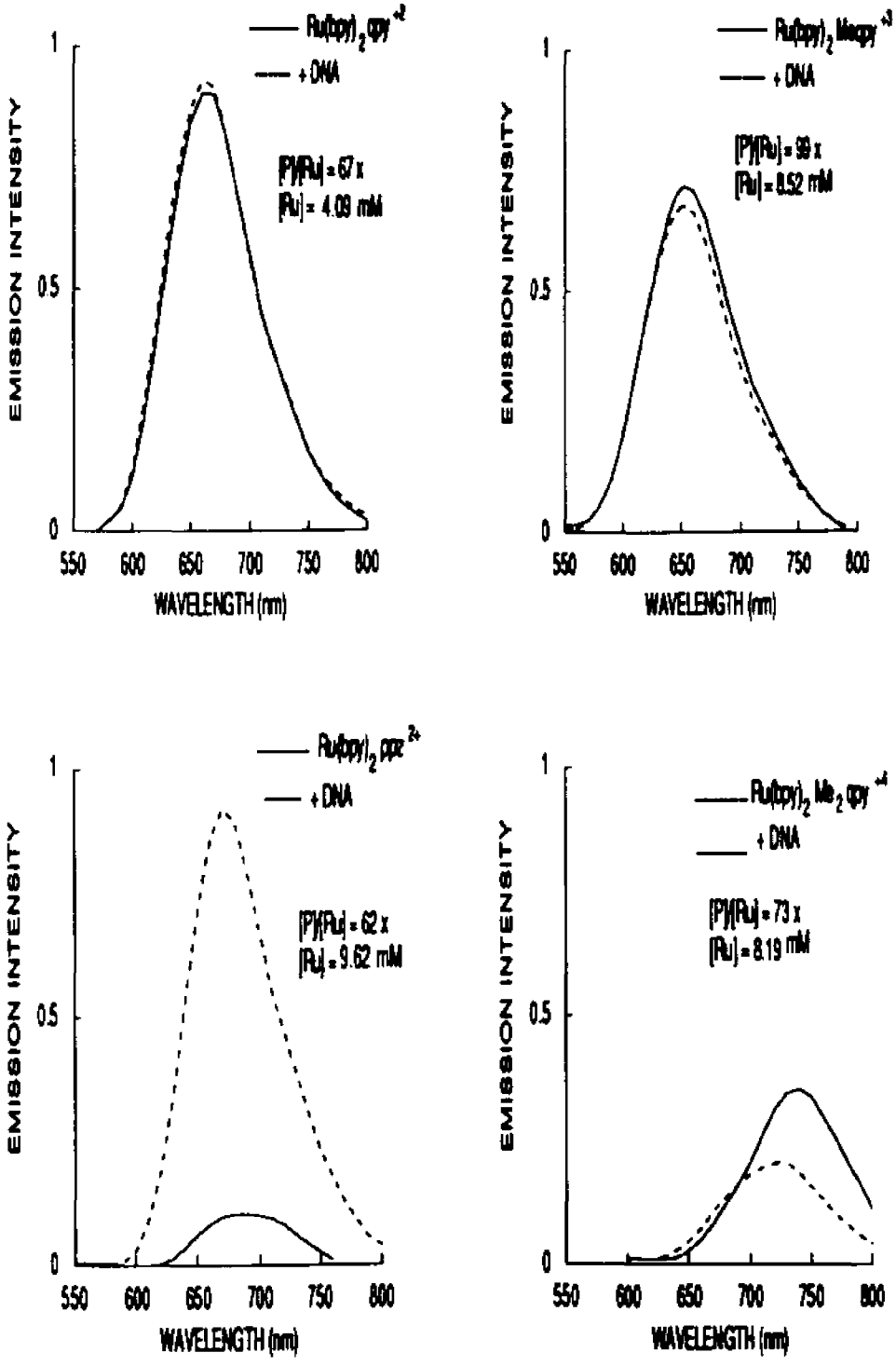

Figure 3. Emission Spectra. All Solutions in 5mM TRIS, pH 7.4, 50 mM NaCl.

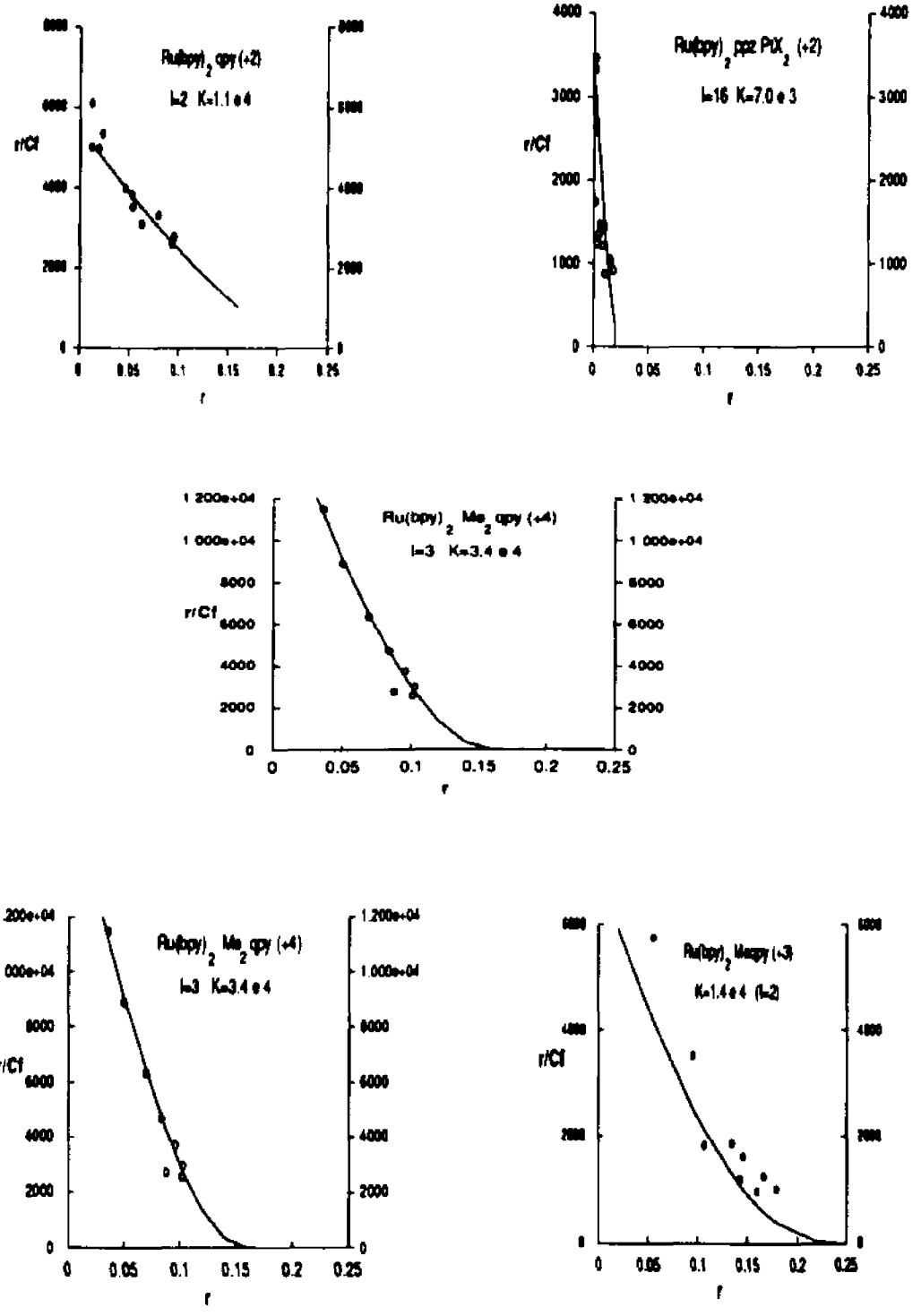

Figure 4. Best fit (——) to the McGhee and von Hippel Equation (See Text) Values of Binding Constant (K_b) and Site Size (I).

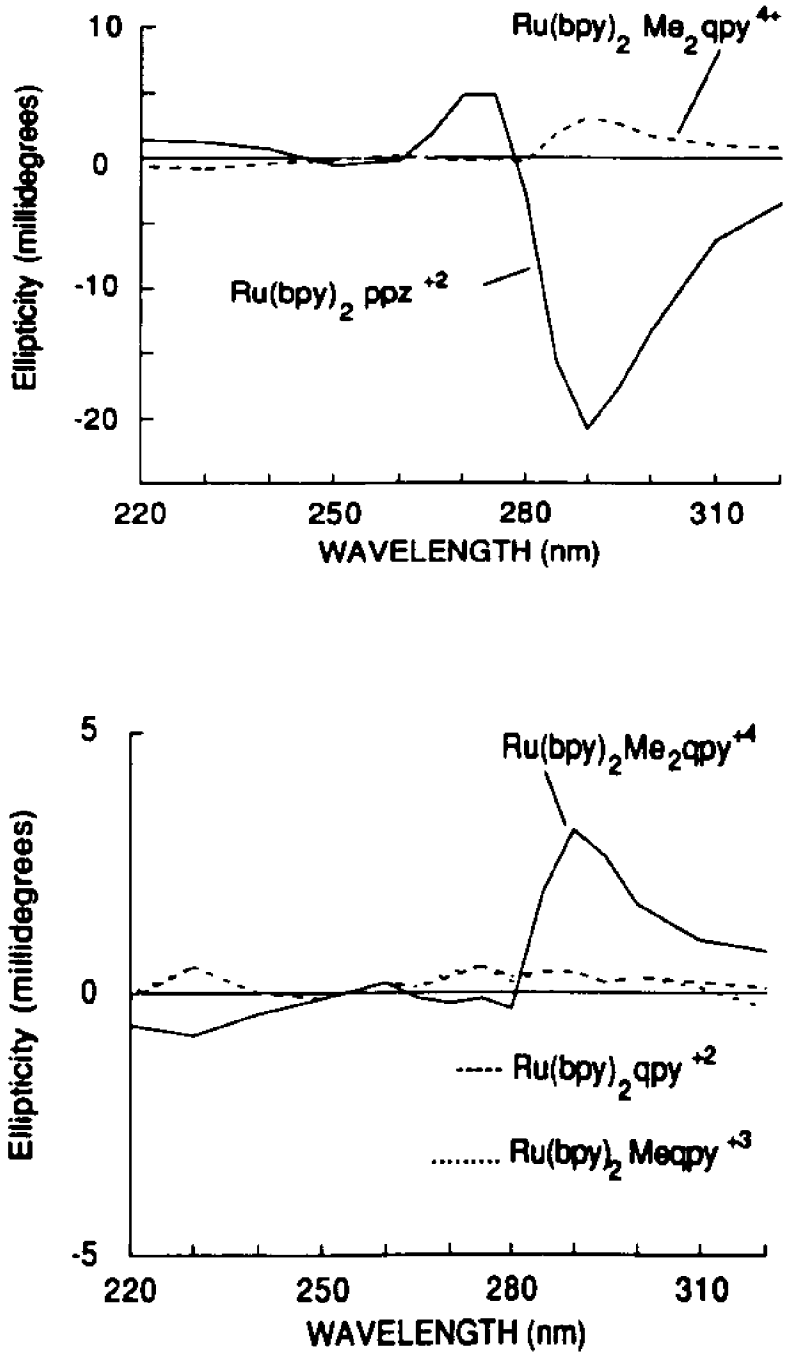

Figure 5. Circular Dichroism Spectra of 41 Hour DNA Dialysates Versus Calf Thymus DNA. All Solutions in 5mM TRIS, pH 7.4, 50 mM NaCl.

Chapter XII. Resolution of $[Ru(bpy)_2ppz]^{2+}$ and $[Ru(phen)_3]^{2+}$ on DNA-Hydroxylapatite

Introduction

This chapter, the second concerning the interaction of $[Ru(bpy)_2L]^{2+}$ type complexes with B-DNA, discusses a method by which racemic metal complexes, which contain a suitable intercalating ligand may be resolved by chromatography on a DNA-hydroxylapatite column.

Results and Discussion

During the course of our investigations we attempted to resolve $[Ru(bpy)_2ppz]^{2+}$ into its Δ and Λ isomers by fractional crystallization with potassium antimony tartrate without success. Because of limited amounts of complex, we have devised a novel means of separation for $[Ru(bpy)_2ppz]^{2+}$ and similar complexes which intercalatively interact with DNA.

A column of hydroxylapatite (BIO-GEL– HTP, Biorad Laboratories) 1.6 cm X 21 cm was first poured and washed with several column volumes of buffer (0.01 M sodium phosphate, pH 6.8; 100 mM NaCl). Calf thymus DNA (Sigma) was dissolved at a concentration of 1 mg/mL in the same buffer and 40 mL of this solution was washed onto the column, followed by several hundred milliliters of buffer. Double-stranded DNA (and some single-stranded, if present) adsorbs[173] to the column under these conditions.

As a test of the resolving capabilities of the column, we passed a 0.100 mL sample of racemic $[Ru(phen)_3]^{2+}$ (1.2 mM) through the column, eluting with the column buffer. Circular dichroism spectra of the fractions eluted showed that the Λ- $[Ru(phen)_3]^{2+}$ elutes first and that the Δ-$[Ru(bpy)_3]^{2+}$ elutes last. This would be expected Because Δ-$[Ru(bpy)_3]^{2+}$ has been shown to bind more strongly to double stranded DNA. A plot of the $\Delta\varepsilon$(267 nm) versus column fraction is presented in Figure 2. The published value[173] of $\Delta\varepsilon$(267 nm) is +540 for the Λ isomer. Clearly, the leading fractions are significantly enriched in the Λ isomer and the tailing fractions in the Δ isomer.

We then proceeded to attempt resolution of $[Ru(bpy)_2ppz]^{2+}$ on the same column. A 1.0 mL sample of the complex (0.7 mM) was eluted through the column and was observed to separate into two distinct bands. The circular dichroism spectra of the bands indicated that they were indeed enriched in the two enantiomers. The first band eluted gave $\Delta\varepsilon$(289 nm)=(-)120 ; $\Delta\varepsilon$(273 nm)=(+)38 while the second band gave $\Delta\varepsilon$(289 nm)=(+)115 ; $\Delta\varepsilon$(273 nm)=(-)32. A second pass of each band through the column gave the same values within a few percent, indicating that the first pass through the column gave approximately 95% enantiometically pure fractions. By analogy with the $[Ru(phen)_3]^{2+}$ results[49], we assign the leading fraction as the Λ isomer and the tailing fraction as the Δ isomer. The maximal values for the Λ isomer are: $\Delta\varepsilon$(289 nm)=(-)130 ; $\Delta\varepsilon$(273 nm)=(+)40; $\Delta\varepsilon$(393 nm)=(+)15.8; $\Delta\varepsilon$(503 nm)=(-)4.0. The Δ isomer has the same values with opposite sign.

Additional trials with several other complexes, including $[Ru(bpy)_2phen]^{2+}$, have indicated that this method is generally useful in accomplishing significant enantiomeric fractionation for complexes of this type, when at least one of the ligands is competent as an intercalator. It has been demonstrated[46,47] that bpy is at best only minimally competent in this regard, because $[Ru(bpy)_3]^{2+}$ shows little or no enantioselectivity in interacting with DNA. Nevertheless, we have demonstrated that complexes of the general formula $Ru(bpy)_2L$, where only Λ is an intercalating ligand are capable of high enantioselectivity in their interaction with B-form DNA. This finding helps to define a minimal complement of ligands capable of enantiospecific interaction with DNA. The greatest degree of enantiospecificity previously reported[48] was for $[Ru(DIP)_3]^{2+}$, whose Λ isomer did not bind to B-form DNA. Because of the size of the DIP (4,7-diphenylphenanthroline) ligands and its non-planarity, the overall interaction of this tris complex, as previously described, is surely quite different from that of a complex such as $[Ru(bpy)_2ppz]^{2+}$. The overall structure of the latter complex is certainly closer to $[Ru(bpy)_3]^{2+}$, but only the ppz ligand intercalates, leaving two bpy ligands to determine the chirality of interaction within the major groove of DNA. The column separation results indicate that this combination of ligands results in significant enantioselective discrimination. We conclude that the favorable intercalative interaction of the ppz ligand is manifested in its tendency

to pull the complex into the major groove sufficiently to favor binding of the Δ isomer over the Λ isomer via the non-bonded interactions of the bpy ligands within the major groove of DNA. This result would support the interpretation[37-40,45] of Barton et al. regarding the more favorable intercalative mode of interaction for the Δ isomer. A recent report has appeared[49] which proposes an alternative model for differential binding of $[Ru(phen)_3]^{2+}$ enantiomers based on linear dichroism results. With the ability to separate enantiomers of such complexes, we look forward to studying, via a variety of spectroscopic methods, the effect of binding individual isomers to DNA and contributing to the resolution of this question.

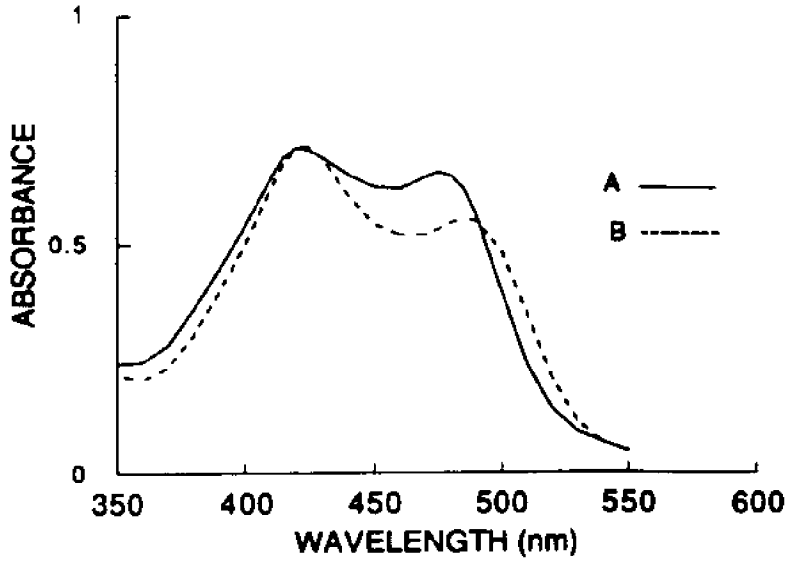

1. Absorption Spectra of $[Ru(bpy)_2ppz]^{2+}$ (A) and With DNA, Mole Ratio of DNA [P]/[Ru] of 20 (B). Complex is 65 mM in both spectra.

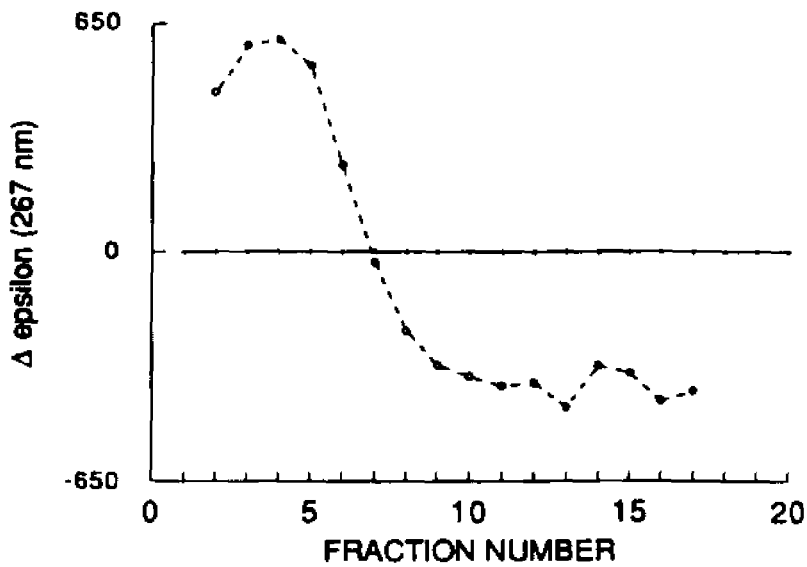

Figure 2. $\Delta\varepsilon$ (267 nm) of Fractions of $[Ru(phen)_3]^{2+}$ Eluted From DNA-Hydroxylapatite Column.

Chapter XIII. Experimental

Materials and Methods

4,4'–bipyridine was obtained from Aldrich as the dihydrate. $RuCl_3$ was obtained as the hexahydrate, and stored at 150 °C for 4 hours prior to use. H_2PtCl_6 was obtained as a 10% solution (Aldrich). Acetonitrile was either Aldrich gold label or Baker HPLC grade. DMF was distilled over CaH_2 prior to use. $Ru(bpy)_2Cl_2$ was either purchased as the hexahydrate, or prepared by existing literature methods[174]. Nitrogen gas was dried by passage through a column of P_2O_5, followed by a column of $CaCl_2$ All other reagents were used as received from chemical suppliers without further purification.

Cyclic Voltammetry

Cyclic voltammograms were recorded on a PAR 173 system as described in our earlier publications[30,31]. Millimolar samples were examined in acetonitrile solution with 0.1M tetra n–butylammonium tetrafluoroborate as the supporting electrolyte. The cell was purged with nitrogen for 20 minutes prior to the recording of the voltammogram. The working electrode was either a glassy carbon or platinum disk, the auxiliary a platinum screen, and potentials were recorded versus the standard calomel electrode (SCE).

Acidity Measurements

A stock solution of the complex to be studied, either $[Ru(bpy)_2qpy]^{2+}(PF_6^-)_2$, $[Ru(bpy)_2qpyme]^{3+}$ $(PF_6^-)_3$ or $[Ru(qpy)_3]^{2+}$ $(PF_6^-)_2$, was adjusted to absorbance 0.8 to 1.5 for absorption measurements, and to 0.6 for emission experiments. The solution was made slightly acidic due to the lack of solubility of some of the complexes in neutral aqueous media. Standard solutions of sulfuric acid and potassium hydroxide were prepared for use as titrants.

A Corning 135 or Digisense LED 5986–10 pH meter was used for pH measurements in

both cases, the meter was first calibrated with standard buffer solutions obtained from Fischer. The Corning meter was calibrated using the two point method. The stock solution of the complex was adjusted to a convenient initial pH. Small aliquots of standard acid or base were added in portions to the stock solution so as to adjust the pH, and its spectrum was recorded. After several measurements, the solution was returned to its original pH, whereupon spectra identical to that of the original solution were obtained. This was the case whether the original solution was first made basic with potassium hydroxide solution or acidic with sulfuric acid. After each series of measurements, the pH meter was rechecked with known buffers to ensure that no significant drift had occurred. In no case was the drift more than 0.02 pH units.

Absorption and Luminescence Measurements

All UV/Vis spectra were recorded on a Cary 14 spectrophotometer, except the DNA interaction data which were recorded on a Perkin Elmer 320. Emission spectra were recorded on a Perkin Elmer Hitachi MPF–2A emission spectrophotometer equipped with a red sensitive Hamamatsu R818 photomultiplier. Emission quantum yields were made relative to $[Ru(bpy)_3]^{2+}$ in the case of the complexes containing a qpy, and to $[Os(bpy)_3]^{2+}$ for the complexes containing 4;7'-phenanthrolino-5',6':5,6-pyrazine, as previously reported[30,31]. Excited state lifetimes were measured by the method described in earlier publications from this laboratory[30,31] and also with a newer system that uses a Quanta–Ray DCR–2A Nd:YAG laser with a 355 nm excitation source. When using the ND:YAG as the source, the luminescence was analyzed at 90° to the direction of excitation by first passing the emitted light through a Bausch and Lomb 33–86–76 monochromator and then into a RCA 31034A photomultiplier. The output of the photomultiplier was sent to a Tektronix 7834 oscilloscope and photographs were taken of the oscilloscope trace. Lifetimes were calculated by the usual method of finding the time for the luminescence decay to 1/e of its intensity at the time of the pulse.

Excited state potentials.

Oxidative and reductive excited state potentials were calculated according to equations (1) and (2) respectively[3b].

$$E(A^*/A^-) = E(A^*/A) - E^{0-0} \qquad (1)$$

$$E(A^-/A^-) = E(A/A^-) - E^{0-0} \qquad (2)$$

Where A^*/A and A/A^- are the potentials for the first reduction and oxidation potentials in the complex, and E^{0-0} is the zero–zero spectroscopic energy of the transition, which was estimated as the maxima of the luminescence spectrum.

Derivation of pK_a Relationships.

For symmetrical polyacids in which the acidic sites are spatially isolated from one another (i.e. non-interacting) the values for the acidity constants can not equal one another, for statistical reasons. In Chapter VII Equation 1 was introduced for the case of a diacid.

$$pK_{a2} = pK_{a1} + Log_{10}(4) \qquad (1)$$

The proof of Equation 1 is as follows.

Consider the case of a diacid:

$$AH_2 \rightleftharpoons A^- + H^+ \qquad K_{a1}$$

$$AH^- \rightleftharpoons A_2^- + H^+ \qquad K_{a2}$$

The rates for the forward reactions, with rate constants k_1 and k_2, are not equal. Because AH_2 can lose a proton from either of the two equivalent sites, and AH^- from only a single site, $k_1 = 2k_2$. For the reverse reaction, $k_{-2} = 2k_{-1}$. Because A^{2-} can be protonated at either of two sites, and AH^- at only one.

Expressing the equilibrium constants as:

$$K_{a1} = k_1/k_{-1} \quad \text{and} \quad K_{a2} = k_2/k_{-2}$$

it follows that

$$K_{a1}/K_{a2} = k_1/k_{-1} \cdot k_{-2}/k_2 \qquad (2)$$

Substituting the rate constant relationships into (2):

$$K_{a1}/K_{a2} = 2k_2k_{-2} / 0.5 \cdot k_{-2}k_2 = 4$$

Thus:

$$Log_{10}[K_{a1}/K_{a2}] = Log_{10}[4]$$

From which Equation (1) follows.

The derivation of the relationships for higher polyacids is similar to that of Equation (1), and the values for di- to hex- acids are given in Table I in Chapter VII.

Column Chromatography.

Excellent samples of all the ruthenium complexes described here can be purified by column chromatography on alumina (neutral, activity I obtained from Baker). The general procedure is to place a plug of glass wool in the column, and fill it with acetone. The stationary phase is poured slowly and allowed to settle. The column is packed under pressure by passing a volume of acetone through it. Two centimeters of sand is then added to the top of the column. The complex to be purified is dissolved in acetonitrile, in the case of the hexafluorophosphate salt, or acetonitrile/methanol in the case of the chloride. The sample is added to the column and allowed to enter the stationary phase, by adding small quantities of acetone (acetone is generally not polar enough to be used as the eluent). The column is then developed with acetone. If the material does not move down the column with acetone, acetonitrile is used. Most samples can be eluted with acetonitrile and a small quantity of methanol. The amount of methanol can be increased until the bands move down the column. The column can be cleaned by passing a volume or so of methanol through it, and prepared for another sample, with a volume of acetone. Alumina has been found to vary from sample to sample, and the amount of methanol in the acetonitrile needed to elute a

particular complex also varies. The gradient method above has been found to be extremely general to the purification of tris–diimine ruthenium(II) complexes.

Preparation of Impregnated Porous Vycor Glasses.

The piece of glass is weighed, and a $1X10^{-5}$ solution of the complex as its hexafluorophosphate salt in acetonitrile is prepared. The initial absorbance (at the visible maximum) of the solution is recorded. The glass is placed in 50 mL of this solution, and the absorbance of both solution and glass are monitored during the soak. When absorbance of the glass is between 0.3 and 0.6, the soak is terminated. Similarly, the absorbance of the solution drops .1 to .2 (as recorded in a 1 cm cell) during this time. The glass is then placed in a vacuum desiccator in the presence of calcium chloride, and the solvent removed at 0.1 torr. The loading of the complex was calculated in mole of complex per gram of PVG. The glasses were thoroughly dried under vacuum, and their absorption spectra recorded.

Equilibrium Dialysis

Equilibrium dialysis experiments were run in a buffer composed of 5mM Tris, pH 7.4 and 50 mM NaCl. 1.0 mL of calf thymus DNA (1 mg/mL), was placed in the buffer, sealed in dialysis tubing, and dialyzed for 48 to 72 hours at 25 °C versus 2.0 ml of ruthenium complex in solution. Concentrations were determined by absorption spectroscopy.

Preparation of Compounds

The procedures for the preparation of the compounds in this work are described below. The ruthenium complexes are always prepared as their hexafluorophosphate salts. In order to prepare the chloride salts (for improved water solubility), the precipitation step is to be neglected, and the samples directly chromatographed, as described above.

2,2":4,4":4',4"'–Quaterpyridyl, qpy.

4,4'–dipyridyl dihydrate (75 g) and 10% Pd/C (10 g) were heated at 125 °C for 72 hours in a round bottom flask equipped with a reflux condenser. After this time, the reaction mixture was cooled. Chloroform (300 mL) was added, and the resulting slurry was refluxed for 30 min. The mixture was filtered, and the chloroform removed by distillation. Acetone (200 mL) was added to the solid residue and the mixture stirred. The slurry so obtained was filtered to yield a crop of the quaterpyridyl which was set aside for later purification. The filtrate was collected and its volume reduced by about 50 mL by partial evaporation of the acetone so as to yield more solid. The solid (a further batch of the quaterpyridyl) was again collected by filtration, and the filtrate once more reduced in volume. In this way ,more quaterpyridyl was obtained. This evaporation/filtration procedure was repeated several times, the acetone volume being reduced in 50 mL increments, until the solid obtained was found to be unreacted starting material (mp 71 °C) rather than the much higher melting quaterpyridyl (mp> 200 °C). The batches of crude quaterpyridyl were combined and recrystallized from ethanol. Samples of high purity could be obtained by sublimation under reduced pressure. The quaterpyridyl is a colorless solid m.p. 235 °C. C,H,N Analysis for qpy·H_2O: Found. (%C 73.02 %H 4.37 %N 17.07) Calc. (%C 73.15 %H 4.91 %N 17.06)

N"–Methylquaterpyridinium Iodide, [qpyme]$^+$(I^-).

500 mg of 2,2':4,4":4',4"'–quaterpyridine was dissolved in 100 mL of methylene chloride and 1.0 mL of methyl iodide added. The resulting solution was stoppered, and allowed to remain at room temperature for 96 hours. The solvent was removed by distillation, the solid residue was refluxed in chloroform (200 mL) for 20 min, and the resulting solution filtered while hot. The yellow solid so obtained (200 mg) was found to be the diquaternary salt (see next preparation (R_f= 0.0, 95% ethanol, alumina). The filtrate containing unreacted 2,2':4,4":4',4"'–quaterpyridine and the monoquaternary salt, was reduced in volume to 50 mL. The monomethylquaternary salt was

precipitated by the addition of hexane, and isolated by crystallization from chloroform or methylene chloride of to yield 500 mg of yellow platelet. C,H,N Analysis Found for the mono hydrate: (%C 53.25 %H 3.70 %N 11.66) Calc. (%C 53.62 %H 4.07 %N 11.96)

N'',N'''–Dimethyl–2,2':4,4':4',4'''–Quaterpyridinium Iodide, $[qpyme_2]^{2+}(I^-)_2$.

50 mg (0.16 mmol) of 2,2':4,4'':4',4'''–quaterpyridine and 2 mL of methyl iodide were refluxed in 50 mL of acetone for 4 hours. The mixture was then filtered and the solid so obtained washed with acetone (20 mL) then chloroform (4 x 20 mL). Recrystallization from ethanol yielded 75 mg of yellow platelet of the diquaternary salt (75%). C,H,N Analysis: Found. (%C 44.03 %H 3.29 %N 9.15). Calc. (%C 44.46 %H 3.39 %N 9.43)

N'',N'''–Dimethyl–2,2':4,4':4',4'''–Quaterpyridinium Hexafluorophosphate, $[qpyme_2]^{2+}(PF_6^-)_2$.

100 mg of N'',N'''–dimethyl–2,2':4,4':4',4''–quaterpyridinium iodide (prepared by the above method) were added to 10 mL of water and heated until all of the solid dissolved. This solution was allowed to cool, and was added to a 15 mL saturated solution of ammonium hexafluorophosphate. The precipitate was allowed to digest at 0 °C for 2 hours, and then the resulting slurry was filtered. The crude product was washed with 5 mL of cold water, and precipitated out of acetone using ether to yield 90 mg of the salt, $[qpyme_2]^{2+}(PF_6^-)_2$. The NMR and UV spectra were identical to that of the iodide salt above. Addition of $AgNO_3$ solution to a solution containing 10^{-2} moles of the PF_6^- salt prepared by the above method gave no detectable precipitate of silver iodide.

N''–Methyl–2,2':4,4':4',4'''–Quaterpyridinium Hexafluorophosphate, $[qpyme]^+(PF_6^-)$.

Prepared as above for N'',N'''–dimethyl–2,2':4,4':4',4'''–quaterpyridinium hexafluorophosphate, substituting $[qpyme]^+(I^-)$ for $[qpyme_2]^{2+}(I^-)_2$.

4;7'-Phenanthrolino-5,6:5,6-Pyrazine, ppz

The following is a modified preparation of that previously reported[31]. 5.0 g of 4,7–phenanthroline–5,6–dione and 1.2 g of ethylene diamine were added to 500 mL of methanol, and stirred for 24 hours. The solvent was removed under reduced pressure, and 50 mL of acetone was added. The slurry was filtered to yield 3.8 g of crude 1,10–phenanthrolino–5,6:5',6'–pyrazine as a pale yellow solid. The solid was dissolved 100 mL of hot methylene chloride, treated with activated carbon, filtered while hot, and precipitated with the addition of ligroin (bp. 60– 90 °C). Filtration of the mixture yielded 3.0 g of 4,7'–phenanthrolino–5,6:5',6'–pyrazine as a white solid mp 268°C

1;10'–Phenanthrolino–5,6:5,6'–Pyrazine, *l*–ppz.

5.0 g of 1,10–phenanthroline–5,6–dione and 1.2 g of ethylene diamine were added to 500 mL of methanol, and stirred for 7 days. The solvent was removed under reduced pressure, and 50 mL of acetone was added. The slurry was filtered to yield 3.8 g of crude 1,10–phenanthrolino–5,6:5',6'–pyrazine as a pale yellow solid. The solid was dissolved 100 mL of hot methylene chloride, treated with activated carbon, filtered while hot, and precipitated with the addition of ligroin (bp. 60– 90 °C). Filtration of the mixture yielded 3.0 g of 1,10'–phenanthrolino–5,6:5',6'–pyrazine as a white solid mp > 260 °C. C,H,N Analysis: Found. (%C 72.63 %H 3.55 %N 24.06). Calc. (%C 72.40 %H 3.47 %N 24.12)

Tris–(2,2'':4,4'':4',4'''–Quaterpyridine)Iron(II) Hexafluorophosphate, $[Fe(qpy)_3]^{2+}(PF_6^-)_2$.

2,2':4,4":4',4"'–quaterpyridine (100 mg, 0.323 mmol) and ferrous chloride (32 mg, 0.108 mmol) were refluxed in 25 mL of 95% ethanol for one hour. The deep purple solution was added dropwise to 20 mL of sat. ammonium hexafluorophosphate, and the solution was cooled to 0 °C for one hour. The resulting mixture was filtered, the crystals washed with 50 mL of water and dried

in air. The complex was precipitated out of acetone by the addition of ether to yield 100 mg of $[Fe(qpy)_3]^{2+}(PF_6^-)_2$. Comparable results are obtained using a stoichiometric amount of ferrous ammonium sulfate as the iron source. C,H,N Analysis: Found (%C 49.50 %H 3.27 %N 11.78) Calc. (%C 49.61 %H 3.12 %N 11.54)

Tris–(N'–Methyl–2,2'':4,4'':4',4'''–Quaterpyridinium)Iron(II) Hexafluorophosphate $[Fe(qpyme)_3]^{6+}(PF_6^-)_6$.

Prepared as above for tris–(2,2'':4,4'':4',4'''–quaterpyridine)iron(II) hexafluorophosphate, substituting $[qpyme]^+$ for qpy.

Tris–(N'',N'''–Dimethyl–2,2':4,4'':4',4'''–Quaterpyridinium)Iron(II) Hexafluorophosphate, $[Fe(qpyme_2)_3]^{8+}(PF_6^-)_8$.

Prepared as above for tris–(2,2'':4,4'':4',4'''–quaterpyridine)iron(II) hexafluorophosphate, substituting $[qpyme_2]^{2+}$ for qpy.

Bis–(2,2'–Bipyridine)–2,2':4,4'':4',4'''–Quaterpyridine Ruthenium(II) Hexafluorophosphate, $[Ru(bpy)_2qpy]^{2+}(PF_6^-)_2$.

$Ru(bpy)_2Cl_2$ (500 mg, 0.92 mmol) and qpy (310 mg, 1.00 mmol) were refluxed in 50 mL of ethanol (95%) for 2 hours. The deep red solution so obtained was filtered while hot. After removing the solvent under reduced pressure a red solid was obtained. This was dissolved in a minimum amount of acetonitrile, and this solution was added dropwise into 20 mL of a saturated aqueous solution of ammonium hexafluorophosphate. The salt which precipitated was collected by filtration, precipitated out of acetone by the addition of ether, and chromatographed on alumina (acetonitrile/methanol) as described above to give 500 mg of $[Ru(bpy)_2qpy]^{2+}(PF_6^-)_2$. C,H,N Analysis Found (%C 47.89 %H 3.16 %N 11.20). Calc. (%C 47.39 %H 2.97 %N 11.01).

Bis–(2,2'–Bipyridine)–N''–Methyl-2,2':4,4'':4',4'''–Quaterpyridine Ruthenium(II) Hexafluorophosphate, $[Ru(bpy)_2qpyme]^{3+}(PF_6^-)_3$.

$Ru(bpy)_2Cl_2$ (300 mg, 0.61 mmol) and N''-methyl-2,2':4,4'':4',4'''–quaterpyridinium iodide ($[qpyme]^+(I^-)$, 276 mg, 0.61 mmol) were refluxed in 100 mL of 50% ethanol/water for 1 h. The deep red solution was concentrated to 30 mL, and added to 10 mL of sat. ammonium hexafluorophosphate, with the immediate formation of a red solid. This precipitate was allowed to digest at 0 °C for 4 hours. The solid was filtered, and washed thoroughly with water (20 mL, 4X). The solid was collected, dissolved in a minimum amount of hot acetone and filtered hot. The volume of acetone was reduced to 30 mL, and the complex was precipitated by the addition of ether. The solid was filtered washed with ether, and allowed to dry. The sample was repeatedly chromatographed on alumina (acetonitrile/methanol) as described above until the emission spectra for the top of the band was identical with that on the bottom of the band. This resulted in 100 mg of $[Ru(bpy)_2qpyme]^{3+}(PF_6^-)_3$. Analysis on the pentahydrate : Found (%C 39.29 %H2.79 %N 8.89). Calc. (%C 39.02 %H 3.12 %N 8.89).

Bis–(2,2'–bipyridine)–N'',N'''–Methyl-2,2':4,4'':4',4'''–Quaterpyridine Ruthenium(II) Hexafluorophosphate, $[Ru(bpy)_2qpyme_2]^{4+}(PF_6^-)_4$.

Prepared as above for bis–(2,2'–bipyridine)–N''–methyl-2,2':4,4'':4',4'''–quaterpyridine ruthenium(II) hexafluorophosphate, substituting $[qpyme_2]^{2+}$ for $[qpyme]^+$. Resulting in 300 mg of $[Ru(bpy)_2qpyme_2]^{4+}(PF_6^-)_4$. C,H,N Analysis Found (%C 37.34 %H 2.74 %N 8.32) Calc. (%C 37.34 %H 2.52 %N 8.50)

Tris–(2,2':4,4'':4',4'''–Quaterpyridine)Ruthenium(II) Hexafluorophosphate, $[Ru(qpy)_3]^{2+}(PF_6^-)_2$.

$Ru(DMSO)_6Cl_2$ (300 mg, 1.18 mmol) and qpy (366 mg, 1.18 mmol) were refluxed, with stirring, in 25 mL of ethylene glycol for 15 min. At that time, the additional 2 equivalents of the quaterpyridyl

were added (732 mg, 2.36 mmol), and heating was continued for 30 min longer. The resulting deep red solution was cooled to room temperature, and added to 10 mL of sat. ammonium hexafluorophosphate. The resulting precipitate was allowed to digest at 0 °C for 4 hours. The solid was filtered and washed thoroughly with water (20 mL, 4X), and chloroform (20 mL, 4X). The solid was precipitated from acetone with ether, and chromatographed on alumina (acetonitrile/methanol) as described above. The procedure results in 300 mg of $[Ru(qpy)_3]^{2+}(PF_6^-)_2$. C,H,N Analysis Found on the octahydrate: (%C 48.71 %H 2.97 %11.52) Calc. (%C 48.55 %H 2.85 %N 11.32)

Tris–(N'–Methyl–2,2'':4,4'':4',4'''–Quaterpyridinium)Ruthenium(II) Hexafluorophosphate. $[Ru(qpyme)_3]^{6+}(PF_6^-)_6$.

The complex was prepared as above for $[Ru(qpy)_3]^{2+}(PF_6)_2$, substituting [qpyme]$^+$ (I^-) for qpy.

Tris–(N'',N'''–Dimethyl–2,2':4,4':4',4'''–Quaterpyridinium)Ruthenium(II) Hexafluorophosphate, $[Ru(qpyme_2)_3]^{6+}(PF_6^-)_6$

The complex likely is formed with the above preparation $[Ru(qpy)_3]^{2+}(PF_6^-)_2$, substituting $[qpyme_2]^{2+}(I^-)_2$ for qpy, but purification using column chromatography is not applicable. The complex binds irreversibly to alumina or silica gel, and cannot be removed even with water/methanol solutions.

Bis–(2,2'–Bipyridine)–4;7'-Phenanthrolino-5',6':5,6-Pyrazine Ruthenium(II) Hexafluorophosphate, $[Ru(bpy)_2ppz]^{2+}(PF_6^-)_2$.

$Ru(bpy)_2Cl_2$ (300 mg, 0.576 mmol) in 200 ml 95% ethanol was added to 4;7'-phenanthrolino-5',6':5,6-pyrazine (250 mg, 1.08 mmol), also in 200 ml of 95% ethanol, over a period of one hour at reflux. After the addition, refluxing was continued for another two hours. The volume was then reduced to 40 mL by distillation under reduced pressure, and the solution

was cooled to room temperature. The complex was then precipitated by addition of the solution to 20 mL of sat. ammonium hexafluorophosphate, and the complex immediately precipitated. The precipitate was allowed to digest at 0 °C for 4 hours; the solid was filtered and washed with water (20 mL, 4X), and chloroform (20 mL, 4X). The solid was dissolved in a minimum amount of hot acetone and filtered while hot. The volume of acetone was reduced to 30 mL, and the complex was precipitated by the addition of ether. The solid was filtered and washed with ether, and allowed to dry. This resulted in 200 mg of crude $[Ru(bpy)_2ppz]^{2+}(PF_6^-)_2$ contaminated with traces of the dimeric species, $[Ru(bpy)_2ppzRu(bpy)_2]^{4+}(PF_6^-)_4$. Pure samples of $[Ru(bpy)_2ppz]^{2+}(PF_6^-)_2$ can be obtained by one of two methods. Column chromatography on alumina with methanol/acetone or (acetonitrile/ethanol) or gel filtration on sephadex LH 60 eluted with acetonitrile/ ethanol. In both procedures there are three major bands observed. The first is composed of $Ru(bpy)_2Cl_2$, next, $[Ru(bpy)_2ppz]^{2+}$ elutes in a yellow band, and finally, the dimer, $[Ru(bpy)_2ppzRu(bpy)_2]^{4+}$ elutes in the a blue/purple band.

$[(bpy)_2RuppzRu(bpy)_2]^{4+}(PF_6^-)_4$.

$Ru(bpy)_2Cl_2$ (300 mg, 0.576 mmol) and ppz (67 mg, 0.289 mmol) were refluxed in 70 mL of 50% ethanol for 2 hours. The volume was then reduced to 25 mL The resulting solution was cooled to room temperature, and added to 50 mL of sat. ammonium hexafluorophosphate. The solution was stored at 0 °C for 4 hours. The solid was filtered and washed with water (20 mL, 4X), and chloroform (20 mL, 4X). Purification is accomplished as for the monomeric species (above).

$[(bpy)_2RuppzPtCl_2]^{2+}(PF_6^-)_2$

H_2PtCl_6 was reduced to K_2PtCl_4 with SO_2 via the method of Keller[162]. The K_2PtCl_4 so obtained was used to prepare the $Pt(DMSO)_2Cl_2$ by a previously described procedure[163]. $[Ru(bpy)_2ppz]^{2+}$ (50 mg, 0.058 mmol) and $Pt(DMSO)_2Cl_2$ (24 mg, 0.058 mmol) were refluxed in 20

mL of ethylene glycol for 1 hour. The resulting solution was cooled to room temperature, and added to 20 mL of sat. ammonium hexafluorophosphate. The solution was stored at 0 °C for 4 hours. The solid was filtered and washed with water (20 mL, 2X). The solid was collected, and dissolved in a minimum amount of hot acetone and filtered hot. The volume of acetone was reduced to 30 mL, and the complex was precipitated by the addition of ether. The solid was filtered, washed with ether, allowed to dry, dissolved in a minimum of acetonitrile, and chromatographed on alumina with an acetonitrile/methanol mobile phase as described above. This procedure result in 50 mg of $[Ru(bpy)_2ppzPtCl_2]^{2+}(PF_6^-)_2$. C,H,N Analysis on the dihydrate: Found (%C 32.79 %H 2.00 %N 8.91) Calc. (%C 32.99 %H 2.28 %N 9.05).

$[(bpy)_2RudppPtCl_2]^{2+}$ $(PF_6^-)_2$

$[Ru(bpy)_2dpp]^{2+}$ (50 mg, 0.058 mmol) and $Pt(DMSO)_2Cl_2$, prepared as above, (24 mg, 0.058 mmol) were refluxed in 20 ml of ethylene glycol for 1 hour. The resulting solution was cooled to room temperature, and added to 20 mL of sat. ammonium hexafluorophosphate. The solution was stored at 0 °C for 4 hours. The solid was filtered and washed with water (20 mL, 2X). The solid was collected, and dissolved in a minimum amount of hot acetone and filtered hot. The volume of acetone was reduced to 30 mL, and the complex was precipitated by the addition of ether. The solid was filtered and washed with ether, and allowed to dry. The solid was dissolved in a minimum of acetonitrile, and chromatographed on alumina with an acetonitrile/methanol mobile phase as described above. This procedure result in 50 mg of $[Ru(bpy)_2dppPtCl_2]^{2+}(PF_6^-)_2$. The complex appears to decompose on the column, and is not stable (Chapter X).

Bis–(2,2'–Bipyridine)–1;10'-Phenanthrolino-5',6':5,6-Pyrazine Ruthenium(II) Hexafluorophosphate, $[Ru(bpy)_2(\mathit{l}\text{–}ppz)]^{2+}(PF_6^-)_2$.

$Ru(bpy)_2Cl_2$ (100 mg, 0.192 mmol) and 1;10'-phenanthrolino-5',6':5,6-pyrazine (83 mg, 0.36

mmol) were refluxed in 100 mL of 50% ethanol for 2 hours. The volume was then reduced to 40 mL by distillation under reduced pressure, and the solution was cooled to room temperature. The complex was then precipitated by addition of the solution to 50 mL of sat. ammonium hexafluorophosphate, and the complex immediately precipitated. The precipitate was allowed to digest at 0 °C for 1 hours. The solid was filtered and washed with water (20 mL, 4X), and then chloroform (20 mL, 4X). The solid was collected, dissolved in a minimum amount of hot acetonitrile, and chromatographed on alumina with acetonitrile/methanol as described above. $[Ru(bpy)_2(i\text{-}ppz)]^{2+}$ is collected as a bright yellow band. The solvent is then allowed to evaporate giving a yield of 100 mg. C,H,N Analysis on the monohydrate: Found. (%C 42.44 %H 2.47 %N 11.54). Calc. (%C 42.82 %H 2.75 %N 11.75)

References

1. Paris, T. P.; Brandt, W. W. *J. Am. Chem. Soc.*, **1959**, *81*, 5001.

2. a) Gafney, H. D.; and Adamson, A. W. *J. Am. Chem. Soc.*, **1972**, *94*, 8238. b) Demas, J. N. and Adamson, A. W. *J. Am. Chem. Soc.* **1973**, *95*, 5159.

3. (a) Kalyanasundaran, K.; Gratzel, M.; Pelizzetti, E. *Coord. Chem. Rev.*, **1986**, *69*, 57-125. (b) Juris, A.; Balzani, V.; Barigelletti, F.; Campagna, S.; Belser, P.; Zelewsky, A. Z., *Coord. Chem. Rev.*, **1988**, *84*, 85- 277.

4. a) Bock, C. R.; Meyer, T. J.; and Whitten, D. G. *J. Am. Chem. Soc.*, **1974**, 96, 4710. b) Young, R. C.; Meyer, T. J.; Whitten, D. G. *J. Am. Chem. Soc.*, **1975**, 97, 781. c) Navon, G.; Sutin, N. *Inorg. Chem.* **1974**, 13, 2159.

5. a) Anderson, C. P.; Salmon, D. J.; Meyer, T. J.; Young, R. C. *J. Am. Chem. Soc.* **1977**, 99, 1980. b) Maestri, M.; Gratzel, M. *Ber. Bunsenges. Phys. Chem.* **1977**, 81, 504. c) Bock, C. R.; Conner, J. A.; Gutierrez, Meyer, T. J.; Whitten, D. G.; Sullivan, B. P.; Nagle, J. K. *J. Am. Chem. Soc.* **1979**, 101, 4815 ; *Chem. Phys. Lett.* **1979**, 61, 522 d) Ballardini, R.; Varani, G.; Indelli, M. T.; Scandola, F.; Balzani, V. J. *Am. Chem. Soc.* **1978**, 100, 7219.

6. (a) Maestri, M.; Sandrini, D. *Nouv. J. Chim.*,**1981**, *5*, 637. (b) Harriman, A.; Mills. *J. Chem. Soc. Faraday. Trans.*, **1981**, *77*, 2111. (c) Shehegoleva, I. S.; Kuchmii, S. Y. *High Energy Chem., USSR*, **1983**, *17*, 81. (d) Nenadovic, M. J.; Micic, O. I.; Rajh, T.; Savic, D.,*J. Photochem.*,**1983**, *21* 35. (e) Launikonis, A., Loder, J. W.; Mau, A. W. H.; Sasse, W. H. F.; Summers, L. A.; Wells, D. *Aust J. Chem.*, **1982**, *35*, 1341. (f) Launikonis, A.; Loder, J. W.; Mau, A. W. H.; Sasse, W. H. F.; Wells, D. *Ir. J. Chem.*,**1982**, *22*, 1587. (g) Frank, A. J.; Stevenson, K. L. *J. Chem. Soc. Chem. Commun.*, **1981**, 593. (h) Crutchley, R. R.; Lever, A. B. P. *J. Am. Chem Soc.*, **1980**, *102*, 7128.

7. (a) Hawecker, J.; Lehn, J.- M.; Ziessel, R. *Nouv. J. Chem.*, **1983**, *7*, 271. (b) Lay. P. A.; Mau, A. W. H.; Sasse, W. H. F.; Creaser, I. I.; Gahan, L. R.; Sargeson, A. M. *Inorg. Chem.*, **1983**, *22*, 2347. (c) Krishnan, C. V.; Sutin, N. *J. Am. Chem. Soc.*, **1981**, *103* 2141.

8. (a) Creutz, C.; Heller, A. D.; Sutin, N.; Zipp, A. P. *J. Am. Chem. Soc.*, **1982**, *104*, 3618. (b) Brunschwig, B. S.; Sutin, N. *Chem. Phys. Lett.*, **1981**, *77*, 63. (c) Chan, S. F.; Chou, M.; Cruetz, C.; Matsubara, T.; Sutin, N. *J. Am. Chem. Soc.*, **1981**, *103*, 369. (d) Giro, G.; Casalbore, G.; DiMarco, P. G. *Chem Phys. Lett.*, **1980**, *71*, 7128.

9. Cruetz, C.; Sutin, N. *Proc. Natl. Acad.* Sci., **1975**, *72*, 2858.

10. (a) Khannov, N. K.; Shafirovich, V. *Dokl. Acad. Nauk, USSR*, **1981**, *260*, 1418. (b) Ghosh, P. K.; Brunschwig, B. S.; Chan, M.; Cruetz, C.; Sutin, N. *J. Am. Chem. Soc.*, **1984**, *106*, 4772. (c) Shafirovich, V. Y.; Khannanov, N. K.; Strelets, V. *Nouv. J. Chim.*, **1980**, *4*, 81. (d) Harriman, A.; Porter G.; Walters, P., *J. Chem. Soc. Faraday. Trans.*, **1981**, *2*, 77, 2373.

11. Gersten, S. W.; Samuels, G. S.; Meyer, T. J. *J. Am. Chem. Soc.*, **1982**, *104*, 4029.

12. Goswami, S.; Chakravarthy, A. R.; Chakravarthy, A. *J. Chem. Soc. Chem. Commun.*, **1982** 1288.

13. (a) Gilbert, J. A.; Eggleston, D. S.; Murphy, D. S.; Geselowitz, D. A.;Gersten, D. A.; Hodgson,

D. J.; Meyer, T. J., *J. Am. Chem. Soc.*, **1985**, *107*, 3855. (b) Honda, K.; Frank, A. J. *J. Chem. Soc., Chem. Commun.*, **1984**, 1635. (c) Lay, P. S.; Sasse, W. H. F. *Inorg. Chem.*,**1985**, *24*, 4707. (d) Collins, J. P.; Sauvage, J. P. *Inorg. Chem.*, **1986**, *25*, 135. (e) Desilvestro, J.; Duonghong, D.; Kleiji, M.; Gratzel, M. *Chimia*, **1985**, *4*, 102. (f) Rotzinger, F. P.; Shekhar, M.; Comte, P.; Hurst, J. P.; Gratzel, M.; Pern, F.-J.; Frank, A. J. *J. Am. Chem. Soc.*, **1987**, *109*, 6619-6626.

14. Dressick, W. J.; Meyer, T. J.; Durham, B.; Rillema, D. P. *Inorg. Chem.*,**1982**, *21*, 3451-3458.

15. Ghosh, K. B. *Coord. Chem. Rev.*, **1989**, *95*, 239.

16. a) Meyer, T. J. *Acc. Chem Res.*, **1978**, *11*, 94. b) Bock, C. R.; Conner, J. A.; Gutierrez, A. R.; Meyer, T. J.; Whitten, D. G.; Sullivan, B. P.; Nagle, J. K.; *J. Am. Chem. Soc.* **1979**, *101*, 4815 . c) Bock, C. R.; Meyer, T. J.; Whitten, D. G. *J. Am. Chem. Soc.*, **1974**, *96*, 4710. d) Navon, G.; Sutin, N., *Inorg. Chem* **1974**, *13*, 2159. e) Gafney, H. D.; Adamson, A. W. *J. Am. Chem. Soc.*, **1972**, *94*, 8238.

17. a) Balzani, V.; Moggi, L.; Manfrin, M. F.; Bolletta, F.; Laurence, G. A. *Coord. Chem. Rev.*, **1975**, *15*, 321. b) Sabbatini, N.; Balzani, V. *J. Am. Chem. Soc.* **1972**, *94*, 7587. c) Demas, J. N.; Adamson, A. W. *J. Am. Chem. Soc.* **1971**, *93*, 1800. d) Lin, C-T.; Bottcher, W.; Chou, M.; Cruetz, C.; Sutin, N. *J. Am. Chem. Soc.* **1976**, *98*, 6536. e) Kane-Maguire, N. A. P.; Langford, C. H. *J. Am. Chem. Soc.* **1975**, *94*, 2125.

18. The area has been reviewed. a) Kalyansundaram, K. *Coord. Chem. Rev,*. **1982**, *46*, 159. b) Wrighton, M. S. Ed. *Adv. Chem. Ser.* **1979**, No 173, Chapters 1,2,4. c) Sutin, N. *J. Photochem.* **1979**, *10*, 19. d) Whitten D. G. *Acc. Chem. Res*, **1980**, *13*, 83. e) Sutin, N.; Creutz, C. *Pure Appl. Chem.* **1980**, *52*, 2717. f) Meyer, T. J. *Acc. Chem. Res.*, **1978**, *11*, 94. g) Crosby, G. A. *Acc. Chem. Res.* **1975**, *8*, 231.

19. a) Della Guardia, R. A.; Thomas, J. K. *J. Phys. Chem.* **1983**, *87*, 990. b) Ghosh, P. K.; Bard, A. J. *J. Phys. Chem.* **1984**, *88*, 5519.

20. Milosavljevic, B. H.; Thomas, J. K. *J. Phys. Chem.* **1983**, *87*, 616.

21. Wheeler, J.; Thomas, J. K. *J. Phys. Chem.* **1982**, *86*, 4540.

22. (a) Kalyanasundaram, K.; Gratzel, M.; Pelizzetti, E. *Coord. Chem. Rev.* **1986**, *69*, 57. (b) Rotzinger, F. P.; Munavalli, S.; Comte, P.; Hurst, J. K.; Gratzel, M.; Pera, F-J.; Frank, A. J. *J. Am. Chem. Soc.*, **1987**, *109*, 6619 (and references therein).

23. a) Balzani, V.; Bolleta, F.; Gandolfi, M. T.; Maestri, M. *Top. Curr. Chem.* **1978**, *75*, 1. b) Sutin, N.; Creutz, C. *Pure Appl. Chem.* **1980**, *52*, 2717. c) Kalyansundaram, K. *Coord. Chem. Rev.* **1982**, *46*, 159.

24. Wilner, I.; Maidan, R.; Mandler, D.; Durr, H.; Dorr, G.; Zengerle, K. *J. Am. Chem. Soc.*, **1987**, *109*, 6080.

25. For a review see: Meyer, T. J. *Acc. Chem. Res.*, **1989**, *22*, 5, 163.

26. Bruinink, J.; Kregting, C. G. A.; Ponjee, J. J. *J. Electrochem. Soc.* **1977**, *124*, 1854.

27. Dose, E.; Wilson, L. J. *Inorg. Chem.* **1978**, *17*, 2660.

28. a) Rillema, D. P.; Mack, K. B. *Inorg. Chem*, **1982**, *21*, 3849. b) Hunziger, M.; Ludi, A. *J. Am. Chem. Soc.* **1977**, 99, 7370. c) Dose, E.; Wilson, L. J. *Inorg. Chem.* **1978**, *17*, 2660.

29. Rillema, D. P.; Callahan, R. W.; Mack, K. B. *Inorg. Chem.* **1982**, *21*, 2589.

30. Braunstein, C. H.; Baker, A. D.; Strekas, T. C.; and Gafney, H. D. *Inorg. Chem.*, **1984**, *23*, 857.

31. Fuchs, Y.; Lofters, S.; Dieter, T.; Wei shi; Morgan, R.; Strekas, T. C.; Gafney, H. D.; Baker, A. D. *J. Am. Chem. Soc.* **1987**, 109, 2691.

32. a) Nasielski-Hinkens, R.; Benedek-Vamos, M. J. *Chem. Soc., Perkin Trans. I*, **1975**, 1229. b) Kirsch-De Mesmaeker, A.; Nasielski-Hinkens, R. Maetens, D.; Pauwels, D.; Nasielski, J. *Inorg. Chem.* **1984**, *23*, 377. c) Kirsch-De Mesmaeker, A.; Maetens, D.; Nasielski-Hinkens, R. *J. Electroanal. Chem. Interfacial Electrochem.* **1985**, *182*, 123. d) Kirsch-De Mesmaeker, A; Maetens, D.;Nasielski-Hinkens, R. *Acta Chim. Hung.* **1985**, *119*, 245. e) Masschelein, A.; Kirsch-De Mesmaeker, A. *Nouv. J. Chim.* **1987**, *11*, 329.

33. Sahai, R.; Baucom, A.; Rillema, P. D. *Inorg. Chem.* **1986**, 3843.

34. Schmehl, R. H.; Auerbach, R. A.; Wacholtz, W. F.; Elliot, C. M.; Freitag, R. A.; Merkert, J. W. *Inorg. Chem.* **1986**, *25*, 2440.

35. Wacholtz, W. F.; Auerbach, R. A.; Schmehl, R. H. *Inorg. Chem.* **1987**, *26*, 2989.

36. Moore, T. A.; Gust, D.; Mathis, P.; Mialocq, J. C.; Chachaty, C.; Bensasson, R. V.; Land, E. J.; Doizi, D.; Lidell, P. A.; Lehman, W. R.; Nemath, G. A.; Moore, A. L. *Nature*, **1984**, *307*, 630.

37. Barton, J.K. *Science* **1986**, 233, 727-734.

38. Pyle, A.M.; Rehmann, J.P.; Meshoyrer, R.; Kumar, C.V.; Turro, N.J.; Barton, J.K. *J. Am. Chem. Soc.* **1989**, 111, 3051-3058.

39. Barton, J.K.; Paranawithana, S.R. *Biochemistry*, **1986**, 25, 2205-2211.

40. Barton, J.K.; Goldberg, J.M.; Kumar, C.V.; Turro, N.J. *J. Am. Chem. Soc.* **1986**, 108, 2081-2088.

41. Kumar, C.V.; Barton, J.K.; Turro, N.J. *J. Am. Chem. Soc.* **1985**, 107, 5518-5523.

42. Barton, J.K.; Raphael, A.L. *Proc. Nat. Acad. Sci. U.S.A.* **1985**, 82, 6460-6464.

43. Barton, J.K.; Lolis, E. *J. Am. Chem. Soc.* **1985**, 107, 708-709.

44. Barton, J.K.; Basile, L.A.; Danishefsky, A.; Axexandrescu; *A. Proc. Nat. Acad. Sci. U.S.A.* **1984**, 81, 1961-1965.

45. Barton, J.K.; Danishefsky, A.; Goldberg, J.M. *J. Am. Chem. Soc.* **1984**, 106, 2172-2176.

46. Barton, J.K.; Dannenberg, J.J.; Raphael, A.L. *J. Am. Chem. Soc.* **1982**, 104, 4967-4968.

47. Norden, B.; Tjernfeld, F. *FEBS Lett.* **1976**, 67, 368-370.

48. Hiort, C.; Norden, B.; Rodger, R. *J. Am. Chem. Soc.* **1990**, 112, 1971-1982.

49. Goldstein, B.M.; Barton, J.K.; Berman, H.M. *Inorg. Chem.* **1986**, 25, 842-847.

50. a) Smith, D. M. "Rodd's Chemistry of Carbon Compounds," Sec. Ed., ed by S. Coffey, Vol. IV (Heterocyclic compounds- Part F), pp 56- 226, Elsevier, Amsterdam (1976). b) Heterocyclic Compounds - Pyridine and its Derivatives," ed by R. A. Abramovitch, Vol. 14, Part 1- 4, John Wily & Sons, New York (1974- 5). c) For an excellent review of bipyridine chemistry see: Summers, L. A. *Adv. Het. Chem*, **1984**, *35*, 281.

51. For a review see: Badger G. M.; Sasse, W. H. F. *Adv. Heterocycl. Chem* **1963**, *2*, 179.

52. Sargeson, A. M. and Sasse, W. H. F., *Proc. Chem. Soc., London*, **1958**, 150.

53. Sasse, W. H. F. and Whittle, C. P. *Aust J. Chem.* **1963**, *16*, 31.

54. Sasse, W. H. F. *J. Chem. Soc.*, **1959**, 3046.

55. Sasse, W. H. F., *Org. Synth*, **1966**, *46*, 5.

56. Land. G. H.; Lang, G. H.; New, R. G. A.; Thompson, J. M. British Patent 899,015 (1962) [*CA* **57**, 6670 (1962)].

57. Belser, P.; von Zelewsky, A. *Helv. Chim. Acta Part A*, **1980**, *63*, 1675.

58. Badger, G. M.; Sasse, W. H. F. *J. Chem. Soc.*, **1956**, 616.

59. Sasse, W. H. F.; Whittle, C. P. *J. Chem. Soc.*, **1961**, 1347.

60. Lang, G. H. British Patent 955,951 (1964) [*CA 61*, 3075 (1964)].

61. Hart, F. A.; Newberry, J. E. *J. Inorg. Nucl. Chem.* **1969**, *31*, 1725.

62. Otroshchenko, O. S.; Ziyaev, A. A.; Sadykov, A. S. U.S.S.R Patent 255,276 (1969) [*CA* **72**, 111307 (1970)].

63. Ziyaev, A. A., Otroshchenko, O. S., Sadykov, A. S., Khalilova, K. D. and Tolkacheva, G. A., *Khim. Geterotsikl. Soedin.*, **1978**, 1224.

64. Jackson, G. D. F.; Sasse, W. H. F.; Whittle, C. P. *Aust. J. Chem.*, **1983**, *16*, 1126.

65. Rapoport, H.; Iwamoto, R.; Tretter, J. R. *J. Org. Chem.*, **1960**, *25*, 372.

66. California Research Corporation, British Patent 915,950 (1963) [*CA* **59**, 11453 (1963)]

67. Lang, G. H. British Patent 981,353 (1965) [*CA* **63**, 14826 (1965)].

68. Lang, G. H.; New, R. G. A. British Patent 1,000,656 (1965) [*CA* **63**, 16315 (1965)].

69. Lang, G. H. British Patent 1,026,822 (1966) [*CA* **65**, 2232 (1966)].

70. Dalton, R. F.; Dowden, D. A.; Lang, G. H. British Patent 1,377,213 (1974) [*CA* **82**, 170703 (1975)].

71. Waddan, D. Y.; Williams, D. German Patent 1,950,074 (1970) [*CA* **73**, 3799 (1970)].

72. Haginiawa, J.; Higuchi, Y.; Maki, I. *Yakugaku Zasshi*, **1977**, *97*, 1261.

73. Vilceanu, R.; Neda, I.; Arsulescu, E.; Leonte, O.; Kutz, S. Romanian Patent 67,302 (1979) [*CA* **94**, 208723 (1981)].

74. Lang, G. H. British Patent 1,014,077 (1965) [*CA* **64**, 11182 (1966)].

75. Haginiwa, J.; Higuchi, Y. *Yakugaku Zasshi*, **1973**, *93*, 144.

76. Haginiwa, T.; Hiuchi, Y.; Fujimoto, Y. Japanese Patent 13,796 (1974) [*CA* **81**, 153148 (1974)].

77. Rosevear, P. E.; Sasse, W. H. F. *J. Heterocycl. Chem.*, **1971**, *8*, 483.

78. Rosevear, P. E.; Sasse, W. H. Australian Patent 466,960 (1975) [*CA* **84**, 74118 (1976)]

79. Weidel, H.and Russo, M. *Monatsh. Chem.*, **1882**, *3*, 850.

80. Smith, C. R. *J. Am. Chem. Soc.*, **1924**, *46*, 414.

81. Anderson, T. *Justus Liebigs Ann. Chem.*, **1870**, *154*, 270.

82. Emmert, B., *Ber. Dtsh. Chem. Ges.*, **1917**, *50*, 31.

83. Setton R. *Hebd. Seances Acad. Sci.*, **1957**, *244*, 1205.

84. Imperial Chemical Industries Ltd., French Patent aw341,585 (1963) [*CA* **60**, 14482 (1964)].

85. Imperial Chemical industries Ltd., French Patent 1,380,806 (1964) [*CA* **62**, 10417 (1965)].

86. Imperial Chemical Industries Ltd., Netherlands Patent 6,603,415 (1966) [*CA* **66**, 28674 (1967)].

87. Imperial Chemical Industries Ltd., Belgian Patent 617,852 (1962) [*CA* **60**, 2907 (1964)].

88. Ahrens, F. B. *Ber. Dtsch. Chem. Ges.*, **1888**, *21*, 2929.

89. Heuser A.; Stoehr, C. *J. Prakt. Chem.* **1889**, *42*, 429.

90. Dimroth, O.; Heene, R. *Ber dtsch. Chem. Ges. B.*, **1921**, *54*, 2934.

91. Dimroth, O.; Frister, F. *Ber Dtsch. Chem. Ges. B.*, **1922**, *55*, 1223.

92. Michaelis, L.; Hill, E.S. *J. Am. Chem. Soc.*, **1933**, *55*, 1484.

93. Szarvas, P.; Emri, J.; Gyori, B.; Nagy, Z.; Punkosti, K.; Bonczor, J.; Arany, S.; Gyori, B. Hungarian
Patent 157,374 (1970) [*CA* **73**, 66444 (1970)]

94. Clarke, A. J.; McNamara, S.; Meth-Cohn, O. *Tett. Lett.*, **1974**, 2373.

95. Newkome, G. R.,; Hager, D. C. *J. Org. Chem.*, **1982**, *47*, 599.

96. Newkome, G. R.; Hager, D. C.; Fronczek, F. R. *J. C. S. Cawm Commun.*, **1981**, 858.

97. Kauffmann, T. *Angew. Chem.*, **1979**, *18*, 1.

98. Kauffmann, T. *Angew Chem.*, **1974**, *13*, 291.

99. Vaughan, L. G. *J. Am. Chem. Soc.*, **1970**, *92*, 730.

100. Wilbaut, J. P.; Overhoff, *Recl. Trav. Chim. Pays- Bas,*, **1928**, *47*, 761.

101. Burstall, F. H. *J. Chem. Soc.*, **1938**, 1662.

102. Geissman, T. A.; Schlatter, M. J.; Webb, I. D.; Roberts, J. D. *J. Org. Chem.*, , **1946**, *11*, 741.

103. Mikhailov, G. I. *Zh. Prikl Chim*, **1955**, *28*, 114.

104. Kulicki, Z.; Karminski, W. *Zesz. Nauk. Politech. Slask., Chem.* **1963**, *16*, 11. [*CA* **62**, 4001,(1965)].

105. Karminski, W.; Kulicki, Z. *Chem. Stosow., Ser. A*, **1965**, *9*, 129. [*CA* **63**, 18018 (1965)].

106. Kulicki, Z.; Karmininski, W.; Kajzerek, B. Polish Patent, 52,038 (1966). [*CA* **68**, 2816 (1968)].

107. Goshaev, M.; Otroshchenko, O. S.; Sadykov, A. S.; Kuznetsova, N. *Izv. Akad. Nauk. Turkm. USSR, Ser. Fiz.-Tekh., Khim. Geol. Nauk.*, **1970**, 114. [*CA* **84**, 105407 (1976)].

108. Fanta, P.E. *Chem. Rev.*, **1964**, 613.

109. den Hertog, H. J. Jr., Wilbaut, J. P. *Rec. Trav. Chim, Pays-Bas* , **1932**, *51*, 381.

110. Goshaev, M.; Otroshchenko, O. S.; Sadykov, A. S.; Kuznetsova, N. *Izv. Akad. Nauk. Turkm. USSR, Ser. Fiz.-Tekh., Khim. Geol. Nauk.*, **1970**, 114. [*CA* **84**, 105407 (1976)].

111. Kurbatov, Y. V.; Otroshchenko, O. S.; Sadykov, A. S.; Goshaev, M. *Tr. Samark. Gos. Univ. im. Alishera Navoi*, **1969**, *167*, 85. [*CA* **73**, 98760 (1970)].

112. Otroshchenko, O. S.; Goshaev, M.; Sadykov, A.S.; Kuznetsova, N. V. U.S.S.R Patent 253,066 (1969) [*CA* **72**, 121372 (1970)].

113. Gali, G.; Honty, K.; Kalaus, G.; Szantay, C.; Hungarian Patent 17,177 (1979) [*CA* **92**, 181024 (1980)].

114. Thompson, W. J.; Gaudino, J. *J. Org. Chem.*, **1984**, *49*, 5237.

115. Davidson, J. M.; Triggs, C. *J. Chem Soc. A*, **1968**, 1324.

116. Haashi, T.; Mitsuo, K.; Kumada, M. *Tett. Lett.*, **1979**, *21*, 1871.

117. Miyaura, N.; Yanagi, T.; Suzuki, A. *Synth. Commun.*,**1981**, *11*, 513.

118. Ishikura, M.; Kamada, M.; Terashima, M. *Synth. Commun.*, **1984**, 936.

119. Thompson, W. J.; Jones, J. H.; Lyle, P. A.; Thies, E. J. *J. Org. Chem.*, **1988**, *53*, 2052.

120. Bishop, J. J.; Davidson, A.; Katcher, D. W.; Lictenberg, R. E.; Merrill, R. E.; Smart, J. C. *J. Organometal. Chem.*,**1971**, *27*, 241.

121. Lang. G. H., German Patent 2,521, 969 (1975) [*CA* **84**, 105407 (1976)].

122. Barnfield, P.; Quan, P. M. *Synthesis*, **1978**, 537.

123. Krohnke, F. *Synthesis*, **1976**, 1.

124. Newkome, G. R.; Lee, H. W. *J. Am. Chem. Soc.*, **1983**, *105*, 5956.

125. Bonnemann, H.; Brinkmann, R. *Synthesis*, **1975**, 600.

126. Ruetman, S. H. U.S. Patent 3,819558 (1974) [*CA* **81**, 91363 (1974)].

127. Darrah, J. I. British Patent 1,491,254 (1977) [*CA* **88**, 190594 (1978).

128. Darragh, J. I. British Patent 1,494,336 (1977) [*CA* **89**, 24154 (1978)].

129. Kurbatov, Y. V.; Kiryukhin, V. K.; Otroshchenko, O. S.; Sadykov, A. S. *Nauchn. Tr. Tashk. Gos. Univ. im. V. I. Lenina* , **1966**, *286*, 92. [*CA* **67**, 82059 (1967)].

130. Rosen, S.; Lerman, O.; Kol, M. J. *J. Chem. Soc., Chem. Commun.*, **1981**, 443.

131. Lerman, O.; Tor, Y.; Hebel, D.; Rosen, S. *J. Org. Chem.*, **1984**, *49*, 806.

132. Rosen, S.; Lerman, O.; Kol, M., Hebel, D. *J. Org. Chem.*, **1985**, *50*, 4753.

133. Hebel, D.; Rosen, S. *J. Org. Chem.*, **1988**, *53*, 1123.

134. Umemoto, T.; Tomizawa G. *Tett. Lett.*, **1987**, *28*, 2705.

135. Sont, W.; Alper, H. *Org. Prep. Proceed. Int.* , **1980**, *12*, 243.

136. Case, F. H. *J. Org. Chem.*, **1962**, *31*, 2398.

137. Haginiwa, J. *J. Pharm. Soc. Jpn.*, **1955**, *75*, 731.

138. Murase, I. *Nippon Kagaku Zasshi*, **1956**, *77*, 682.

139. Simpson, P. G.; Vinciguerra, A; and Quagliano, J. V. *Inorg. Chem.*, **1963**, *2*, 282.

140. Castellano, S.; Gunther, H.; Ebersole, S. *J. Phys. Chem.*, **1965**, *69*, 4166.

141. Keats, N. G.; Summers, L. A. *J. Heterocyclic Chem.*, **1976**, *13*, 369.

142. Keats, N. G.; Summers, L. A. *J. Heterocyclic Chem.*, **13**, 753.

143. Osbourne, A. G. *Spect. lett.*, **1972**, 10(10), 777.

144. De Koning, A.J.; Budzelaar, P.H.M.; Boersma, J.; Van Der Kerk, G.J.M. *J. Organomet. Chem*, **1980**, 199, 153-169.

145. Spotswood, T. McL.; Tanzer, C. I. *Aust J. Chem.* **1967**, 20, 1227-42.

146. Curphey, T. J.; Prasad, K. S. *J. Org. Chem.*, **1972**, *37*, 2259.

147. Calvet, J. M.; Caspar, J. V.; Binstead, R. A.; Westmoreland, T. D.; Meyer, T. J. *J. Am. Chem. Soc.*, **1982**, *104*, 6620.

148. See ef 3b (Above).

149. Polcyn, D. S.; Shain,I., *Anal. Chem.*, **1956**, *38*, 371.

150. Strekas, T. C.; Mandal. S. K. *J. Raman Spect.* **1984**, 15, 109.

151. Tokel-Takvoryan, N. E.; Hemingway, R. E.; Bard, A. J. *J. Am. Chem. Soc.* **1973**, *95*, 6582.

152. Saji, T.; Aoyagui, S. *J. Electroanal. Chem. Interfacial Electrochem.*, **1975**, *58*, 104.

153. Yersin, H.; Gallhuber, E. *J. Am. Chem. Soc.*, **1984**, *106*, 6582.

154. Meyer, T. J. *Pure & Appl. Chem*, **1986**, *58* (no. 9), 1193.

155. Vogt, L. H. Jr.; Katz, J. L.; Wiberly, S. E. *Inorg. Chem.* **1965**, 4, 1157.

156. Linsky, J. P.; Pierport, C. G. *Inorg. Chem.* **1973**, 7, 2959.

157. Creutz, C; Sutin, S. *Inorg. Chem.* **1976**, 15, 496.

158. Crutchley, R. J., Kress, N., and Lever, A. B. P., *J. Am. Chem. Soc.*, **1983**, *105*, 1170-1178.

159. Shinozaki, M.; Kaizu, Y.; Hirai, H.; Kobayashi, K. *Inorg. Chem.* **1989**, *28*, 3675.

160. Hosek, W.; Tysoe, S. A.; Gafney, H. D.; Baker, A. D.; Strekas, T. C. *Inorg. Chem.*, **1989**, 1228.

161. Evans, J. P.; Spencer, A.; Wilkinson, G. *J. Chem. Soc. (Dalton)* **1973**, 204.

162. Keller, R. N., *Inorganic Syntheses*, Vol II, pp 247-249.

163. Price, J. H.; Williamson, A. N.; Schramm, R. P.; Wayland, B. B. *Inorg Chem.*, **1972**, 11, 1280-1284.

164. Sahai, R.; Baucom, D. A.; Rillema, P. D. *Inorg. Chem.*, **1986**, *25*, 3843-3845.

165. Berger, R.M. *Inorg. Chem.* **1990**, *29*, 1920.

166. Berger, R. M.; McMillin, D. R. *Inorg. Chem.* **1988**, *27*, 4245.

167. Heath, G.A.; Yellowlees, L.J.; Braterman, P.S. *J. Chem. Soc., Chem. Commun.*, **1981**, 287.

168. Kelly, J.M.; Tossi, A.B.; McConnell, D.J.; OhUigin, C. *Nucleic Acids Res.* **1985**, 13, 6017-6034.

169. Tossi, A.B.; Kelly, J.M. *Photochem. Photobiol.*, **1989**, 5, 545-556.

170. Wang, A.H.J.; Nathans, J.; van der Marel, G.; van Boom, J.H.; Rich, A. *Nature* **1978** 276, 471-474.

171. Cooper, J.B.; MacQueen, D.B.; Petersen, J.D.; Wertz, D.W. *Inorg. Chem.*, **1990** 29, 3701-3705.

172. (a) Britten, R.J.; Graham, D.E.; Neufeld, B.R. *Meth. Enzymol.* **1974**, 29, 363-441.
(b) Richards, E.J. *in Short Protocols in Molecular Biology* **1989** pp. 80-81; Ausubel, F.M.; Brent, R.; Kingston, R.E.; Moore, D.D.; Seidman; J.G.; Smith, J.A.; Struhl, K.; Eds.; Greene Publishing Associates and Wiley-Interscience.

173. Mason, S.F.; Peart, B.J. *J. Chem. Soc., Dalton Trans* **1973**, 949-955.

174. Sullivan, B. P.; Salmon, D. J.; Meyer T. J. *Inorg. Chem.*, **1978**, *17*, 3334.